

REPORT NO.  
UCB/EERC-84/08  
AUGUST 1984

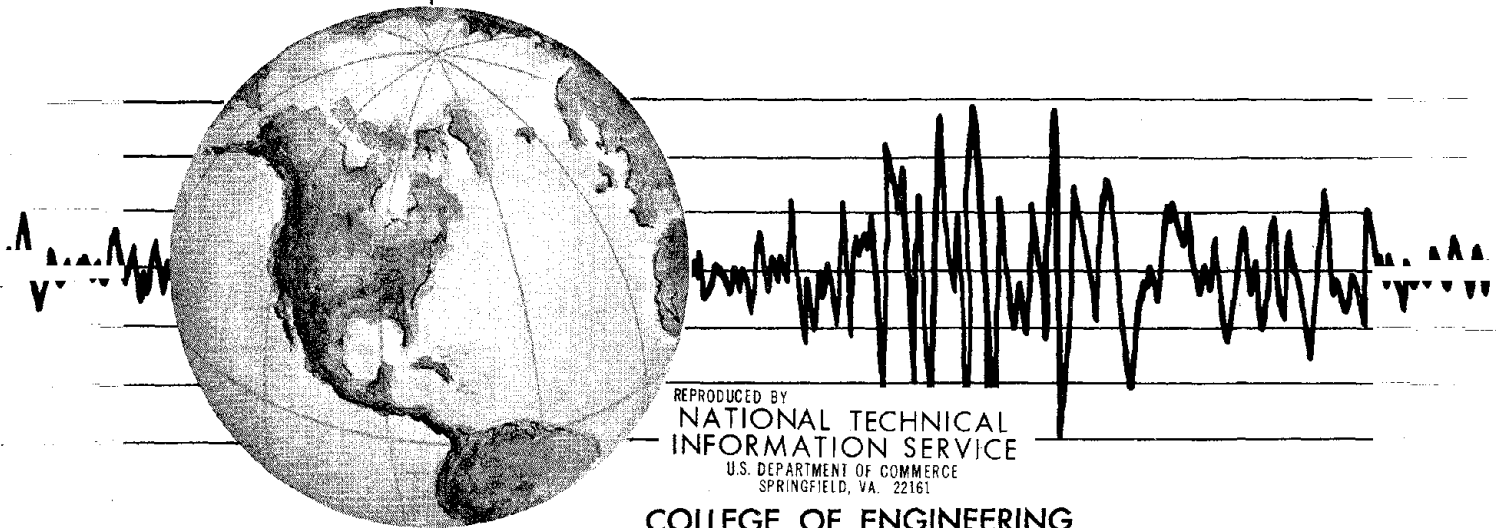
EARTHQUAKE ENGINEERING RESEARCH CENTER

# EXPERIMENTAL STUDY OF THE SEISMIC RESPONSE OF A TWO-STORY FLAT-PLATE STRUCTURE

by

JACK P. MOEHLE  
JOHN W. DIEBOLD

Report to the National Science Foundation



REPRODUCED BY  
NATIONAL TECHNICAL  
INFORMATION SERVICE  
U.S. DEPARTMENT OF COMMERCE  
SPRINGFIELD, VA. 22161

COLLEGE OF ENGINEERING

UNIVERSITY OF CALIFORNIA • Berkeley, California

For sale by the National Technical Information Service, U.S. Department of Commerce, Springfield, Virginia 22161.

See back report for up to date listings of EERC reports.

#### DISCLAIMER

Any opinions, findings and conclusions or recommendations expressed in this publication are those of the authors and do not necessarily reflect the views of the National Science Foundation or the Earthquake Engineering Research Center, University of California, Berkeley.

TITLE PAGE NSF/CEE-84030		Publication No. PB86 1225537AS	
<b>4. Title and Subtitle</b> Experimental Study of the Seismic Response of a Two-Story Flat-Plate Structure		<b>5. Report Date</b> August 1984	
<b>7. Author(s)</b> Jack P. Moehle and John W. Diebold		<b>8. Performing Organization Rept. No.</b> UCB/EERC-84/08	
<b>9. Performing Organization Name and Address</b> Earthquake Engineering Research Center University of California, Berkeley 1301 So. 46th Street Richmond, Calif. 94804		<b>10. Project/Task/Work Unit No.</b>  <b>11. Contract(C) or Grant(G) No.</b> (C) (G) CEE-81-10050	
<b>12. Sponsoring Organization Name and Address</b> National Science Foundation 1800 G. Street, N.W. Washington, D.C. 20550		<b>13. Type of Report &amp; Period Covered</b>  <b>14.</b>	
<b>15. Supplementary Notes</b>			
<b>16. Abstract (Limit: 200 words)</b> <p>A three-tenths scale, two-story reinforced concrete flat-plate structure was tested on the earthquake simulator at the Earthquake Engineering Research Center of the University of California, Berkeley. The test structure modeled a prototype structure with three bays in one direction and multiple bays in the transverse direction. The floor slab was supported on columns without interior beams, drop panels, or slab shear reinforcement. A shallow spandrel beam spanned the perimeter.</p> <p>The design seismic lateral forces were as specified for Zone 2 by the 1982 Uniform Building Code. The earthquake motions simulated were the North-South and vertical components of the El Centro, 1940 Imperial Valley earthquake.</p> <p>This report documents the design, fabrication, testing, and observed response of the test structure. Interpretations of the observed response are presented. Correlations obtained using modal analyses, linear elastic frame analyses, nonlinear frame analyses, and limit analyses are presented. Observations from isolated component experiments are summarized, and comparisons between component and test structure behavior are made.</p>			
<b>17. Document Analysis a. Descriptors</b>  <b>b. Identifiers/Open-Ended Terms</b>  <b>c. COSATI Field/Group</b>			
<b>18. Availability Statement:</b> Release Unlimited		<b>19. Security Class (This Report)</b>	<b>21. No. of Pages</b> 260
		<b>20. Security Class (This Page)</b>	<b>22. Price</b>



EXPERIMENTAL STUDY OF THE SEISMIC RESPONSE  
OF A TWO-STORY FLAT-PLATE STRUCTURE

by

Jack P. Moehle  
Assistant Professor of Civil Engineering  
University of California, Berkeley

and

John W. Diebold  
Formerly Research Assistant  
University of California, Berkeley

Report to Sponsor:  
National Science Foundation

Report No. UCB/EERC-84/08  
Earthquake Engineering Research Center  
College of Engineering  
University of California  
Berkeley, California

August 1984



## ABSTRACT

A two-story reinforced concrete flat-plate structure was built at three-tenths of full scale and tested on the earthquake simulator at the Earthquake Engineering Research Center of the University of California at Berkeley. The test structure models a prototype structure having three bays in one direction and multiple bays in the transverse direction. The floor slab was supported on columns without interior beams, drop panels, or slab shear reinforcement. A shallow spandrel beam spanned the perimeter.

Proportions of the structure were determined according to conventional design practice, with design seismic lateral forces as specified for Zone 2 of the 1982 Uniform Building Code. Details satisfy requirements of the ACI Building Code for structures located in regions of moderate seismic risk.

The experiments include earthquake simulation tests having one horizontal component (parallel the three-bay direction of the test structure) and one vertical component, with accelerations histories modeled after the North-South and vertical records obtained in El Centro during the 1940 Imperial Valley earthquake. Several earthquake simulations were conducted, having intensities ranging from low to high.

This report documents design, fabrication, testing, and observed response of the test structure. Interpretations of observed response are presented. Correlations obtained using modal analyses, linear elastic frame analyses, nonlinear frame analyses, and limit analyses are presented. Observations from isolated component experiments are summarized, and comparisons between component and test structure behavior are made.



## ACKNOWLEDGMENT

The work described in this report was part of an investigation to study seismic response of complete structural systems being carried out at the Earthquake Engineering Research Center of the University of California at Berkeley, California. The work was sponsored by the National Science Foundation under Grant No. CEE-81-10050. Opinions, findings, conclusions, and recommendations in this report are those of the authors and do not necessarily represent those of the National Science Foundation.

Appreciation is expressed for the kind, patient, and expert assistance of many persons who were involved with the project. Professors Clough, Mahin, Scordelis, and Wilson of the Department of Civil Engineering of the University of California at Berkeley are thanked for criticisms, advice, and assistance. S. Fung assisted ably with preliminary designs. F. Charney offered welcome assistance in deciphering the data reduction procedure. H. Zee is thanked for careful conduct of tests on interior and exterior slab-column connections, and for providing data and discussions willingly.

R. Lawrence and P. Quinn are thanked for supervision of machine shop and instrumentation facilities and personnel. R. Parsons was invaluable for his supervision and assistance in construction of the model. D. Clyde calibrated and operated all instrumentation and test apparatus without apparent fault. M. Edwards, G. Feazell, and R. Steele prepared several of the ink drawings.

A portion of this report was prepared as partial fulfillment of requirements for the degree of Master of Engineering of the second author under the supervision of the first.



TABLE OF CONTENTS

ABSTRACT . . . . . i

ACKNOWLEDGMENT . . . . . iii

TABLE OF CONTENTS . . . . . v

LIST OF TABLES . . . . . ix

LIST OF FIGURES . . . . . xi

1. INTRODUCTION . . . . . 1

    1.1 Statement of the Problem . . . . . 1

    1.2 Objectives and Scope . . . . . 2

    1.3 Performance History of Flat-Plate Frames . . . . . 5

    1.4 Previous Research . . . . . 7

2. DESIGN OF PROTOTYPE AND TEST STRUCTURE . . . . . 15

    2.1 Structure Description . . . . . 15

    2.2 Outline of the Design . . . . . 17

3. DESCRIPTION OF THE EXPERIMENT . . . . . 27

    3.1 Fabrication of the Test Structure . . . . . 27

    3.2 Experimental Setup . . . . . 29

    3.3 Description of Tests . . . . . 30

    3.4 Instrumentation and Data Recording . . . . . 32

    3.5 Sign Convention . . . . . 34

4. MEASURED RESPONSE OF THE TEST STRUCTURE . . . . . 35

    4.1 General Comments Regarding Data Presentation . . . . . 35

    4.2 Global Response . . . . . 42

    4.3 Response Spectra and Spectrum Intensities . . . . . 37

    4.4 Reinforcement Strains . . . . . 37

    4.5 Base Shear-Top Displacement Relations . . . . . 38

    4.6 Observed Damage . . . . . 38

5.	DISCUSSION OF OBSERVED RESPONSE . . . . .	40
5.1	Base Motions . . . . .	40
5.2	Global Response Trends . . . . .	43
5.3	Variation of Dynamic Properties . . . . .	45
5.4	Load-Displacement Response . . . . .	51
5.5	Summary of Response . . . . .	53
6.	INTERPRETATIONS USING LINEAR-ELASTIC MODELS . . . . .	59
6.1	Introductory Remarks . . . . .	59
6.2	Description of the Basic Analytical Models . . . . .	59
6.3	Effect of Transducers on Lateral-Load Stiffness . . . . .	62
6.4	Comparison Between Computed and Initial Measured Lateral Load Stiffnesses . . . . .	63
6.5	Comparison of Computed and Measured Stiffness During Earthquake Simulations . . . . .	64
6.6	An Equivalent Frame to Model Variation of Lateral Load Stiffness . . . . .	67
6.7	Interpretation of Maximum Displacement Responses Using Response Spectrum Analysis . . . . .	69
7.	INTERPRETATIONS OF STRENGTH AND INELASTIC RESPONSE . . . . .	76
7.1	Introductory Remarks . . . . .	76
7.2	Summary of the Component Tests . . . . .	76
7.3	Comparison Between Apparent Component and Complete Structure Behaviors . . . . .	78
7.4	Analysis of Inelastic Load-Deformation Response of the Test Structure . . . . .	80
7.5	Lateral-Load Capacity . . . . .	83
7.6	Interpretation of Test-Structure Overstrength . . . . .	90
8.	SUMMARY AND CONCLUSIONS . . . . .	94
8.1	Description of the Ptototype Structure . . . . .	94
8.2	Description of the Test Structure and the Experiments . . . . .	95
8.3	Conclusions . . . . .	96

REFERENCES . . . . .	102
TABLES . . . . .	107
FIGURES . . . . .	117
APPENDIX A: DESCRIPTION OF EXPERIMENTAL WORK . . . . .	200
A.1 Chronology of the Experiments . . . . .	200
A.2 Test Structure . . . . .	200
A.3 Instrumentation and Data Descriptions . . . . .	208
APPENDIX B: NOTATION . . . . .	237



LIST OF TABLES

Table	Page
2.1 Required and Provided Slab Reinforcement . . . . .	107
2.2 Direct Shears and Unbalanced Moments Used in Design . . . . .	108
3.1 Test Sequence . . . . .	109
4.1 Peak Values Recorded During Earthquake Simulations . . . . .	110
4.2 Spectrum Intensities for Horizontal Base Motions . . . . .	111
4.3 Maximum Strain Gage Readings During Earthquake Simulations . . . . .	112
5.1 Vibration Periods and Damping Ratios of the Test Structure . . . . .	113
6.1 Computed Mode Shapes and Periods . . . . .	114
6.2 Comparison Between Measured and Calculated Top Slab Drifts . . . . .	115
7.1 Capacities Used in Limit Analysis . . . . .	116
A.1 Chronology of Experiments . . . . .	214
A.2 Comparison Between Nominal and Measured Dimensions . . . . .	215
A.3 Vertical Weight Distribution . . . . .	216
A.4 Summary of Concrete Properties . . . . .	217
A.5 Description of Recorded Data . . . . .	218



LIST OF FIGURES

Figure	page
1.1 Plan and Section View of Prototype . . . . .	117
1.2 Longitudinal and Transverse Section of Model . . . . .	117
2.1 Plane-Frame Model Used for Design Lateral-Load Analysis . . . . .	118
2.2 Slab Design Moments . . . . .	119
2.3 Slab Reinforcement Details . . . . .	120
2.4 Edge-Beam Reinforcement Details . . . . .	122
2.5 Column Reinforcement Details . . . . .	123
2.6 Theoretical and Design Column Axial Load-Moment Interaction Diagrams . . . . .	124
3.1 Photograph of Test Structure on Shaking Table . . . . .	125
3.2 Schematic View of Test Structure Orientation Relative to the Shaking Table . . . . .	126
3.3 Test Setup for Free-Vibration and Static Tests . . . . .	126
4.1 Typical Recorded Horizontal Base Motions Lasting 35 Seconds . . .	127
4.2 Global Response of the Test Structure to Test EQ 1 . . . . .	128
4.3 Global Response of the Test Structure to Test EQ 2 . . . . .	130
4.4 Global Response of the Test Structure to Test EQ 3 . . . . .	132
4.5 Global Response of the Test Structure to Test EQ 4 . . . . .	134
4.6 Global Response of the Test Structure to Test EQ 5 . . . . .	136
4.7 Global Response of the Test Structure to Test EQ 6 . . . . .	138
4.8 Global Response of the Test Structure to Test EQ 7 . . . . .	140
4.9 Global Response of the Test Structure to Test EQ 8 . . . . .	142
4.10 Global Response of the Test Structure to Test EQ 9 . . . . .	144
4.11 Global Response of the Test Structure to Test EQ 10 . . . . .	146
4.12 Global Response of the Test Structure to Test EQ 11 . . . . .	148

Figure	page
4.13 Linear Elastic Response Spectra for Horizontal Base Motions of Test EQ 1 . . . . .	150
4.14 Linear Elastic Response Spectra for Horizontal Base Motions of Test EQ 2 . . . . .	151
4.15 Linear Elastic Response Spectra for Horizontal Base Motions of Test EQ 3 . . . . .	152
4.16 Linear Elastic Response Spectra for Horizontal Base Motions of Test EQ 4 . . . . .	153
4.17 Linear Elastic Response Spectra for Horizontal Base Motions of Test EQ 5 . . . . .	154
4.18 Linear Elastic Response Spectra for Horizontal Base Motions of Test EQ 6 . . . . .	155
4.19 Linear Elastic Response Spectra for Horizontal Base Motions of Test EQ 7 . . . . .	156
4.20 Linear Elastic Response Spectra for Horizontal Base Motions of Test EQ 8 . . . . .	157
4.21 Linear Elastic Response Spectra for Horizontal Base Motions of Test EQ 9 . . . . .	158
4.22 Linear Elastic Response Spectra for Horizontal Base Motions of Test EQ 10 . . . . .	159
4.23 Linear Elastic Response Spectra for Horizontal Base Motions of Test EQ 11 . . . . .	160
4.24 Slab Reinforcement Strains During Test EQ 6 . . . . .	161
4.25 Slab Reinforcement Strains During Test EQ 9 . . . . .	162
4.26 Column Longitudinal Reinforcement Strains During Test EQ 6 . . . .	163
4.27 Column Longitudinal Reinforcement Strains During Test EQ 9 . . . .	164
4.28 Relation Between Base Shear and Top Floor Displacement During Test EQ 4 . . . . .	165
4.29 Relation Between Base Shear and Top Floor Displacement During Test EQ 6 . . . . .	166
4.30 Relation Between Base Shear and Top Floor Displacement During Test EQ 9 . . . . .	167
4.31 Relation Between Base Shear and Top Floor Displacement During Test EQ 10 . . . . .	168

Figure	page
4.32 Relation Between Base Shear and Top Floor Displacement During Test EQ 11 . . . . .	169
4.33 Crack Patterns Observed Before Testing . . . . .	170
4.34 Crack Patterns Observed Following Test EQ 4 . . . . .	171
4.35 Crack Patterns Observed Following Test EQ 6 . . . . .	172
4.36 Crack Patterns Observed Following Test EQ 9 . . . . .	173
4.37 Crack Patterns Observed Following Test EQ 10 . . . . .	174
4.38 Crack Patterns Observed Following Test EQ 11 . . . . .	175
4.39 Photographs of Typical Damage Following Test EQ 11 . . . . .	176
5.1 Variation of Peak Horizontal and Vertical Base Accelerations with Test Number . . . . .	178
5.2 Variation of Five-Percent Damped Spectrum Intensities with Test Number . . . . .	178
5.3 Variation of Peak Second-Floor Relative Displacement with Five-Percent Damped Spectrum Intensity . . . . .	179
5.4 Variation of Peak Second Floor Acceleration with Five- Percent Damped Spectrum Intensity . . . . .	179
5.5 Variation of Peak Base Shear with Five-Percent Damped Spectrum Intensity . . . . .	180
5.6 Variation of Peak Base Shear with Peak Second-Floor Relative Displacement . . . . .	180
5.7 Fourier Amplitude Spectra of First-Floor Free-Vibration and Earthquake Simulation Acceleration Responses . . . . .	181
5.8 Variation of Apparent First-Mode Vibration Periods with Maximum Second-Floor Relative Displacement . . . . .	185
5.9 Variation of Apparent First and Second Mode Vibration Periods with Maximum Second-Floor Relative Displacement . . . . .	185
5.10 Variation of First-Mode Equivalent Viscous Damping with Maximum Previous Second-Floor Relative Displacement . . . . .	186
5.11 Variation of Inertial Forces During Test EQ10 . . . . .	187
5.12 Envelope Relation Between Base Shear and Second-Floor Relative Displacement . . . . .	187
6.1 Effective Beam Width Model . . . . .	188

Figure	page
6.2 Equivalent Frame Model . . . . .	188
6.3 Comparison Between Computed and Measured Lateral-Load Stiffnesses . . . . .	189
6.4 Stiffness Variation of Equivalent Frame Models Modified to Account for Effects of Cracking Due to Applied Loads . . . . .	189
6.5 Ratios Between Calculated and Measured Second Floor Displacement Maxima for the "Experimental Model" . . . . .	190
6.6 Ratios Between Calculated and Measured Second Floor Displacement Maxima for the "Equivalent Frame Model" . . . . .	191
7.1 Idealizations of Slab-Column Connection Experiments . . . . .	192
7.2 Load-Displacement Relations of Slab-Column Connections . . . . .	193
7.3 Progression of Visible Damage in Slab-Column Connections . . . . .	195
7.4 Computed Moment-Rotation Behavior of Columns . . . . .	197
7.5 Derived Moment-Rotation Behavior of Slabs . . . . .	198
7.6 Computed and Measured Relations Between Structure Base Shear and Top Displacement . . . . .	199
7.7 Computed Collapse Mechanism . . . . .	199
A.1 Foundation Details . . . . .	221
A.2 Footing Details . . . . .	222
A.3 Photographs of Reinforcement Cages Before Casting . . . . .	223
A.4 Dimensions of Lead Pig . . . . .	225
A.5 Locations and Magnitudes of Lead-Pig Reactions . . . . .	225
A.6 Calculated Ideal and Actual Slab Gravity-Load Moments . . . . .	226
A.7 Concrete Stress-Strain Relations . . . . .	227
A.8 Slab Reinforcing Bar Dimensions . . . . .	227
A.9 Stress-Strain Relation of 4.5-mm Slab Bar . . . . .	228
A.10 Stress-Strain Relation of 6.4-mm Bar . . . . .	228
A.11 Photographs of Instrumentation . . . . .	229
A.12 DCDT Locations . . . . .	232

Figure	page
A.13 Details of DCDT Connections . . . . .	233
A.14 Locations of Linear Potentiometers (1-8), DCDTs for Measurement of Relative Displacements (D30, D32), and Transducers (T1-T8) . . . . .	234
A.15 Locations and Orientations of Accelerometers . . . . .	235
A.16 Configuration of Shear and Moment Transducer . . . . .	236
A.17 Locations of Reinforcement Strain Gages . . . . .	236



## 1. INTRODUCTION

### 1.1 Statement of the Problem

Many regions of the United States are classified by geologists as being regions of low or moderate seismic risk. This classification indicates the likelihood of a damaging earthquake occurring in a given region, and is not a direct measure of the expected ground motion intensity. Historical records indicate that strong ground motions do occur in low and moderate risk regions [3]\*. Despite the historical record, many structures in such regions are designed and constructed with little regard for the possible consequences of strong ground shaking. Because of the extensive construction in regions of lower seismic risk, and because of the potential for catastrophic damage in the event of a strong earthquake in these regions, it is important to undertake research to mitigate the seismic hazard. This report documents a study of the potential hazards associated with reinforced concrete slab-column frames subjected to low, moderate, and strong base motions.

The slab-column structural system typically comprises multiple stories of reinforced concrete slabs cast monolithically with reinforced concrete columns. In its simplest form, the slab-column frame is constructed without drop panels or capitals, in which case the system is designated a "flat-plate" frame. In many cases, the flat plate has a spandrel beam around the perimeter of the floor. The simple geometry makes the flat plate a popular gravity load floor system for structures in which spans and loads are limited. It is simple to design, simple to construct, and often offers various architectural advantages.

---

\* References are given in brackets [ ], and are listed alphabetically at the end of this report.

In many structures, the advantages of flat-plate construction may be outweighed by several disadvantages relative to the performance of the flat plate. These disadvantages include relatively low lateral load stiffness and relatively low toughness of the connection region, both of which are significant considerations in seismic design. Consideration should be given to effects of excessive lateral drifts on nonstructural damage and on P-delta effects. Appropriate provisions are also necessary to ensure sufficient toughness of the connection so that possibilities of punching and progressive collapse are minimized.

Although significant advances have been made in recent years to improve the state of practice in seismic design of slab-column frames, much is still in question regarding performance of this structural system. This report describes a research program that was undertaken to address some of these questions.

## 1.2 Objectives and Scope

Specific objectives of the research reported herein are (1) to study the effects of low, moderate, and high intensity seismic loadings on the behavior of a multistory, multibay, flat-plate frame that was the primary lateral load resisting system, (2) to observe the adequacy of current code requirements for design and detailing of structures in regions of moderate seismic risk, (3) to investigate the use of traditional plane-frame modeling techniques for combining component behavior to predict global behavior of a complete flat-plate structure, and (4) to investigate simple design-oriented analytical models that may be capable of approximating response of a flat plate under lateral loads.

The form of the research program was directed by the aforementioned

objectives and by several practical considerations, as follows.

- (1) The complexity of the problem precluded the possibility of a purely analytical study, and led to a combined analytical and experimental study.
- (2) Recent research [15] emphasizes the importance of redistribution in complete three-dimensional structures. This redistribution often is not apparent in experiments on isolated components of a structure. Thus, a model comprising "multiple" stories and bays was desirable.
- (3) Interest in dynamic effects, and particularly the seismic "demand" on the flat plate, led toward a dynamic shaking table study as opposed to a static experiment.

The prototype structure selected for study is depicted in Fig. 1.1. The structure comprises two stories with three bays in one direction and multiple bays in the other. Slabs having thickness of 203 mm (8 in.) are supported on columns having 457 by 457-mm (18 by 18-in.) cross sections and spaced 6.1 m (20 ft) on centers. A shallow edge beam having 381-mm (15-in.) depth and 457-mm (18-in.) width is provided around the slab perimeter at each floor. Story heights from top of footing or slab to top of slab are 3.05 m (10 ft). The structure is envisioned as being supported on reinforced concrete footings on a stiff soil.

The prototype structure is designed to resist gravity and seismic loads. Design gravity service loads are self weight plus a live load of 11.6 kPa (60 psf). The structure is constructed in a seismic risk zone classified as Zone 2 by the 1982 Uniform Building Code (UBC [50]), which may be expected to experience a design earthquake having Intensity VII of the Modified Mercalli Intensity Scale of 1931. Gravity load effects are determined according to design procedures of the ACI Building Code (ACI 318-83, [7]). Seismic loads are obtained using the equivalent static lateral loads specified by the UBC.

Load combinations are according to ACI 318-83. Reinforcement details correspond to requirements of Section A.9 of ACI 318-83, which pertains to frames in regions of moderate seismic risk.

To study seismic behavior of the prototype structure, a model was constructed at a scale equal to three-tenths of full scale (Fig. 1.2). The model was nominally identical to the prototype with four major exceptions: (1) All dimensions were scaled by the factor of 0.3. (2) Only a portion of the structure extending a length equal to two bays was constructed in the multiple-bay direction. (3) The structure was supported on very stiff reinforced concrete footings rather than footings supported on stiff soil. (4) Self weight of the scaled model was "simulated" (in a manner described in Chapter 3) using nonstructural lead weights.

Behavior during earthquake motions was studied by subjecting the model to earthquake simulations of various intensities on a shaking table [41]. The simulations included one horizontal component and one vertical component of base motion. The base motions model the North-South and vertical components of the records obtained at El Centro during the 1940 Imperial Valley earthquake. Continuous response measurements are used to monitor behavior of the specimen. A record of visible damage was also maintained.

Analytical studies of the model response were made to verify measurements and to determine the reliability of existing analysis techniques. Included are studies of lateral stiffness, dynamic behaviors, and ultimate lateral resistance. Analytical models are tempered by and correlated with experimental observations made during reversed load tests conducted on subassemblies of the complete structure [56].

This report documents the model design, fabrication, and testing. It

also includes descriptions and results of the analytical studies. Conclusions are made relative to the success of the structural system, its design, and methods of analysis.

A review of performance of flat-plate structures and of previous research follow in Sections 1.3 and 1.4. Model design and detailing are described in Chapter 2. A description of fabrication and the experiment is presented in Chapter 3. Chapter 4 presents highlights of observed behavior. Interpretations of behavior are given in Chapters 5, 6, and 7. Conclusions and overall recommendations are in Chapter 8.

### 1.3 Performance History of Flat-Plate Frames

The flat-plate structural system has seen many years and instances of successful applications, marred by several cases of less than adequate structural performance. It is these latter cases that have provided the impetus for numerous research studies on flat plates (as outlined in Section 1.4). Some of the cited failures have been associated with lateral loads, often during earthquake response. Other failures have occurred under predominantly gravity loads. Some representative failures are described in this section to give a perspective on problems associated with the flat plate.

Common problems under gravity loads include excessive longterm deflections and progressive collapse. Of these, the problem of progressive collapse has seen the most publicity in recent years. In many cases, progressive collapse is initiated during construction, at which time a young concrete may be called upon to carry heavy construction loads. A typical case history of progressive collapse during construction has been reported for a sixteen-story, flat-plate building in Boston [8]. According to the report,

the collapse resulted as a consequence of a critical combination of inconsistent structural drawings, errors in placement of reinforcement, cold-weather concreting, and overloads on the recently poured sixteenth floor. This led to a shear failure and subsequent progressive collapse of two thirds of the structure.

Similar problems with connection toughness have been cited as having led to collapse of structures during seismic loading. As an example, the J. C. Penney building [4] suffered a partial collapse during the Anchorage Alaska earthquake of 1964 that was partially attributable to flat-plate connection failure. The J. C. Penney building comprised a reinforced concrete flat-plate floor system stiffened against lateral loads by shear walls. According to the report, the unsymmetric arrangement of lateral load resisting elements contributed to excessive torsional response, which forced the slab-column connections to carry bidirectional lateral forces in addition to gravity loads. Some interior column connections failed, and one corner of the building collapsed. Although the primary failure can be attributed to nonsymmetry in the building plan, the inability of the flat plate to act as a tough secondary lateral load resisting system resulted in the final collapse. Other cases of severe damage attributable to slab-column connection failures during strong earthquakes have been reported [53].

Insufficient lateral-load stiffness of flat-plate framing has also been cited as a problem in lateral-load performance. As an example, the Holiday Inn structure in Los Angeles, California is a conventional seven-story flat-plate structure in which lateral loads are resisted by the flat-plate frame. Extensive nonstructural damage occurred during the 1971 San Fernando Earthquake [42], which has been attributed to excessive flexibility of the flat-plate frame.

Hindsight in reviewing the case histories of failures indicates that the failures could likely have been avoided given a little more foresight in design and detailing of the complete structural system. However, the fact that the failures have occurred points out the susceptibility of the flat plate to punching shear failures, excessive lateral drift, and progressive collapse. These problems have given rise to numerous research investigations. Several such investigations are described in the following section.

#### 1.4 Previous Research

Performance of flat-plate construction subjected to vertical and lateral loads has been the subject of numerous analytical and experimental studies. In addition, several shaking table studies of reinforced concrete frame structures (not generally flat plates) have been undertaken. Pertinent aspects of some of the research are discussed in the following paragraphs.

##### (a) Experimental Research

The structural performance of flat slabs has been the subject of numerous experimental studies dating from 1911 [49]. Many of the early studies were designed to illustrate the static gravity load capacity of this type of construction. More recently, several experiments have been conducted to establish design considerations related to problems of progressive collapse and problems related to lateral loading. It is these latter studies that are of primary interest in the present report, and that are highlighted in the following paragraphs.

Experimental research on lateral load resistance of flat plates has covered a broad spectrum of variables. Included in various studies are interior, edge, and corner connections, tested either as isolated components

or tested in combinations involving more than one connection. A range of load histories, aspect ratios of column-to-span dimension and column-to-slab thickness, longitudinal slab reinforcement ratios and arrangements, vertical slab shears, and slab shear reinforcements have been studied. Experiments have primarily been conducted using slowly varying load reversals, although some studies of isolated connections have been conducted on shaking tables.

General characteristics of behavior under lateral load are similar to characteristics observed for conventional beam-column connections. An initially "stiff" loading slope is followed by a gradual reduction in stiffness as cracking spreads, and a more rapid reduction as yield begins. Because inelastic action in the slab spreads gradually away from the column in the transverse direction, the stiffness changes associated with cracking and yielding tend to be less distinct than in a conventional beam-column connection.

Concentration of stresses in the slab near the column is likely to cause some inelastic action to occur in the slab even under service loads. As a consequence, experimentally measured initial stiffnesses are typically less than stiffnesses computed assuming elastic response [35, 52]. In many experiments [20, 33] significant yield in the overall connection moment-rotation response has been observed not to occur until lateral interstory drifts reach or exceed one percent of interstory height. It is usual that lateral drifts will be controlled to values of this order during the design earthquake. Thus, many flat-plate designs will be controlled by lateral drift considerations rather than strength considerations. For such designs, it is important that elastic stiffnesses, including effects of cracking under service loads, be accurately estimated.

Slip of slab reinforcement from the column has a significant influence on the stiffness of the connection after cracking. Experiments reported by Hawkins [19] indicate the flexibility attributable to slip can be of the same order as that attributable to slab flexure at service level lateral loads. Thus, it is important when testing reduced scale structures to "model" the reinforcement-to-concrete bond as closely as practicable.

As with reinforced concrete beam-column connections, plate-column connections experience stiffness and strength deterioration with cyclic loading in the inelastic range. Unbalanced moment strength may be reduced by ten percent under cyclic loads as compared with monotonic loads [21]. The load-deformation relation is usually pinched under reversed loads, such that energy dissipation is characteristically low, and stiffness following yield is dependent both on the magnitude of maximum previous deformation and on the magnitude of current deformation.

Hawkins has conducted experiments in which the total amount of slab reinforcement has been held constant, but the distribution of the reinforcement varied [20,21]. It was observed that unbalanced moment capacity is enhanced by concentrating slab reinforcement near the column. In seismic design, it is likely that reinforcement banded near the columns improves overall framing continuity. For nonseismic design, ACI 318-83 [7] requires banding of reinforcement within 1.5 slab thicknesses either side of the column to resist a portion of the unbalanced moment. For slab-column frames in regions of moderate seismic risk, Appendix A of ACI 318-83 stipulates further requirements regarding banded reinforcement. Although some reported experiments have used banded reinforcement, the majority have used a uniform mesh of slab bars across the slab width.

Failure of plate-column connections under lateral and vertical loads can occur by punching of the slab around the column. Some researchers have found that an increase in the magnitude of direct shear carried in the slab around the column can significantly reduce the unbalanced moment strength and deformation capacity [20], while other researchers have found the effect to be small in some cases [33]. It has also been argued [34] that punching typically occurs at drifts beyond those of practical interest. To avoid the shear controversy, it is preferable in tests of slab-column frames to "simulate" effects of vertical gravity loads.

As noted previously, continuous top and bottom slab reinforcement concentrated near the columns is helpful in ensuring continuity under seismic lateral loads. In the event of punching, top reinforcement will not be able to develop sufficient dowel action to support the plate and may be torn out of the slab [22]. Continuous bottom reinforcement over the column may be capable of acting as a net to suspend the slab following punching and has been recommended for this purpose. Standard codes of practice do not require such reinforcement for nonseismic zones but recommend it for regions of moderate seismic risk [7]. Design procedures have been recommended [22].

Hawkins presents a summary of the influence of shear reinforcement on lateral load response of slab-column connections [20]. As noted in that summary, shear reinforcement in the form of closed stirrups increases both moment capacity and ductility. Hawkins also notes that shearheads increase moment capacity but have little effect on ductility. It should be noted that the tendency to punch appears to depend on the magnitude of the direct shear and on the magnitude of lateral drift imposed on the connection. In many typical design situations, the critical shears and drifts may be well beyond those anticipated in design, thus, slab shear reinforcement may not be

necessary. In practice, slab shear reinforcement is not often used because of complications in design and construction.

The majority of experiments on isolated connections have been for interior connections. More recently experiments have been conducted on edge and corner connections [1,20]. Although the UBC requires an edge beam in seismic zones, and edge beams are often required in nonseismic regions for transfer of unbalanced moment due to gravity loads alone, only a limited number of experiments have been conducted on specimens having edge beams [24,40,56]. An edge connection with edge beam, having dimensions identical to those of the test structure described in this report, and subjected to reversed lateral loads, is reported in Reference 56.

In general, edge connections without edge beams behave in a manner similar to interior connections, but typically exhibit greater ductility and hysteretic damping [20]. Edge beams can enhance the strength by improving the slab contribution, and can be designed to preclude punching shear failure [56].

Experiments on specimens comprising more than one plate column connection have also been conducted [1,29]. In general, these experiments have confirmed results observed for the isolated plate-column specimens. These experiments have all been conducted statically, such that dynamic effects were not observed. A dynamic vibration test on a small-scale multistory flat-plate frame has also been reported [18]. Response was limited to the elastic range, such that inelastic behavior under strong ground motions could not be inferred.

Shaking table experiments on isolated interior plate-column connections [34] indicate that load-deformation behavior under dynamic loadings is similar

to that under slow load reversals. Morrison and Sozen [34] have noted that dynamic effect on tensile properties of concrete are more pronounced than on tensile properties of steel or compressive properties of concrete. Because punching shear may be a tensile failure phenomenon, it can be hypothesized that fast loading rates tend to materially strengthen the connections against shear failure such that flexural failure modes are more likely. Significant increases in deformation capacity attributable to fast loading rates (on the order of those that might occur during seismic loading) have been observed [16].

Numerous shaking table experiments on reinforced concrete frames have been reported [eg., 31,5]. A primary advantage of shaking table tests is that they enable in-depth studies of effects of realistic earthquake motions on complex structural systems. Analysis of results of such experiments has enabled improved developments in the area of structural dynamic analysis. To the knowledge of the authors, no shaking table experiments of flat-plate frames have been reported.

(b) Analytical

The majority of analytical work has on lateral-load resistance of slab-column construction has emphasized interior plate-column connections. Analytical methods are available for modeling initial stiffness, ultimate strength, the entire monotonic load-deformation behavior to failure, and the hysteretic behavior under inelastic load reversals. Some of these will be summarized briefly and qualitatively in the following paragraphs.

Vanderbilt and Corley [52] discuss analytical modeling of lateral-load stiffness of slab-column frames under working loads. Two models summarized in that paper appear amenable to typical design practice. The first, the

effective beam width model, uses a plane-frame model of beams connecting to columns, the slab being replaced by a beam having depth equal to slab depth and width equal to the product between slab width and an effective width factor. Effective width factors are determined using elastic plate analysis, and have been reported for interior flat-plate connections [52] and interior flat-slab connections [13]. The second, the equivalent frame model, represents the structure by beams that connect to the columns through "transverse torsional members." The model is similar to the equivalent frame model for gravity load analysis described in ACI 318-83. It should be emphasized that both of these models are based essentially on elastic properties of the structure. Effects of service load cracking on stiffness reduction, which may be significant, are not considered directly.

Several analytical procedures for estimating shear and unbalanced moment strength of slab-column connections are summarized in Reference [21]. One of the models envisions a linear variation of shear stress on a critical slab section induced by the shear and unbalanced moment. Failure is predicted when the nominal shear stress reaches a critical value. The method gives reasonably conservative estimates of strength for interior and exterior plate-column connections, and is the method recommended in ACI 318-83. The method is not amenable to exterior connections with edge beams.

Several beam analogies to determine connection strength have been proposed [21,37]. A plate-column connection is envisioned as comprising "beams" framing into the front, back, and side faces of the column. Strength of a connection is obtained by summing strengths of the beams on each face of the column, considering flexure, shear, and torsion. The method is difficult to apply to interior connections because numerous failure possibilities must be checked. The procedure can be applied more readily to exterior connections

with edge beams simply by summing the torsional strengths of the edge beams to the flexural strength of the slab framing into the front face of the column. Under short-term monotonic loading, Rangan and Hall [40] have demonstrated that torsional strength of the edge beams is enhanced significantly because of longitudinal restraint provided to the beams by the slab. Effectiveness of the restraint under longterm or cyclic loading is uncertain.

The beam analogy model has been extended to enable approximate construction of the complete load-deformation response of plate-column connections under monotonic or cyclic load histories [1,19]. This is achieved by describing appropriate load-deformation behaviors of elements connecting to the column faces, and connecting them together to obtain the entire connection load-deformation behavior. The model has been used successfully to "predict" responses of numerous single and multiple column test specimens [1]. Earthquake response analyses of the Holiday Inn (discussed in Section 1.3) have been carried out also [1]. The model has good potential in research for modeling global behavior of complex flat-plate structures. Its usefulness for design is limited by the complexity of its application.

Grid models [34,44] and finite element models [51,55] for computing inelastic response of plate-column assemblies have also been proposed and verified with experimental data. The models are not currently amenable to typical design office practice.

## 2. DESIGN OF PROTOTYPE AND TEST STRUCTURE

This chapter describes design of the test structure. General configurations of the prototype and test structures are described first, followed by a description of the design methods and resulting details.

### 2.1 Structure Description

#### (a) Prototype

The research described in this report is based on measured behavior of a test structure that was tested using simulated earthquake motions on a shaking table. The test structure is modeled after a full-scale prototype structure. While having proportions typical of many flat-plate structures, the prototype is not intended to mimic any particular structure. Rather, it has been designed specifically for this experimental study.

The prototype is a two story flat plate building (Fig. 1.1). Each story is 3.05 m (10 ft) tall. Three bays span one direction, with multiple bays in the transverse direction. Each bay measures 6.10 m (20 ft) in both directions. Slab thickness is 203 mm (8 in.). Column capitals, drop panels, and shear reinforcement are not used. Interior columns support the slab without beams. A spandrel beam which is 457 mm (18 in.) wide by 356 mm (14 in.) deep frames into the exterior columns. All columns have square cross sections of dimension 457 mm (18 in.). Columns are supported on footings in stiff soil.

The structure is to be designed for combined gravity and seismic loads. Service gravity loads comprise self weight plus a live load of 2.87 kPa (60 psf). The structure is located in a region classified as Zone 2 in the 1982 Uniform Building Code (UBC, [50]), and may be expected to experience a design

seismic event corresponding to Intensity VII on the Modified Mercalli Intensity Scale [3].

(b) Test Structure

The prototype is modeled by the test structure shown in Fig. 1.2. A three bay frame resists earthquake input along its principal direction. Transverse to the input, two bays model the multibay direction of the prototype building (Fig. 1.1 and 1.2). Model lengths are scaled to three tenths of the prototype lengths. Story heights measure 914 mm (36 in.). Each bay spans 1.83 m (6.0 ft) in the two principal directions. Slab thickness is 61 mm (2.4 in.). Spandrel beams are 137 mm (5.4 in.) wide and 107 mm (4.2 in.) deep. The edge beams are located along opposite sides of the three bay direction, spanning transverse to the direction of horizontal base motion (Fig. 1.2). The slab is supported by eight columns each having a square cross section of 137 mm (5.4 in.). At the ground level, columns are cast monolithically with footings. Shear and moment measuring transducers support the footings, anchoring the structure to a steel foundation frame (not shown in Fig. 1.2). The foundation frame is prestressed to the shaking table during the experiment. Lead weights are tied to each slab to simulate self weight of the prototype slab. Weight distribution is described in Chapter 3, and Appendix A.

The design of the test structure is outlined in the following sections. To facilitate comparison with observed behavior, all design values are presented for the scaled test structure rather than the prototype. Design compressive strength of concrete is taken as 27.6 MPa (4000 psi), and steel yield stress is taken as 414 MPa (60,000 psi).

## 2.2 Outline of the Design

### (a) General

The structure was designed to satisfy overall requirements for serviceability and strength as specified in ACI 318-83 [7]. Gravity load effects were determined based on the moments and shears obtained using the design coefficients of the Direct Design Method as described in ACI 318-77 [6].

Design seismic lateral loads were from the UBC [50] for a structure located in Zone 2 as defined in that code. Lateral load analysis used a plane frame model as depicted in Fig. 2.1. For that model, columns are represented directly, and slabs are represented by beams connecting between columns. The beams have depth equal to slab depth and width equal to width of the column strip. Gross section properties are assumed for columns and slabs in the analytical model. A vibration period of 0.21 sec is calculated for the test structure using this analytical model. This corresponds to a period of 0.38 sec in the prototype structure.

According to the UBC, the design base shear is given by Eq. 2.1.

$$V = ZICSKW \dots\dots\dots(2.1)$$

where V = service level design base shear, Z = numerical coefficient dependent on the zone (Z = 3/8 for Zone 2), I = 1.0, S = numerical coefficient for site-structure interaction (taken as 1.5), K = a numerical coefficient dependent on framing type (taken as 1.0), W = weight (taken for design to include 25 percent of live load), and C is given by Eq. 2.2.

$$C = 1/(15\sqrt{T}) \leq 0.12 \dots\dots\dots(2.2)$$

where  $T$  = vibration period (0.38 sec). According to the UBC, the product  $CS$  need not be taken to exceed 0.14. The base shear from Eq. 2.1 is 11.6 kN (2.61 kip), which corresponds to 5.3 percent of self weight of the structure.

Following the procedure in the UBC, the base shear is distributed to the floor slab centerlines, the second floor force taken as twice the first for the test structure (Fig. 2.1). Computed second floor lateral displacement of 0.03 percent of structure height is well within accepted limits.

Moments and shears produced by the design loads are combined using load combination factors of ACI 318-83. As required in Section A.9 of ACI 318-83, moments and shears in the slab due to lateral loads are assumed to be taken by the column strip alone.

(b) Slab Design

Slab thickness is controlled by minimum thickness requirements of ACI 318-83, resulting in thickness of 61 mm (2.4 in.) in the model. In the prototype structure, the thickness is 203 mm (8.0 in.), resulting in a service dead load of 4.79 kN/m<sup>2</sup> (100 psf). The model structure is designed for the same dead load plus the service live load of 2.87 kN/m<sup>2</sup> (60 psf).

Total column and middle strip slab moments and direct shears due to factored gravity loads are determined using the Direct Design Method. Maximum moments are plotted in Fig. 2.2a and 2.2b. Values presented near the columns are the slab moments at column faces. Corresponding moments due to service level design seismic loads are given in Fig. 2.2c, and envelopes for the most critical load combination as required by ACI 318-83 are in Fig. 2.2d.

As can be seen in Fig. 2.2, load combinations are such that slab moments due to combined gravity and lateral loads are approximately the same as those

due to gravity loads alone. Thus, total amounts of slab flexural reinforcement are essentially controlled by gravity load requirements.

Maximum strip design moments, required steel ratios, and supplied reinforcement are listed in Table 2.1. At interior columns and at midspans, provided column strip reinforcement matches closely the reinforcement required for strength. For simplicity of construction, column strip negative moment reinforcement at the exterior columns was made the same as at interior columns, even though the required capacity is only three-quarters of that at the interior sections. Middle strip design moments are relatively small, hence, provided steel is based on minimum reinforcement requirements of ACI 318-83.

While gravity loads tend to produce the majority of total moment, and hence to control the total amount of reinforcement, seismic design loads have greater influence on the "unbalanced" moment at critical sections, and seismic detailing requirements have considerable influence on distributions of that total reinforcement. The following requirements of Section A.9 of ACI 318-83 affect arrangement of slab reinforcement.

(1) The column strip is required to resist the unbalanced moment,  $M_s$ , with 40 percent of  $M_s$  transferred to the column by eccentricity of slab shears, and the remainder transferred by flexure. The flexural moment is to be resisted by flexural reinforcement placed within the slab effective width of  $c + 3h$ , where  $c$  = the column cross section width, and  $h$  = the slab thickness. This requirement does not necessarily require addition of more slab steel, but will likely affect the distribution of bars.

(2) At least 50 percent of the column strip reinforcement at the support shall be placed within the  $c + 3h$  width.

(3) Continuous column strip bottom reinforcement at the support shall be at least one-third of the top steel at the support.

(4) At least 25 percent of top reinforcement and 50 percent of bottom reinforcement in the column strip must be continuous.

In addition to these requirements, it is noted that ACI 318-83 requires that design shears be determined based on either (a) the shear associated with development of flexural hinging, or (b) twice the shear calculated from the design seismic forces. The latter option is selected for shear design of the slab.

The requirements listed above are satisfied in the test structure by using the minimum depth slab and the arrangement of slab bars indicated in Fig. 2.3. All slab bars are specially manufactured 4.5 mm (0.178 in.) diameter deformed bars having properties representative of Grade 60 reinforcement. The bars and their manufacture are described in detail in Appendix A.

It is noted that four extra short bottom bars in each direction are provided over interior columns as a safeguard against progressive collapse. These bars are in addition to the requirements of ACI 318-83

Required direct shear and unbalanced moment capacities are listed in Table 2.2. Direct shears are calculated by tributary areas for gravity loads and are obtained directly from the analysis model for lateral loads. Unbalanced moments for lateral loads are obtained directly from the analysis model. Exterior unbalanced moment due to gravity loads are corrected to the column centerline by summing the slab edge moment from the Direct Design Method and the product between connection shear and half the column width. Interior unbalanced gravity load moments are calculated using the procedure in

ACI 318-83, which assumes a pattern live load equal to half the factored live load on one of the adjacent panels. Unbalanced lateral load moments are combined with gravity moments according to ACI load combination requirements.

ACI 318-83 defines a nominal direct shear stress on a critical section around the column as the ratio between the direct shear force and the area of the critical section. The maximum direct shear stress due to factored gravity loads is  $0.198\sqrt{f'_c}$  MPa ( $2.40\sqrt{f'_c}$  psi) for the test structure. Nominal shear stress capacity according to ACI 318-83 is  $0.33\sqrt{f'_c}$  MPa ( $4\sqrt{f'_c}$  psi), while design stress capacity with a capacity reduction factor of 0.85 is  $0.28\sqrt{f'_c}$  MPa ( $3.4\sqrt{f'_c}$  psi). Thus, it may be concluded that direct punching is not critical for the test structure.

With regard to design for shear and unbalanced moment transfer at interior connections, ACI 318-83 specifies that 40 percent of the unbalanced moment be carried by eccentric shear. For the full factored design loads and the design section properties, an unbalanced moment of 4.06 kN-m (36.0 kip-in.) can be carried by eccentric shear (according to ACI 318-83, with capacity reduction factor of 0.85). This value is 17 percent in excess of required capacity (Table 2.2).

ACI 318-83 also requires that the portion of unbalanced moment not carried by eccentric shear (ie., 60 percent of the unbalanced moment) shall be carried in flexure by slab reinforcement placed within a width  $c + 3h$  centered on the column. Summing the flexural strength of both top and bottom slab bars within the width  $c + 3h$ , and dividing by 0.6 (the reciprocal of 60 percent), the computed capacity based on flexure is 4.90 kN-m (43.4 kip-in.) (using capacity reduction factor of 0.9), versus the required value of 3.48 kN-m (30.8 kip-in.). It is noted that the overstrength is a consequence of minimum

thickness and detailing requirements.

At exterior connections, unbalanced moment strength can be limited by slab flexural strength (formation of a yield line across the slab width) or by the combined slab-spandrel strength (formation of a yield line in the slab at the column face plus development of spandrel torsion capacities). Using a capacity reduction factor of 0.9, design flexural strength of the full panel width in negative moment is 6.67 kN-m (59.0 kip-in.). ACI 318-83 requires that the column strip be capable of resisting the entire unbalanced moment at the edge. The design flexural strength of the column strip is 4.23 kN-m (37.4 kip-in.), which is 6 percent in excess of required (Table 2.2). Requirements of the combined slab-spandrel strength are discussed in Section 2.2(c).

Slab bar cut-offs are chosen to satisfy continuity and anchorage requirements of ACI 318-83. Hooked slab bars were used in edge panels to anchor slab bars within the edge beam (Fig. 2.4c). At cantilever edges, slab bars extend to within 13 mm (0.5 in.) of the edge of the slab, at which point they are discontinued.

#### (c) Edge Beam Design

Gross-section dimensions of the spandrel beams were selected on the "small" side during preliminary design, resulting in a more critical test of the design procedure for spandrel beams. Final dimensions are a width of 137 mm (5.4 in.) and depth of 107 mm (4.2 in.). The width was selected to match the column dimension, thereby simplifying formwork. The depth was arbitrary.

Edge beam details are shown in Fig. 2.4. Longitudinal steel comprised 6.4-mm (0.25-in.) Grade 60 deformed bars. Four such bars, one in each corner of a stirrup, are continuous over the beam length. A center longitudinal bar

alternates between the top and bottom. Transverse reinforcement comprised plain wire having diameter of 3.0 mm (0.12 in.) and yield stress of 622 MPa (90.2 ksi). The wire was bent in the form of closed stirrups. Stirrup spacings were approximately according to minimum requirements of Section A.9.3 of ACI 318-83, which requires stirrups at  $d/4$  for a distance  $2d$  from the column face, and at  $d/2$  beyond that, where  $d$  is the beam effective depth.

Gravity load requirements for the edge beam were determined using the Direct Design Method. The required flexural capacity at the column face is 1.71 kN-m (15.1 kip-in.), which is 63 percent of the provided capacity. No provision is made to provide extra flexural strength to resist possible seismic actions in the transverse direction. The excess flexural capacity is required for torsional considerations.

According to ACI 318-83, the edge connection should be capable of developing the flexural strength of the slab column strip. This is a reasonable requirement for seismic design where the internal forces may well reach values corresponding to provided strengths. At exterior connections, a portion of the unbalanced moment enters the column by direct flexure in the slab, the remaining portion being transferred to the column by torsion in the spandrel beams. In design of the test structure, it was assumed that five top slab bars were anchored directly in the column (Fig. 2.3). The remaining column strip bars on either side of the column possess a nominal flexural strength of 1.53 kN-m (13.53 kip-in.), which is considered the ultimate torque to be resisted by each spandrel. For simplicity, the spandrel shears were each taken as one third the direct shear in Table 2.2, the remaining third assumed to be carried by the slab.

The procedure in ACI 318-83 for combined shear and torsion design is

followed in designing the spandrels. According to the procedure, an amount of transverse reinforcement is determined to resist the combined shear and torsion. The computed quantity of transverse reinforcement required for torsion ( $A_t/s$ , where  $A_t$  = area of a stirrup leg and  $s$  = stirrup spacing) is 0.358 mm (0.0141 in.), which compares with the provided quantity of 0.371 mm (0.0146 in.). ACI 318-83 also requires that the volume of longitudinal reinforcement provided in addition to flexural reinforcement be equal to the total volume of transverse reinforcement required for torsion. Accordingly, 54 mm<sup>2</sup> (0.083 in.<sup>2</sup>) reinforcement should be added both top and bottom to the beam. Only 36 mm<sup>2</sup> (0.055 in.<sup>2</sup>) of top reinforcement are nominally available in addition to nominal flexural requirements. More than sufficient bottom steel is available.

(d) Column Design

Columns were proportioned with the intention that (1) primary inelastic action at slab-column connections would be limited to the slabs and beams, and (2) shear failure would be unlikely in the event that flexural hinges occurred at both ends of a column.

Column details are presented in Fig. 2.5. Gross cross sections were 137 by 137 mm (5.4 by 5.4 in.). Longitudinal reinforcement consisted of eight 6.4 mm (0.250 in.) diameter Grade 60 deformed bars. The bars were continuous through the footing and were welded to a steel plate at the base of the footing. A welded splice at midheight of the second story was required as a consequence of a fabrication error. Each longitudinal bar was tied in the corner of a column tie. Ties were 3 mm (0.120 in.) diameter plain wires having yield stress of 622 MPa (90.2 ksi). Spacings followed minimum requirements of Section A.9.5.3 of ACI 318-83, which requires ties to be

spaced at a maximum of  $8d_b$  over a length  $l_o$  from the slab-column or beam-column joint, where  $d_b$  is the longitudinal bar diameter and  $l_o$  is the minimum of one-sixth the clear height or the maximum column dimension. Outside this region, ties are required at the lesser of  $16d_b$  or the minimum column dimension. Extra ties were provided along the longitudinal bar splice (Fig. 2.5b).

The axial load-bending moment column interaction diagram for a column was derived using design material properties and assuming maximum concrete strain of 0.003. Capacity reduction factors according to ACI 318-83 were used to determine the "design" interaction relation. Both the theoretical and design interactions are shown in Fig. 2.6. Maximum axial force and moment due to design lateral loads occur at the base of the columns, and are well below the provided capacities.

To ensure that the primary inelastic action would be limited to the slab, a criterion was established requiring that column flexural strength at every connection exceed the unbalanced moment strength of the slab-column connection. For simplicity, the unbalanced moment strength was taken equal to the sum of flexural strengths of slab column strips framing into an interior connection. At the upper floor, where a single column must resist the slab, the strengths are closely matched (Fig. 2.6). At the first floor, the sum of column strengths significantly exceeds the slab strength.

The capacity design method described in the preceding paragraph is not required by ACI 318-83 for frames in regions of moderate seismic risk, nor is it generally recognized as being necessary in such regions. The method was used in this experimental study because the primary objective was to study inelastic behavior of the slab as opposed to the column.

The shear strength provided by the minimum ties is sufficient to carry the shear which develops when plastic hinges develop at both ends of the column. There are no special requirements for confinement similar to those for ductile frames in regions of high seismic risk. However, the configuration and spacing of column transverse and longitudinal reinforcements (Fig. 2.5) are likely to result in well-confined concrete at column ends.

### 3. DESCRIPTION OF THE EXPERIMENT

This chapter describes test structure fabrication, experimental setup, test sequence, instrumentation, and recording of data. The descriptions are intended to provide a general view of the experiments without complicated details. Details of the experiment are in Appendix A.

#### 3.1 Fabrication of the Test Structure

The test structure was fabricated to match the design requirements described in Chapter 2. As mentioned in that chapter, the test structure scale was selected to be three-tenths of the prototype. Efforts were made to follow standard construction practice where practicable. However, certain deviations were required in the experimental environment. A major difference between the prototype and the test structure was that the test structure could not be cast on a real soil foundation. Instead, it was cast atop load transducers fixed to a steel foundation frame (Fig. 1.2). An overall view of the completed test structure on the test platform of the shaking table is in Fig. 3.1. Fabrication is outlined in the following paragraphs.

Test structure fabrication was begun by casting reinforced concrete footings. The footings were cast separate from the steel foundation frame, and later blocked into place above the foundation frame (Fig. 3.1). Column reinforcement for the upper two floors was in place at the time the footings were cast. The column reinforcement was welded to a base plate in the bottom of the footing to ensure anchorage.

Following curing of the footings, the remainder of the test structure was constructed one floor at a time. Reinforcement was placed in the forms as shown in Fig. A.3. Details of reinforcement layout are in Chapter 2 (Fig. 2.3

to 2.5). Concrete was placed for columns, slab, and edge beams of an entire floor in a single casting. Following an appropriate curing period for the first floor, the sequence was repeated for the second floor. Formwork for both floors was subsequently removed. The structure was then painted with thinned latex paint to facilitate observation of cracking during the experiments. (A chronology of the construction is presented in Appendix A.)

Longitudinal reinforcement for columns and edge beams comprised deformed 6.4 mm (0.25 in.) bars having mean measured yield stress of 481 MPa (69.8 ksi) and ultimate strength of 691 MPa (100 ksi). Transverse reinforcement for columns and edge beams comprised plain 3.0 mm (0.12 in.) wire having yield stress of 622 MPa (90.2 ksi). Slab reinforcement was deformed 4.5 mm (0.178 in.) diameter bar having mean measured yield stress of 435 MPa (63 ksi) and ultimate strength of 671 MPa (97.3 ksi). Column and edge beam reinforcement was purchased in the form used in the test structure. Slab reinforcement was purchased smooth and was cold rolled and heat treated to obtain desired properties.

Concrete for the test structure had 9.5 mm (0.375 in.) maximum size aggregate and Type II cement. Concrete for footings was batched in Davis Hall at the University of California, Berkeley. Concrete for each of the two stories was ready-mixed and delivered to the Earthquake Simulator Laboratory. A single batch was used for each floor. Compressive strengths were obtained from compression tests on 76 by 152 mm (3 by 6 in.) cylinders conducted at the time of the earthquake simulator tests. Measured mean compressive strength was 37.2 MPa (5400 psi) for the first floor and 35.9 MPa (5200 psi) for the second floor.

### 3.2 Experimental Setup

Following removal of formwork, the test structure was braced and moved (on rollers) from the location where it had been cast to the shaking table test platform. After careful positioning, the steel foundation frame was prestressed to the test platform. Hydrostone was placed to ensure a close fit. Absence of cracking in the hydrostone during the experiments verified that the foundation frame was adequately fixed to the test platform.

The bare test structure is shown schematically on the shaking table platform in Fig. 3.3. The three-bay direction of the test structure is orientated in the East-West direction.

The reduced scale of the test structure resulted in length dimensions scaled by a factor of 0.3. As a consequence of scaling relations, column and slab stresses of the bare test structure due to dead loads were 0.3 times those anticipated for the prototype. The low stress level results in stiffnesses and strengths that are different from those anticipated for the prototype. To compensate for this condition, subsidiary lead weights were attached to the top of each floor slab. A total of 160 individual weights was placed on each slab. A photograph of the test structure with the lead weights in place is shown in Fig. 3.1.

The total amount of lead weight added to each slab was 69.0 kN (15.5 kips). This amount of subsidiary weight, when added to the self weight of the test structure slab, results in an average slab dead load of 4.87 kN/m<sup>2</sup> (102 psf). This corresponds closely with the prototype slab dead weight of 4.79 kN/m<sup>2</sup> (100 psf). As discussed in detail in Appendix A, the distribution of subsidiary weights produces approximately the correct magnitude and distribution of slab dead load shear and moment in both the longitudinal and

transverse directions. No loads were added to simulate slab live loads.

The weights were held in place with a connection system designed to ensure that the weights moved with the slab, but that the weights did not stiffen or strengthen the slab. Analyses of dynamic experiments before and after the addition of the weights were used to verify that the weights did not stiffen the slab significantly. These analyses are presented in Chapter 5.

### 3.3 Description of Tests

Experiments included static tests, free-vibration tests, and earthquake simulation tests. The static tests were conducted before any earthquake simulations. Some free vibration tests were conducted before the earthquake simulations, and others were interspersed with the earthquake simulations. The sequence and designation of free-vibration and earthquake simulation tests are in Table 3.1.

As indicated in Table 3.1, eleven earthquake simulations, designated EQ1 through EQ11, were conducted. Following each earthquake simulation, a check was made for visible damage, and then a free vibration test was conducted. In addition to examining the test structure for structural damage, all instrumentation and connections were checked for looseness following each simulation with the aid of a checklist.

More detailed descriptions of the tests follows.

#### (a) Static Tests

Static tests were conducted before subjecting the test structure to any earthquake simulations. The tests were conducted by applying lateral loads in increments at one of the two floor levels. The test arrangement is shown

in Fig. 3.4. After each loading increment, lateral displacements of each floor were measured relative to the exterior wall of the earthquake simulator laboratory. Examination of lateral load-displacement relations following the experiments revealed that the displacement data were polluted by wind-induced oscillations of the laboratory wall. For this reason, further information on these tests is not presented in this report. However, it is noted that no damage to the test structure was observed as a consequence of the static tests.

(b) Free-Vibration Tests

The free-vibration test setup was identical to the setup used for the static tests (Fig. 3.4). A test was conducted by first pulling the structure with a cable attached at the first floor (the cable applied a force having a horizontal component of 4.45 kN [1.0 kip]), and then suddenly releasing the structure by cutting the cable. Response was monitored by accelerometers attached to the top of the floor slabs.

Seven free-vibration tests were conducted before any earthquake simulations. These are designated tests FV0.A through FV0.G. As noted in Table 3.1, tests were conducted at the construction site and on the test platform of the shaking table, either with or without the lead weights in place on the floor slab. For some of the tests, the test platform was blocked (wooden blocks wedged against the test platform to ensure base fixity). Others were without blocking. Because the observed effect of blocking was negligible, it was discontinued following test FV0.F.

A free-vibration test followed each earthquake simulation. These are designated FV1 through FV11.

(c) Earthquake Simulation Tests

The test structure was tested with eleven base motions with successively increasing intensity. The simulations are designated EQ1, EQ2,..., EQ11. Peak base accelerations ranged from 0.012g to 0.83g in the horizontal direction. All tests had horizontal input parallel to the three bay direction of the model (Fig. 3.3). Four of the tests combined vertical and horizontal motion simultaneously. All tests having both horizontal and vertical components followed simulations of similar horizontal intensity, but having only the horizontal component. The test sequence is listed in Table 3.1.

The base motions model the North-South and vertical acceleration records obtained in El Centro during the 1940 Imperial Valley Earthquake. Base displacement records model those obtained by integration of the corrected prototype acceleration records (47). To ensure that base motion and test structure frequencies are properly related, the time scale of the prototype motion was scaled by the ratio  $1 : \sqrt{3}$ . El Centro 1940 was selected for its broad frequency content, and because it has been used in numerous other research investigations.

(d) Damage Observation

Visible damage was observed and recorded on the structure immediately following each earthquake simulation. Each test was marked with a different color felt tip pen. Damage was photographed and traced on graph paper, providing a record of the damage level after each earthquake.

3.4 Instrumentation and Data Recording

Instrumentation was arranged to provide information on both global and local responses of the test structure. A total of 112 data channels were

recorded. Data from a number of these channels are presented in detail in this report. These include the following:

(i) Table instrumentation measured base accelerations and displacements.

(ii) Accelerometers measured absolute accelerations of floor slabs parallel to the horizontal base motion.

(iii) Direct Current Differential Transformers (DCDTs) measured displacements of floor centerlines relative to the base of the test structure.

(iv) Weldable strain gages attached to selected slab and column longitudinal bars measured reinforcement strains.

(v) Transducers measured shear and moment below column footings.

In addition to these instruments, instruments were arranged as follows:

(vi) Accelerometers measured absolute vertical and transverse slab accelerations.

(vii) Linear potentiometers measured absolute slab displacements in both the longitudinal and transverse directions.

(viii) DCDTs measured deformations of the footings and of columns and slabs near slab-column and column-footing connections.

Story shears were derived from the sum of products between average floor accelerations and calculated floor masses. Floor and base moments were determined as the sum of products between story shears and story heights. P-delta moments (product between weight and lateral displacement) were computed and are included in reported moments.

All data were recorded digitally. Data samples during dynamic tests were taken at 0.01 second intervals, and read in bursts of 1/20,000 second. All channels were filtered identically using a 100 Hz filter. The maximum time lag between any two channels is less than 0.006 seconds.

### 3.5 Sign Convention

Orientation of the test structure on the shaking table test platform is indicated in Fig. 3.3. The test was oriented such that the horizontal component of base motion is in the East-West direction. Lateral displacements and accelerations of the test platform or of the test structure are considered positive in the West direction. Positive moments and shears are produced at the base of the columns by displacing the structure in the positive direction. Transverse displacements or accelerations are positive in the South direction. Vertical accelerations are considered positive up. Strain gages indicate positive strain when strained in tension. DCDTs attached to measure relative deformations between slabs and columns at connections, and between the footings and the foundation, measure positive relative displacements when the distance between the instrument and target increases.

#### 4. MEASURED RESPONSE OF THE TEST STRUCTURE

This chapter presents data on response of the test structure to the earthquake simulation tests described in Chapter 3. Global response histories (lateral displacements, lateral accelerations, base forces, and base motions) and linear elastic response spectra are presented for all tests. Selected maximum values of input and response for all tests are presented in tabular form. Strain-gage histories, relations between top displacement and base shear, and observed cracking and spalling are presented only for some of tests EQ4, EQ6, EQ9, EQ10, and EQ11, so that the progression of damage can be traced. Descriptions of response in this chapter are intended to be objective. The data presented serve as a basis for interpretations in subsequent chapters.

##### 4.1 General Comments Regarding Data Presentation

###### (a) Duration of Strong Motions

Base motions for earthquake simulations were scaled from the records presented in Reference 47. Typical recorded horizontal base displacement and acceleration histories are plotted in Fig. 4.1. Although the recorded duration extends through 35 sec, the duration of significant strong base acceleration lasts only through approximately the first 18 sec. So that the significant response can be examined in greater detail, only the first portion of the response records are shown in all subsequent response history plots in this section.

###### (b) Synchronization and Accumulation of Data Offsets

For each response history, data are synchronized by aligning the point in time where peak table displacement occurred. Zero offsets for the responses

were determined by averaging data readings for a one second interval before and after each test. For all but accelerometers, offsets that trailed the responses were accumulated in subsequent response histories. Accelerometer offsets were not accumulated. It is noted that strain gages were zeroed shortly before testing, such that gravity load strains are not recorded.

#### 4.2 Global Response

Global response history data are presented in Figures 4.2 to 4.12. The first page of each figure depicts the average acceleration histories for the floor slabs and for the test platform. For the first floor, accelerometers 4 and 5 (Fig. A.15) were averaged to obtain the overall floor slab acceleration, while for the second floor, accelerometers 8 and 9 (Fig. A.15) were averaged. Horizontal and vertical table accelerations are averages for the test platform.

The second page of each figure presents displacement histories of the first and second floor (relative to the bottom of the shear and moment transducers [Fig. 1.2]), the transducer base shear history, and the moment measured at the base of the columns (at the top of the footings). Although floor relative displacements are measured relative to the base of the transducers, it is noted that the maximum lateral distortion of the transducers and footings was at all times less than three percent of top slab relative displacement, thus, the relative displacement data can be considered to be effectively relative to the top of the footings. As noted in Chapter 3, base shears are the sum of shears measured by the transducers, and base moments are derived from floor level accelerations, masses, and lateral displacements (including the P-delta moment). It is noted that P-delta moments were an order of magnitude smaller than total base moments.

Table 4.1 presents peak values of these measured global responses.

#### 4.3 Response Spectra and Spectrum Intensities

Response spectra for linear elastic single degree of freedom systems were constructed for measured horizontal base accelerations for several values of viscous damping. The spectra are plotted in Fig. 4.13 through 4.23. The plots include absolute acceleration and relative displacement spectra plotted on linear scales, and psuedo-relative velocity plotted on a tri-partite graph.

Housner spectrum intensities [23] were calculated for various damping levels. In this report, spectrum intensity is defined as the area under the velocity spectrum between periods of 0.058 and 1.44 sec. This period range is compressed from that given by Housner [23] to accomodate the time scale of the base motion used in the experiments. Spectrum intensities are tabulated for horizontal base motions in Table 4.2.

#### 4.4 Reinforcement Strains

Strain-gages were attached to selected slab and column bars as indicated in Fig. A.17. Slab bar strain histories for tests EQ6 and EQ9 are plotted in Fig. 4.24 and 4.25. Column bar strain histories for the same tests are plotted in Fig. 4.26 and 4.27. The dashed line on the graphs at a strain value of 0.002 indicates approximately the strain at which yielding of the steel is expected. Table 4.3 presents peak strains for all gages and all tests. It is noted that several of the strain gages had malfunctioned by the end of test EQ11.

#### 4.5 Base Shear-Top Displacement Relations

A measure of the global hysteretic behavior of the structure is obtained by plotting relations between base shear and top slab lateral displacement (relative to the base). The measured relations for tests EQ4, EQ6, EQ9, EQ10, and EQ11 are plotted in Fig. 4.28 through 4.32. In each figure, response for selected periods of time is broken into several successive short time intervals so that only a few response cycles are plotted in each of several individual graphs. The time segments plotted on each graph are indicated, with subsequent segments plotted adjacent to each other. Horizontal and vertical scales are identical for each plot in a given figure, but scales vary for the different figures.

Previous experimental studies [25,34] have noted that time lags in recorded data can occur as a consequence of signal conditioning equipment used to condition data. These time lags can cause significant errors in hysteretic plots such as those shown in Fig. 4.28 through 4.32. These errors are believed not to be present in the data presented in this report because all data were conditioned with the same equipment, such that any lag in time between measurement and recording of data is nominally identical for all data channels.

#### 4.6 Observed Damage

Concrete cracking and spalling were observed during the experiments. This damage was traced on the structure. A grid of squares measuring 305 mm (12 in.) was marked on the slab surfaces to facilitate accurate location of cracks and transfer of crack locations to data sheets.

Apparent damage before testing comprised hairline cracks. Locations of

cracks on slabs, columns, and edge beams are indicated in Fig. 4.33.

The progression of cracking and spalling observed following tests EQ4, EQ6, EQ9, EQ10, and EQ11 is indicated in Fig. 4.34 through 4.38. In those figures, the regular grid is indicated by solid lines, cracking is indicated by solid curves, and spalling is indicated by the hachured regions.

It is noted that damage before test EQ6 was slight, consisting of limited extensions of existing cracks. Damage for all tests, with the exception of test EQ11, consisted of narrow cracks, and minor spalling in columns at slab-column and footing-column interfaces. Damage for test EQ11 included more extensive spalling, including spalling of concrete in the spandrel beam near its connection to columns. Typical spalling damage is shown in Fig. 4.39. In addition, the slab around an interior column appeared to have dropped a small distance (1 to 2 mm), indicating the possibility of an incipient punching failure. A photograph of this region is shown in Fig. 4.39. Because of the small amount of movement, it is not apparent in the photograph. Bar buckling was not observed during any of the tests.

## 5. DISCUSSION OF OBSERVED BEHAVIOR

This chapter discusses behavior of the test structure during the earthquake simulation and free-vibration tests. The discussion begins with an interpretation of base motion intensities. General characteristics of measured responses, and variations of those characteristics as the experiments progressed, are described also.

### 5.1 Base Motions

Base accelerations recorded during the tests are plotted in Fig. 4.2 through 4.12. The base acceleration records for all tests generally have similar shapes, the main differences being peak acceleration and the presence or absence of vertical motion concurrent with the horizontal motion. The variation of peak base accelerations with test number is tabulated in Table 4.1.

Variation of peak horizontal and vertical base accelerations with test number is plotted in Fig. 5.1. It is apparent that peak accelerations tended to increase with successive tests. Peak vertical accelerations were typically 25 percent of horizontal accelerations for tests with both horizontal and vertical inputs. Vertical accelerations are relatively lower for tests without vertical input signals (Tests EQ1, EQ3, EQ4, EQ5, EQ6, EQ8, and EQ10). Vertical accelerations in these tests resulted from inability of the shaking table to totally suppress extraneous vertical accelerations.

The similarity in frequency content for all base motions is apparent by examining response spectra for horizontal base motions (Fig. 4.13 through 4.23). Overall, the shapes of the spectra are similar to those obtained for the prototype North-South record obtained in El Centro during the 1940

Imperial Valley Earthquake, with the exception of the frequency shift of  $\sqrt{3}$  that results from time compression of the test structure base motion. In addition, the base displacement record (Fig. 4.1) is nearly identical to the record derived by integration from the corrected accelerograms reported in Reference 47. Thus, it may be concluded that the base motion represented properly the frequency content of the prototype motion as presented in Reference 47. The very long period content of the prototype motion (periods beyond approximately 10 sec in the prototype scale) is not included in Reference 47 and is not modeled by the test motion.

The variation of base-motion intensity is conveniently represented by the Housner spectrum intensity [23]. It is noted that the spectrum intensity does not reflect the duration of strong shaking, thus, it is not a complete measure of intensity for structures responding in the inelastic range. However, considering that durations of all base motions were the same during the experiments, it is an acceptable measure of intensity. As noted in Chapter 4, spectrum intensities were computed for a frequency range of 0.58 sec to 1.443 sec, which has been shifted from the range suggested by Housner to account for time compression of the base motions.

Spectrum intensities of horizontal motions are tabulated for several values of damping in Table 4.2. Variation of the five-percent damped spectrum intensity versus test number is in Fig. 5.2. Relative variations at other damping values are similar. The data in Fig 5.2 indicate a gradual increase in intensity through test EQ9, followed by significantly more intense motions for tests EQ10 and EQ11.

It should be noted that nearly identical horizontal intensities were calculated for tests EQ1 and EQ2, for tests EQ6 and EQ7, and for tests EQ8 and

EQ9 (Fig. 5.2). The test pairs differ primarily in that the latter of each pair includes vertical base motion in addition to the horizontal motion.

The spectrum intensity of the test motions can be compared approximately with the scaled spectrum intensity of the prototype North-South El Centro 1940 motion. As reported by Housner [23], the twenty percent damped spectrum intensity for the prototype motion is 0.826 m (2.71 ft). At the time scale used for the tests (equal to  $1/\sqrt{3}$ ), this scales to a spectrum intensity of 0.275 m (0.902 ft). The ratios between spectrum intensity for the test motions and the scaled spectrum intensity for the prototype El Centro motion are given below.

Test	Spectrum Intensity Ratio	Arbitrary Intensity Rating
EQ1	0.03	Low
EQ2	0.03	Low
EQ3	0.10	Low
EQ4	0.10	Low
EQ5	0.21	Low
EQ6	0.44	Moderate
EQ7	0.44	Moderate
EQ8	0.89	High
EQ9	0.89	High
EQ10	1.96	High
EQ11	2.71	High

Based on the preceding analysis, if a low intensity motion is assumed to have spectrum intensity less than one quarter of the El Centro intensity, all tests up to and including test EQ5 can be classified as low intensity tests. Defining a moderate base motion as having half the intensity of El Centro,

tests EQ6 and EQ7 may be classified as moderate. Defining the El Centro motion as strong, all tests after test EQ7 may be considered strong motions. Tests EQ10 and EQ11, having intensities approximately two and three times that of El Centro 1940, may have unrealistically intense motions.

## 5.2 Global Response Trends

Variations of global responses with increasing test intensity followed logical patterns. The patterns are discussed in this section.

### (a) Displacements

The variation of second floor relative displacement with horizontal base motion intensity (as represented by Housner spectrum intensity at five percent damping) is plotted in Fig. 5.3. The displacement increases at a moderately increasing rate with increasing spectrum intensity. However, the overall trend could be represented reasonably well by a linear variation of displacement with spectrum intensity. Similar trends have been observed in other experiments [9,32].

Tests EQ6 and EQ7 were tests for which horizontal motions were nearly identical (spectrum intensity of approximately 0.2 m in Fig. 5.3). However, test EQ7 has a vertical base motion in addition to the horizontal motion. Test EQ6 results in a peak horizontal second floor displacement of 5.11 mm (0.20 in.). Test EQ7 results in a displacement of 9.86 mm (0.39 in.), which is nearly twice the corresponding value for Test EQ6. The higher displacement in test EQ7 could result from many causes. For example, the test structure begins test EQ7 having been previously softened by test EQ6. The larger initial period may result in correspondingly larger displacement. Another possibility is that the combined vertical and horizontal input results in

larger inelastic drifts than does the horizontal motion alone. The observed behavior is not an anomaly, as a similar trend is observed for tests EQ8 and EQ9 (spectrum intensity of approximately 0.4 m in Fig. 5.3).

(b) Accelerations

Variation of peak second floor slab acceleration as a function of five percent damped spectrum intensity is plotted in Fig. 5.4. The variation is approximately linear to a spectrum intensity of 0.4 m, beyond which it increases at a lower rate to a maximum of nearly 1 g. The initial linear portion is consistent with the linear trend observed for displacements (Fig. 5.3). Beyond a spectrum intensity of approximately 0.4 m (Fig. 5.4), it is possible that significant yield in the structure limited the magnitude of inertial force that could be developed, thus, accelerations were limited. This observation is supported by observations made in Section 5.2c.

Acceleration amplification is calculated as the ratio between peak top floor acceleration and peak horizontal base acceleration. The mean amplification was 2.0, but values occurred over a wide range bounded by values of 1.3 and 3.3. Table 4.1 presents peak accelerations from which amplifications can be derived.

(c) Base Shear

Variation of peak base shear with spectrum intensity is shown in Fig. 5.5. The same trend observed for accelerations occurs for base shears, that is, an approximately linear variation is followed by a plateau beginning at spectrum intensity of 0.4 m. The plateau indicates the onset of significant structural yielding, beyond which point there is relatively less increase in base shear with increasing lateral displacement.

### 5.3 Variation of Dynamic Properties

#### (a) Vibration Periods

Measures of vibration periods were obtained by three different methods, as follows: (1) The time between three successive zero crossings of the top floor displacement during the peak displacement cycle of earthquake response. (2) An average period during the earthquake simulation, as obtained from the peaks of the Fourier Amplitude spectrum of the first floor acceleration response. (3) An average period during the free-vibration test following an earthquake simulation, as obtained from peaks of Fourier Amplitude spectra of first floor acceleration response. The Fourier Amplitude spectra of first floor acceleration responses during earthquake simulation and free-vibration tests are plotted in Fig. 5.6 for reference. Measured vibration periods are tabulated in Table 5.1.

As noted in Chapter 3, some free-vibration tests were conducted before the earthquake simulations. Some of the tests were conducted before placement of the lead ingots, and some afterwards. The vibration periods measured before placement of lead ingots were relatively constant, indicating that little damage occurred before placement of the ingots (Tests FV0.A, FV0.B, and FV0.C in Table 5.1). The period increased substantially following addition of the lead ingots (Test FV0.D in Table 5.1). The change in period can be attributed in part to change in structure mass after placement of the lead, but could also be affected by a change in stiffness. To check if any measurable stiffness change occurred, a simple analysis was made, as outlined in the following paragraph.

The vibration period of the test structure,  $T$ , is proportional to the square root of the ratio between structure weight,  $W$ , and structure stiffness,

K. Thus, assuming distributions of stiffness and weight do not change, the ratio between final period and initial period,  $T_f/T_o$ , should be equal to the square root of the ratio between  $W_f/W_o$  and  $K_f/K_o$ , where the subscripts f and o refer to values after and before placement of weights, respectively. Mean values of  $T_f$  and  $T_o$  from Table 5.1 are 0.209 sec and 0.117 sec, respectively. From Table A.3, the values of  $W_f$  and  $W_o$  are 211 kN and 71.6 kN, respectively. Thus, the ratio between final stiffness and initial stiffness is given by the Eq. 5.1.

$$\frac{K_f}{K_o} = \frac{W_f}{W_o} \left(\frac{T_o}{T_f}\right)^2 = \frac{211.}{71.6} \left(\frac{0.117}{0.209}\right)^2 = 0.92 \dots\dots\dots 5.1$$

The comparison between weights and periods (Eq. 5.1) indicates that a small reduction in stiffness has occurred. From this reduction, it is possible to conclude that either (a) the weights cracked the structure, thereby reducing the average stiffness to 92 percent of the initial value, or (b) the weights cracked the structure to reduce stiffness to less than 92 percent of the initial value, but contributed to stiffness by an amount to bring the final stiffness up to 92 percent of the initial value. It is noted that the above calculation assumes mass distribution does not change significantly with addition of the lead ingots. As verified by elastic modal analyses, this assumption results in only a marginal error in computed periods because the majority of mass is in the slabs and the centroid of the added mass is close to the slab.

Vibration periods also changed as testing proceeded. The variations of the first-mode period (obtained by each of the three measures described previously) are plotted versus the peak top floor displacement during the earthquake simulation in Fig. 5.7. As can be seen in that figure, each

different method for measuring period produces a different period estimate. In general, the period obtained from the time between zero crossings during the peak response is the median period. The average period during the earthquake response (obtained by the peak of the Fourier Amplitude spectrum) was generally longer than the period during the peak cycle. This longer period results because average stiffness during moderate amplitude responses following the peak response is less than during the peak. This is evident as pinching in the hysteretic loops (Fig. 4.28 through 4.32). In flat plates, this pinching has been attributed to opening and closing of cracks and to bar slip [19]. The shortest period estimate is obtained by Fourier Amplitude spectra of free vibration responses. It is probable that the force levels during free vibration responses were insufficient to induce bar slip, thus, the somewhat stiffer response was observed.

A general trend was for first and second mode vibration periods to increase with increasing maximum displacement (Fig. 5.7 and 5.8). This is indicative of the reduction in average stiffness as the structure was loaded further into the inelastic range of response. The change in period can be checked approximately with measured stiffness changes by assuming the period at any stage of response is proportional to the inverse of the square root of the secant stiffness at that stage of response. Instantaneous secant stiffness,  $K_i$ , can be read from the the measured peaks of the shear-displacement relations (see Section 5.5). Using the stiffness,  $K_{EQ5}$ , and period,  $T_{EQ5}$ , measured during peak response of test EQ5 as reference values, instantaneous vibration periods,  $T_i$ , can be computed approximately by Eq. 5.3.

$$T_i = \sqrt{K_{EQ5}/K_i} T_{EQ5} \dots\dots\dots 5.3$$

Figure 5.7 compares measured periods with periods calculated by Eq. 5.3. The

calculated periods compare most closely with periods measured during the peak response cycles. This is not unexpected, as the stiffnesses used in Eq. 5.3 were obtained at times corresponding to measured peak responses.

The rate at which second mode period varies is similar to the rate at which the first mode period varies. Initially, the ratio between the first and second mode periods is approximately 3.5. The value of the ratio varies in an apparently random manner about the initial value as testing proceeds.

(b) Equivalent Viscous Damping

A measure of equivalent viscous damping can be obtained using the logarithmic decrement of measured first-floor accelerations during free-vibration tests. The response decay over several cycles was measured for each test. Calculated damping ratios are tabulated in Table 5.1. Values were not obtained for Tests FV0.1 through FV0.G. However, because damping values obtained for several tests following Test EQ1 remained relatively constant, it is likely that values were similar before Test EQ1.

The initial equivalent viscous damping was in the range between 1.1 and 1.5 percent of critical (Tests FV1 through FV5 in Table 5.1). Similar values have been reported previously [17,32] for "uncracked" reinforced concrete structures. The low damping suggests that the lead ingots fixed to the slabs did not affect energy dissipation appreciably, at least for low-amplitude responses.

Variation of damping with maximum previous second-floor displacement is plotted in Fig. 5.9. As noted in the preceding paragraph, equivalent viscous damping was effectively constant at approximately 1.5 percent of critical for all low amplitude tests (up to and including test EQ5), indicating that

minimal damage was incurred during these tests. Damping increased gradually with increasing displacement, starting with test EQ6.

The maximum damping observed was approximately seven percent of critical following Test EQ11. Considering that the structure was probably near collapse during that test, the equivalent viscous damping ratio of seven percent of critical probably indicates an upper bound. However, it should be noted that these values of damping were obtained during very low amplitude free vibration responses. Effective damping for an equivalent elastic structure would probably be higher at the higher displacement amplitudes observed during the earthquake simulations [17].

(c) Variation of Apparent Modal Contributions

In this report, response is described as being predominantly in the first mode if waveforms at each of two floor levels vary approximately in phase, without significant oscillations out of phase. "Second-mode response" is essentially out of phase at the two floor levels. By these definitions, displacement responses can be classified as being predominantly in the first mode, whereas acceleration responses typically exhibit some second-mode response in addition to the first-mode response. Base shears and base moments, having frequency contents that comprise both the apparent first and second mode frequencies, are considered to have response contributions from both modes. However, the "first-mode" component of both base shear and base moment significantly exceeds the "second-mode" component. These characteristics can be observed in Figs. 4.2 through 4.12.

The relations between the apparent first and second mode responses can be seen in the Fourier Amplitude spectra of first-floor acceleration responses in Fig. 5.6. In those spectra, the peak corresponding to the apparent first mode

has the highest peak, and is normalized to a value of unity. The relative areas of the peaks associated with each mode is a measure of the relative energy associated with that mode of response. Examination of the spectra for the free-vibration tests (right-hand side of Fig. 5.7) indicates that the relative energy associated with the second mode response increases progressively starting with test FV6.

A similar trend is less apparent, but discernible, for the earthquake simulations (left-hand side of Fig. 5.6). The greater relative contributions of the second mode during earthquake simulations can be explained in terms of the response spectrum (Figs. 4.13 through 4.23), as follows. As the structure became more damaged, both the first and second mode periods lengthened. As a consequence, the first mode moved into a portion of the spectrum having lower spectral acceleration (below approximately three Hz), while the second mode moved into a portion having higher spectral acceleration (approximately 10 Hz).

A peculiar feature of the apparent second-mode response is shown in Fig. 5.10, which depicts variations of total base shear, first-floor inertial force, and second-floor inertial force, as measured during a portion of test EQ10. Distributions of lateral inertial forces at times of peak base shear are plotted above the waveforms. As indicated in the force distributions, lateral forces tended to be nearly uniform over height at times when the largest base shears were reached. At other times, the second-floor force tended to be larger than the first-floor force. This trend was not apparent in the early tests, becoming apparent only during the latter tests when base-shear capacity was being approached.

Simple limit analyses [30] indicate that a larger base shear capacity can

be realized by a frame structure if lateral forces are concentrated towards the lower floors rather than the upper. The data for the test structure (and data from other experiments, eg., Reference 32) indicate that when the structure is responding near its capacity, lateral force distributions tend toward the distributions that result in the largest base force capacity of the structure. The tendency for lateral forces to redistribute to accommodate a given base force may have important implications as regards collapse of structures. Further research is necessary before firm conclusions can be drawn from the observations.

#### 5.4 Load-Displacement Response

Measured relations between base shear and top floor relative displacement for tests EQ4, EQ6, EQ9, EQ10, and EQ11 are plotted in Fig. 4.28 through 4.32. The relations show progressive softening of the structure with increasing displacement amplitude. This is indicative of the progressive development of concrete cracking and reinforcement yielding. In addition, the hysteretic curves display the characteristic "pinched" hysteretic loops of reinforced concrete, the pinching becoming more pronounced as the displacement amplitudes are increased.

The hysteretic relations between base shear and top floor relative displacement for each test were superimposed to construct an envelope relation between base shear and top floor displacement (Fig. 5.11). The relation indicates an initially "stiff" response, followed by a gradual reduction in stiffness, with a nearly plastic response at drifts exceeding approximately two percent of structure height (height not including footings and transducers).

The initially stiff response (Fig. 5.11) corresponds to the effectively

"uncracked" structure. Gradual reduction in stiffness is apparent at a top level drift of approximately 0.2 percent of structure height. The base shear coefficient (base shear divided by total structure weight) is 0.24 by the time the drift level reaches 0.2 percent. It is noteworthy that this value is larger than the service level design base shear coefficient of 0.053 (Eq. 2.1) used to design the test structure.

The test structure did not develop significant yield in the overall load-displacement relation until drifts reached approximately 1.5 percent of structure height (Fig. 5.11), after which the structure displayed a relatively plastic response to lateral drifts exceeding 5 percent of structure height. The large deformation capacity without collapse suggests that the structure possessed necessary attributes for seismic resistance, provided that lateral drifts could be reasonably controlled. A survey by Algan [2] indicates that significant damage can be expected in a building at drifts exceeding approximately 1.5 percent of structure height, thus, it can be argued that lateral drifts should be controlled to values less than 1.5 percent. For the test structure, significant yield in the overall load-displacement relation (Fig. 5.11) does not occur until drifts of approximately 1.5 percent of structure height. Thus, if drifts are properly controlled, response of the test structure examined in this report is essentially within the elastic range.

The occurrence of first yielding in selected slab and column longitudinal reinforcement is indicated in Fig 5.11. Yield is first detected in longitudinal reinforcement at the footing level of an interior column during test EQ8. The corresponding lateral drift is approximately 0.5 percent of structure height. Yield is next detected in top and bottom reinforcement of the slab at the first floor exterior connection at top level drift of

approximately 1 percent. Yield of top slab reinforcement at the first floor interior connection occurs at approximately the same drift, followed immediately by yield of reinforcement in interior columns at the top of the first and second stories. Slab bottom reinforcement at the first floor interior connection indicates yield at drift of approximately 1.5 percent. Bottom slab reinforcement in the second floor exterior connection experiences yield at approximately the same drift. No yield is detected in the second floor slab at the interior connection.

It is noted that the strain gage attached to the top slab reinforcement at the second floor exterior connection malfunctioned, so that the occurrence of yield at that location could not be determined. It is also noted that gravity load strains were not monitored during the tests, and that yield was defined when gages indicated strains due to lateral loads that were in excess of the yield strain. Gravity load strains are probably negligible in the slab at exterior joints, and in all columns. Slab reinforcement at the interior connections is likely to be stressed by gravity loads, but the effect cannot be determined precisely. As an approximation, if the service load column strip moment obtained from the Direct Design Method of ACI 318-77 is assumed to be spread uniformly across the slab column strip, computed top reinforcement strain due to gravity loads is one-third of the yield strain.

## 5.5 Summary of Response

This section provides a qualitative overview of the condition of the test structure before testing, and the effects of low, moderate, and high intensity earthquake simulations. The designations of low, moderate, and high intensity are somewhat arbitrary. The basis for the designations is discussed in Section 5.1.

(a) Initial Condition of the Test Structure

Before the earthquake simulations, the test structure was examined for surface cracking. As indicated in Fig. 4.33, a few hairline were observed. Based on the limited visible cracking, it is reasonable to conclude that the structure was in an effectively "uncracked" state prior to the earthquake simulations. The low equivalent viscous damping ratios (less than or equal to 1.5 percent of critical) measured during free-vibration tests before the earthquake simulations support this conclusion. However, as indicated by analyses presented in Section 5.3a, some slab cracking (and corresponding stiffness reduction) probably occurred due to slab gravity loads.

(b) Responses to Low-Intensity Earthquake Simulations

As described in Section 5.1, Tests EQ1 through EQ5 are considered to have low-intensity base motions on the basis that spectrum intensities were less than one-quarter of the scaled intensities of the prototype El Centro N-S, 1940 record. Cracking attributable to these tests was limited to minor extensions of existing cracks (Fig. 4.34). During free-vibration tests, vibration periods and equivalent viscous damping were essentially unchanged from values measured before the earthquake simulations (Table 5.1).

Hysteretic relations between base shear and top floor relative displacement (eg., Fig. 4.28) reveal essentially linear elastic response. Maximum top floor relative displacement reached 0.11 percent of structure height during Test EQ5, and maximum base shear reached 14 percent of structure weight. Even though these values are larger than corresponding design values (Chapter 2), the response was well below capacity of the test structure (Fig. 5.11). Strain gages attached to slab and column reinforcement revealed negligible strain except for column longitudinal bars at the bottom of the

first story where strains reached approximately one-quarter of the yield strain (Table 4.3).

(c) Responses to Moderate-Intensity Earthquake Simulations

Tests EQ6 and EQ7 are designated in this report to be of "moderate intensity", on the basis that spectrum intensities were equal to 44 percent of the scaled intensity of the prototype motion. The intensities qualify these tests as being representative of design motions for the test structure. Test EQ 6 had horizontal base motion only, whereas Test EQ7 had both horizontal and vertical base motion.

Peak top displacements were 0.27 and 0.54 percent of the structure height for test EQ6 and EQ7, respectively. Peak base shear during the respective tests reached 28 and 44 percent of structure weight. Examination of the maximum response relative to the overall response envelope (Fig. 5.11) indicates that response during these tests was well below capacity of the structure.

Several measures provide evidence of limited inelastic action. Vibration periods increased during the earthquake simulations, and periods exceeding the initial periods were apparent in subsequent free-vibrations as well (Table 5.1). The logarithmic decrement of free-vibration responses indicates equivalent viscous damping increased from 1.5 to 2.4 percent of critical (Table 5.1). Hysteretic plots of base shear versus top displacement (Fig. 4.29) indicate an average stiffness reduction compared with previous tests. In addition, the hysteretic loops have a more irregular appearance, depicting slightly wider hysteretic loops, yet a slight amount of pinching. Although maximum reinforcement strains did not reach yield, several gages

approached yield (Table 4.3), and slight offsets are observed in some gages (Fig. 4.24 and 4.26).

Some surface cracking was observed following these tests (Fig. 4.35). No spalling was found. The observed damage was of sufficiently limited nature that it would probably not be cause for concern during post-earthquake inspection.

(d) Responses to High-Intensity Earthquake Simulations

Tests EQ8, EQ9, EQ10, and EQ11 are defined in this report as "high-intensity" tests because they have spectrum intensities nearly equal to or exceeding the scaled intensity of the prototype El Centro base motion. Maximum base accelerations and spectrum intensities are tabulated in Tables 4.1 and 4.2, respectively. It is noted that tests EQ8 and EQ9 have identical intensities for horizontal base motions. They differ in that test EQ9 has vertical input whereas test EQ8 does not. It is also noted that tests EQ10 and EQ11 may be unrealistically intense motions, given that spectrum intensities are considerably in excess of the intensity of the prototype base motion.

Peak top level displacements increase progressively from test to test (Fig. 5.3). Given as a percentage of total structure height, top level drifts are 1.1, 1.6, 3.4, and 5.2 for tests EQ8, EQ9, EQ10, and EQ11. The large lateral drifts sustained during the latter two tests are significant in that they exceed by a considerable margin the maximum drift reasonably expected for a well designed structure [2]. Thus, the test structure demonstrates that reliably tough slab-column connections can be achieved given the proper details.

Peak base shears (Fig. 5.5) increase at a less rapid rate than do displacements. Given as a fraction of the total structure weight, the base shear coefficients are 0.64, 0.69, 0.77, and 0.81 for tests EQ8, EQ9, EQ10, and EQ11. These base shears are considerably above the design shear.

Hysteretic relations between base shear and top displacement appear progressively more erratic as test intensity increases, with reduced average stiffness and increased pinching (Fig. 4.30 through 4.32). As would be expected given the degrading stiffness of the test structure, vibration periods increase progressively for each test (Table 5.1). Damping during free vibration response also increases progressively (Table 5.1), reaching a maximum of 7.1 percent of critical following test EQ11.

Slab strain gages indicated yield at the first floor slab level during test EQ8 (Table 4.3). Yield in the top slab was not reached until test EQ10, by which time the first floor slab indicated significant offsets. Columns first yielded at the footing level during test EQ8 (Table 4.3). Columns at the slab-column connections approach yield during test EQ8 (Table 4.3). Significant offsets and several gage fractures are apparent by the end of test EQ11.

The progression of visible damage is indicated in Fig. 4.36 to 4.39. During tests EQ8 and EQ9, the slab developed more extensive cracking around columns and along edge beams, with a few cracks extending across the full slab width (Fig. 4.36). During test EQ10 and EQ11, the slabs developed numerous cracks extending across the full width on both the top and bottom slab surfaces (Fig. 4.37 and 4.38). For any given test, slab damage was more pronounced at the first level than at the second level. After the end of test EQ11, a slight vertical displacement of the first floor slab surrounding one

interior column indicated possibility of punching failure if testing had been continued.

Inclined cracks observed in edge beams near the columns (Fig. 4.36 to 4.38) indicate torsional "distress" in the spandrel beams. Intersecting inclined cracks that occurred as a consequence of reversed torsional moments eventually resulted in some loss of concrete cover after test EQ11 (Fig. 4.39). Spalling occurred in columns at the base level (Fig. 4.39). Inclined cracks on North and South column faces were observed, although their width did not exceed approximately 0.3 mm (0.01 in.).

## 6. INTERPRETATIONS USING LINEAR-ELASTIC MODELS

### 6.1 Introductory Remarks

Interpretations of response using relatively simple linear-elastic analytical models are of value because of the prevalent use of such methods in design and because of the vulnerability of flat-plate construction to experience drift problems within the effectively elastic range of response. Elastic analysis methods should be valid for earthquake simulations EQ 1 through EQ 5 because response during these tests did not deviate significantly from linearly elastic. Responses during subsequent tests displayed increasing levels of inelastic response, and consequently may be less amenable to interpretation by elastic methods. Nonetheless, the conventional practice of using elastic analytical models in design for anticipated inelastic responses (as is done, for example, in seismic design) deserves examination.

This chapter examines elastic analytical models for lateral load analysis of slab-column frames. The presentation begins with discussion of two conventional analytical models, and describes an extension to one of the models that enables consideration of effects of cracking due to applied loads. In subsequent sections, elastic responses to earthquake simulations are interpreted using linear elastic modal spectral analysis methods.

### 6.2 Description of the Basic Analytical Models

In slab-column construction, the slab frames around the columns as well as directly into the columns, such that two adjacent slab spans are never isolated from one another by the column. Special modeling techniques are often required to model this framing action. Two elastic analytical models are commonly used for lateral-load analysis of slab-column frames [52]. These

are the effective beam width model and the equivalent frame model. The basic premises of each model are described in this section.

The effective beam width model represents a slab-column structure by conventional plane frames comprising beams and columns (Fig. 6.1). The columns of the real structure are represented directly. The slab of the real structure is represented by beams having depth equal to slab depth and width equal to the product between the full panel slab width and an effective width coefficient. The effective width coefficient accounts approximately for the fact that the slab is not fully effective across its full transverse width in transferring unbalanced moments due to lateral loads. Gross-section properties are typically assumed for beams and columns. As used in this report, rigid beam-column joints are included in the analytical model. The joints have width equal to column width and depth equal to slab or spandrel beam depth, as appropriate.

Effective width coefficients for use in the effective beam width model are usually calculated assuming elastic properties for the slab. Corley and Vanderbilt present a summary of available solutions [52]. In some of the solutions, the region of the slab common to the column is permitted to deform. Solutions in which the slab-column connection has been assumed rigid are usually preferable. In this report, only those solutions assuming the rigid joint are used. For the proportions of the interior connections used in the test structure, Pecknold recommends [39] an effective width coefficient of 0.54. Although a larger effective width is appropriate for the exterior connections because of the edge beam [56], identical values are usually assumed for both interior and exterior connections. The same practice is followed in this report.

The equivalent frame model for lateral load analysis is identical to the equivalent frame model described in ACI 318-83 [7]. The model represents a slab-column structure by columns, slab-beams, and transverse torsional members (Fig. 6.2). The columns of the real structure are represented directly, and have rigid zones equal to slab or edge beam depth, as appropriate. The slab-beams are continuous over multiple spans, connecting to columns only through the transverse torsional members. Along the slab clear span, flexural inertia of the slab-beam is equal to that of the full slab panel width. Within a length equal to the column dimension, the moment of inertia of the slab-beam is amplified as required by ACI 318-83. The torsional member has cross section comprising the slab of width equal to the column for the interior connections, and comprising the edge beam plus portion of slab extending a distance equal to the projection of the beam below the slab for the exterior connection. Rotational stiffness of the torsional member is computed according to ACI 318-83. For all cross sections, stiffnesses are based on gross-section properties.

As noted in the Commentary to the ACI Code [12], the equivalent frame model was developed for gravity load analysis, and its use for lateral-load analysis may result in underestimates of lateral drift unless reduced stiffnesses are used.

Vibration frequencies and lateral load responses were computed for the effective beam width and equivalent frame models using the computer program SAP 80 [54]. For the lateral load calculations, lateral loads were applied at slab middepths, the second-floor force being twice the first-floor force. Flexural and shearing deformations were permitted for beams (slab-beams) and columns. Axial deformations were permitted also for columns in the effective beam width model (they were observed to have negligible effect). Flexural,

axial, and shear rigidities of footings and transducers were considered (see Appendix A for description of transducers and their stiffness). The transducers were assumed to be fixed to a rigid platform at the base. Concrete modulus was 25500 MPa (3700 ksi), and steel modulus was 200000 MPa (29000 ksi) for all calculations. Average measured cross-sectional dimensions were assumed (Table A.2).

### 6.3 Effect of Transducers on Lateral-Load Stiffness

Before examining the correctness of the analytical models in estimating lateral-load stiffness, it is of interest to determine the effect on stiffness of the combined transducer-footing system (Fig. 1.2) that supported the test structure. For this purpose, a dynamic analysis of the effective beam width model with lead weights was conducted. An effective width coefficient of 0.54 was assumed, as recommended by Pecknold [39]. Three analyses are considered, designated Analyses B, C, and D in Table 6.1. For Analysis B, the test structure was assumed fixed at the base of the columns, for Analysis C, the test structure was fixed at the base of the footings, and for Analysis D, the test structure was assumed fixed at the base of the transducers.

Comparison between Analyses B and D indicates that the combined transducer-footing system lengthened the calculated initial periods by ten percent, which indicates that the overall structural stiffness with transducers was approximately 83 percent of stiffness without transducers. The reduction in elastic stiffness is not unexpected, and is not unrealistic for structures supported on footings on stiff soil. Because the effect is not insignificant, the transducer flexibility will be taken into account in all subsequent calculations unless otherwise noted.

#### 6.4 Comparison Between Computed and Initial Measured Lateral-Load Stiffnesses

Initial lateral load stiffnesses were gaged from free-vibration tests conducted before and after placement of subsidiary lead weights on the floor slabs. Vibration periods are listed in Table 5.1. Periods were calculated using the effective beam width model with effective width coefficient of 0.54. Masses were taken equal to values without and with lead weights, as tabulated in Table A.3. The mass assumed at each floor includes mass of the floor slab, subsidiary lead weights, and tributary portions of columns and edge beams. Although mass centroids were calculated to be slightly eccentric from slab middepth, the eccentricity was found not to have significant effect on computed response. Thus, masses are assumed at slab middepths.

Computed first and second mode vibration periods before placement of lead weights are 0.102 and 0.0284 sec (Analysis A, Table 6.1). These values are 88 and 90 percent of measured values of 0.116 and 0.0316 sec (Test FV0.A, Table 5.1). The close comparison suggests that the analytical model represents the structure closely. Because concrete structures tend to crack due to service loads and time-dependent effects, it is typical for calculated periods to be shorter than measured periods [32].

Measured first and second mode periods increased to approximately 0.21 and 0.060 sec after placement of lead weights on the slabs. Computed periods are 0.179 and 0.0498 sec (Analysis D, Table 6.1), or approximately 84 percent of measured.

The ratio between measured and calculated periods before placement of weights on the floor slab suggests that measured stiffness was approximately 77 percent of calculated (obtained by squaring the period ratio). A similar calculation indicates that stiffness after placement of weights was reduced to

70 percent of calculated. Although the apparent change in stiffness could arise in part from errors in assumed mass distribution. However, it is likely that a major portion of the change is attributable to cracking in the slab as a consequence of placement of the weights on the slab.

To investigate the extent of slab cracking, Analysis E (Table 6.1) was conducted for which the slab effective width factor was taken equal to half of the theoretical elastic value of 0.54. With the reduced analytical slab stiffness, computed first mode period is equal to measured. Some discrepancy remains between measured and computed second mode periods.

Cracking of the slab is likely as a consequence of slab self weight, construction loads, temperature variations, and shrinkage. Considering that construction loads were significantly below the service live load (estimated at one quarter of the design service live load) and that the test structure was stored in a laboratory that did not experience wide fluctuations in temperature and humidity, the reduction in stiffness attributed to cracking is noteworthy. Effects of cracking are likely to be more significant in typical structures subjected to a wider range of loading and environmental conditions.

#### 6.5 Comparison of Computed and Measured Stiffness During Earthquake Simulations

Lateral-load stiffnesses were measured during earthquake simulation responses, starting with test EQ4. Measured and computed stiffnesses are compared in Fig. 6.3. In that figure, measured simultaneous occurrences of base shear and peak lateral displacement during cycles of increasing displacement amplitude are represented by open circles. Measured lateral loads were distributed approximately in the inverted triangular distribution

for the data in Fig. 6.3. Stiffnesses computed for the effective beam width model ( $\beta = 1$  in Fig. 6.3) were obtained using an effective width coefficient of 0.54 as described previously. Stiffnesses for the ACI Equivalent Frame Method ( $\beta = 1$  in Fig. 6.3) are shown also.

From the data in Fig. 6.3, it is apparent that the effective beam width model is too stiff to represent initial lateral-load stiffness at small drifts. This conclusion is supported by data presented in Section 6.4, which compare measured and computed initial vibration periods.

Initial lateral-load stiffnesses are better modeled using the equivalent frame model ( $\beta = 1$  in Fig. 6.3). Considering that the equivalent frame has been devised to match experimentally observed behavior under gravity loads, and that moments and stiffnesses at low drifts are not significantly different from those under gravity loads alone, the close correlation is not beyond reason.

It is apparent in Fig. 6.3 that lateral load stiffness varies with the magnitude of lateral loads. Thus, the appropriate stiffness to be used in design depends on the level of lateral loading, that is, the working loads for the building. Two definitions of working loads may apply in a given design, as follows: (1) If the building design is controlled by strength considerations, then the working load will be some percentage of the lateral-load strength. In this report, 40 percent of lateral strength will be considered the working load. (2) If the building design is controlled by lateral drift considerations, then the working load will be that load corresponding to the limiting lateral drift limit. For wind design, many engineers limit the maximum interstory drift to  $0.002H$ , where  $H$  = interstory height [52]. For seismic design, a value of  $0.005H$  under the code service

level lateral forces is typical [50].

Lateral-load stiffnesses obtained by the effective beam width and equivalent frame models ( $\beta = 1$ ) are plotted in Fig. 6.3 for comparison with measured stiffnesses. Both are considerably too stiff at working loads. Apparently, some stiffness reduction is necessary to properly model working load stiffness.

Vanderbilt and Corely have recommended [52] that a lower bound to lateral load stiffness can be obtained using an equivalent frame having slab-beam inertia reduced to one-third of the gross-section value. The resulting stiffness is plotted in Fig. 6.3 ( $\beta = 1/3$ ). Correspondingly, a stiffness for the effective beam width model with an effective width coefficient of one-third of the elastic value of 0.54 is also plotted ( $\beta = 1/3$  in Fig. 6.3).

The following observations are made regarding the accuracy of the models at working loads.

(i) At the working load limit defined by 40 percent of the structure strength, both the reduced equivalent frame and the reduced effective beam width models produce close estimates to stiffness.

(ii) At the working load limit defined by the drift of  $0.002H$ , the reduced stiffnesses are too soft. The original equivalent frame model estimates the stiffness reasonably well. Although not shown in Fig. 6.3, the equivalent beam width model requires an effective width of approximately one-half the elastic value to match stiffness at this level of loading.

(iii) The working load limit of  $0.005H$  is close to the limit based on 40 percent of the strength for the test structure, and the corresponding observations are valid.

## 6.6 An Equivalent Frame to Model Variation of Lateral Load Stiffness

The preceding discussion indicates that modifications to the effective beam width or equivalent frame models are necessary to correctly represent lateral-load stiffness at "working loads." The reduction of slab-beam stiffness to one-third of its gross-section stiffness as suggested by Vanderbilt and Corley [52] is simple but is not likely to produce consistently accurate stiffness estimates. A rational approach to estimating lateral-load stiffness is desirable.

As one approach, the Commentary to ACI 318-83 states that an effective moment of inertia of slab members may be computed using the fully-cracked section. For the test structure, this would result in an effective inertia approximately 15 percent of the gross-section inertia, a value that is overconservative. As an alternative, it is suggested [12] that a stiffness based on Eq. 6.1 is reasonable.

$$I_e = \left(\frac{M_{cr}}{M_a}\right)^3 I_g + \left[1 - \left(\frac{M_{cr}}{M_a}\right)^3\right] I_{cr} \dots\dots\dots 6.1$$

in which  $I_e$  = effective slab inertia,  $M_{cr}$  = cracking moment,  $M_a$  = applied moment,  $I_g$  = gross-section moment of inertia, and  $I_{cr}$  = cracked-section moment of inertia. Eq. 6.1 can be written in a more convenient form (for discussion purposes) given by Eq. 6.2.

$$R = \left(\frac{M_{cr}}{M_a}\right)^3 + \left[1 - \left(\frac{M_{cr}}{M_a}\right)^3\right] \frac{I_{cr}}{I_g} \dots\dots\dots 6.2$$

in which  $R$  = ratio between effective inertia and gross-section inertia. No explicit guidance is given in the ACI 318-83 Commentary on the application of Eqs. 6.1 or 6.2. However, it seems reasonable that the effective stiffness ratio,  $R$ , should be based on moments and stiffnesses for a width less than the full slab width, because the full slab width is not effective in resisting

lateral loads. Likewise, it seems reasonable to reduce the torsional member stiffness by the same (if not greater) ratio as the slab-beam stiffness because the torsional member represents the slab connection to the column and should therefore experience at least as large a stiffness reduction due to cracking in the connection region.

The application of Eq. 6.2 for estimating lateral-load stiffness of the test structure was investigated analytically for base shears up to 60 percent of base-shear capacity. Beyond this base shear, yielding was computed in the structure, so the elastic model is not likely to be appropriate. The procedure is as follows:

- (1) Lateral loads are applied to an equivalent frame having gross-section stiffnesses as specified in ACI 318-83.
- (2) Column strip gravity load moments (from the Direct Design Method) and total slab lateral-load moments are summed at column faces and at midspans to obtain values of total moment,  $M_a$ , for use in Eq. 6.2.
- (3) At the column face and midspan of each slab span, the reduction in slab inertia,  $R$ , is computed using Eq. 6.2 with moments and flexural inertias based on values for the column strip. (This width is used because it is close to the elastic effective width.) An average value of  $R$  for the entire slab span is then computed as the average between the midspan and average end values of  $R$ . Flexural inertia of the slab-beam is taken as the product between  $R$  and the gross-section inertia for the full slab width. Torsional member stiffness is reduced by the same ratio  $R$ . Effective inertia of columns is determined with Eq. 6.1 using appropriate column moments and inertias.
- (4) The equivalent frame with the effective inertias is reanalyzed to determine lateral drifts.

The relation between base shear and top displacement obtained by the

procedure outlined in the preceding paragraph is shown in Fig. 6.4. The computed response is consistently more stiff than measured, although deviations are small and overall trends are matched closely. If a width equal to  $c + 3h$  (where  $c$  = column width and  $h$  = slab thickness) is used in Eq. 6.2 rather than the column strip, computed stiffnesses fall generally on the soft side relative to measured values (Fig. 6.4). For comparison, stiffnesses obtained using total moments and the full panel width are shown also (Fig. 6.4). It is apparent that a reduction based on the full width is unsatisfactory, and that better results are obtained using the column strip width or the width  $c + 3h$ .

Similar analyses carried out using the effective beam width model produced similar trends. However, as noted previously, the effective beam width model was initially too stiff. Thus, although the trends of stiffness reduction were generally correct, the model remained consistently too stiff relative to the measured response.

Although seemingly rational in its derivation, the procedure presented in this section may be excessively complex to justify its application in design office practice. Simple procedures such as that outlined by Vanderbilt and Corley [52], in which an arbitrary reduction is applied universally, may be the more appropriate. Further study of this topic is recommended.

## 6.7 Interpretation of Maximum Displacement Responses Using Response Spectrum Analysis

### (a) General Comments

Responses to tests EQ 1 through EQ 5 were essentially in the elastic range, and levels of inelastic response to tests EQ 6 and EQ 7 were sufficiently small that interpretations using elastic dynamic models should be

possible. Research reported elsewhere [17,45] indicates that if suitable effective elastic properties are selected, responses well into the inelastic range can also be predicted using elastic methods. This section of the report discusses the suitability of elastic response spectrum techniques for interpreting measured elastic and inelastic responses of the test structures.

Response spectrum analysis requires descriptions of the ground motions and of the structural properties. Linear elastic response spectra for different viscous damping ratios and for each earthquake simulation are shown in Figs. 4.13 through 4.23. For the analyses described herein, unless otherwise noted, spectral displacements are read from the pseudo-velocity response spectra shown in those figures. Because displacement responses were dominated by the apparent first mode, only the first mode is considered in the analysis. Structural properties for several different analyses are described in the following subsections.

(b) "Experimental Model"

Response spectrum analyses were first conducted using a model that is designated the "experimental model." The model has vibration period equal to the period measured during the cycle of peak displacement during the earthquake simulation. The mode shape is taken equal to the displaced shape at the time of peak displacement. (It is noted that measured displacements were dominated by the first mode, and that the displaced shape did not change significantly during the response.) Because effective damping during earthquake simulations is not known, three different values (2, 5, and 10 percent of critical damping) are investigated. These values are near the range measured during free-vibration tests (Table 5.1) and within the range typical for reinforced concrete structures [9,17,31,34,45,46].

Maximum calculated and measured top slab displacements, and ratios between calculated and measured top slab displacements, are listed in Table 6.2. To facilitate interpretations, ratios between calculated and measured top slab displacements are plotted in Fig. 6.5 (no values are plotted for tests EQ1 through EQ3 because displacements were not measured accurately). Responses for tests with horizontal motions only are shown with solid symbols, and those having both horizontal and vertical are with open symbols.

Low-amplitude responses (test EQ 4) are reasonably well estimated with two percent damping (Fig. 6.5). As response amplitude increases, the general trend is that response is better estimated by a higher damping. However, the value of damping that gives the best response estimate varies somewhat erratically from test to test. The erratic variation is not unexpected, considering that the structure is not responding elastically as has been assumed in the analysis. For inelastic responses, maximum displacement response is reasonably well estimated using a model having period corresponding to the period during maximum response with equivalent viscous damping of ten percent of critical. Other researchers have made similar observations for reinforced concrete structures [32,46].

It was noted previously that tests EQ 6 and EQ 7, and tests EQ 8 and EQ 9, were pairs of tests for which horizontal spectrum intensities were nearly identical. The primary variable between the first and second test of each pair was that the first test had horizontal input only, whereas the second test combined the corresponding vertical motion with horizontal motion. Maximum measured responses for the tests with combined vertical and horizontal motions were significantly higher than responses for tests with horizontal motions alone. In contrast, computed responses (5 or 10 percent damping in Table 6.2) indicate that nearly equal maximum displacements should have

occured for the two tests of each pair. The discrepancy between measured and calculated responses may simply be a manifestation of the inherent variability of the calculation method, which assigns fictitious elastic properties to an inelastic system. In particular, it is noted that the test structure begins the combined test having been previously damaged by a base motion of similar strength. The fact that the structure has been previously damaged will generally result in different response characteristics during the second test.

(b) "Equivalent Frame Model"

The "equivalent frame model" has properties determined by the procedure described in Section 6.6. As noted in that section, stiffness is dependent on the magnitude of lateral load. For simplicity, stiffness of the equivalent frame model was determined for lateral drift approximately equal to the maximum measured lateral drift for the earthquake simulation in question. As for the "experimental model" described previously, three different values of effective damping were investigated (2, 5, and 10 percent of critical damping).

Computed responses are listed in Table 6.2, and ratios between computed and measured responses are plotted in Fig. 6.6. Values are not presented beyond test EQ6, because the magnitude of lateral drift for subsequent tests exceeded the elastic limit for which the equivalent frame model was valid. Overall trends of computed responses are similar to trends noted previously for the "experimental model." In particular, it is noted that computed responses compare well with measured responses for damping in the range between 5 and 10 percent of critical damping.

(c) "Effective Beam Width Model"

It is common in structural design to compute maximum expected displacements during an earthquake using the elastic response spectrum and calculated elastic properties of the structure. To investigate this procedure, an effective beam width model was selected. The effective width coefficient was reduced to one-third of the elastic value of 0.54, which, as discussed previously in this chapter, results in elastic stiffness near the measured stiffness at working loads. Five percent of critical damping was assumed. Maximum responses were computed using the acceleration response spectra of Fig. 4.13 through 4.23.

Computed responses are listed in Table 6.3. It is apparent from the data in that table that the model correctly anticipated maximum responses for tests prior to test EQ7. The good correlation is not unexpected considering that the test structure responded essentially in the elastic range of response for these first tests. For subsequent tests, inelastic response was evident.

Newmark [36] has noted that if the initial elastic period of a structure is in the constant velocity range of response, maximum displacement during inelastic responses will be approximately equal to response computed for the elastic structure. If the structure has initial period shorter than the period corresponding to the constant velocity range, the inelastic response is likely to exceed the computed elastic response. The test structure falls into the latter class of structures. Thus, it is reasonable that maximum measured responses after test EQ6 exceed the computed elastic responses.

(d) Comparison With the Design Model

The test structure was designed for seismic zone 2 of the UBC [50] as

described in Chapter 2. An effective beam width model, with effective width coefficient of 0.5, was used to determine lateral drift under the code service level forces. The computed top floor displacement was 0.03 percent of structure height, or approximately 0.5 mm.

The UBC designation of a region as "zone 2" does not clearly describe the expected intensity of base motion for that region. The UBC base-shear coefficients provide one measure of the implied intensity. The intensity for zone 2 is three-eighths of the intensity for zone 4. Considering the prototype 1940 El Centro motion as a typical design motion for zone 4, an equivalent design motion for zone 2 would have approximately three-eighths the intensity of the prototype. As noted in Section 5.1 of this report, test EQ6 has approximately this intensity. In addition, it is noted that test EQ6 had peak base motion of 0.189 g, which is a reasonable effective peak base acceleration for many zone 2 regions [3]. Thus, test EQ6 can be considered to be a fair representation of the design base motion for the test structure.

In contrast to the anticipated 0.03 percent lateral drift, the test structure experienced a maximum lateral drift of 0.28 percent. The discrepancy is attributed to (1) excessive stiffness of the analytical model because effects of service load cracking have not been considered in the design model, and (2) implied inelastic response, which is reflected in design code forces that are significantly less than forces obtained from an elastic response analysis. The first effect can be taken into consideration by recognizing that the computed lateral-load stiffness is approximately 2 times the measured stiffness (Fig. 6.3). Chopra [11] has noted that for short period structures (eg., the test structure), the elastic spectrum forces are 4 or more times the forces given by the UBC. Thus, lateral displacements should be anticipated on the order of  $0.03 \times 2 \times 4 = 0.24$  percent of height.

Measured lateral drift of 0.28 percent is within the expected scatter about this value.

## 7. INTERPRETATIONS OF STRENGTH AND INELASTIC RESPONSE

### 7.1 Introductory Remarks

The shaking table model was part of an experimental program designed to examine methods for analysis, design, and construction of flat-plate structural systems. In addition to the shaking table model, the research program included an experimental study of interior and exterior slab-column components of the shaking table model. Thus, the research also provides an opportunity to compare behavior of the components and of the whole structure, so that relationships between the parts and the whole can be better understood. Those relationships are the subject of the first portion of this chapter.

The second portion of this chapter examines analytical methods for calculating strength of the test structure. As noted in previous chapters, the test structure possessed a base-shear strength many times the design strength. Given the excessive overstrength, it is important that methods of strength evaluation be examined and that the sources of overstrength in the design be identified.

### 7.2 Summary of the Component Tests

An interior slab-column connection and an exterior slab-column-spandrel connection were constructed and tested as a part of the research on seismic response of flat-plate construction. The connections were nominally identical in size and details to first-floor connections of the shaking table model. They were loaded to simulate effects of gravity loads and reversed seismic loads. Behavior of the connections was studied to obtain a detailed appreciation of connection behaviors and to obtain a more clear understanding

of the relation between component behavior and complete structure behavior. The experiments are summarized briefly in this section. Further details are presented elsewhere [56].

The test specimens and test arrangement are idealized in Fig. 7.1. For each specimen, columns extended above and below the slab to a location corresponding to column midheight in the shaking table model. The slab extended in the longitudinal and transverse directions to lines corresponding to panel centerlines in the shaking table model. Roller supports along the slab transverse edges (Fig. 7.1) were simulated by mechanical links that were calibrated to determine the reaction at the edge. Longitudinal slab edges were unrestrained. The bottom column was pinned at its base. Lateral load was applied at the top of the upper column.

Gravity loads were simulated by placing lead ingots (the same ingots used for the shaking table model) on the slab surface. Analyses reported by Zee and Moehle [56] indicate that the slab of the interior connection was loaded to approximately the correct moment at the column face, but with shear around the critical section approximately 15 percent in excess of that anticipated in the shaking table model. The exterior connection had very small gravity moment at the connection, and approximately the correct gravity shear. Reversed lateral loads were applied at increasing amplitudes until failure was achieved.

Measured relations between lateral load and lateral interstory drift for the connections are shown in Fig. 7.2. The relations are typical of those for reinforced concrete slab-column connections, indicating a relatively low initial stiffness, deterioration of the initial stiffness at relatively low loads, and pinched hysteretic response for repeated inelastic loadings.

Slab surface crack patterns observed at different levels of lateral drift are sketched in Fig. 7.3.

The interior slab-column assembly failed by an apparent punch through of the column at lateral drift of 4.4 percent of specimen height. The failure was sudden and accompanied by a sharp sound indicative of brittle shear failure. The failure cone was apparent only on the side of the slab where the top surface was in tension due to unbalanced moment, and broke through the top surface at approximately 1.7 slab depths from the slab-column interface. The exterior slab-column-spandrel assembly failed under negative unbalanced moment by apparent torsional failure of the spandrel beam at a lateral drift of 5.5 percent of specimen height. Cover in the edge beam spalled to expose the reinforcement. Whereas the interior connection failure was rather sudden and brittle, the exterior connection continued to support load at increasing drifts after spalling of concrete on the spandrel.

### 7.3 Comparison Between Apparent Component and Complete Structure Behaviors

Qualitative comparisons of slab cracking patterns and failure modes are possible without extensive analyses. Analytical comparisons are made in subsequent sections.

#### (a) Crack Patterns

Visible cracking in the first floor of the test structure at any given level of interstory drift (Fig. 4.33 through 4.38) was similar to that observed in the component tests at similar drifts (Fig. 7.3). This is apparent by comparison between first-floor slab cracking in the structure after test EQ10 (Fig. 4.37, maximum drift of 3.4 percent) and component cracking at 3.5 percent drift (Fig. 7.3). Visible second-floor slab damage

was less severe than visible first-floor damage in the test structure, apparently because the slab was stronger than the columns at the second-floor level.

(b) Failure Mode

The test structure achieved lateral drifts of 5.3 percent of structure height without collapse during Test EQ11. After this test, severe spalling in one of the first-floor spandrel beams was noted near the columns, and one of the first-floor interior columns appeared to have begun to punch through the slab. The exterior component experienced a similar failure of the spandrel beam at a similar lateral drift. The interior component experienced punch-through at lateral drift of approximately 4.4 percent. It is noted that the interior component suffered substantial loss of load-carrying capacity when failure was observed. In contrast, the shake table structure did not collapse, nor did it experience an apparent overall loss in lateral-load carrying capacity (see graph for 2.00 to 3.00 sec, Fig. 4.32), even though it underwent more load reversals than the components, and experienced lateral drift in excess of component failure drifts.

Based on the preceding discussions, it is concluded that the component tests provided good measures of expected crack development and failure modes, but an incorrect measure of the effect of a local failure on response of the complete structure. Whereas failure of a connection in an isolated connection test resulted in nearly complete loss of capacity, apparent failure of a connection in the complete structure did not cause any apparent loss of overall capacity. This is attributed to the capacity for redistribution of internal forces in the statically indeterminate test structure.

#### 7.4 Analysis of Inelastic Load-Deformation Response of the Test Structure

Measured behavior of the interior and exterior connections can be assembled analytically to determine an analytical load-deformation response of the shaking table model. The correlation between the analytical prediction and measured response provides a further indication of whether behavior of slab-column components can be used to interpret behavior of complete structures. The procedure and results are documented in this section.

##### (a) Description of the Analytical Model

The test structure was modeled using an assemblage of columns and beams that is similar to the effective beam width model described previously (Fig. 6.1). Beam-column joints were rigid. Deformations of footings and transducers were included. Analytical inelastic response of the structure under monotonically increasing lateral loads was computed using the computer program ULARC [48]. The program considers elements having elastic-perfectly plastic moment-rotation behavior. Actual behavior of reinforced concrete elements is more complex, and can be simulated in the computer program by connecting several elastic-plastic elements in parallel, each having different elastic stiffness and yield moment. Three members in parallel were used for each slab and column of the test structure so that a trilinear moment-rotation response was simulated.

Moment-curvature behaviors of columns under monotonically increasing load were computed using the assumptions for flexural analysis given by Kent and Park [26]. Measured dimensions and material properties were used. Confinement effects were taken into account using the modified Kent-Park relation [38]. Axial load effects on stiffness and strength were included, with axial load equal to the gravity axial load determined by tributary area

methods. Moment-rotation behaviors of the columns were derived from the calculated moment-curvature relations by assuming inflection points fixed at column midheights. The calculated moment-rotation behaviors are in Fig. 7.4. Idealized trilinear relations are also in that figure. The breakpoints of the idealized relations were selected to obtain an average response that was representative of the computed response. The breakpoints do not correspond to physical cracking and yielding.

Moment-rotation behaviors of beams in the analytical model were derived from moment-rotation responses measured during static tests of the interior and exterior slab-column subassemblies. As noted in Section 7.2 and analyzed in detail elsewhere [56], initial total slab moments at the column face were nearly the same in the test structure and in the subassemblies. Because of the similarity in initial moments, measured moment-rotation behaviors of the components can be used directly with little error to represent moment-rotation behaviors of the beams for the inelastic analysis. The measured and idealized envelope relations between total slab moment (excluding gravity moment) and joint rotation are in Fig. 7.5.

(b) Computation of Response

Response of the test structure to monotonically-increasing lateral loads was computed for lateral loads applied in small increments at slab middepths. Several analyses were conducted. For each analysis, the ratio between second and first floor lateral force was held constant. Different ratios were used for different analyses (ratios investigated were second:first = 2:1, 1.5:1, 1:1, 0.5:1, and 0.33:1). Analyses were carried out until lateral drifts were well beyond the maximum drifts experienced during the tests. For each analysis, lateral load, lateral drift, and internal member forces were

monitored at each load increment. Partial results of the analyses are presented in Section 7.4 (c).

(c) Computed Response

Computed relations between base shear and top slab displacement are compared with the measured envelope relation in Fig. 7.6. For the analysis in which the second slab lateral force was equal to twice the first floor force (load distribution of 2:1 in Fig. 7.6), computed response is nearly identical to measured response during the initially elastic range of response (drifts less than approximately 0.5 percent of structure height). Beyond this drift level, the measured envelope relation is more stiff and strong than the response calculated for the inverted triangular load distribution. Beyond drift levels corresponding to approximately 2 percent drift, the measured relation is best represented by the loading distribution having the ratio between second and first slab forces equal to 0.5:1.

The observation that the measured relation between base shear and top displacement is best modeled with the load distribution having ratio of 2:1 during early tests is consistent with measured lateral load distributions. As discussed in Section 5.3c, the lateral load distribution varied throughout the tests, but tended to be predominated by the apparent first-mode distribution during early tests. This distribution has a second floor force approximately twice the first floor force. As testing progressed, the loading distribution varied more erratically, and during peak base shear responses the loading tended to be skewed more heavily toward the first floor, typically in a nearly uniform distribution (Fig. 5.10). Thus, it is reasonable that a uniform lateral-load distribution should be used to best match measured behavior at this stage of testing. It is noted that computed response with the uniform

loading falls short in terms of strength and stiffness of the measured response (Fig. 7.6). As discussed in Section 7.5, it was not possible in the course of this investigation to account for the full measured base-shear strength.

Based on the preceding discussion, it is concluded that the static analysis adequately represents the global response of the structure, with the limitation that the most appropriate distribution of static lateral loads may vary depending on the range of response for which the calculations are to be made. The uniform distribution appears to be a reasonable "average" for response over the entire range (Fig. 7.6).

#### 7.5 Lateral-Load Capacity

The test structure sustained a maximum base shear equal to  $0.84W$ , where  $W$  = total structure weight excluding footings. This base shear is approximately 16 times the design value. In the interest of verifying methods for lateral strength predictions and of understanding the sources of the overstrength, lateral load strength of the test structure was investigated using existing procedures for computation of connection and structure strength. The study is documented in the following paragraphs, which discuss sequentially the strengths of interior connections, exterior connections, columns, and the structure as a whole. The reasons why the strength exceeded the design strength by such a significant margin are discussed in Section 7.6.

##### (a) Strength of Interior Connections

Various procedures have been proposed for computation of shear and unbalanced moment strength of interior slab-column connections. Those investigated in this study include the procedure recommended in ACI 318-83

[7], the beam analogy proposed by Park and Islam [37], and the beam analogy proposed by Hawkins [21]. Measured strength of the interior slab-column connection (see Section 7.2) is the basis for determining the correctness of the analytical procedures as applied to the test structure. It is noted that concrete strength in the component was less than that in the test structure, so some interpretations are required.

#### ACI 318-83 Design Procedure

The design procedure in ACI 318-83 assumes that vertical shear and a portion of the unbalanced moment are resisted by a linear variation of shear stress around a critical section. For the proportions of the test structure, the design procedure assigns 40 percent of the unbalanced moment to be carried by eccentric shear. Using this procedure, with no capacity reduction factor and with vertical shear due to gravity loads acting on the test structure, calculated unbalanced moment strength is 9.70 kN-m (85.8 kip-in.).

According to the design procedure, the portion of unbalanced moment not carried by eccentric shear (60 percent in this case) is to be carried in flexure by slab reinforcement placed within a width  $c + 3h$  centered about the column. Including all top and bottom slab bars within this width (that is, the sum of positive capacity on one side of the column and negative capacity on the other side), unbalanced moment strength in flexure is 9.76 kN-m (86.4 kip-in.).

As noted in the report by ASCE-ACI Committee 426 [43], strength in excess of that indicated by the slab flexural capacity is likely for large moment to shear ratio, as is the case for the test structure. In addition, earlier proposals [14] recommend that total connection strength can be estimated as the direct sum of strengths in eccentric shear and in flexure. If that

procedure is used, calculated unbalanced moment strength is 9.74 kN-m (86.2 kip-in.). Using the same approach, computed strength of the interior slab-column subassembly [56] is 8.33 kN-m (73.7 kip-in.), which is 81 percent of the maximum measured unbalanced moment.

#### Park and Islam Beam Analogy

The beam analogy of Park and Islam [37] envisions the slab-column connection comprising beams framing into all four faces of the column at a distance  $d/2$  from the column face. The beams each have width of  $c + d$  and otherwise have properties identical to those of the slab that frames into each column face. Unbalanced moment strength is computed simply as the sum of flexural and shear strengths of beams framing into the front and back faces and of torsional strengths of beams framing into the side faces. Torsional strengths in the presence of shear are calculated using the procedure for plain concrete beams that is recommended in ACI 318-83, but with shear stress capacity double that permitted for beams. Using this analogy, calculated unbalanced moment capacity is 7.39 kN-m (65.4 kip-in.). Corresponding calculated strength of the interior component [56] is 6.57 kN-m (58.1 kip-in.), which is 64 percent of measured strength. The lower computed strength may occur because torsional strengths are based on concrete capacity with no consideration of slab reinforcement. Experiments [27] have indicated nominal torsional stress capacities significantly in excess of the value assumed by the analogy.

#### Hawkins Beam Analogy

The beam analogy of Hawkins [21] includes effects of slab reinforcement on torsional strengths, with torsional strength computed by the procedure recommended by ACI 318-83 for beams. If it is assumed that flexural

capacities are reached on front and back faces, combined torsion-shear capacities on side faces, and shear capacity on the front face, computed unbalanced moment capacity is 11.3 kN-m (99.9 kip-in.). The corresponding value calculated for the interior component is 9.03 kN-m (79.9 kip-in.), which is 88 percent of measured strength. The discrepancy may be attributable to effects of reversed loads [20] and inaccuracy of the analytical model.

### Summary

From the preceding discussion it is concluded that the beam analogy of Hawkins results in the best estimate of interior connection strength, with computed strength 12 percent less than measured component strength. The procedure recommended by ACI 318-83 underestimates strength by 19 percent, whereas the beam analogy of Park and Islam results in a 36 percent underestimate.

### (b) Strength of Exterior Connections

Strength under monotonic loading of exterior connections having spandrel beams has been studied by Jirsa, et. al. [24] and Rangan and Hall [40]. Two modes of failure are likely, one in which a yield line forms in the slab at the face of the spandrel, the other in which the slab yields at the column and the spandrels fail in torsion. It has been observed that axial growth of the spandrel may induce the slab to participate indirectly in the beam torsional resistance, thereby enhancing the torsional strength. However, it may be unwise to include such effects where severe cyclic loads may deteriorate the strength enhancement.

For the test structure, formation of a yield line at the face of the edge beam results in calculated unbalanced negative and positive moment strengths

(corrected to the column centerline by the ratio between center-to-center span and clear span) of 8.39 and 6.09 kN-m (74.2 and 53.9 kip-in.), respectively. Torsional strengths are calculated using the space truss theory for torsion [28] with linear interaction between shear and torsion. Taking the unbalanced moment strength in the torsional mode as the sum of spandrel torsional strengths plus flexural strength of the slab of width  $c + d$  at the front face of the column (corrected to the column centerline), the computed strengths in negative and positive unbalanced moment are 6.85 and 6.31 kN-m (60.6 and 55.9 kip-in.). Comparing these strengths with those for formation of yield lines across the slab width, it appears the connection should fail in the torsional mode when subjected to negative unbalanced moment. The closeness between computed strengths for the two failure modes for positive bending moment precludes predetermining the failure mode. Examination of the test structure following the tests revealed some torsional distress, and the formation of yield lines on the bottom slab surface at the face of edge beams (Fig. 4.38 and 4.39).

For the exterior component [56], calculated strengths in negative and positive unbalanced moment are 6.28 and 5.64 kN-m (55.6 and 49.9 kip-in.). Failure occurred in the torsional mode while subjected to negative moment. The ratio between calculated and measured strength is 0.86. Owing to the failure under negative unbalanced moment, the ultimate positive moment capacity was not reached during the tests. The maximum measured positive moment was 78 percent of calculated capacity.

(c) Strength of Columns

Column strengths were computed as described in Section 7.4(a). Computed ultimate flexural capacities are 9.93, 9.44, 9.44, and 9.13 kN-m (87.9, 83.5,

83.5, and 80.8 kip-in.) for first-floor interior, first-floor exterior, second-floor interior, and second-floor exterior columns, respectively.

(d) Strength of the Test Structure

Given the capacities of the components (and assuming component capacities are realized simultaneously in the structure), total strength of the structure under any given loading can be calculated using simple limit analysis. The process of estimating strength during earthquake loadings is complicated because the lateral load distribution changes rapidly with time, as discussed in Section 5.3c. During the effectively elastic tests, it was typical for the second-floor lateral force to be approximately twice the first-floor force at times of peak response. During the last tests, when base-shear capacities were apparently achieved, the lateral forces tended to be distributed approximately uniformly over height at times of peak base forces. Similar observations have been made previously from experimental [30] and analytical [10] data.

Because strength of a structure under lateral load varies with the distribution of lateral forces, it is logical that strength estimates should be made using lateral loads typical of those occurring at times of peak base forces. Thus, equal lateral loads will be assumed at the centerline of each floor level. Using this load distribution, base shear capacity can be calculated using limit analysis assuming all components are at capacities simultaneously. Using calculated component capacities (strength of interior connections based on the value obtained from the Hawkins beam analogy), computed base shear capacity is 159 kN (35.6 kips). This is 91 percent of the maximum measured value of 175 kN (39.3 kip).

That the measured strength exceeds the calculated strength is not

unexpected. Higher apparent capacity of the test structure could arise from many sources, including (1) imperfections in the theory used to compute component strengths, (2) strain rate effects, (3) strain hardening of reinforcement, (4) redistribution of internal actions, (5) inaccuracies in assumed critical lateral load distribution, and (6) membrane action which is more effective in continuous structures than in isolated components. Considering only inaccuracies in the theories, it was noted in Section 7.5(a) and 7.5(b) that measured interior and exterior slab-column connection strengths exceeded calculated strengths by 14 and 16 percent, respectively. If corresponding strengths for the limit analysis are amplified by these percentages, computed structure strength increases to 166 kN (37.3 kip), which is 95 percent of measured capacity. Any one of the other factors alone could conceivably account for the remaining overstrength.

The computed collapse mechanism (Fig. 7.7) is consistent with the pattern of damage and yield in reinforcement. During the tests, yield occurred predominantly in the slab and in the columns at the base, although yield was also indicated for upper interior columns. Apparently, strength of the slab exceeded that of the columns at top floor interior connections. Formation of slab positive moment yield lines near midspan was not apparent from the experiments, and was not indicated in the analysis.

The close correlation between measured and calculated collapse quantities supports the validity of existing analysis methods. Considering the simplicity and accuracy of the procedure, it is concluded that limit analysis is a suitable means of investigating upper bound lateral loads for seismic design and determining likely patterns of plastic hinges.

## 7.6 Interpretation of Test-Structure Overstrength

The test structure was designed according to conventional practice as documented in Chapter 2 of this report. Based on requirements of the UBC [50], the design base shear (without load factors) was  $0.053W$ , where  $W$  = structure self weight. During the dynamic experiments, the maximum measured base shear was equal to  $0.84W$ . Thus, the structure demonstrated a base shear capacity approximately 16 times the design capacity. The significant magnitude of this overstrength may be cause for concern relative to the accuracy and consequences of current building design provisions. To arrive at an understanding of the source of the overstrength, an analysis was conducted to determine the influence of various factors on strength. The analysis begins with the service level design forces, and follows sequentially through various factors that resulted in the overstrength. Results of the analysis are discussed in this section. Refer to Table 7.1 for a numerical summary of the analysis.

Analysis A: The test structure was designed using the static lateral force method of the UBC. For zone 2 of the UBC, the design base shear is 11.6 kN (2.61 kips). If the structure is analyzed for the code forces using the effective beam width model with effective width factor of 0.54, column and connection service load moments are as tabulated for Analysis A in Table 7.1. If the test structure is assumed to possess strengths equal to those given in Table 7.1, and a limit analysis is conducted using the inverted triangular lateral load distribution, the computed base-shear capacity is equal to the design value of 11.6 kN (2.61 kips), as it must be. However, if a uniform distribution of lateral loads is assumed for the limit analysis (as was measured during the last several earthquake simulations) the theoretical base-shear capacity is increased by 11 percent. Thus, it is noted that the

lateral-load distribution influences lateral-load strength.

Analysis B: Design of the test structure required consideration of simultaneous effects of gravity and seismic loads. Seismic and gravity load effects are combined according to load combinations of ACI 318-83 (ultimate load effects equal to  $0.75[1.4 \times \text{dead} + 1.7 \times \text{live} + 1.87 \times \text{earthquake}]$ ). The resulting required moment capacities are tabulated for Analysis B in Table 7.1. It is noted that some element capacities are increased significantly, resulting in computed base-shear capacity that is 2.31 times the capacity determined for Analysis A. In part, the increase in capacity is attributable to the effective seismic load factor of  $0.75 \times 1.87 = 1.40$ . Extra strength arises from the combined gravity and seismic effects as follows: (1) Required interior connection strengths are boosted by the code requirement that gravity pattern loads be considered. (2) Exterior connection negative moments are boosted by unbalanced gravity moments, and design exterior positive moments are reduced to zero (because gravity-load effects predominate), with the net effect that the sum of exterior connection unbalanced positive and negative moment capacities is boosted significantly.

Analysis C: Proportions of the interior and exterior connections were selected to satisfy requirements of ACI 318-83. In Table 7.1, provided connection capacities (computed according to methods of ACI 318-83 and including capacity reduction factors) are tabulated for Analysis C. It is noted that exterior connection capacities are taken equal to flexural capacities of the column strip, whereas interior connection capacities are limited by eccentric shear stresses. (Column base moment capacities for Analysis C are unchanged from the required values tabulated for Analysis B.) For the tabulated strengths, computed base-shear capacity is boosted to 1.86 times that computed for Analysis B. The overstrength results from the

following: (1) Section A.9 of ACI 318-83 requires that design strengths associated with shear (unbalanced moment capacity of the interior connections is controlled by eccentric shear stress) be taken equal to factored strengths with seismic effect equal to twice the code seismic effect. The intention of this requirement is to force failure to the more ductile flexural mode. However, reinforcement detailing requirements of the same code section boosted slab flexural strength by an even greater margin, such that strength was controlled by eccentric shear. (2) Moderate overstrengths arise in the proportioning of all connections because of limitations in available reinforcement and section sizes.

Analysis D: Although not required by ACI 318-83 for frames in regions of moderate risk, columns were proportioned to ensure that column strengths would exceed slab column strip flexural strengths, with the intention that primary inelastic action would be limited to the slabs. Provided connection and column strengths for Analysis D are tabulated in Table 7.1. All strengths are computed according to ACI 318-83, and include capacity reduction factors. The computed base-shear capacity is boosted to 1.54 times the capacity obtained in Analysis C. It is concluded that capacity design of columns can have a significant effect on strength of a structure, particularly for low-rise structures.

Analysis E: ACI 318-83 requires that provided ultimate strengths (nominal strength reduced by a capacity reduction factor) exceed the required ultimate capacities determined for factored loads. If provided nominal strengths are considered (Analysis E) rather than provided ultimate strengths (Analysis D), the computed base-shear capacity is boosted to 1.26 times the capacity obtained in Analysis D.

Analysis F: All previous analyses were based on the slab carrying the full factored dead and live loads (ie.,  $0.75[1.4 \times \text{dead} + 1.7 \times \text{live}]$ ). For the experiments, the structure carried only dead load. The reduction in slab loads results in an increase in interior connection strengths, and increases the computed base-shear to 1.09 times the strength obtained in Analysis E.

Analysis G: All previous analyses were based on nominal material strengths. If nominal member/connection strengths are recomputed according to ACI 318-83, with measured material properties rather than design properties, computed base-shear strength is boosted to 1.09 times the capacity of Analysis F.

Analysis H: All previous analyses were based on strengths computed according to ACI 318-83. If connection and column capacities are computed according to the best procedures described in Section 7.5 of this report, computed base-shear capacity is boosted to 1.22 times the capacity obtained in Analysis G.

Analyses A through H, as described in the previous paragraphs, indicate several factors that influence the theoretical strength of the test structure. Some of the factors are likely to apply in seismic design of any flat-plate frame. Others are most significant in low-rise construction. Taken individually, the factors may not appear to be a great significance. However, it is noted that the effects are not additive, but multiplicative, such that a significant overstrength is possible by the successive application of each effect.

Analysis G is based on nominal element strengths computed according to procedures currently recommended by ACI 318-83. The computed base-shear strength by that analysis model is 74 percent of measured capacity. It is concluded that strength calculation procedures of ACI 318-83 provide a reasonably close estimate of real strength.

## 8. SUMMARY AND CONCLUSIONS

A combined experimental and analytical study was undertaken to examine the seismic response of reinforced concrete slab-column frames. In the course of the study, a slab-column frame was designed, fabricated, and tested on an earthquake simulator. Measured responses were discussed and compared with expectations of various analytical methods. Conclusions are drawn regarding overall performance characteristics, the design procedure, and the applicability of analytical methods. The study and its conclusions are summarized in this chapter.

### 8.1 Description of the Prototype Structure

A fictitious prototype slab-column frame was selected for detailed study (Fig. 1.1). The frame had two stories, with three bays in one direction and multiple bays in the transverse direction. A shallow spandrel beam spanned the perimeter of the floor slabs. There were no interior beams, drop panels, capitals, or slab shear reinforcement. The structure supported self weight plus 11.k kPa (60 psf) service live load. It was located in a region classified as seismic zone 2 by the Uniform Building Code (UBC, Reference 50).

The prototype structure was designed for combined gravity and seismic effects. The Direct Design Method of the ACI Building Code (ACI 318-83, Reference 7) was used to determine gravity-load effects. The UBC static lateral force procedure was used to determine seismic effects. All strengths and details were provided to satisfy requirements of ACI 318-83, including special provisions for frames and two-way slabs in regions of moderate seismic risk.

As determined in the design, the service level seismic base shear was

equal to  $0.053W$ , where  $W$  = self weight of the structure. Under this loading, computed lateral drift was 0.03 percent of structure height, a value well within accepted limits. Being a low-rise structure, total factored moments due to gravity loads alone were computed to be equal to factored moment due to combined gravity and seismic effects. Thus, seismic effects did not directly influence the total required slab reinforcement. However, reinforcement details were controlled by Appendix A of ACI 318-83, which pertains to two-way slabs in regions of moderate seismic risk. In particular, it is noted that slab reinforcement was banded near the column lines, and that minimum percentages of both top and bottom slab bars were continuous throughout the slab. In addition, column flexural strengths were made sufficiently large that primary inelastic action at slab-column connections was limited to the slab. The direct shear stress on the slab critical section at interior connections under the influence of factored gravity loads only was  $0.2\sqrt{f'_c}$  MPa ( $2.4\sqrt{f'_c}$  psi).

## 8.2 Description of the Test Structure and the Experiments

A test structure was selected to model the prototype structure at three-tenths of full scale. The test structure had three bays in one direction and "two" bays in the transverse direction (Fig. 1.2). It was constructed in a manner similar to that expected for a typical full-scale structure. All longitudinal reinforcement was deformed and had properties typical of Grade 60 reinforcement (minimum yield stress of 414 MPa [60 ksi]). Concrete had mean compression strength of 36 MPa (5300 psi). Nonstructural lead weights were affixed to floor slabs to increase slab and column gravity-load stresses to values expected for the full-scale prototype structure.

The test structure was mounted atop a stiff foundation frame that was

prestressed to the test platform of an earthquake simulator. Tests included free-vibration tests and earthquake simulation tests. During the earthquake simulations, base motions were imparted to the test structure with a single horizontal component parallel to the three-bay direction. Vertical base motions were input concurrently with some of the horizontal base motions. The base motions modeled records obtained in El Centro during the 1940 Imperial Valley Earthquake.

Several earthquake simulation tests were conducted. The first tests had intensities sufficiently low that no damage was noted. Intensities of later tests were sufficient to induce significant inelastic response. Continuous records of base motions, displacements, accelerations, reinforcement strains, and base forces were obtained for each test. Visible damage was recorded at the end of each test.

Experiments were also conducted on interior and exterior connections of the test structure. Observations from the connection experiments are used in this report to interpret behavior of the shaking table test structure. Complete details of these experiments are reported elsewhere [56].

### 8.3 Conclusions

Eleven earthquake simulation tests were conducted. Housner spectrum intensities [23] of horizontal base motions were computed for each, and a spectrum intensity ratio was defined as the ratio between spectrum intensity of a test and scaled spectrum intensity of the prototype El Centro, 1940, NS record. Spectrum intensity ratios varied from 0.03 for the first test to 2.71 for the last test.

The maximum spectrum intensity ratio for any of the first five earthquake

simulations was 0.21. During these tests, measured relations between base shear and top displacement were effectively linear elastic, and vibration periods and equivalent viscous damping ratios were unchanged from values measured before the onset of testing. It is concluded that negligible damage was induced by the first five tests.

The sixth earthquake simulation had peak horizontal base acceleration of 0.189 g and spectrum intensity ratio of 0.44 (there was no vertical base motion for this test). On the basis of these numbers, it is concluded that this test adequately represents the design test for a region classified as zone 2 by the UBC. Peak base shear was 0.28W, and maximum top-level displacement was 0.0027H. Although these values significantly exceed values anticipated by the design analysis, only limited inelastic action was observed. During a subsequent test, the same horizontal base motion was input with the corresponding vertical base motion. Maximum lateral drift and base shear were nearly double the values obtained from the previous test. Significant inelastic action was not observed.

The four last earthquake simulations had spectrum intensity ratios ranging between 0.89 and 2.71. Although the last two of the four test motions may have been unrealistically intense, the test structure survived without collapse. Maximum lateral drift reached 5.2 percent of structure height. Maximum base shear reached 0.84W. Yield was detected in reinforcement and was apparent in the overall load-displacement response of the test structure which indicated a nearly plastic response by the end of testing. Although visible damage suggested that torsional capacity of an edge beam and shear and unbalanced moment capacity of an interior connection had been reached, there was no apparent loss in overall structure resistance.

Although yield was detected in some reinforcement at lower drifts, significant yield in the overall structural shear-displacement relation was not apparent until lateral drifts reached approximately 1.5 percent of structure height. It was noted that it is typical in seismic design to limit lateral drifts to values near 1.5 percent. Thus, it is concluded that a well-designed slab-column frame having properties similar to the test structure would not be expected to experience severe inelastic response to a design earthquake.

The maximum lateral drift of  $0.052H$  during the last earthquake simulation is well beyond the maximum drift reasonably expected for a well-designed structure. Thus, the test structure demonstrates that reliably tough slab-column connections can be achieved given the proper design proportions and details. This conclusion is qualified by the fact that the test structure was subjected to base motions having only a single horizontal component. Response may have been less favorable under bidirectional horizontal base motions. Further research on this topic is recommended.

The maximum measured base shear of  $0.84W$  is approximately 16 times the service level design base shear. An analysis was conducted to determine the sources of overstrength. The following were identified as having contributed to the overstrength: lateral-load distribution, load factors, capacity-reduction factors, gravity-load design requirements, seismic proportioning requirements, column capacity design, differences between design and actual material properties, and inaccuracies in theories used to compute member strengths. The analysis is summarized in Section 7.6 of this report.

Measured vibration periods varied depending on (1) the amplitude of response during which the period was measured and (2) the maximum response

experienced by the structure prior to measurement of the vibration period. In general, vibration periods increased with increasing previous maximum displacement. The change in period was shown to be related approximately to the change in secant stiffness during the previous maximum response.

Equivalent viscous damping was determined from the logarithmic decrement of measured low-amplitude free-vibration responses. Before testing, damping was measured to be approximately 2 percent of critical damping. Damping increased with increasing state of apparent damage. Following the last earthquake simulation, damping was approximately 7 percent of critical. It is noted that damping values given in this paragraph were effective during the low-amplitude tests from which they were determined. The same values may not be applicable at different response amplitudes.

Lateral-load stiffness was observed to be a function of load history. Analyses indicated that overall lateral-load stiffness was reduced by less than ten percent as a consequence of placing subsidiary lead weights on the slab surface. The reduction is attributed in part to slab cracking due to gravity-induced stresses. Lateral-load stiffness at working loads was notably less than initial stiffness.

Lateral-load stiffness was examined using the effective beam width model and the equivalent frame model. It was found that the effective beam width model (using theoretical elastic effective beam widths) was too stiff to model initial stiffness. Reductions of effective beam widths to between one-third and one-half the theoretical elastic values was required to match effective stiffnesses. The equivalent frame model matched initial stiffness closely, but was too stiff for lateral drifts equal to  $0.005H$ , a drift often cited as an elastic drift limit for code service-level seismic forces. The equivalent

frame matched stiffness at that drift limit if slab-beam inertia was reduced to one-third of the gross-section inertia. An equivalent frame model is described that was capable of modeling the change in lateral stiffness with increasing lateral drift.

Maximum responses to simulated earthquakes was interpreted using elastic response spectrum techniques. Effectively elastic measured responses correlated well with responses computed using elastic equivalent frame or effective beam width models. For inelastic responses, it was found that maximum displacement responses compared well with computed responses if the period was selected to match the period measured during the maximum response and if equivalent viscous damping between five and ten percent of critical was assumed.

Behavior of isolated slab-column connections under slowly-reversing lateral loads was observed to be similar to behavior of the connections within the test structure. Visible damage was similar, and by combining measured connection behaviors using conventional plane-frame modeling techniques, it was possible to reconstruct the overall load-displacement relation of the complete structure. However, whereas failure of a connection in an isolated connection test resulted in sudden loss of capacity, apparent failure of a connection in the test structure did not result in an apparent loss in overall structure capacity. The latter phenomenon is attributed to the capacity for redistribution between connections in the complete structure.

Strengths of connections and of the complete structure were studied using existing analytical methods. Unbalanced moment strengths of connections could be reconciled closely with some of the analytical methods. Using these methods, it was possible to account for 90 percent of measured structure base-

shear strength. Using calculation procedures given in the ACI Building Code, computed strength was 74 percent of measured strength. It is concluded that currently available analytical techniques can be used to obtain a reasonably close estimate of real strength of slab-column structures.

## REFERENCES

1. Akiyama, H., and Hawkins, N. M., "Response of Flat-Plate Concrete Structures to Seismic and Wind Forces," Structures and Mechanics Report SM 84-1, University of Washington, Seattle, July 1984, 267 pp.
2. Algan, B. B., "Drift and Damage Considerations in Earthquake-Resistant Design of Reinforced Concrete Buildings," Ph. D. Thesis, Graduate College, University of Illinois at Urbana-Champaign, Urbana, Illinois, 1982, also available from University Microfilms International, Ann Arbor, Michigan, 1983, 481 pp.
3. Algermissen, S. T., An Introduction to the Seismicity of the United States, Earthquake Engineering Research Institute, Berkeley, California, August 1983, 148 pp.
4. "Anchorage and the Alaska Earthquake," American Iron and Steel Institute, New York, 1964.
5. Bertero, V. V., Clough, R. W., and Oliva, M., "Use of Earthquake Simulators and Large-Scale Loading Facilities in ERCBC," Proceedings of a Workshop on Earthquake-Resistant Reinforced Concrete Building Construction, University of California, Berkeley, July 11-15, 1977, pp. 1652-1681.
6. Building Code Requirements for Reinforced Concrete (ACI 318-77), American Concrete Institute, Detroit, 1977, 102 pp.
7. Building Code Requirements for Reinforced Concrete (ACI 318-83), American Concrete Institute, Detroit, 1983, 111 pp.
8. "Building Collapse Blamed on Design, Construction," Engineering News Record, July 15, 1971, p. 19.
9. Cecen, H., "R/C Frame Models: Observed Seismic Response," Journal of Structural Engineering, ASCE, Vol. 110, No. 12, Dec. 1984, pp. 3015-3030.
10. Charney, F. A., and Bertero, V. V., "An Evaluation of the Design and Analytical Seismic Response of a Seven-Story Reinforced Concrete Frame-Wall Structure," Report No. UCB/EERC-82/08, Earthquake Engineering Research Center, University of California, Berkeley, August 1982, 176 pp.
11. Chopra, A. K., Dynamics of Structures: A Primer, Earthquake Engineering Research Institute, Berkeley, California, 1981, 126 pp.
12. Commentary on Building Code Requirements for Reinforced Concrete (ACI 318-83), American Concrete Institute, Detroit, 1983, 155 pp.
13. Darvall, P., and Allen, F., "Lateral Load Effective Width of Flat Plates with Drop Panels," ACI Journal, Vol. 81, No. 6, Nov.-Dec., 1984, pp. 613-617.

14. DiStasio, J., and Van Buren, M. P., "Transfer of Bending Moment Between Flat Plate Floor and Column," ACI Journal, Vol. 57, No. 3, Sept., 1960, pp. 299-314.
15. Earthquake Effects on Reinforced Concrete Structures, U. S.-Japan Research," SP-84, American Concrete Institute, Detroit, 1985, 440 pp.
16. Ghali, A., Elmasri, M. Z., and Dilger, W., "Punching of Flat Plates Under Static and Dynamic Horizontal Forces," ACI Journal, Vol. 76, No. 10, Oct. 1979, pp. 566-572.
17. Gulkan, P., and Sozen, M. A., "Inelastic Responses of Reinforced Concrete Structures to Earthquake Motions," ACI Journal, Vol. 71, No. 12, Dec. 1974, pp. 604-610.
18. Hartley, G., Rainer, J. H., and Ward, H. S., "Static and Dynamic Properties of a Reinforced Concrete Building Model," Building Research No. 140, Division of Building Research, National Research Council of Canada, Ottawa, April 1979.
19. Hawkins, N. M., "Lateral Load Design Considerations for Flat-Plate Structures," Nonlinear Design of Concrete Structures, CSCE-ASCE-ACI-CEB International Symposium, University of Waterloo, Ontario, Canada, Aug. 7-9, 1979, pp. 581-614.
20. Hawkins, N. M., "Seismic Response Constraints for Slab Systems," Proceedings of a Workshop on Earthquake-Resistant Reinforced Concrete Building Construction, University of California, Berkeley, July 11-15, 1977, pp. 1253-1275.
21. Hawkins, N. M., "Shear Strength of Slabs with Moments Transferred to Columns," SP-42, Shear in Reinforced Concrete, American Concrete Institute, Detroit, 1973, pp. 817-846.
22. Hawkins, N. M., and Mitchell, D., "Progressive Collapse of Flat-Plate Structures," ACI Journal, Vol. 76, No. 7, July 1979, pp. 775-808.
23. Housner, G. W., "Behavior of Structures During Earthquakes," Journal of the Engineering Mechanics Division, ASCE, Vol. 85, No. EM4, Oct. 1959, pp. 108-129.
24. Jirsa, J. O., Baumgartner, J. L., and Mogbo, N. C., "Torsional Strength and Behavior of Spandrel Beams," ACI Journal, Vol. 66, No. 11, Nov. 1969, pp. 926-932.
25. Kabe, A. M., and Rea, D., "Inelastic Earthquake Response of Steel Structures," Journal of Structural Engineering, ASCE, Vol. 109, No. 3, March 1983, pp. 705-720.
26. Kent, D. C., and Park, R., "Flexural Members with Confined Concrete," Journal of the Structural Division, ASCE, Vol. 97, No. ST7, July 1971, pp. 1969-1990.

27. Konah, Y., and Yoshizaki, S., "Strength of Slab-Column Connections Transferring Shear and Moment," ACI Journal, Vol. 76, No. 3, March 1979, pp. 461-478.
28. Lampert, P., and Collins, M. P., "Torsion, Bending, and Confusion - An Attempt to Establish the Facts," ACI Journal, Vol. 69, No. 8, August, 1972, pp. 500-504.
29. Long, A. E., and Kirk, D. W., "Lateral Load Stiffness of Slab-Column Structures," SP-63, Reinforced Concrete Structures Subjected to Wind and Earthquake Forces, American Concrete Institute, Detroit, 1980, pp. 197-220.
30. Moehle, J. P., "Seismic Response of Vertically Irregular Structures," Journal of Structural Engineering, ASCE, Vol. 110, No. 9, Sept. 1984, pp. 2002-2014.
31. Moehle, J. P., "Strong Motion Drift Estimates for R/C Structures," Journal of Structural Engineering, ASCE, Sept. 1984. pp 1988-2001.
32. Moehle, J. P., and Sozen, M. A., "Experiments to Study Earthquake Response of R/C Structures with Stiffness Interruptions," Civil Engineering Studies, Structural Research Series No. 482, University of Illinois at Urbana-Champaign, Urbana, Illinois, August 1980, 421 pp.
33. Morrison, D. G., Hirasawa, I., and Sozen, M. A., "Lateral-Load Tests of R/C Slab-Column Connections," Journal of Structural Engineering, ASCE, Vol. 109, No. 11, Nov. 1983, pp. 2698-2714.
34. Morrison, D. G., and Sozen, M. A., "Response of Reinforced Concrete Plate-Column Connections to Dynamic and Static Horizontal Loads," Civil Engineering Studies, Structural Research Series No. 490, University of Illinois at Urbana-Champaign, Urbana, Illinois, April 1981, 560 pp.
35. Mulcahy, J. F., and Rotter, J. M., "Moment Rotation Characteristics of Flat Plate and Column Systems," ACI Journal, Vol. 80, No. 2, March-April, 1983, pp. 85-92.
36. Newmark, N. M., and Rosenblueth, E., Fundamentals of Earthquake Engineering, Prentice-Hall, Inc., Englewood Cliffs, New Jersey, 1971.
37. Park, R., and Islam, S., "Strength of Slab-Column Connections with Shear and Unbalanced Flexure," Journal of the Structural Division, ASCE, Vol. 102, No. ST9, Sept. 1976, pp. 1879-1901.
38. Park, R., Priestly, M. J. N., and Gill, W. D., "Ductility of Square-Confined Concrete Columns," Journal of the Structural Division, ASCE, Vol. 108, No. ST4, April 1982, pp. 929-950.
39. Pecknold, D. A., "Slab Effective Width for Equivalent Frame Analysis," ACI Journal, Vol. 72, No. 4, April 1975, pp. 135-137.
40. Rangan, B. V., and Hall, A. S., "Moment and Shear Transfer Between Slab and Edge Column," ACI Journal, Vol. 80, No. 3, May-June 1983, pp. 183-191.

41. Research Facilities at the Richmond Field Station of the Earthquake Engineering Research Center, EERC, University of California, Berkeley, May 1974.
42. "San Fernando, California, Earthquake of February 9, 1971," U. S. Department of Commerce, National Oceanic and Atmospheric Administration, Washington, D. C., 1973, Building Reports 29 and 30, John Blume and Associates, Vol. 1, Part A, pp. 359-422.
43. "The Shear Strength of Reinforced Concrete Members - Slabs," reported by ASCE-ACI Committee 426, Journal of the Structural Division, ASCE, Vol. 100, No. ST8, August 1974, pp. 1543-1591.
44. Sheu, M. S., and Hawkins, N. M., "Grid Model for Predicting the Monotonic and Hysteretic Behavior of Slab-Column Connections Transferring Moments," SP-63, Reinforced Concrete Structures Subjected to Wind and Earthquake Forces, American Concrete Institute, Detroit, 1980, pp. 79-112.
45. Shibata, A., and Sozen, M. A., "Substitute Structure Method for Seismic Design in R/C," Journal of the Structural Division, ASCE, Vol. 102, No. ST1, Jan. 1976, pp. 1-18.
46. Sozen, M. A., "Lateral Drift of Reinforced Concrete Structures Subjected to Strong Ground Motions," Proceedings, Third South Pacific Regional Conference on Earthquake Engineering, Wellington, New Zealand, 9-12 May, 1983.
47. "Strong Motion Earthquake Accelerograms," Report No. EERL 71-50, Earthquake Engineering Research Laboratory, California Institute of Technology, Pasadena, California, Vol. 2, Part A, Sept. 1971, pp. 32-34.
48. Sudhakar, A., "Computer Program for Small Displacement Elasto-Plastic Analysis of Plane Steel and Reinforced Concrete Frames," CE 299 Report No. 561, Division of Structural Engineering and Structural Mechanics, Department of Civil Engineering, University of California, Berkeley, Dec. 1972.
49. "Test of a Concrete Floor Reinforced in Two Directions," Proceedings ACI, Vol. 8, 1912, pp. 132-157.
50. Uniform Building Code, International Conference of Building Officials, Whittier, California, 1982, 780 pp.
51. Van Greunen, J., "Nonlinear Geometric, Material, and Time Dependent Analysis of Reinforced and Prestressed Concrete Slabs and Panels," Structural Research Report No. UCB/SESM 79-3, University of California, Berkeley, Oct. 1979.
52. Vanderbilt, M. D., and Corley, W. G., "Frame Analysis of Concrete Buildings," Concrete International, American Concrete Institute, Dec. 1983, pp. 33-43.
53. "The Venezuela Earthquake, July 29, 1967," American Iron and Steel Institute, New York, 1969.

54. Wilson, E. L., "The SAP-80 Series of Structural Analysis Programs," Version 84.00, SAP, Incorporated, El Cerrito, California, Jan. 1983.
55. Yamazaki, J., and Hawkins, N. M., "Finite Element Predictions of the Behavior of Slab-Column Connections Transferring Moment," SP-63, Reinforced Concrete Structures Subjected to Wind and Earthquake Forces, American Concrete Institute, Detroit, 1980, pp. 49-78.
56. Zee, H. L., and Moehle, J. P., "Behavior of Interior and Exterior Flat-Plate Connections Subjected to Inelastic Load Reversals," Report No. UCB/EERC-84/07, Earthquake Engineering Research Center, University of California, Berkeley, Aug. 1984.

Table 2.1 Required and Provided Slab Reinforcement

Required Moment, kN-m		Required steel ratio	Required number of bars	Supplied number of bars	Supplied steel ratio	Supplied Moment, kN-m
Column Strip:						
Edge	2.95	0.0037	10.3	14.	0.0050	3.97
Midspan	2.09	0.0026	7.4	8.	0.0028	2.31
Interior	3.95	0.0049	13.7	14.	0.0050	3.97
Middle Strip:						
Edge	0.08	0.0018*	5.1	8.	0.0028	2.31
Midspan	1.41	0.0018*	5.1	8.	0.0028	2.31
Interior	1.33	0.0018*	5.1	8.	0.0028	2.31

Strength Properties and Dimensions Assumed for Design

concrete compressive strength = 27,600 kN/m<sup>2</sup>  
 steel yield stress. . . . . = 414,000 kN/m<sup>2</sup>

section width . . . . . = 0.914 m  
 depth to tensile steel. . . . = 0.0495 m  
 Area of slab bar. . . . . = 16 mm<sup>2</sup>

\* This required steel ratio is based on the limiting value for temperature and shrinkage control, and to keep the spacing between bars in critical regions below 122 mm (4.8 in).

Table 2.2 Direct Shears and Unbalanced Moments Used in Design

Location/Action	Load Combination		
	$U_g = 1.4D + 1.7L$	$0.75(U_g + 1.87E)$	$0.75(U_g + 1.87[2E])$
Exterior Shear, kN	19.2	15.2	16.0
Interior Shear, kN	38.3	28.7	28.8
Exterior Moment, kN-m	4.25	3.94	4.69
Interior Moment, kN-m	0.89	2.07	3.48

Table 3.1 Test Sequence

Designation	Description
FV0.A	Free Vibration, at Construction Location, w/o Lead Weight
FV0.B	Free Vibration, at Construction Location, w/o Lead Weight
FV0.C	Free Vibration, on Test Platform, w/o Lead Weight, Blocked
FV0.D	Free Vibration, on Test Platform, with Lead Weight, Blocked
FV0.E	Free Vibration, on Test Platform, with Lead Weight, Blocked
FV0.F	Free Vibration, on Test Platform, with Lead Weight, Unblocked
FV0.G	Free Vibration, on Test Platform, with Lead Weight, Unblocked
EQ1	Earthquake Simulation, 0.015 g Horizontal
FV1*	Free Vibration
EQ2	Earthquake Simulation, 0.012 g Horizontal, 0.005 g Vertical
FV2	Free Vibration
EQ3	Earthquake Simulation, 0.047 g Horizontal
FV3	Free Vibration
EQ4	Earthquake Simulation, 0.048 g Horizontal
FV4	Free Vibration
EQ5	Earthquake Simulation, 0.092 g Horizontal
FV5	Free Vibration
EQ6	Earthquake Simulation, 0.189 g Horizontal
FV6	Free Vibration
EQ7	Earthquake Simulation, 0.202 g Horizontal, 0.042 Vertical
FV7	Free Vibration
EQ8	Earthquake Simulation, 0.284 g Horizontal
FV8	Free Vibration
EQ9	Earthquake Simulation, 0.252 g Horizontal, 0.106 g Vertical
FV9	Free Vibration
EQ10	Earthquake Simulation, 0.606 g Horizontal
FV10	Free Vibration
EQ11	Earthquake Simulation, 0.827 g Horizontal, 0.197 g Vertical
FV11	Free Vibration

\* All free vibration tests following earthquake simulations are on test platform with lead weights and table unblocked.

Table 4.1 Peak Values Recorded During Earthquake Simulations

Test No.	Acceleration (g)				Displacement (mm)		Base Shear (kN)	Base Moment (kN-m)
	Second Floor	First Floor	Base Horiz.	Base Vert.	Second Floor	First Floor		
EQ1	0.0251	0.0189	0.015	0.004	*	*	4.07	6.54
EQ2	0.0240	0.0182	0.012	0.005	*	*	4.13	6.53
EQ3	0.0898	0.0728	0.047	0.004	*	*	16.1	25.0
EQ4	0.0901	0.0626	0.048	0.005	1.05	0.64	15.5	23.7
EQ5	0.160	0.135	0.092	0.009	2.06	1.16	30.6	44.8
EQ6	0.348	0.284	0.189	0.015	5.11	2.95	61.9	91.2
EQ7	0.494	0.413	0.202	0.042	9.86	5.76	93.3	140.
EQ8	0.734	0.665	0.284	0.065	20.4	12.0	137.	199.
EQ9	0.832	0.681	0.252	0.102	29.7	16.9	148.	230.
EQ10	1.04	0.860	0.606	0.106	61.9	35.1	165.	268.
EQ11	1.08	0.785	0.827	0.197	95.5	56.6	175.	272.

\* Value too small to read accurately.

Table 4.2 Spectrum Intensities for Horizontal Base Motions, meter

Test No.	Damping, Percent of Critical				
	0	2	5	10	20
EQ1	0.0265	0.0176	0.0140	0.0112	0.00834
EQ2	0.0260	0.0172	0.0137	0.0109	0.00821
EQ3	0.0902	0.0597	0.0472	0.0377	0.0283
EQ4	0.0893	0.0588	0.0464	0.0372	0.0280
EQ5	0.183	0.119	0.0938	0.0752	0.0569
EQ6	0.392	0.256	0.202	0.161	0.121
EQ7	0.397	0.257	0.203	0.162	0.122
EQ8	0.779	0.509	0.404	0.325	0.244
EQ9	0.775	0.506	0.399	0.321	0.242
EQ10	1.77	1.14	0.906	0.725	0.539
EQ11	2.44	1.57	1.24	0.997	0.744

Table 4.3 Maximum Strain Gage Readings During Earthquake Simulations

Gage No.	Test Number										
	EQ1 (x10 <sup>-5</sup> )	EQ2 (x10 <sup>-5</sup> )	EQ3 (x10 <sup>-5</sup> )	EQ4 (x10 <sup>-5</sup> )	EQ5 (x10 <sup>-5</sup> )	EQ6 (x10 <sup>-4</sup> )	EQ7 (x10 <sup>-4</sup> )	EQ8 (x10 <sup>-4</sup> )	EQ9 (x10 <sup>-4</sup> )	EQ10 (x10 <sup>-3</sup> )	EQ11 (x10 <sup>-3</sup> )
1	6.0	9.2	20.	23.	49.	11.	17.	45.	93.	**	**
2	3.9	6.0	21.	15.	41.	11.	19.	61.	92.	**	**
3	2.8	2.8	6.6	5.9	9.9	9.1	18.	55.	129.	**	**
4	3.1	4.5	8.4	5.6	12.	9.5	19.	68.	95.	**	**
5	2.3	4.0	5.3	3.7	7.9	2.8	11.	23.	23.	6.4	11.
6	2.7	3.1	7.4	4.9	8.8	2.2	5.3	16.	22.	2.8	3.5
7	1.9	1.8	4.2	4.2	6.3	1.5	2.3	9.6	11.	1.6	1.7
8	1.6	4.0	4.4	4.5	5.9	1.2	1.8	5.6	6.2	0.93	1.1
9	2.4	3.3	7.4	6.6	12.	5.6	9.5	20.	25.	12.	23.
10	2.6	2.8	5.9	5.6	10.	4.6	8.0	18.	32.	14.	17.
11	3.2	3.6	10.	8.1	16.	5.3	13.	26.	40.	15.	19.
12	2.6	3.6	6.9	5.7	10.	2.9	3.4	8.8	12.	3.6	8.8
13	3.4	2.3	5.7	5.1	9.4	1.9	2.5	7.5	12.	3.4	30.
14	5.0	6.5	9.5	9.1	13.	3.9	11.	24.	27.	14.	25.
15	3.3	2.3	7.1	5.9	9.8	4.2	7.9	15.	19.	8.5	9.1
16	3.0	4.2	6.9	4.9	12.	5.0	7.6	13.	15.	2.5	4.8
17	2.8	2.7	4.3	5.3	5.8	1.3	1.9	9.7	16.	3.3	7.6
18	3.6	2.2	4.6	3.4	5.6	0.78	1.1	2.2	3.1	0.12	0.37
19	2.7	2.3	4.4	3.7	6.3	1.4	1.8	3.9	3.2	0.45	0.56
20	***	***	***	***	***	***	***	***	***	***	***
21	2.5	2.4	3.6	3.2	4.9	1.5	2.7	6.5	9.5	1.6	1.6
22	3.0	2.9	4.1	3.3	6.3	1.6	3.0	6.0	6.6	1.1	1.3

\* See Fig. B. for gage locations.  
 \*\* indicates gage fractured during test.  
 \*\*\* indicates malfunctioning gage.

Table 5.1 Vibration Periods and Damping Ratios of the Test Structure

Test No.	Vibration Period (sec)				Damping (% of critical)
	EQ Simulation*		Free Vibration**		Free Vibration
	Mode 1	Mode 1    Mode 2	Mode 1    Mode 2	Mode 1	
0.A			0.116    0.0316		
0.B			0.115    -----		
0.C			0.121    0.0329		
0.D			0.210    0.0593		
0.E			0.204    0.0594		
0.F			0.210    0.0601		
0.G			0.211    0.0612		
1		0.219    0.0572	0.214    0.0617	1.5	
2		0.220    0.0588	0.220    0.0615	1.1	
3		0.224    0.0596	0.208    0.0616	1.3	
4	0.227	0.224    -----	0.205    0.0615	1.5	
5	0.236	0.229    -----	0.210    0.0620	1.4	
6	0.256	0.270    -----	0.226    0.0658	2.5	
7	0.281	0.280    0.0978	0.237    0.0687	2.3	
8	0.339	0.348    0.111	0.268    0.0754	2.7	
9	0.390	0.406    0.131	0.314    0.0809	4.9	
10	0.540	0.566    0.119	0.449    0.104	4.9	
11	0.683	0.745    0.149	0.576    0.124	7.1	

\* Vibration period estimated as the time between three successive zero crossings of the top level displacement during the peak response cycle.

\*\* Vibration period estimated from peaks on Fourier Amplitude spectra of first floor acceleration responses.

Table 6.1 Computed Mode Shapes and Periods<sup>a</sup>

Modal Para- meter <sup>b</sup>	Analysis A		Analysis B		Analysis C		Analysis D		Analysis E	
	Mode 1	Mode 2								
x <sub>2</sub>	1.000	1.000	1.000	1.000	1.000	1.000	1.000	1.000	1.000	1.000
x <sub>1</sub>	0.517	-1.935	0.445	-2.249	0.454	-2.202	0.517	-1.935	0.464	-2.155
x <sub>f</sub>	0.060	-0.408	0.000	0.000	0.004	-0.031	0.060	-0.408	0.045	-0.441
x <sub>t</sub>	0.027	-0.196	0.000	0.000	0.000	0.000	0.027	-0.196	0.020	-0.211
T, sec	0.102	0.0284	0.163	0.0450	0.165	0.0456	0.179	0.0498	0.213	0.0534

a See Section 6.4 and 6.5 for description of the models.

b  
 x<sub>2</sub> = ordinate of mode shape at second slab level.  
 x<sub>1</sub> = ordinate of mode shape at first slab level.  
 x<sub>f</sub> = ordinate of mode shape at top of footing.  
 x<sub>t</sub> = ordinate of mode shape at top of transducer.  
 T = vibration period.

Table 6.2 Comparison Between Measured and Calculated Top Slab Driftsa

Test	Damping Ratio, Percent of Critical		
	2	5	10
"Experimental Model" <sup>b</sup>			
EQ4	1.24 (1.19)	0.82 (0.78)	0.61 (0.58)
EQ5	3.14 (1.53)	2.10 (1.02)	1.77 (0.86)
EQ6	12.8 (2.50)	9.09 (1.78)	6.61 (1.29)
EQ7	10.7 (1.08)	9.26 (0.94)	7.74 (0.78)
EQ8	32.0 (1.57)	27.3 (1.34)	22.4 (1.10)
EQ9	44.4 (1.50)	28.1 (0.95)	21.8 (0.73)
EQ10	130. (2.11)	103. (1.66)	70.6 (1.14)
EQ11	156. (1.63)	124. (1.30)	95.9 (1.00)
"Equivalent Frame Model" <sup>b</sup>			
EQ1	0.28 (----) <sup>c</sup>	0.23 (----) <sup>c</sup>	0.19 (----) <sup>c</sup>
EQ2	0.27 (----) <sup>c</sup>	0.23 (----) <sup>c</sup>	0.20 (----) <sup>c</sup>
EQ3	0.99 (----) <sup>c</sup>	0.84 (----) <sup>c</sup>	0.77 (----) <sup>c</sup>
EQ4	1.00 (0.95)	0.82 (0.79)	0.65 (0.62)
EQ5	2.51 (1.22)	1.78 (0.87)	1.73 (0.84)
EQ6	8.65 (1.69)	6.82 (1.33)	5.34 (1.04)

a Calculated values are shown with ratios between calculated and measured values given in parenthesis.  
b See Chapter 6 for description of the models.  
c Values too small to be measured accurately.

Table 7.1 Capacities Used in Limit Analysis

Quantity	Analysis A	Analysis B	Analysis C	Analysis D	Analysis E	Analysis F	Analysis G	Analysis H
<b>First-Floor Column</b>								
Strengths, kN-m								
Interior:	0.92 (1.00)	1.29 (1.40)	1.29 (1.40)	6.60 (7.17)	8.64 (9.40)	8.02 (8.72)	9.13 (9.93)	9.93 (10.80)
Exterior:	0.83 (1.00)	1.17 (1.40)	1.17 (1.40)	6.00 (7.22)	7.44 (8.95)	7.12 (8.57)	8.09 (9.74)	9.44 (11.36)
<b>First-Floor Connection</b>								
Strengths, kN-m								
Interior:	1.01 (1.00)	2.09 (2.06)	4.44 (4.39)	4.44 (4.39)	6.03 (5.96)	8.10 (8.00)	9.70 (9.58)	11.29 (11.15)
Exterior (+):	0.54 (1.00)	0.00 (0.00)	2.69 (4.99)	2.69 (4.99)	2.98 (5.53)	2.98 (5.53)	3.14 (5.83)	6.09 (11.30)
(-):	0.54 (1.00)	3.96 (7.35)	4.62 (8.57)	4.62 (8.57)	5.13 (9.52)	5.13 (9.52)	5.39 (10.0)	6.85 (12.70)
<b>Second-Floor Connection</b>								
Strengths, kN-m								
Interior:	0.67 (1.00)	1.61 (2.40)	4.44 (6.63)	4.44 (6.63)	6.03 (9.01)	8.10 (12.1)	8.10 (12.1)	9.44 (14.08)
Exterior (+):	0.38 (1.00)	0.00 (0.00)	2.69 (7.17)	2.69 (7.17)	2.98 (7.95)	2.98 (7.95)	3.14 (8.37)	6.09 (16.23)
(-):	0.38 (1.00)	3.73 (9.94)	4.62 (12.3)	4.62 (12.3)	5.13 (13.7)	5.13 (13.7)	5.39 (14.4)	6.85 (18.25)
<b>Base-Shear</b>								
Strength, kN								
Triangular Load:	11.6 (1.00) [0.07]	26.8 (2.31) [0.15]	49.9 (4.30) [0.29]	77.0 (6.64) [0.44]	97.1 (8.36) [0.55]	106. (9.10) [0.61]	117. (10.0) [0.67]	142. (12.2) [0.81]
Uniform Load:	12.9 (1.11) [0.07]	29.8 (2.57) [0.17]	55.6 (4.79) [0.32]	85.8 (7.39) [0.49]	108. (9.32) [0.62]	118. (10.2) [0.67]	130. (11.2) [0.74]	158. (13.6) [0.90]

Note: \* See Section 7.6 for a description of the analyses.

\* Values given in parentheses ( ) are ratios between computed strength and strength required for UBC service loads.

\* Values given in brackets [ ] are ratios between computed base shear strength and measured base shear strength.

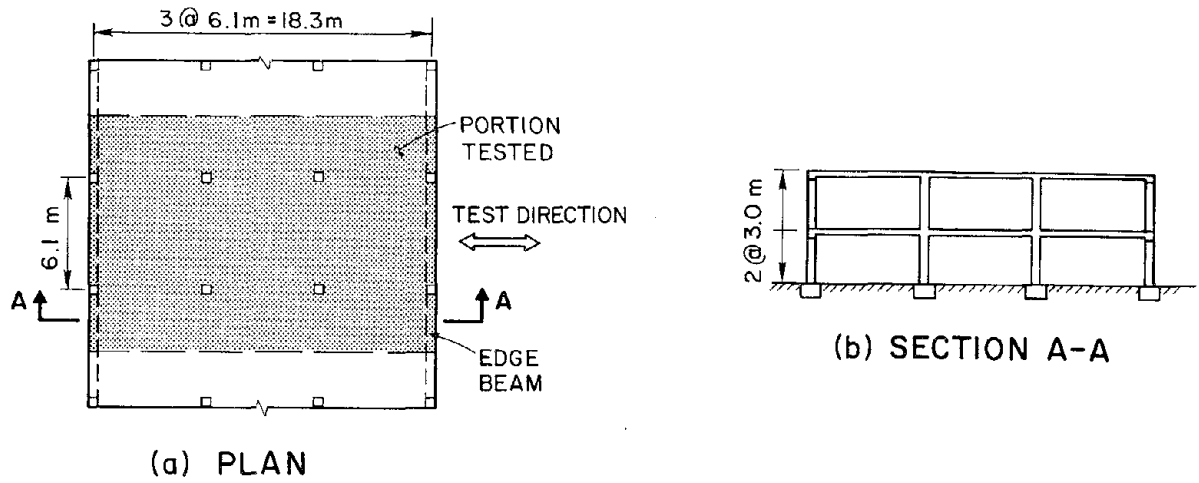


Fig. 1.1 Plan and Section View of Prototype

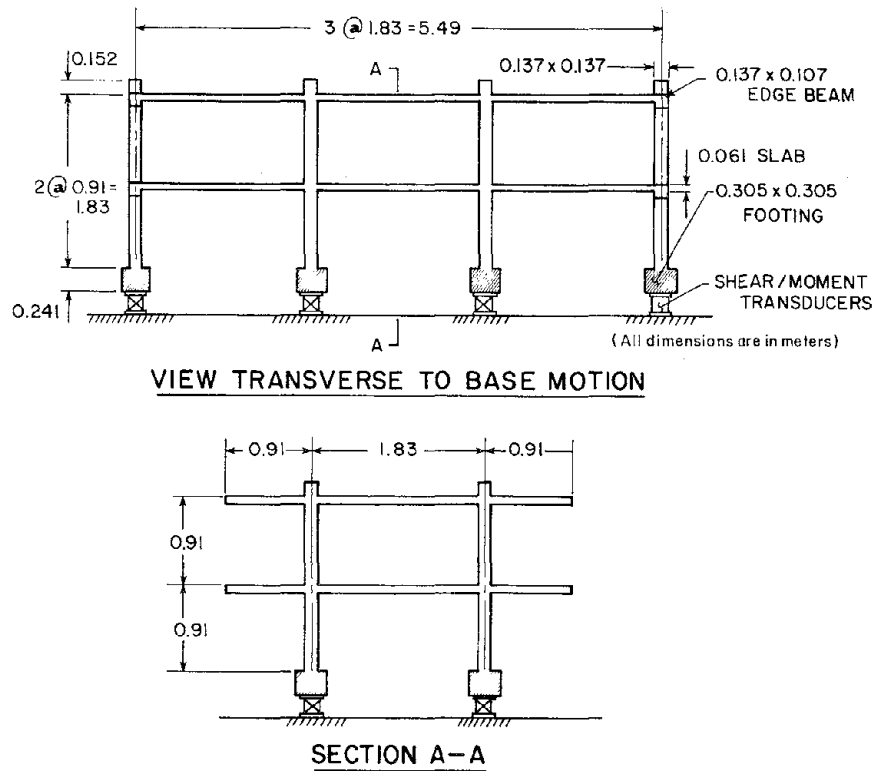
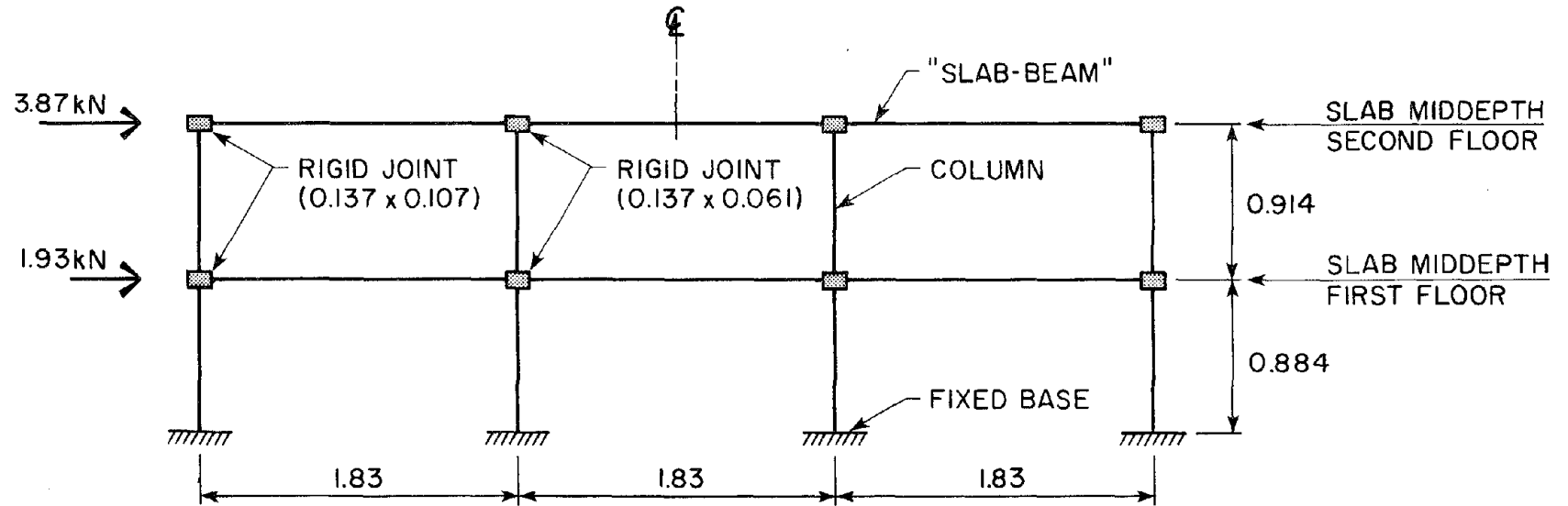
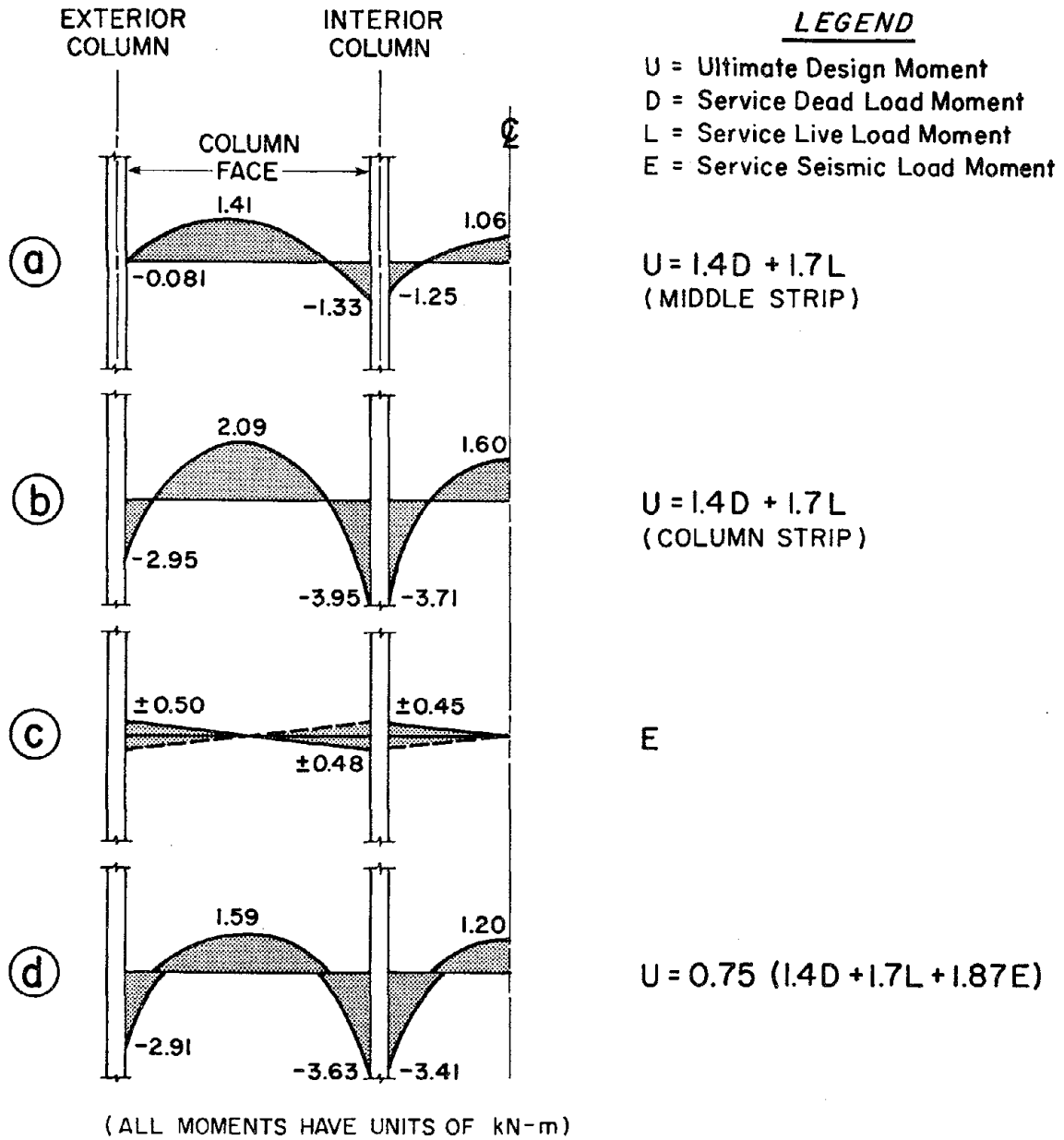


Fig. 1.2 Longitudinal and Transverse Section of Model



**NOTE :** Seismic Lateral Loads Are For One-Half Of Structure.  
All Dimensions Are In Meters.

Fig. 2.1 Plane-Frame Model Used for Design Lateral-Load Analysis



**LEGEND**

- U = Ultimate Design Moment
- D = Service Dead Load Moment
- L = Service Live Load Moment
- E = Service Seismic Load Moment

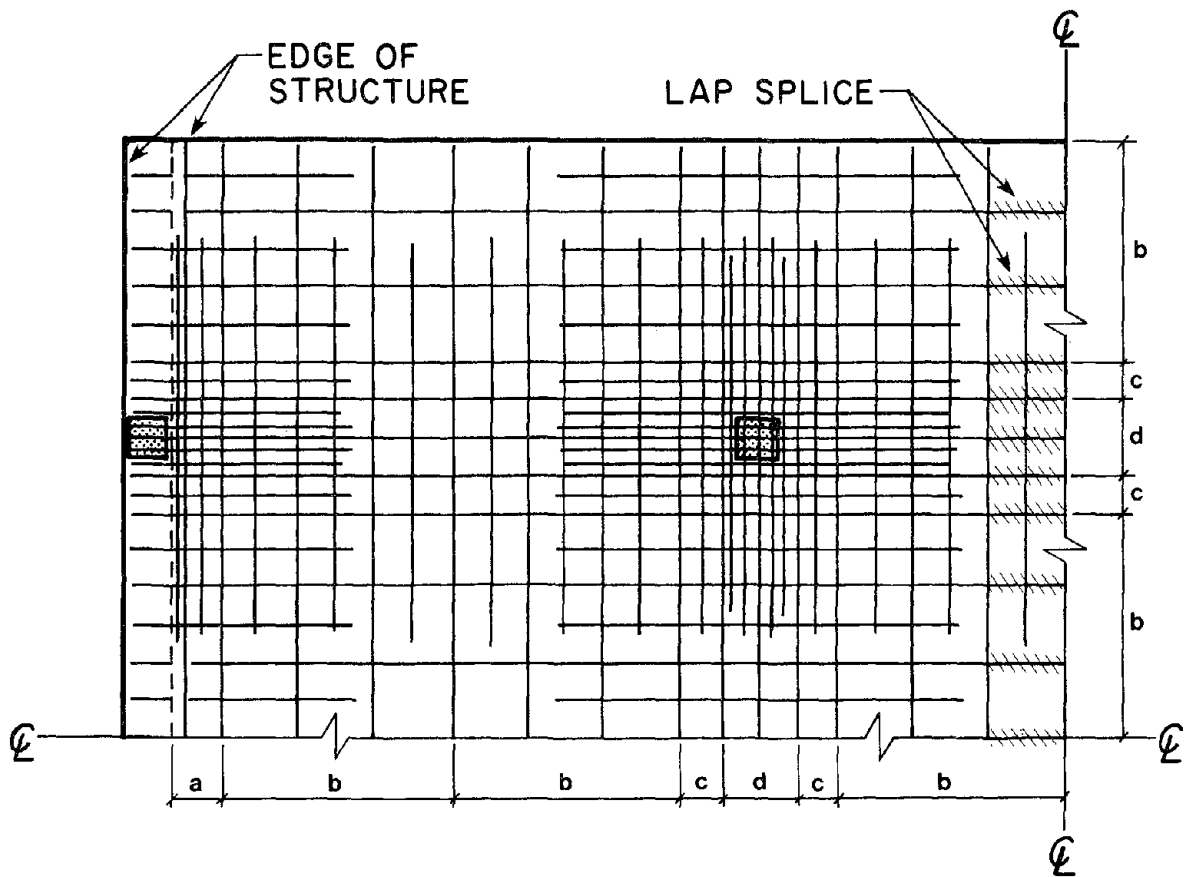
$U = 1.4D + 1.7L$   
(MIDDLE STRIP)

$U = 1.4D + 1.7L$   
(COLUMN STRIP)

E

$U = 0.75 (1.4D + 1.7L + 1.87E)$

Fig. 2.2 Slab Design Moments

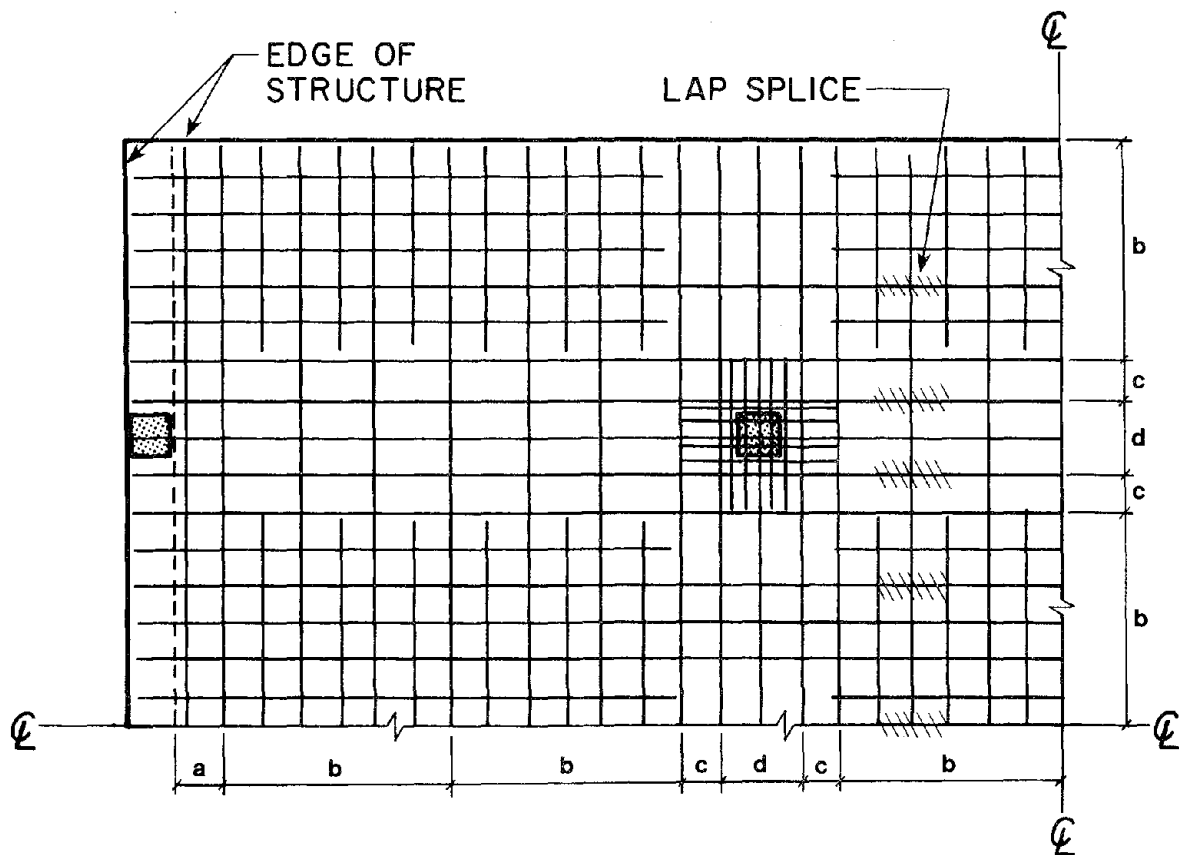


MARK	WIDTH	SPACING	BAR LENGTHS
a	0.152	0.038	1 at 1.22 1 at 3.63 1 at 1.22
b	0.686	0.114	3 at 1.22 4 at 3.63
c	0.114	0.057	1 at 1.22
d	0.229	0.038	2 at 1.12 2 at 1.22 2 at 3.63

(ALL DIMENSIONS IN METERS)

### (a) TOP REINFORCEMENT

Fig. 2.3 Slab Reinforcement Details



MARK	WIDTH	SPACING	BAR LENGTHS
a	0.152	0.114	1 at 3.63
b	0.686	0.114	3 at 1.37 4 at 3.63
c	0.114	NO BARS IN THIS SPACE	
d	0.229	0.038	4 at 0.46 3 at 3.63

(ALL DIMENSIONS IN METERS)

## (b) BOTTOM REINFORCEMENT

Fig. 2.3 (cont'd.) Slab Reinforcement Details

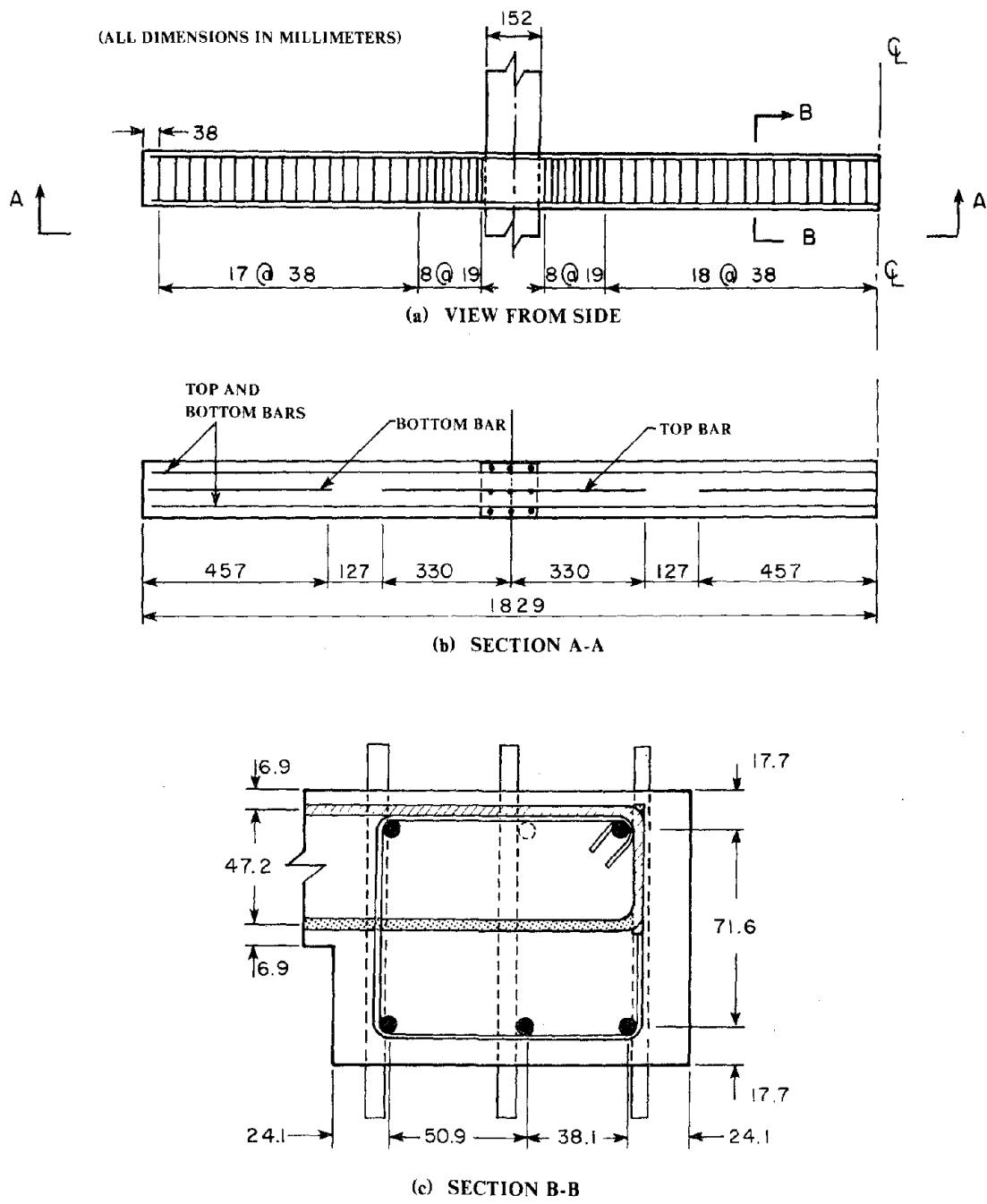


Fig. 2.4 Edge-Beam Reinforcement Details

(ALL DIMENSIONS IN MILLIMETERS)

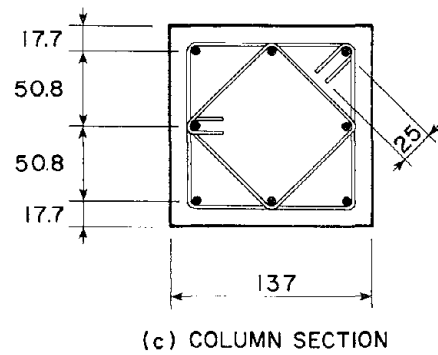
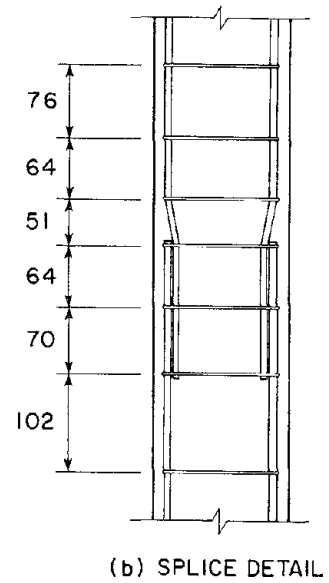
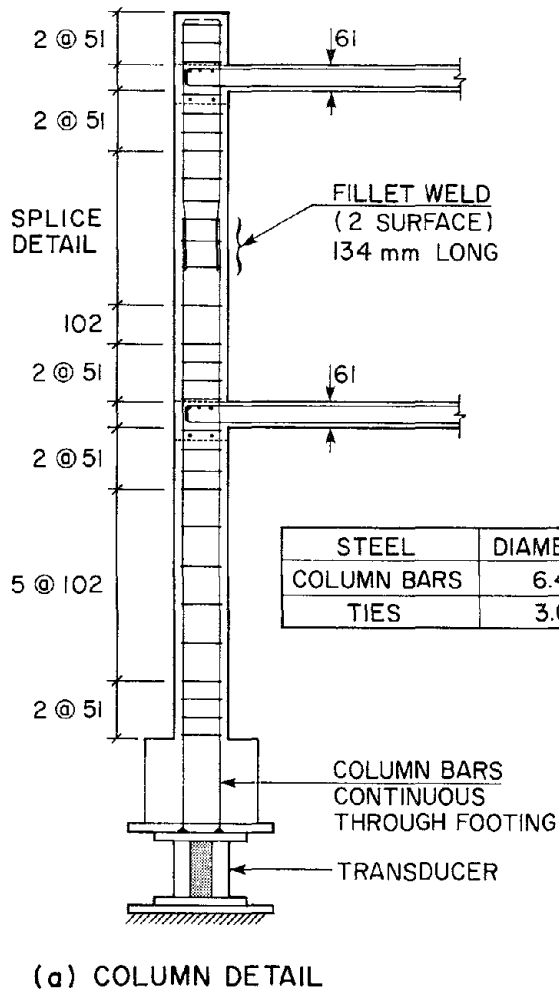


Fig. 2.5 Column Reinforcement Details

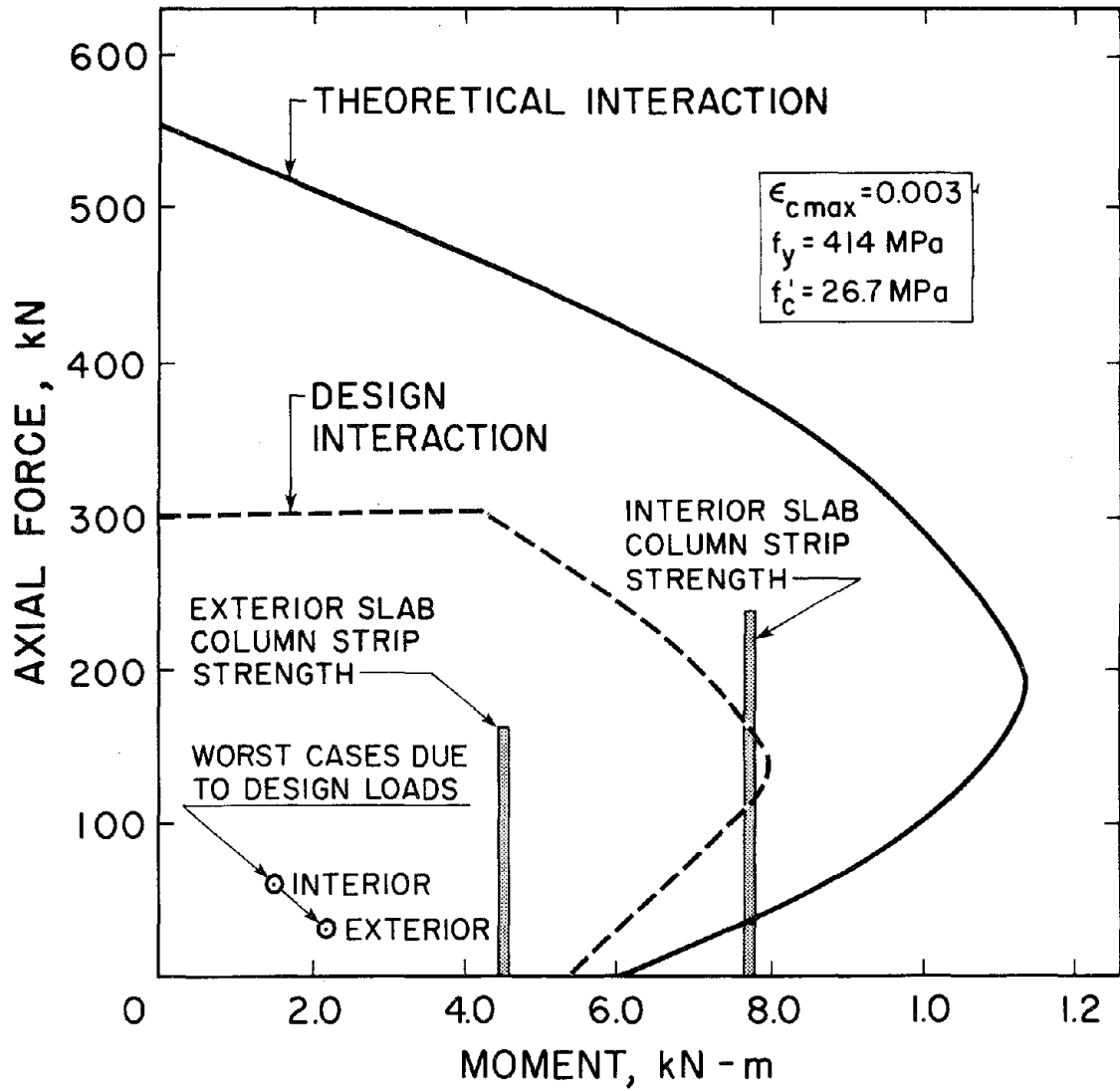


Fig. 2.6 Theoretical and Design Column Axial Load-Moment Interaction Diagrams

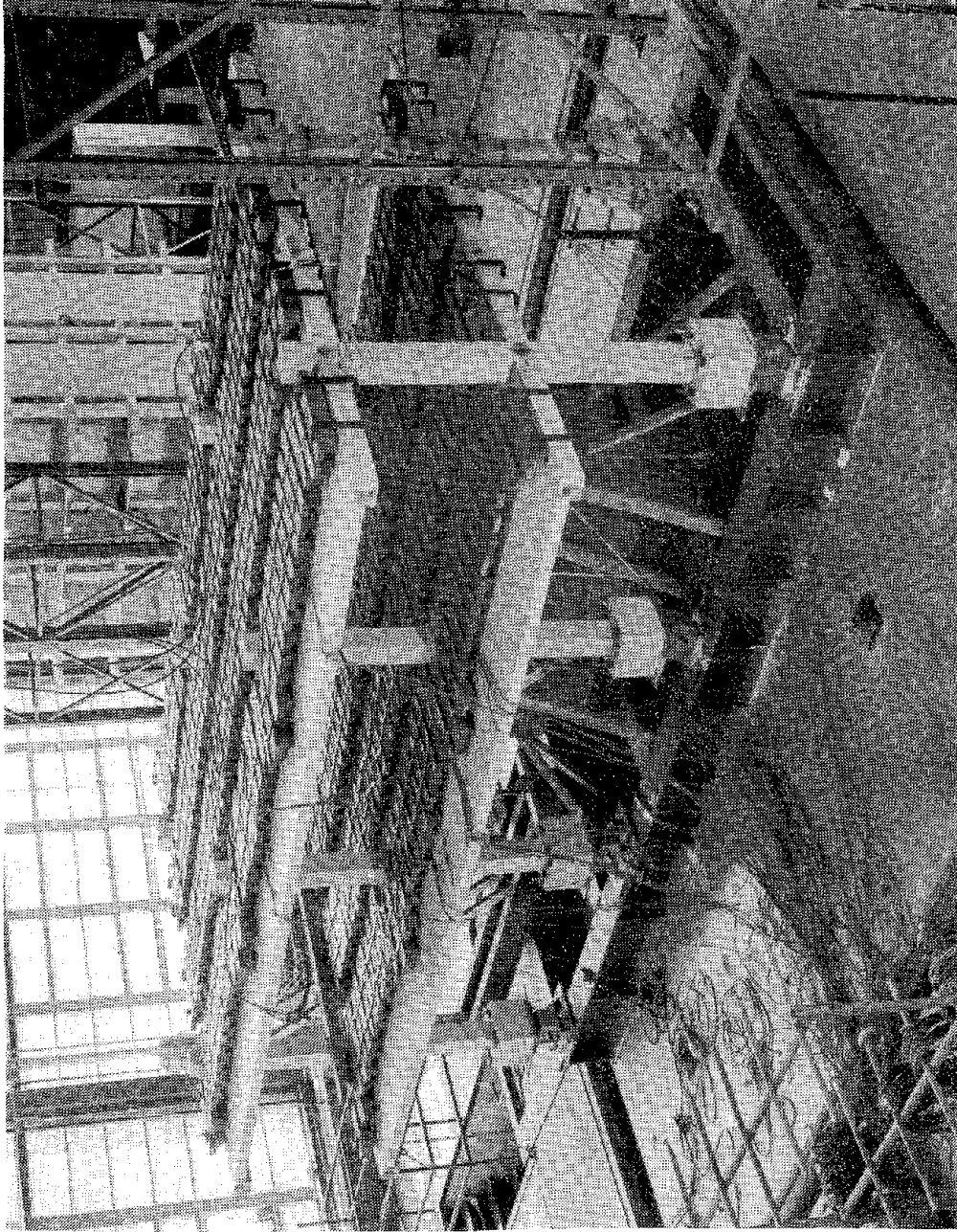


Fig. 3.1 Photograph of Test Structure on Shaking Table

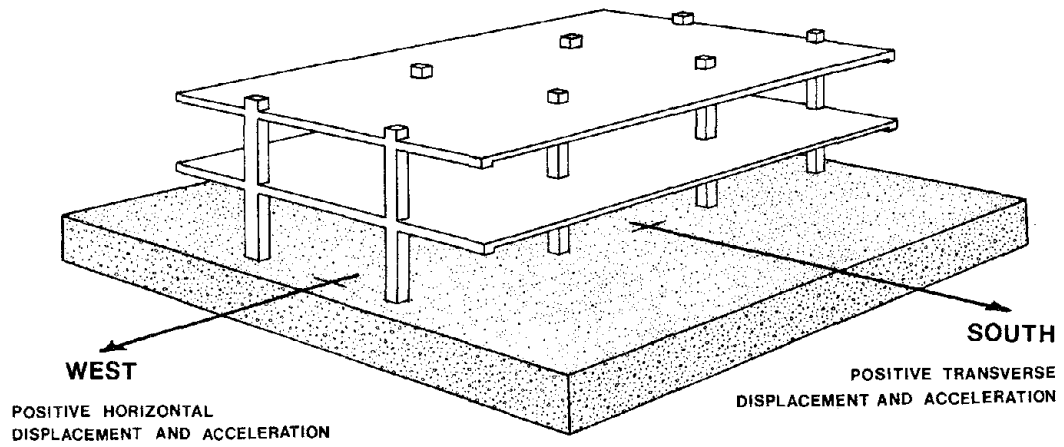


Fig. 3.2 Schematic View of Test Structure Orientation Relative to the Shaking Table

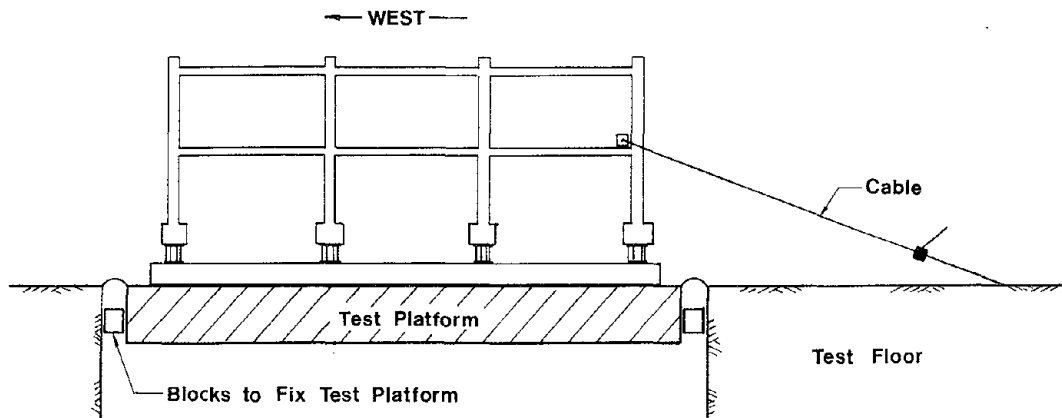


Fig. 3.3 Test Setup for Free-Vibration and Static Tests

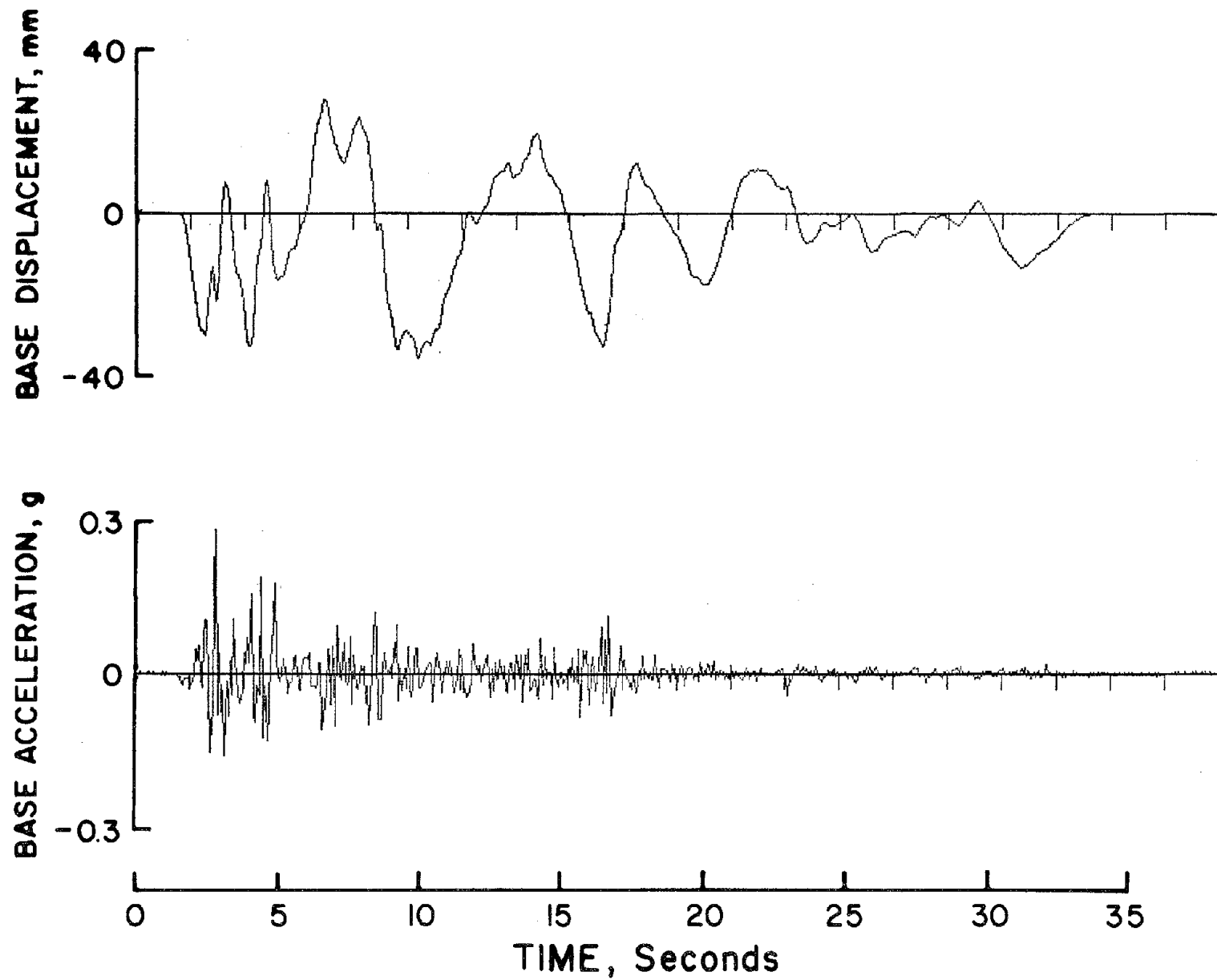


Fig. 4.1 Typical Recorded Horizontal Base Motions Lasting 35 Seconds

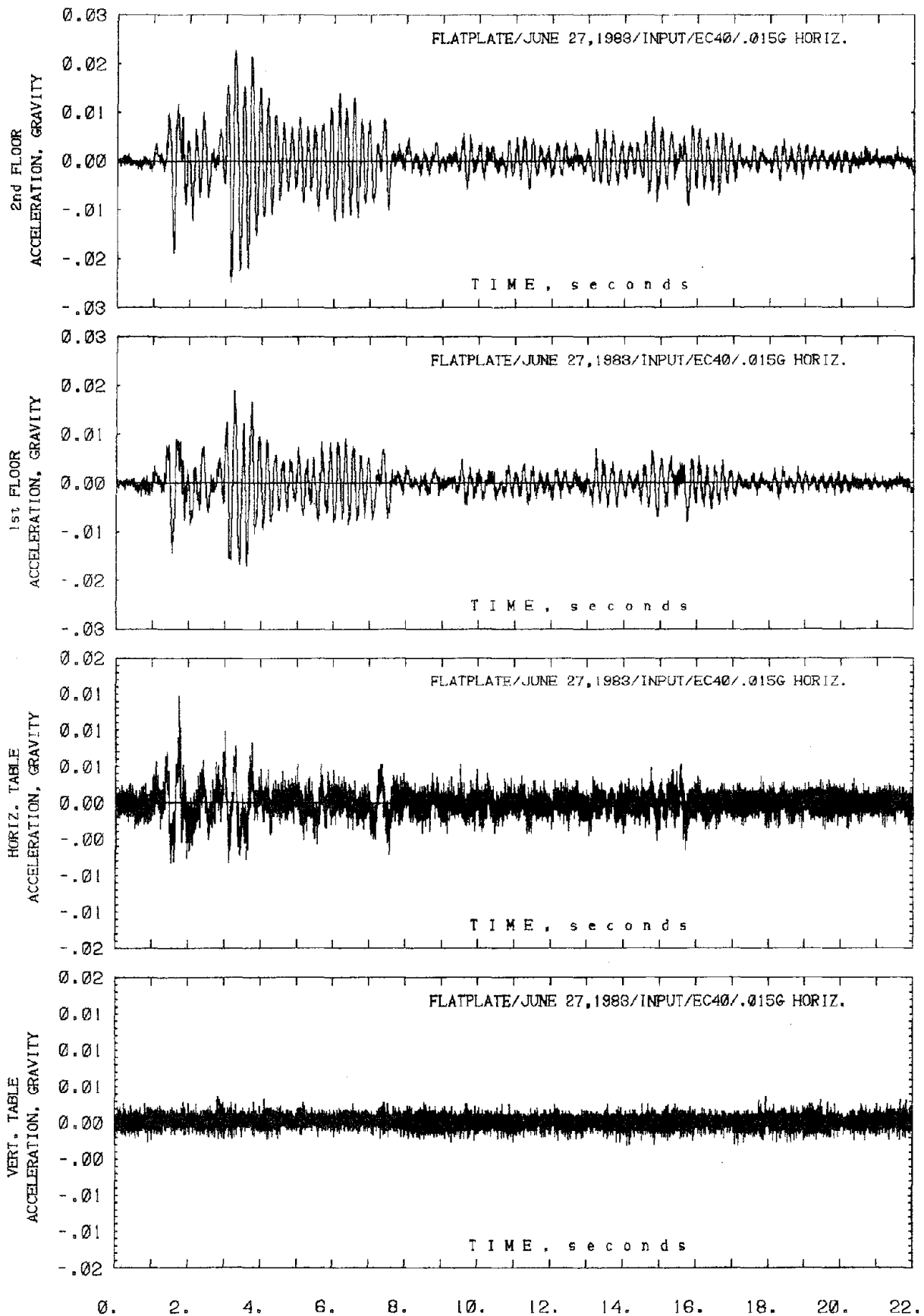
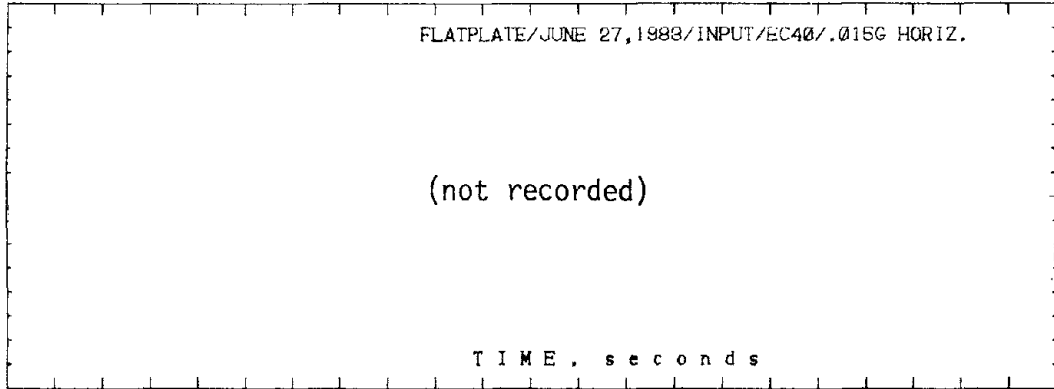
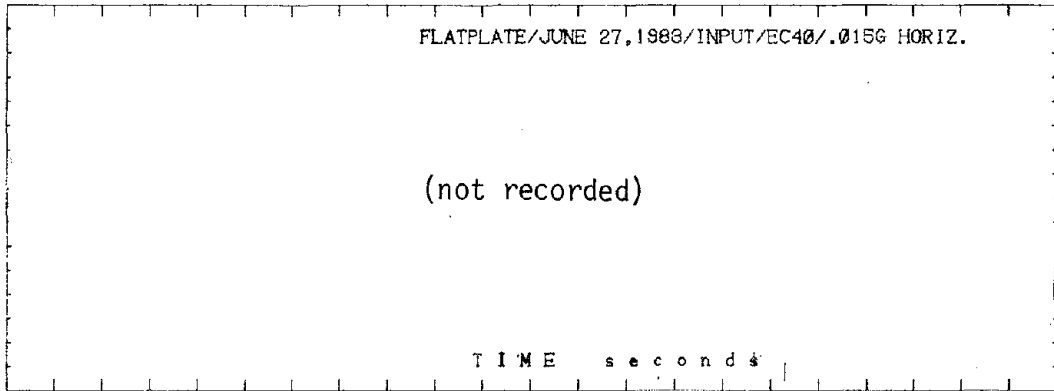


Fig. 4.2 Global Response of the Test Structure to Test EQ 1

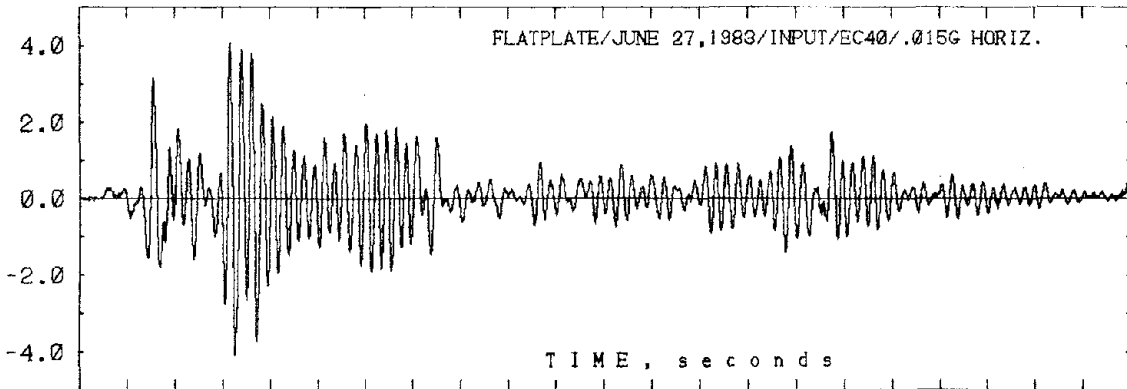
2nd FLOOR RELATIVE  
DISPLACEMENT, mm/mm



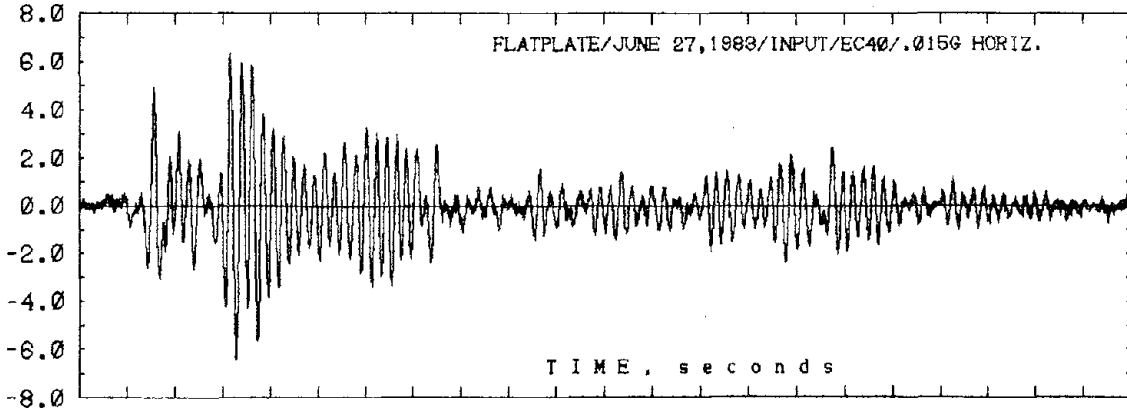
1st FLOOR RELATIVE  
DISPLACEMENT, mm/mm



TRANSDUCER BASE SHEAR,  
KILONEWTONS



BASE MOMENT, KN-METERS



0. 2. 4. 6. 8. 10. 12. 14. 16. 18. 20. 22.

Fig. 4.2 (cont'd.) Global Response of the Test Structure to Test EQ 1

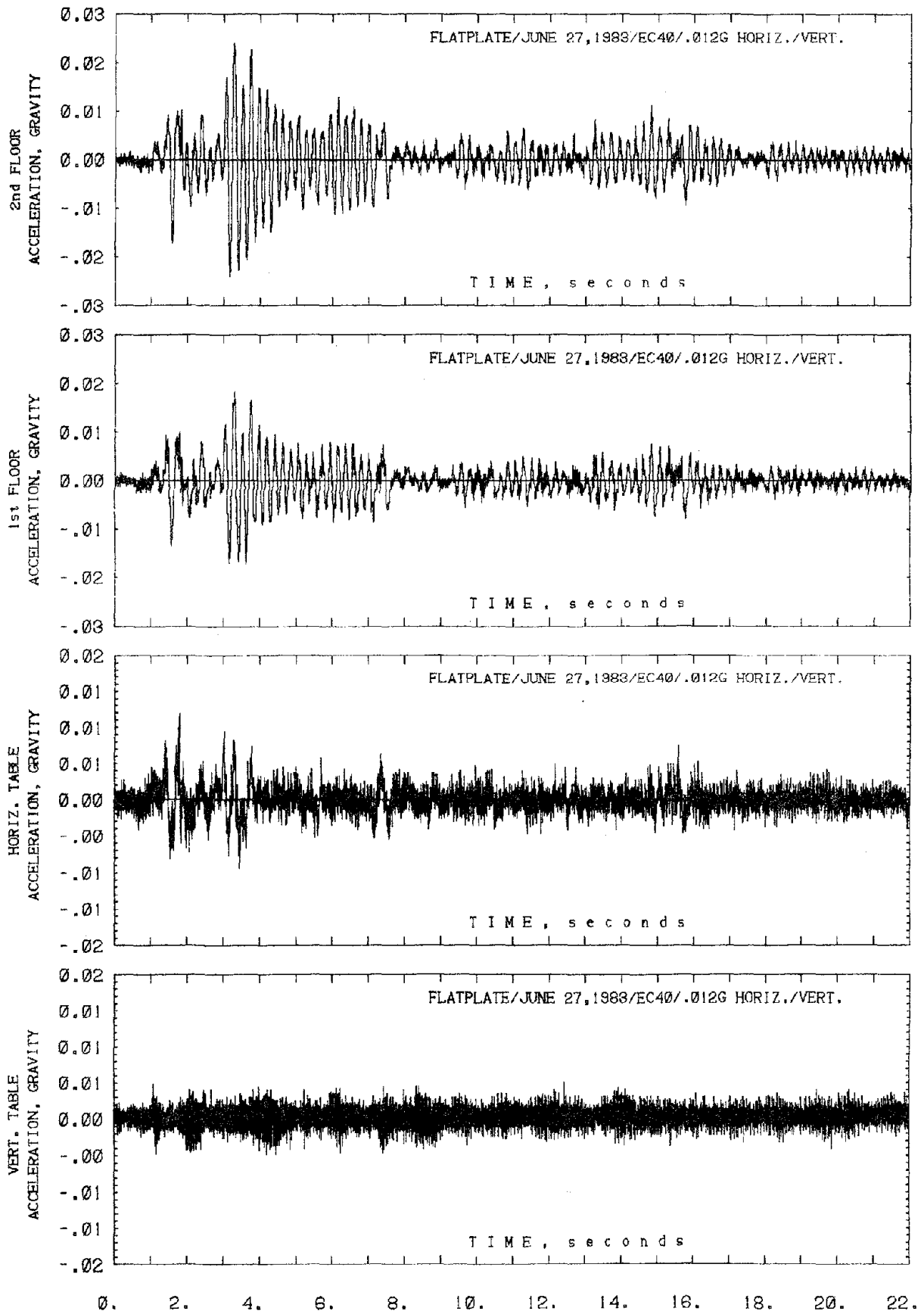


Fig. 4.3 Global Response of the Test Structure to Test EQ 2

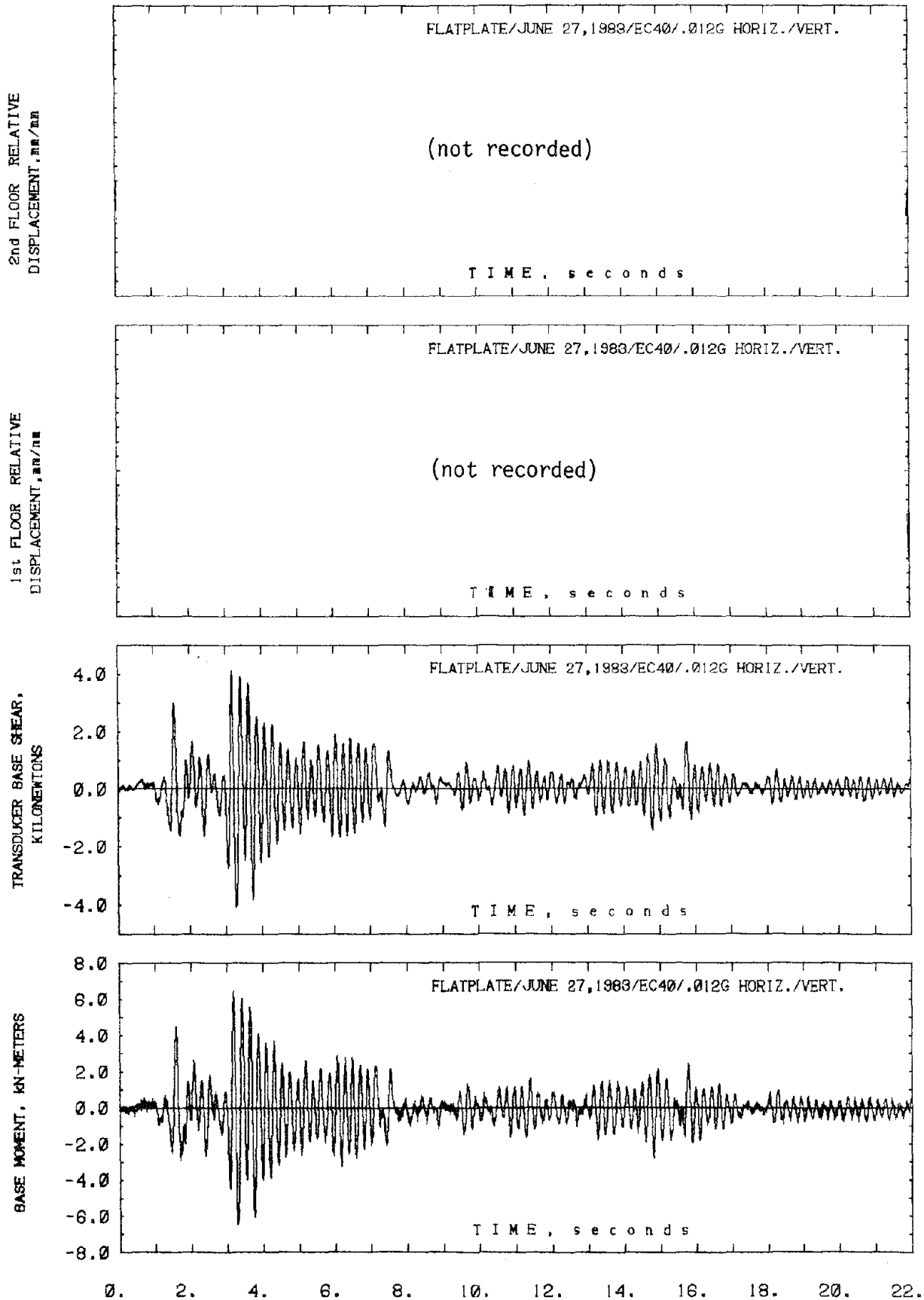


Fig. 4.3 (cont'd.) Global Response of the Test Structure to Test EQ 2

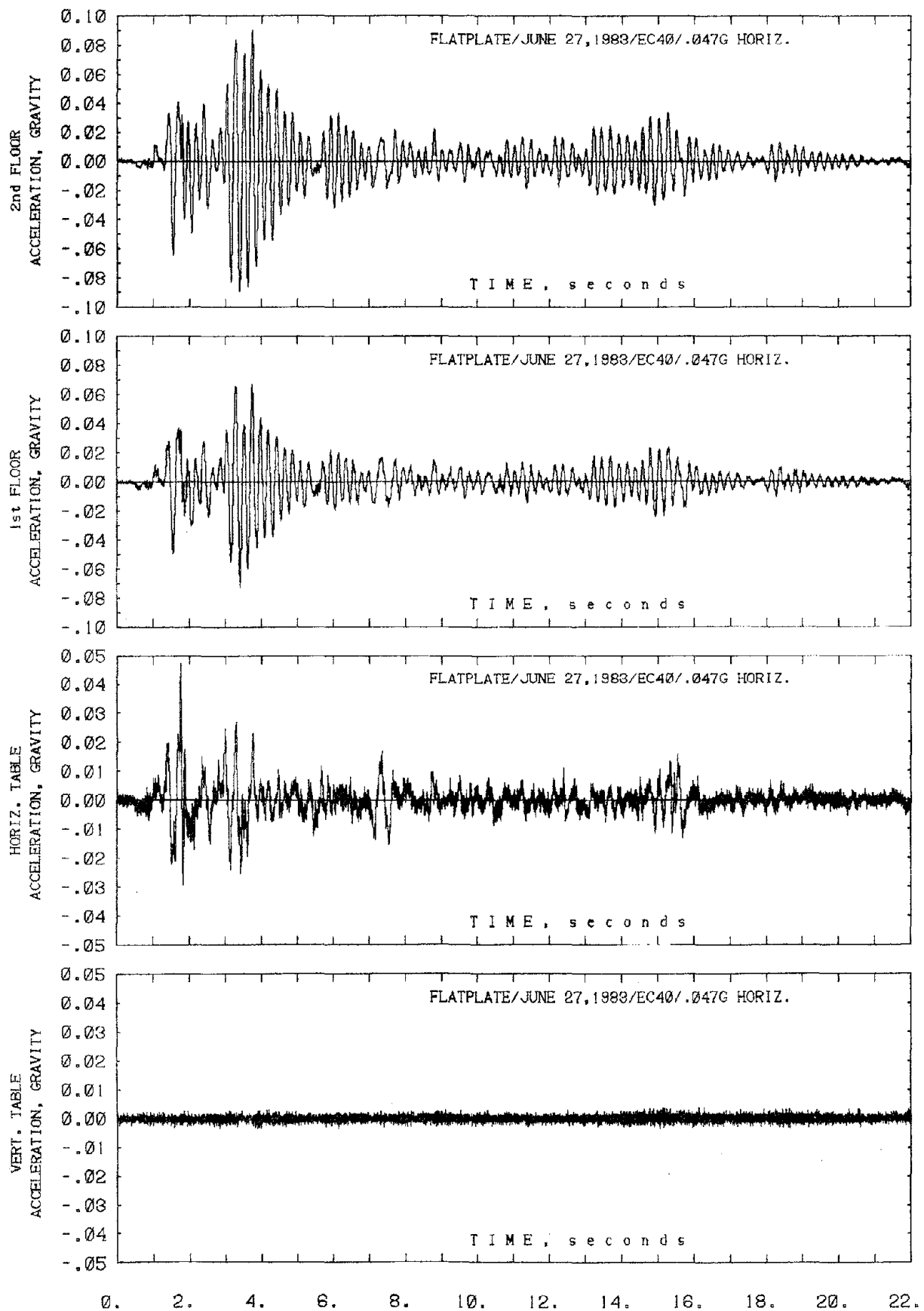


Fig. 4.4 Global Response of the Test Structure to Test EQ 3

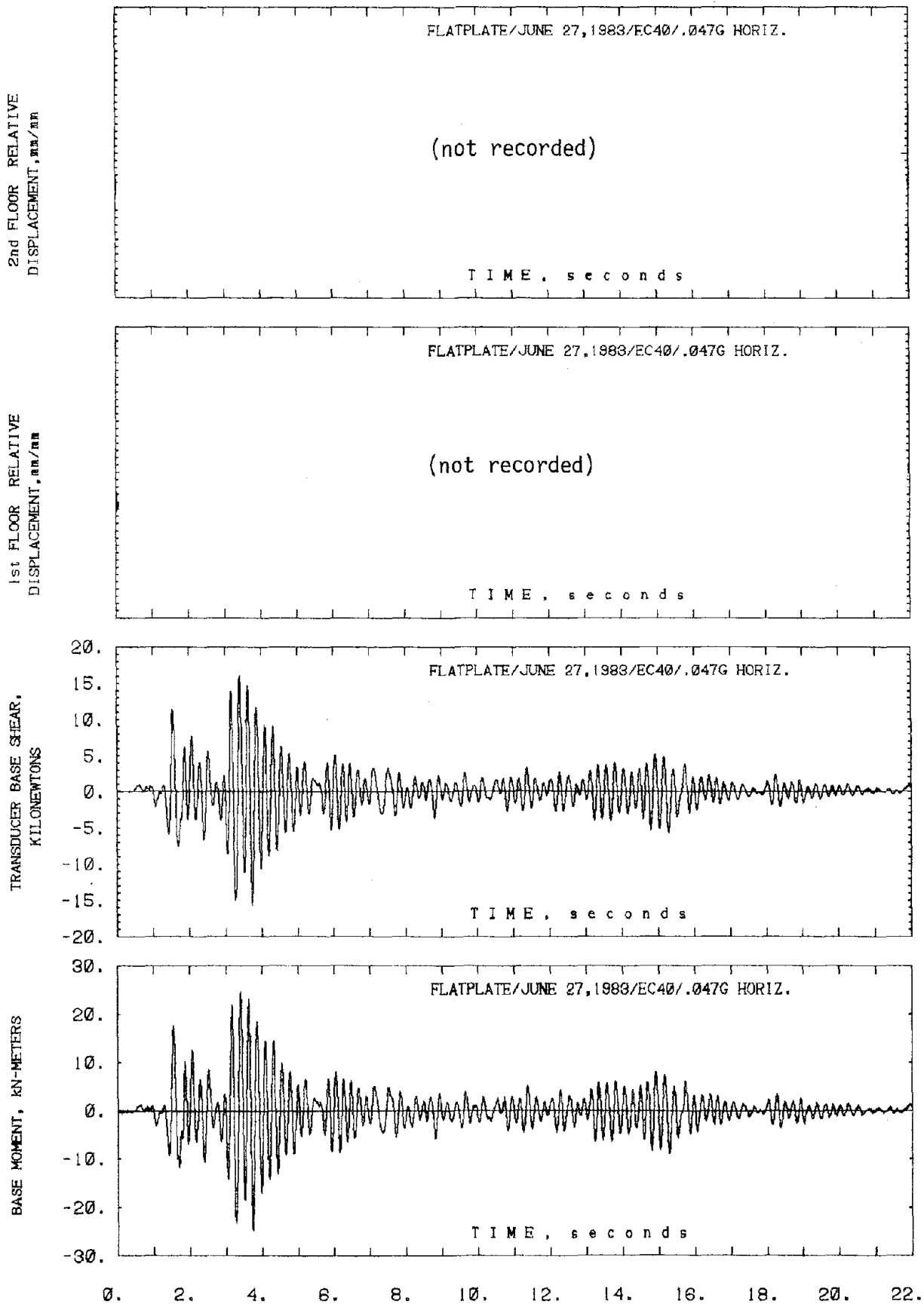


Fig. 4.4 (cont'd.) Global Response of the Test Structure to Test EQ 3

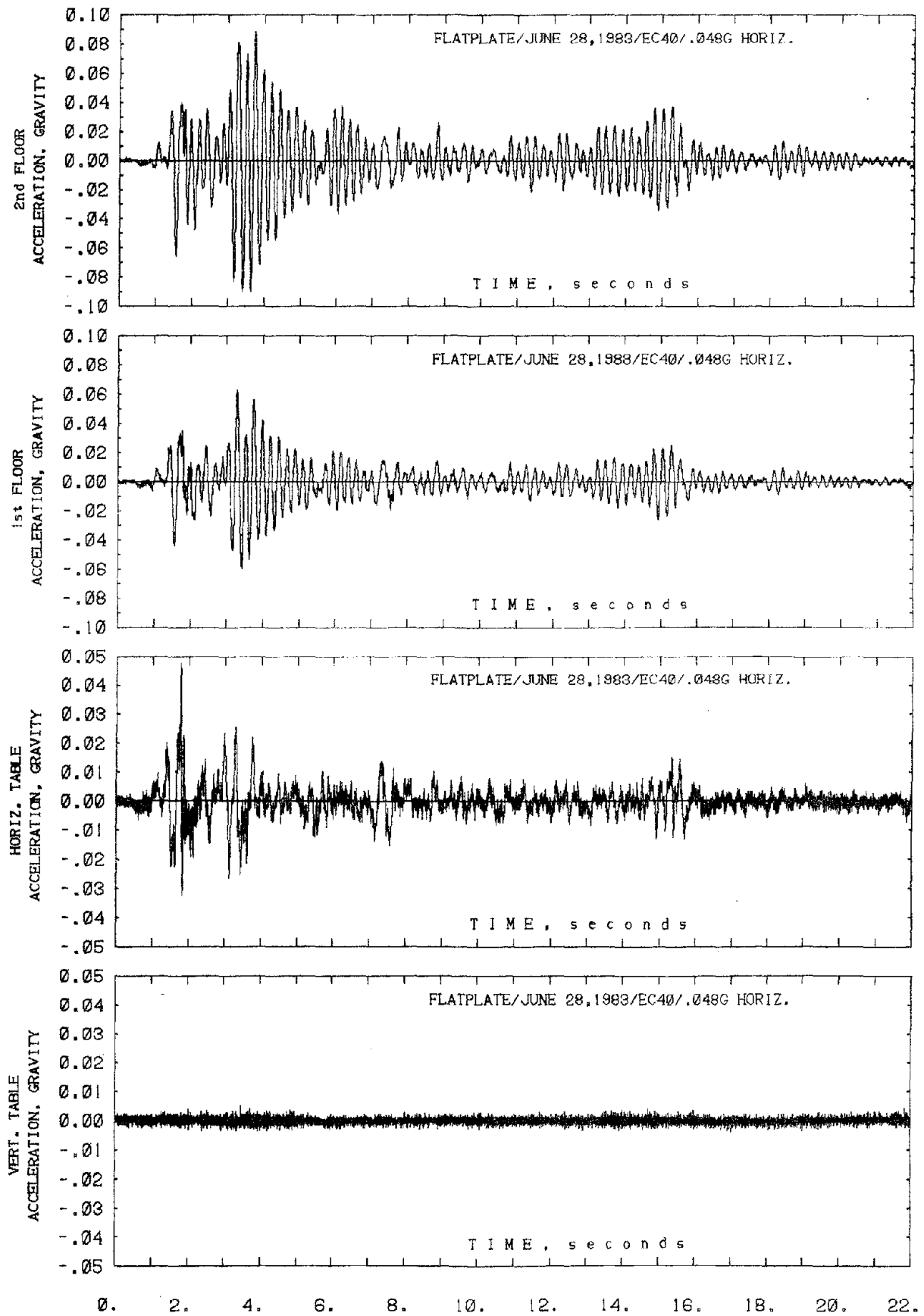


Fig. 4.5 Global Response of the Test Structure to Test EQ 4

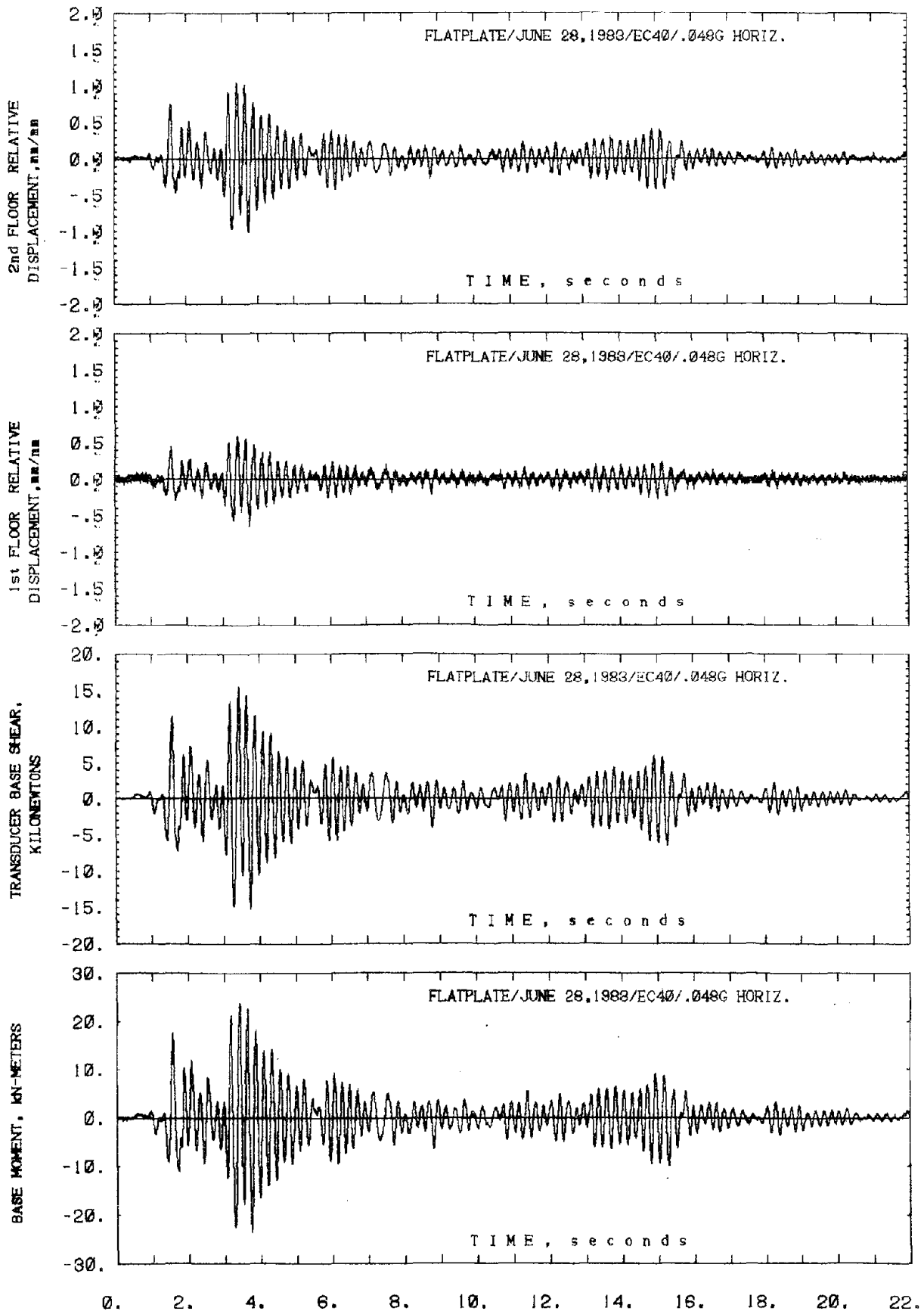


Fig. 4.5 (cont'd.) Global Response of the Test Structure to Test EQ 4

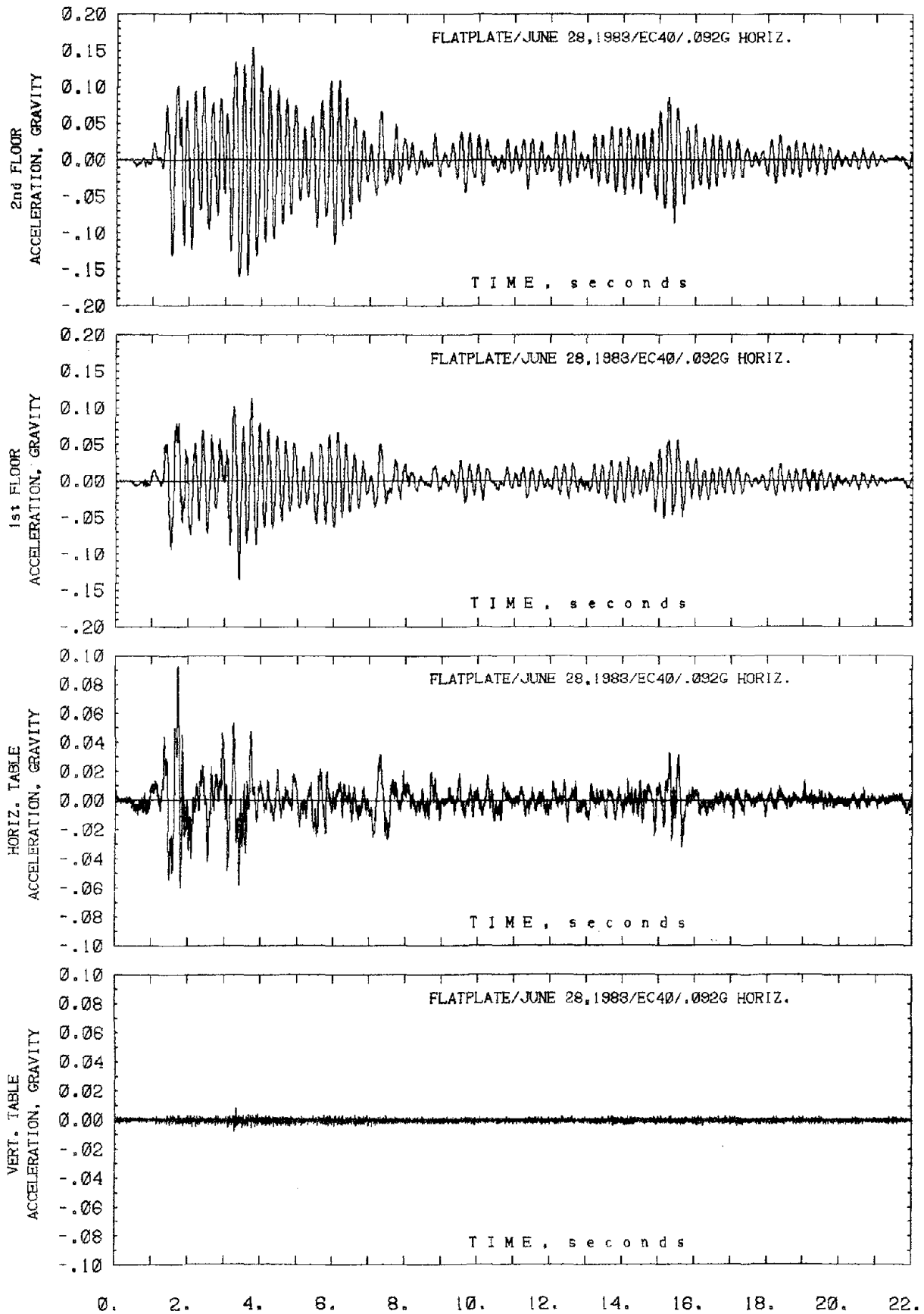


Fig. 4.6 Global Response of the Test Structure to Test EQ 5

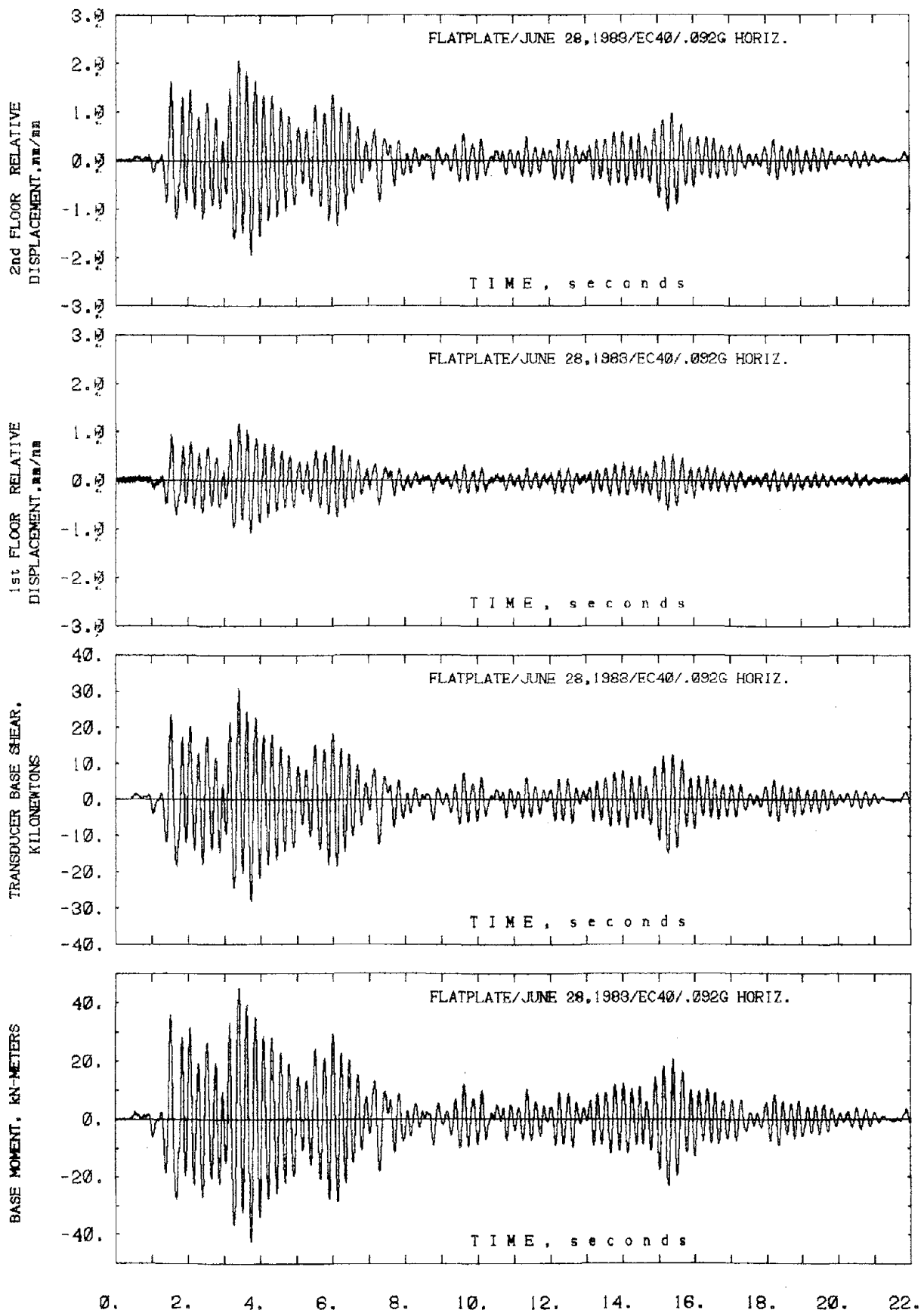


Fig. 4.6 (cont'd.) Global Response of the Test Structure to Test EQ 5

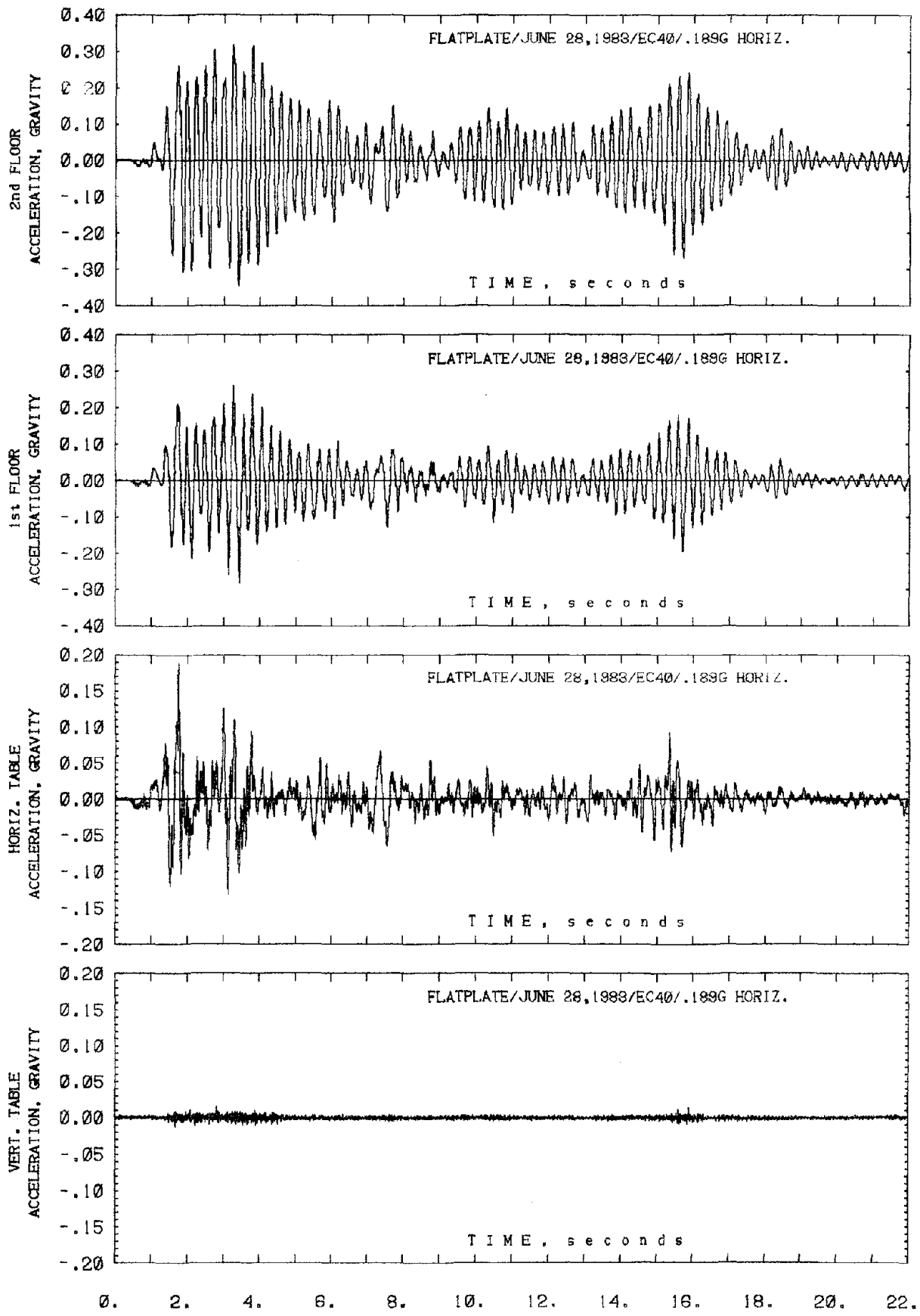


Fig. 4.7 Global Response of the Test Structure to Test EQ 6

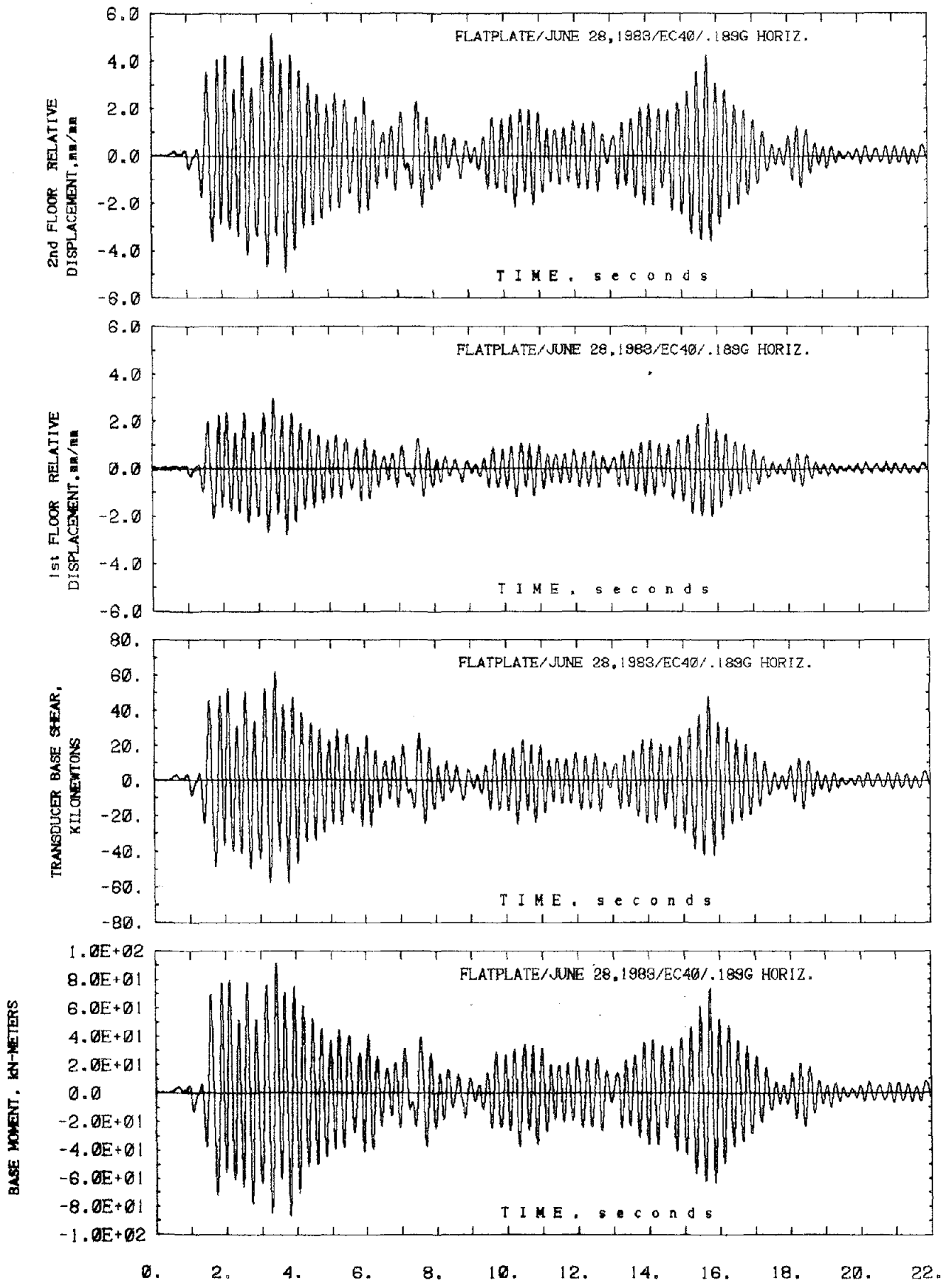


Fig. 4.7 (cont'd.) Global Response of the Test Structure to Test EQ 6

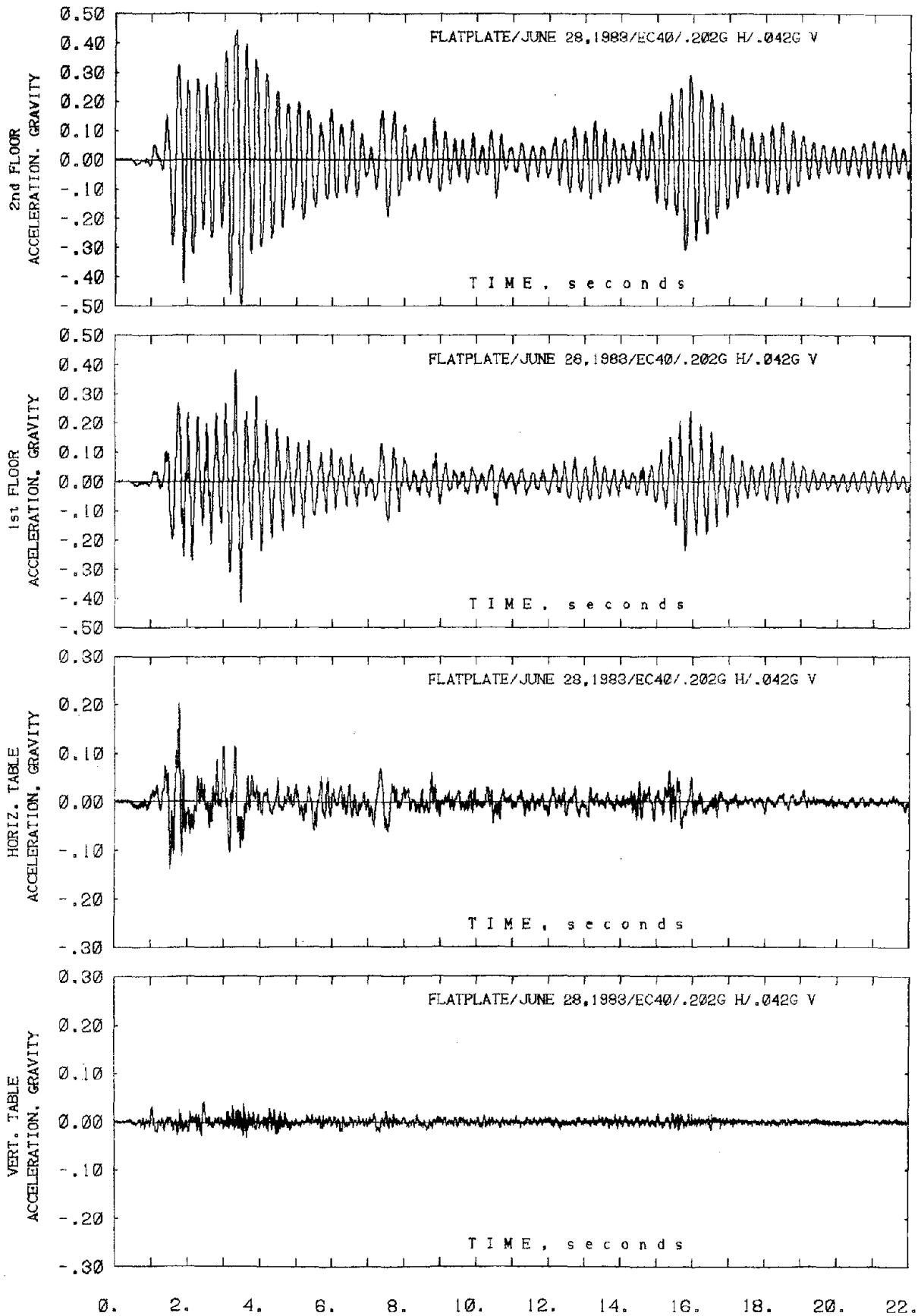


Fig. 4.8 Global Response of the Test Structure to Test EQ 7

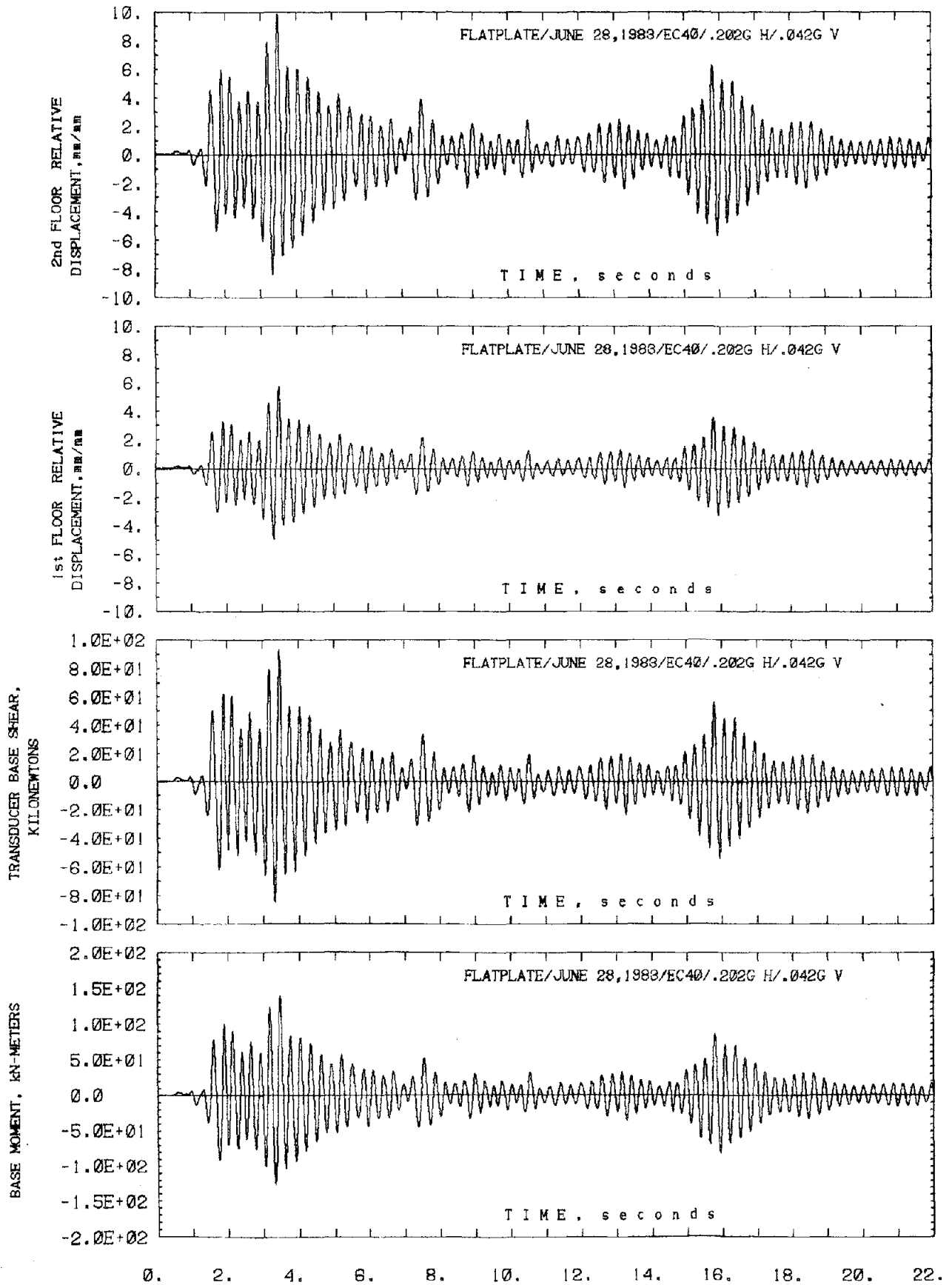


Fig. 4.8 (cont'd.) Global Response of the Test Structure to Test EQ 7

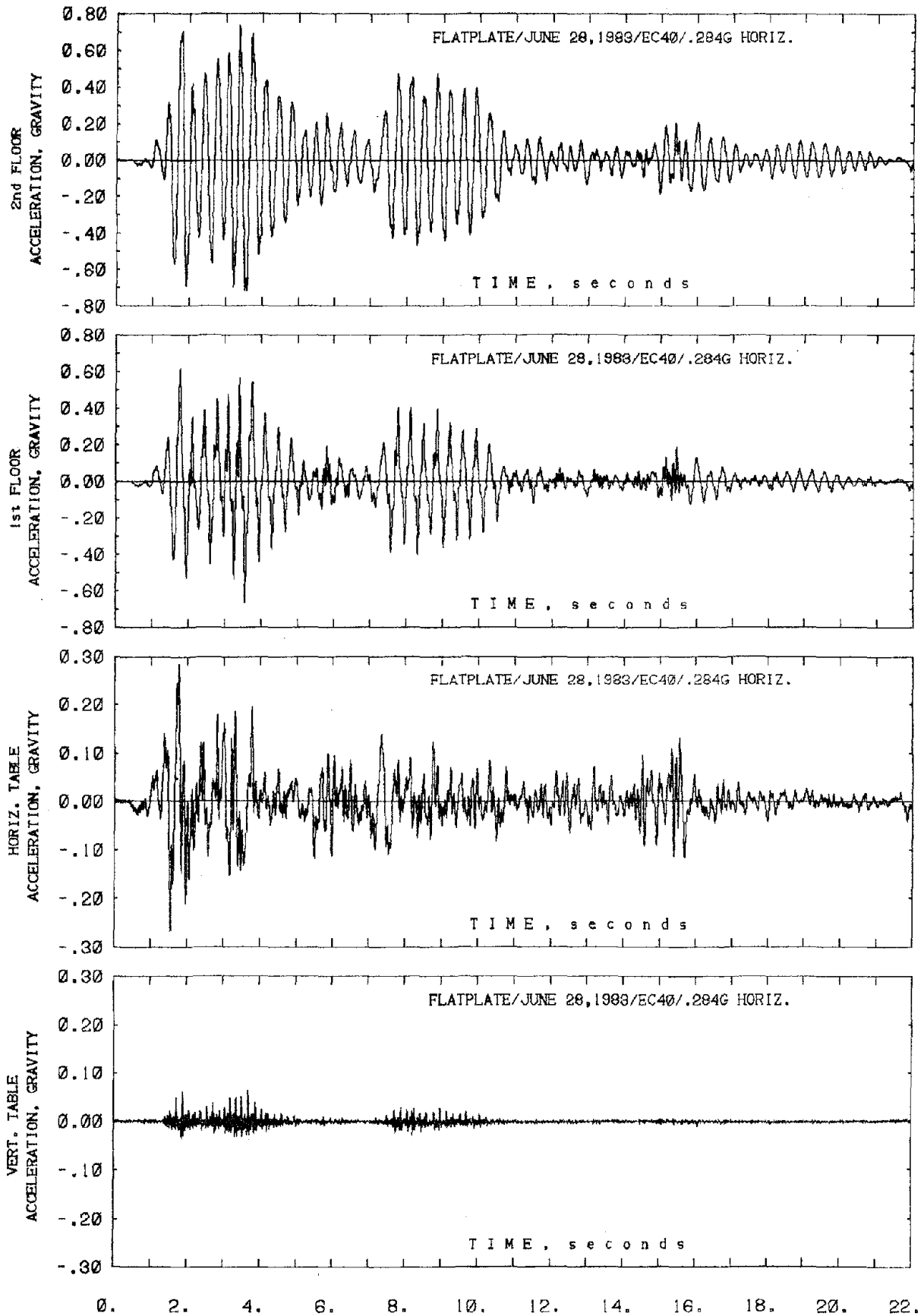


Fig. 4.9 Global Response of the Test Structure to Test EQ 8

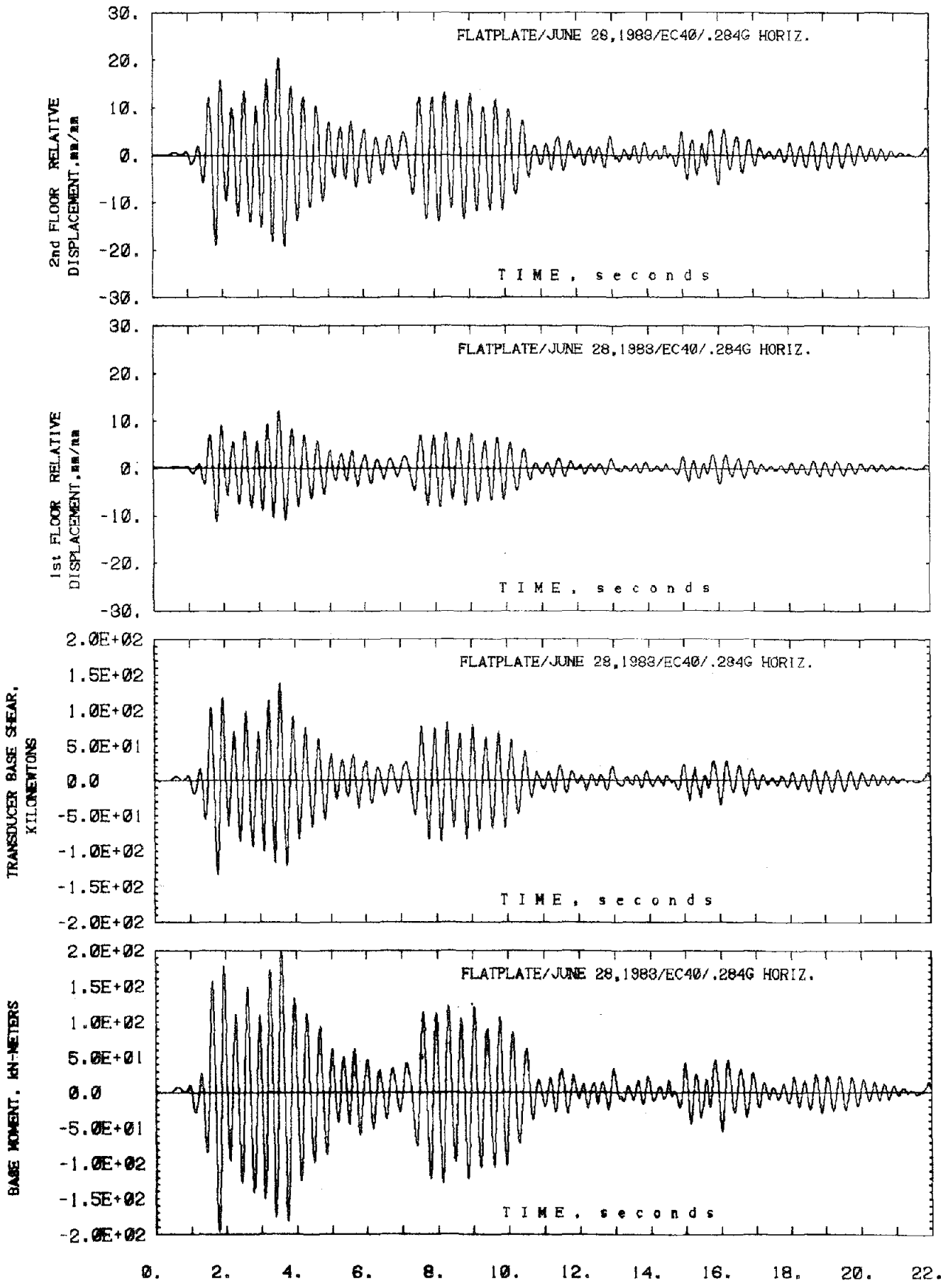


Fig. 4.9 (cont'd.) Global Response of the Test Structure to Test EQ 8

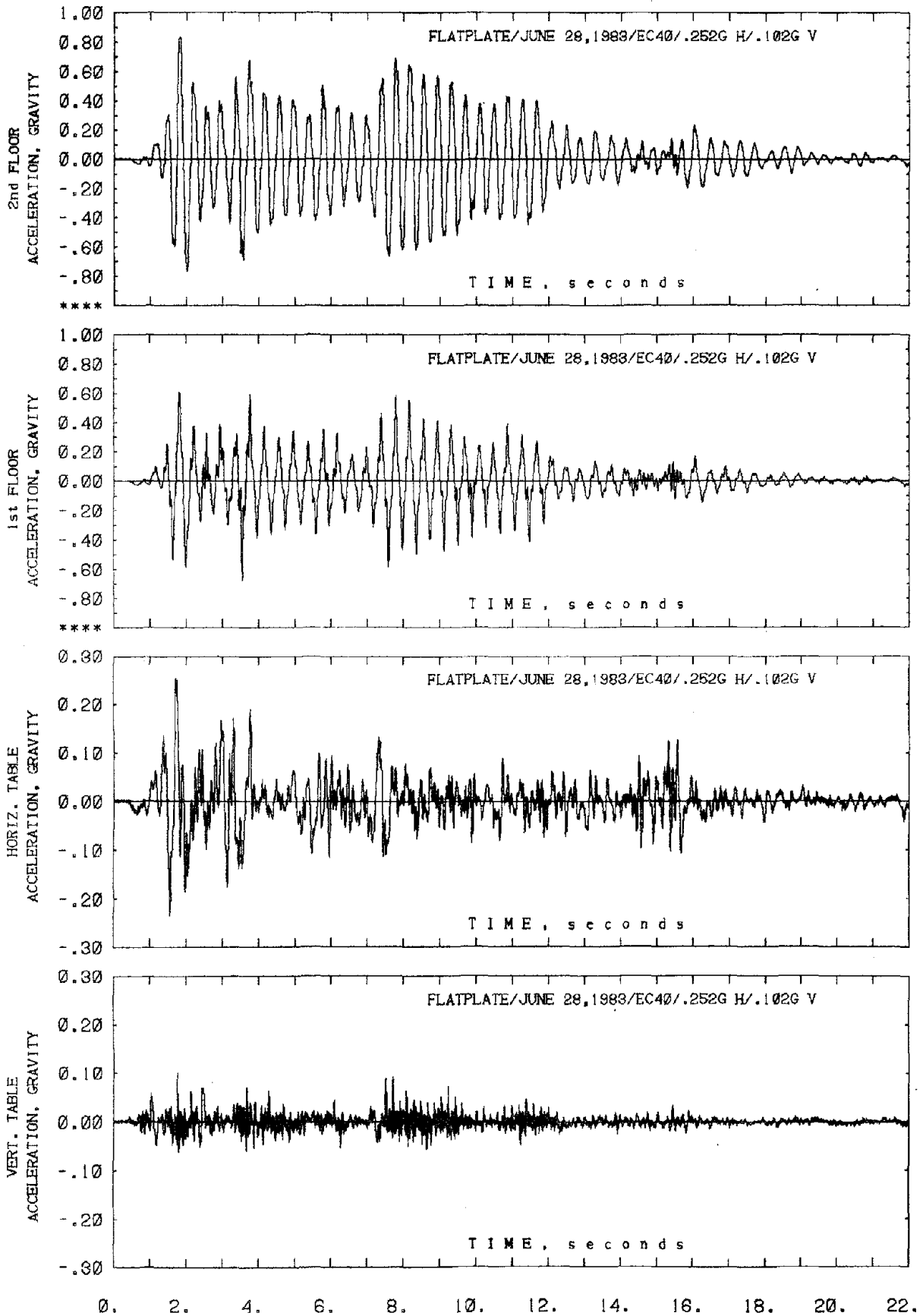


Fig. 4.10 Global Response of the Test Structure to Test EQ 9

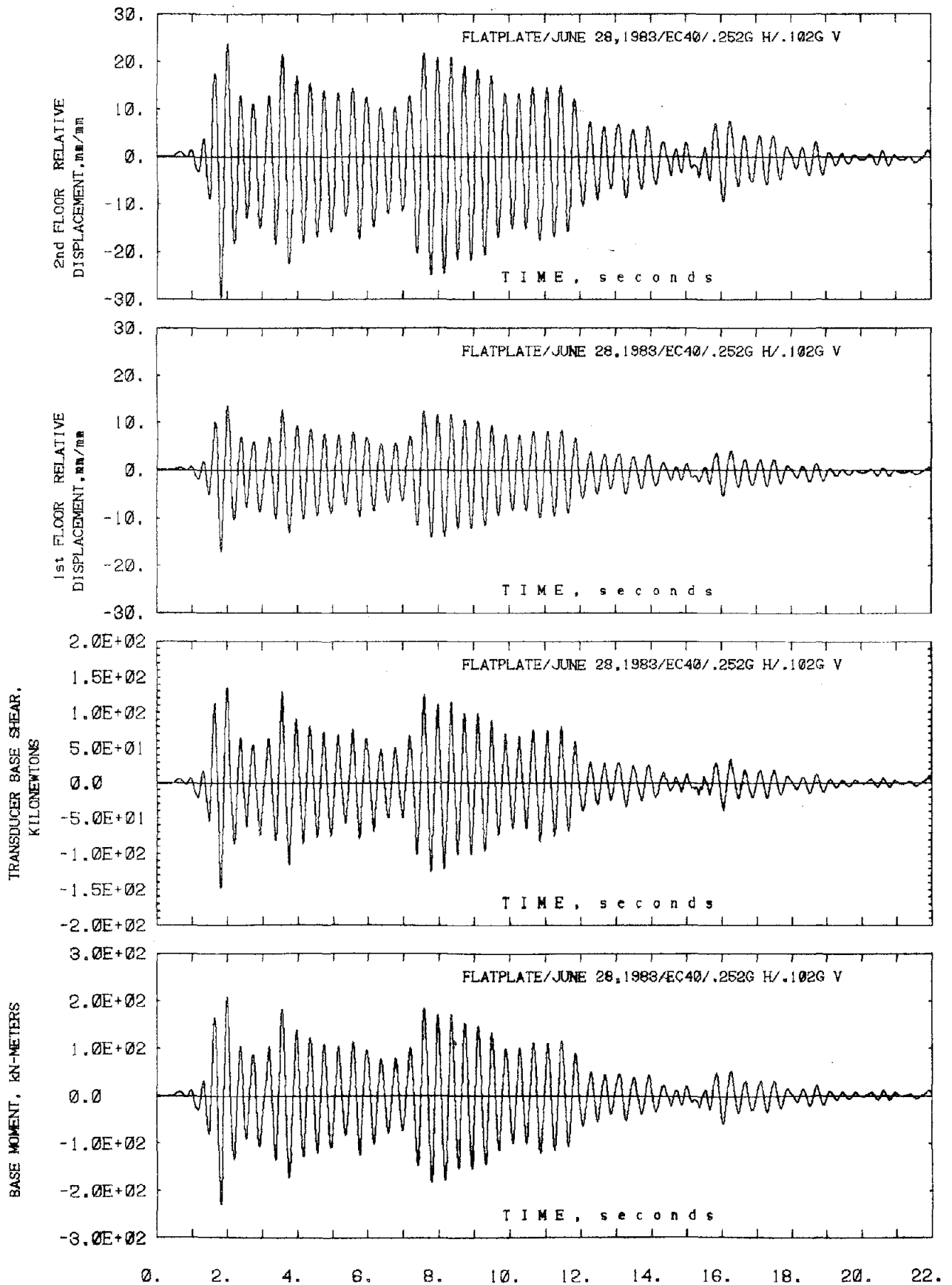


Fig. 4.10 (cont'd.) Global Response of the Test Structure to Test EQ 9

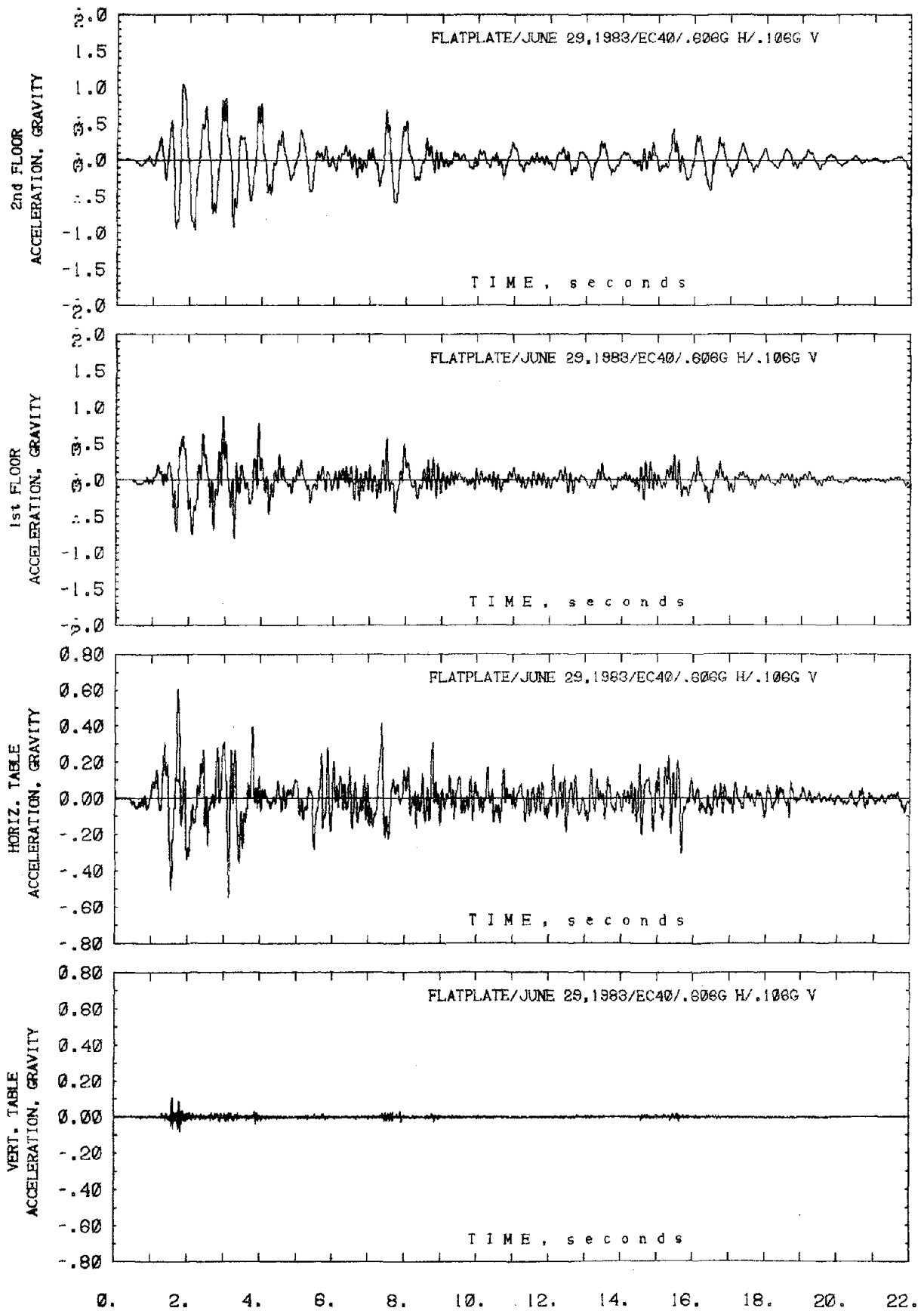


Fig. 4.11 Global Response of the Test Structure to Test EQ 10

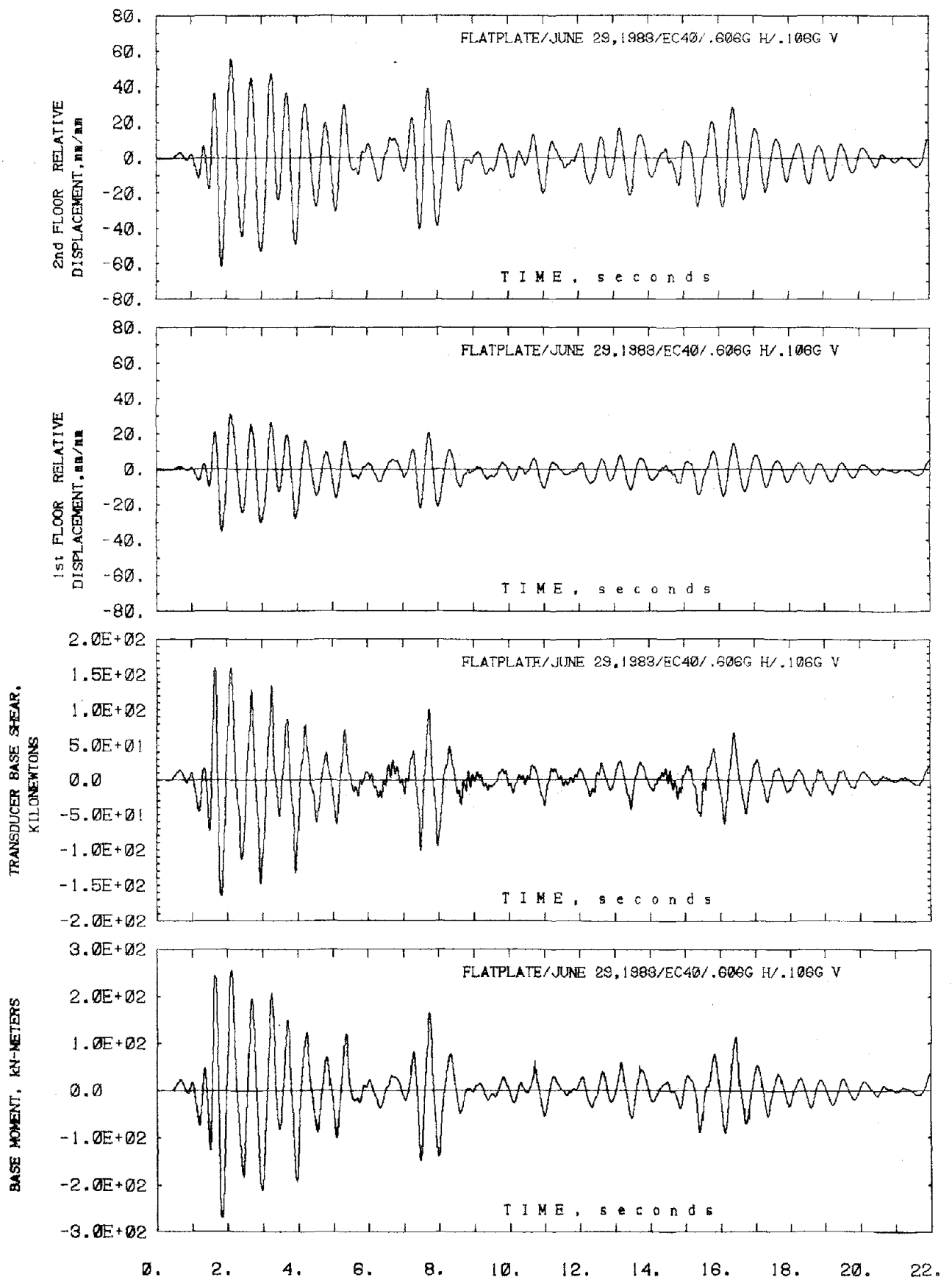


Fig. 4.11 (cont'd.) Global Response of the Test Structure to Test EQ 10

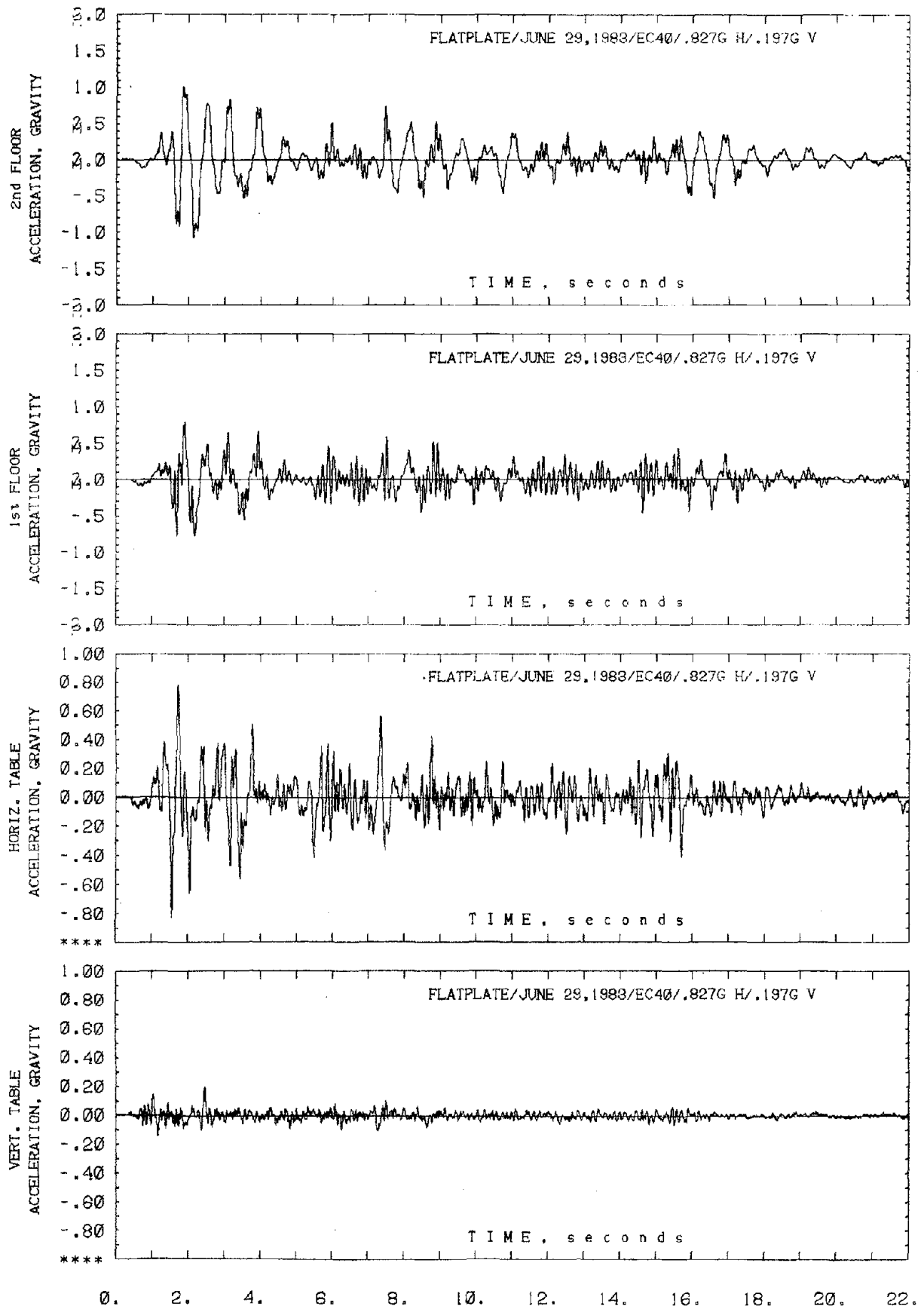


Fig. 4.12 Global Response of the Test Structure to Test EQ 11

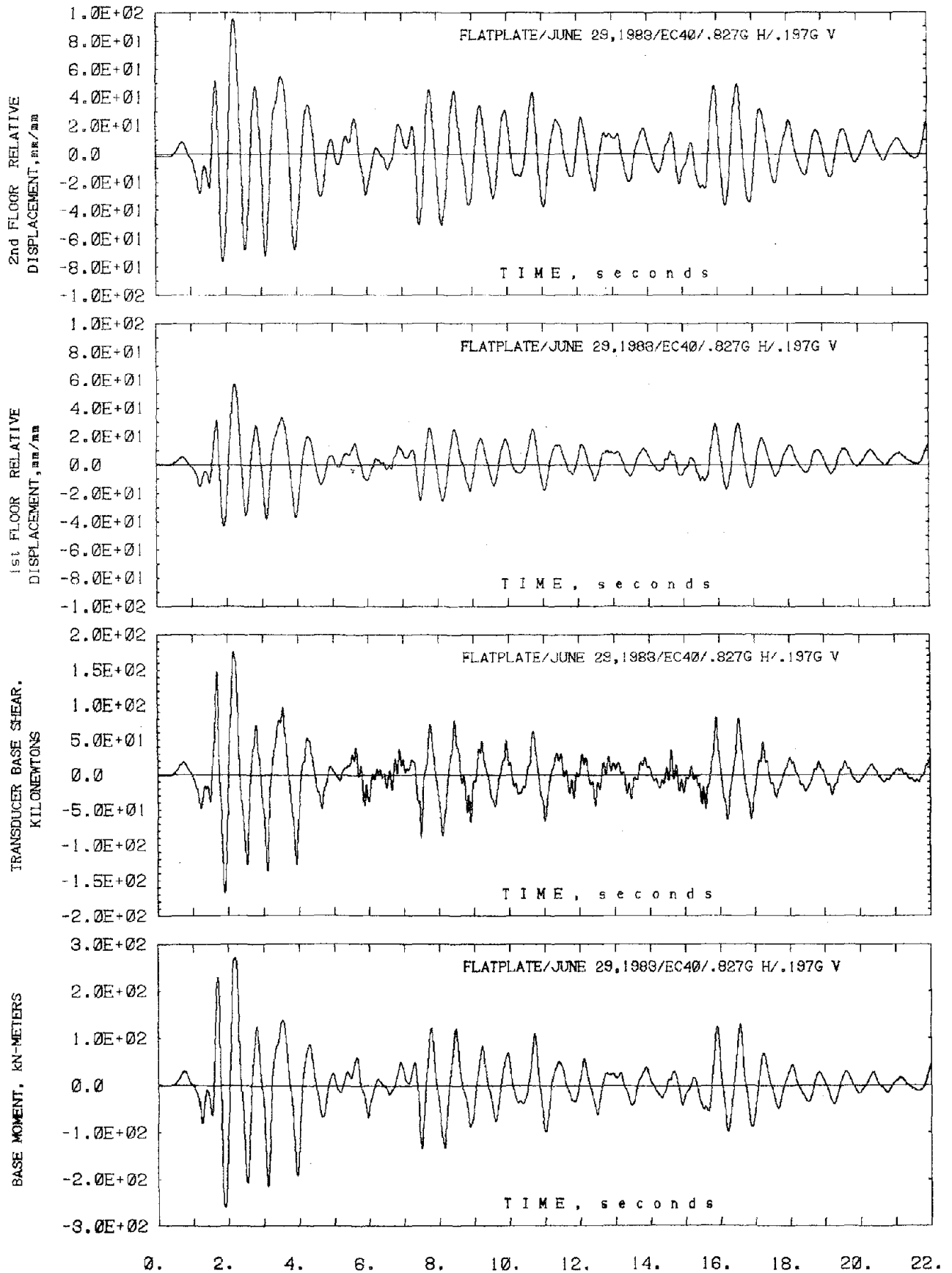


Fig. 4.12 (cont'd.) Global Response of the Test Structure to Test EQ 11

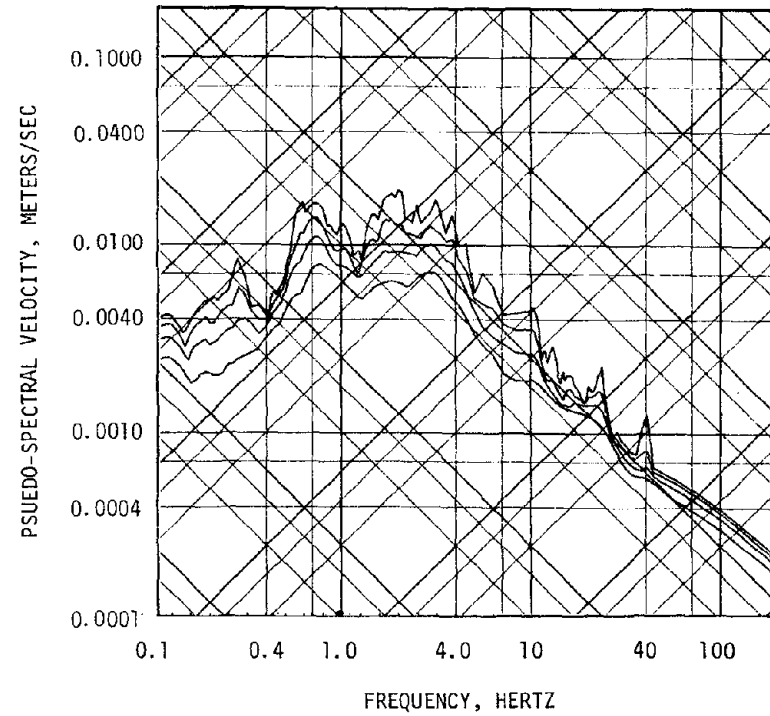
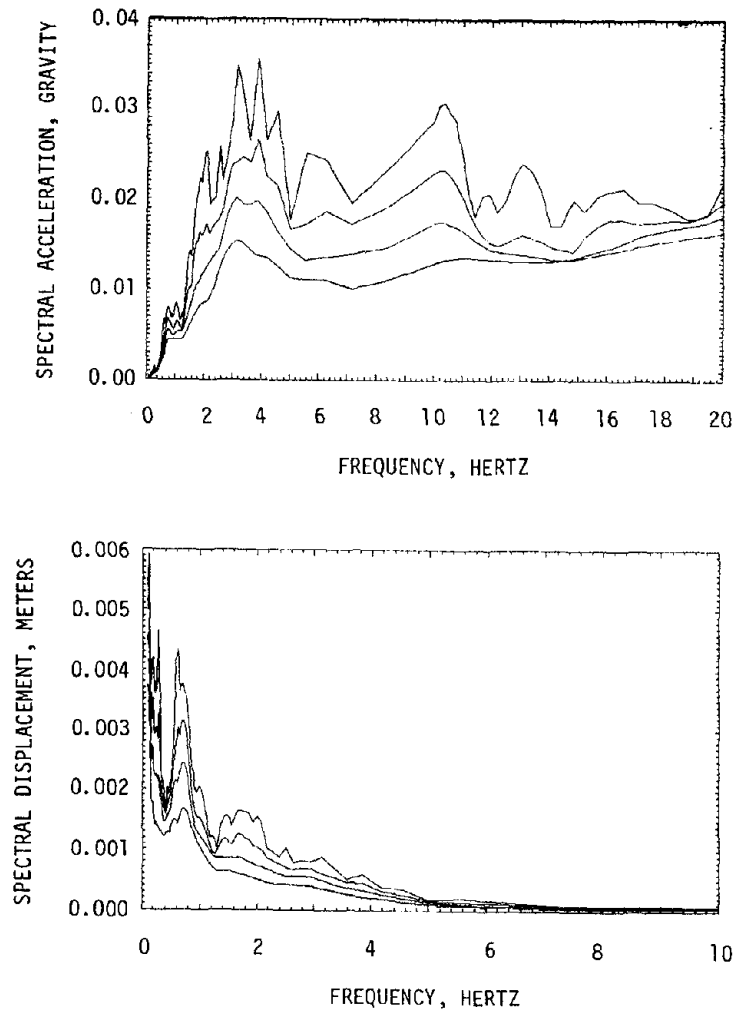


Fig. 4.13 Linear Elastic Response Spectra for Horizontal Base Motions of Test EQ 1

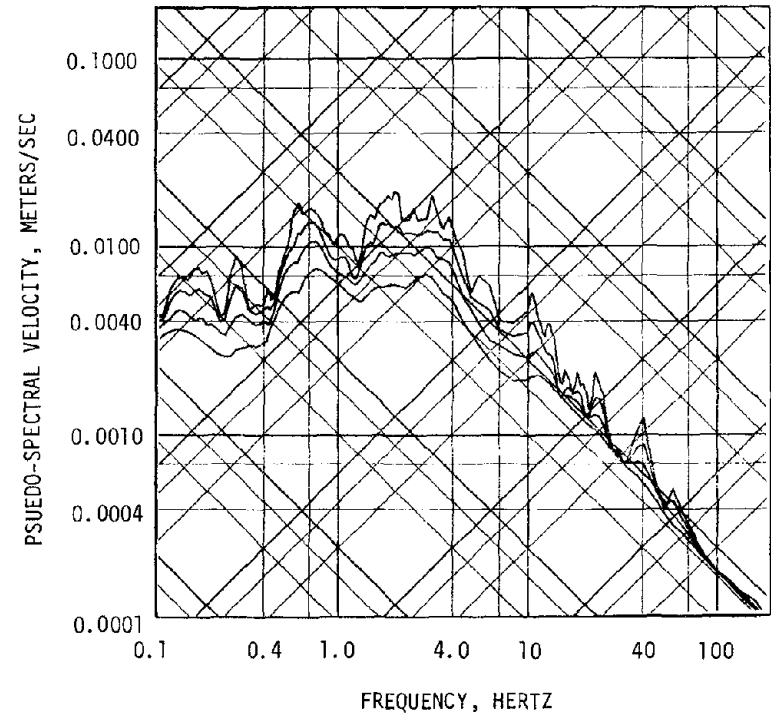
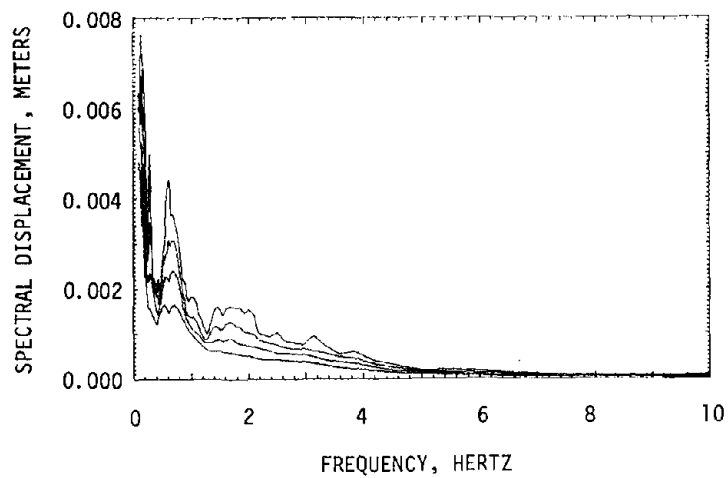
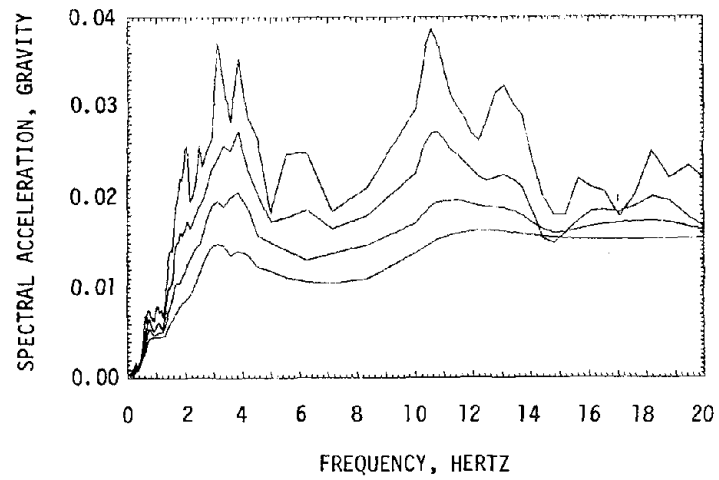


Fig. 4.14 Linear Elastic Response Spectra for Horizontal Base Motions of Test EQ 2

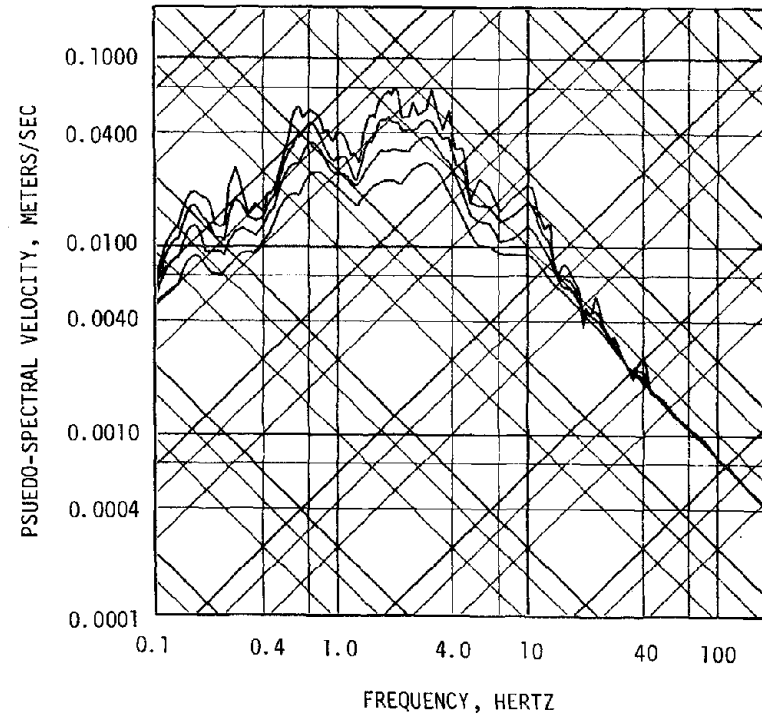
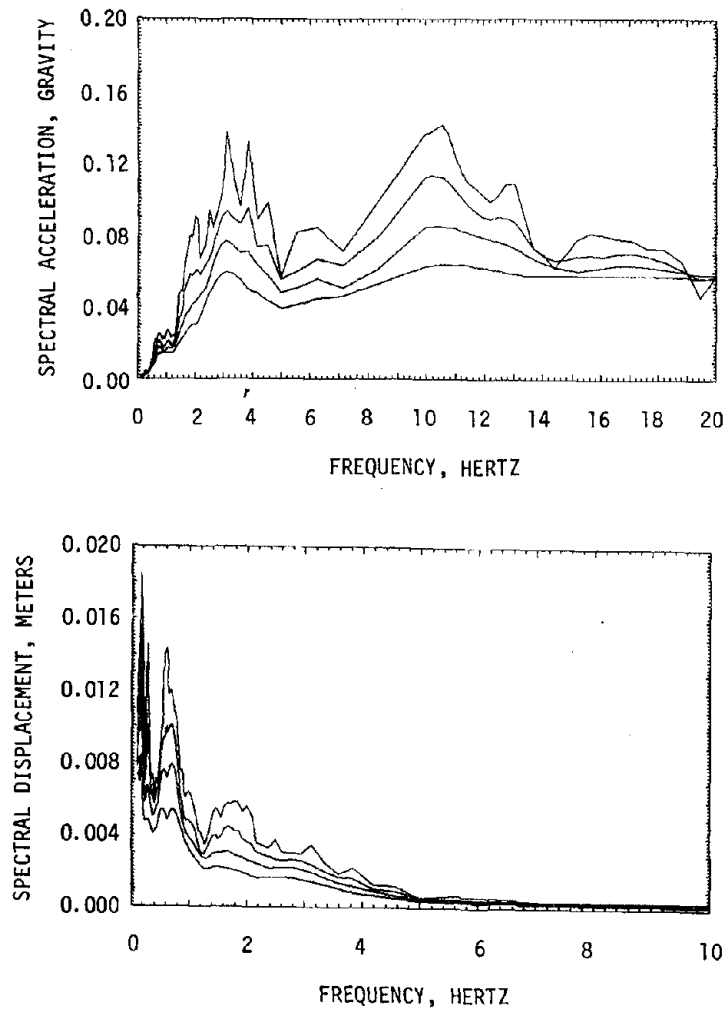


Fig. 4.15 Linear Elastic Response Spectra for Horizontal Base Motions of Test EQ 3

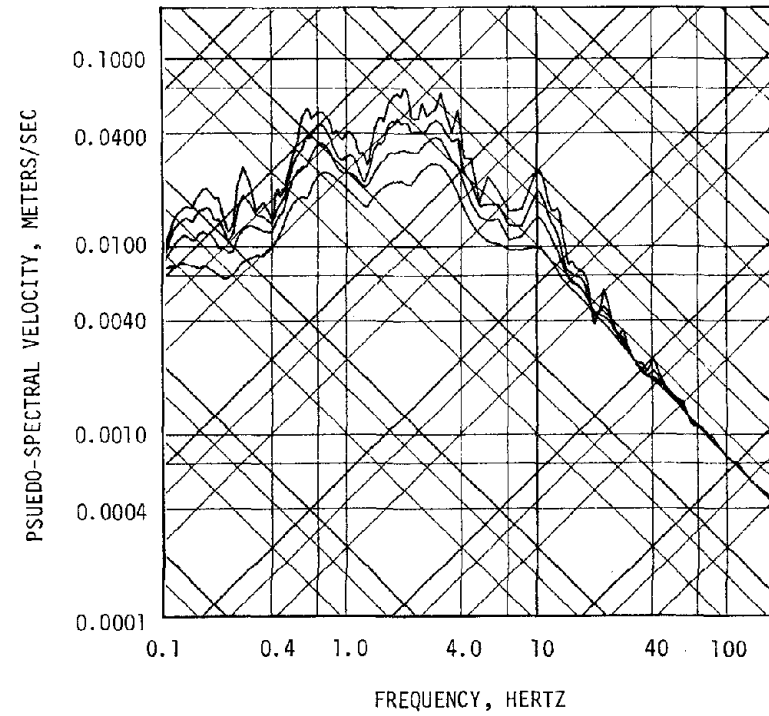
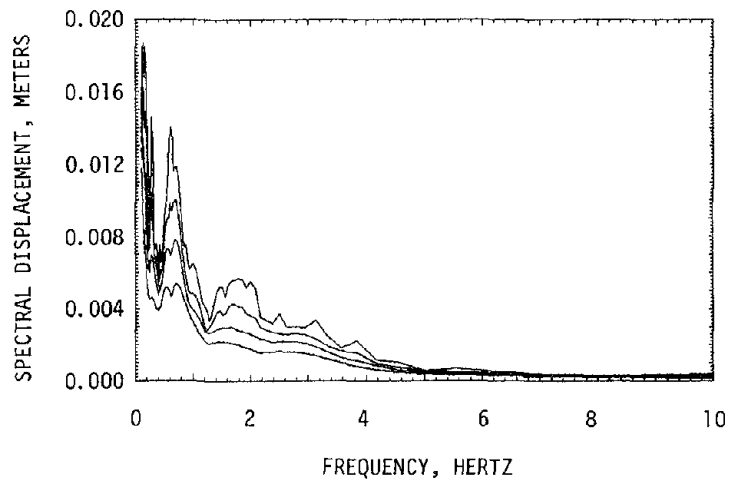
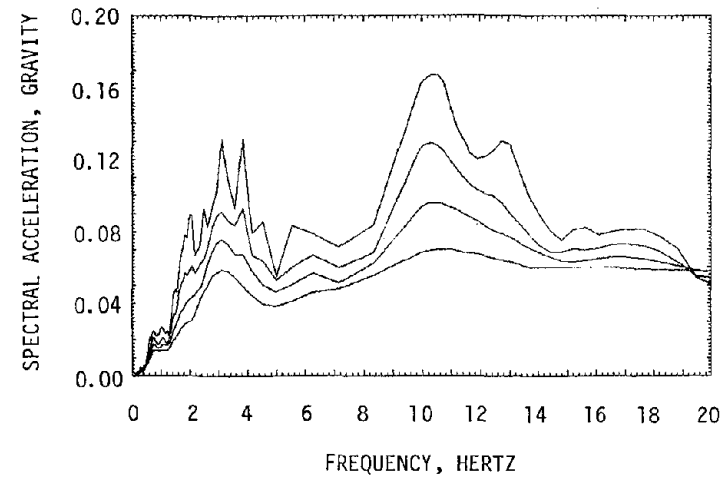


Fig. 4.16 Linear Elastic Response Spectra for Horizontal Base Motions of Test EQ 4

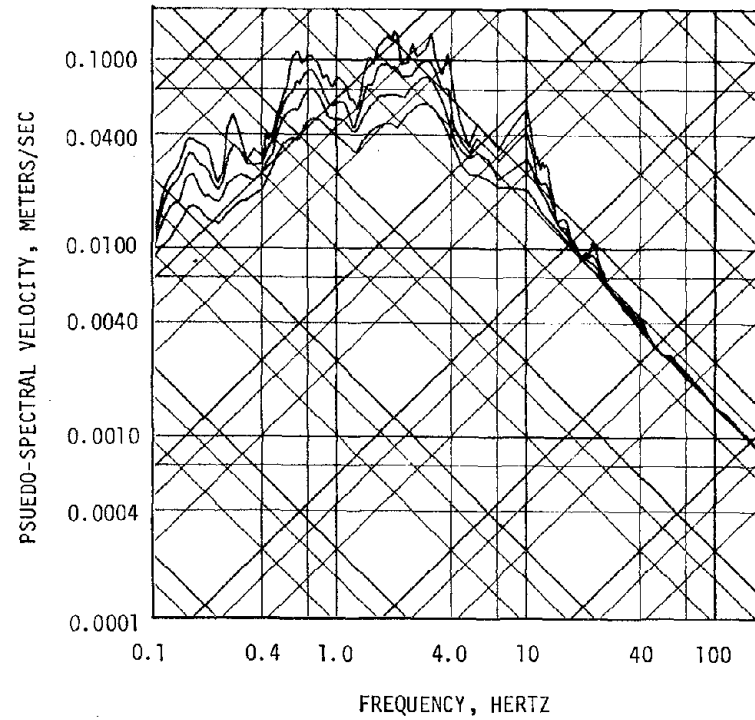
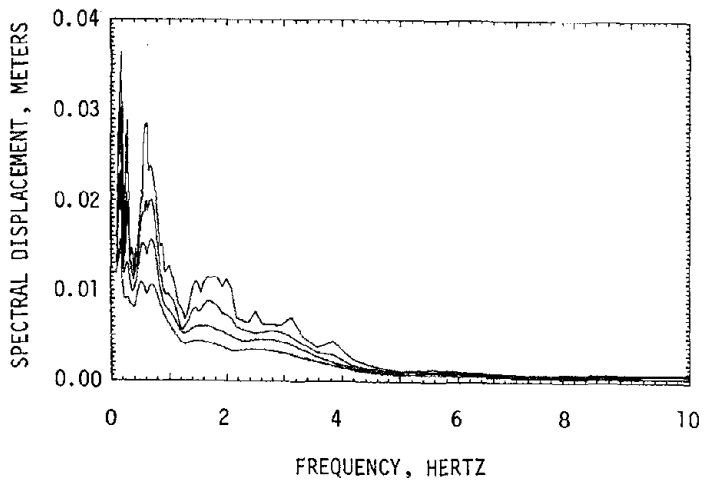
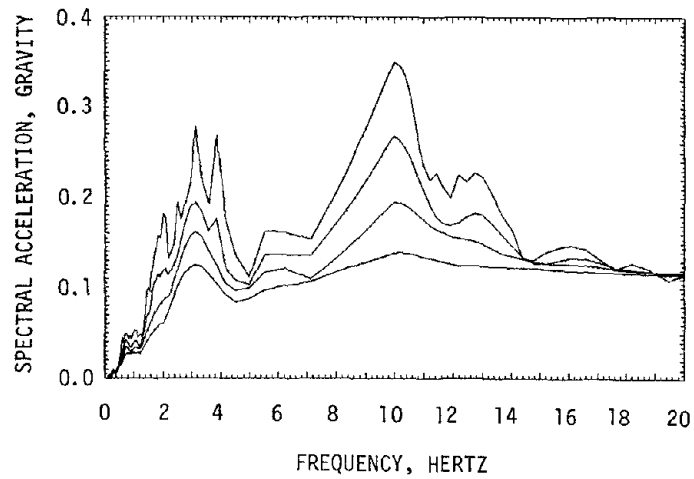


Fig. 4.17 Linear Elastic Response Spectra for Horizontal Base Motions of Test EQ 5

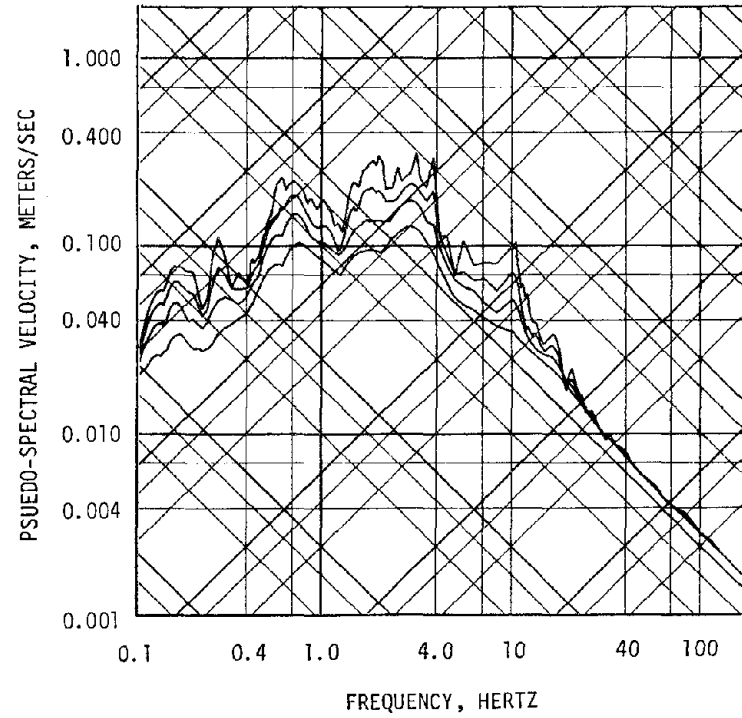
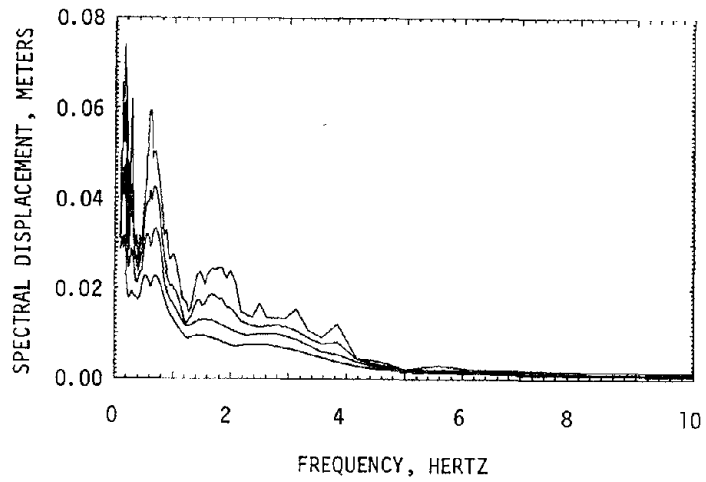
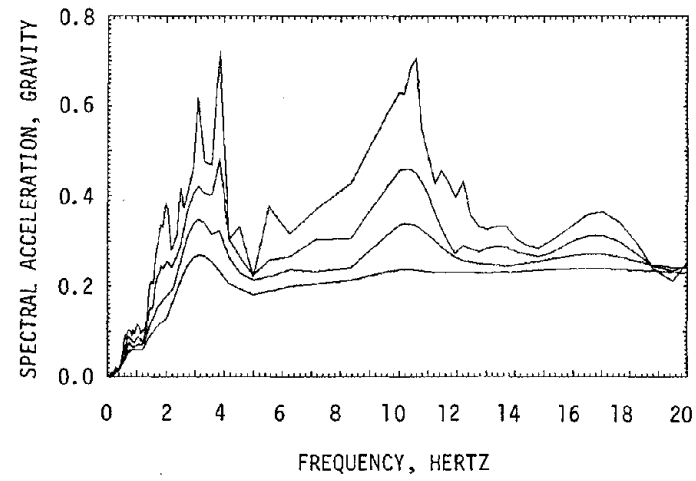


Fig. 4.18 Linear Elastic Response Spectra for Horizontal Base Motions of Test EQ 6

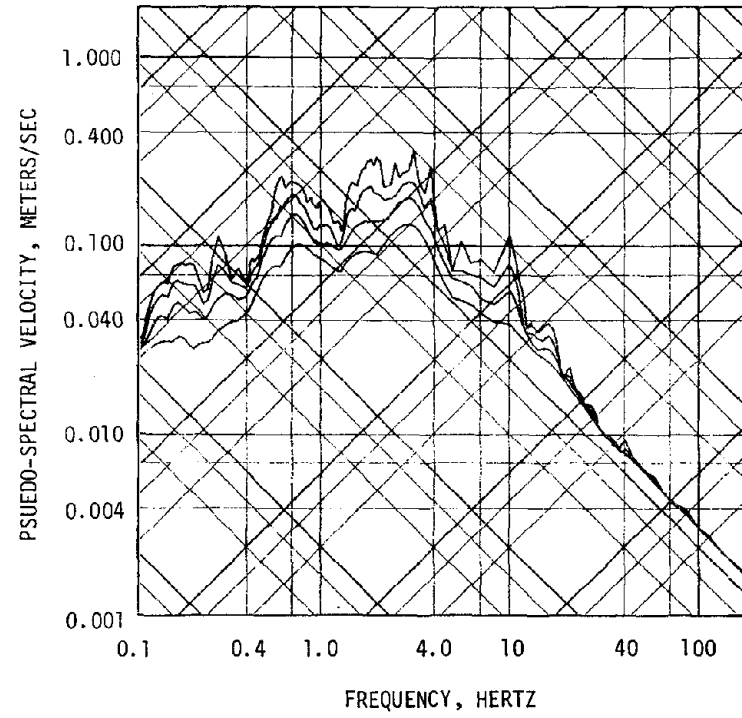
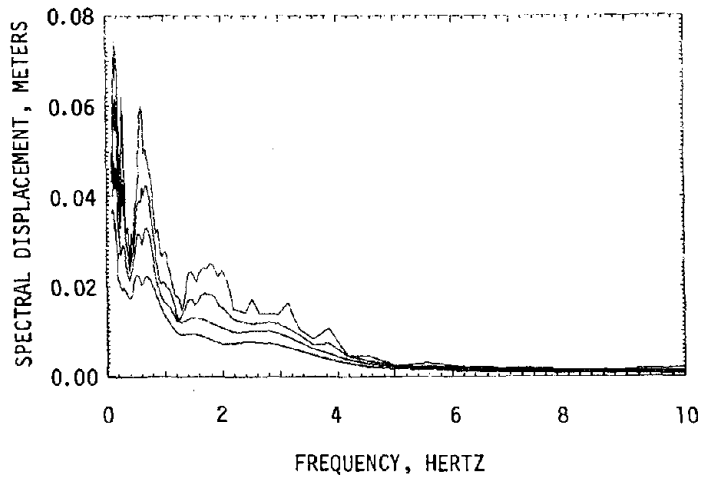
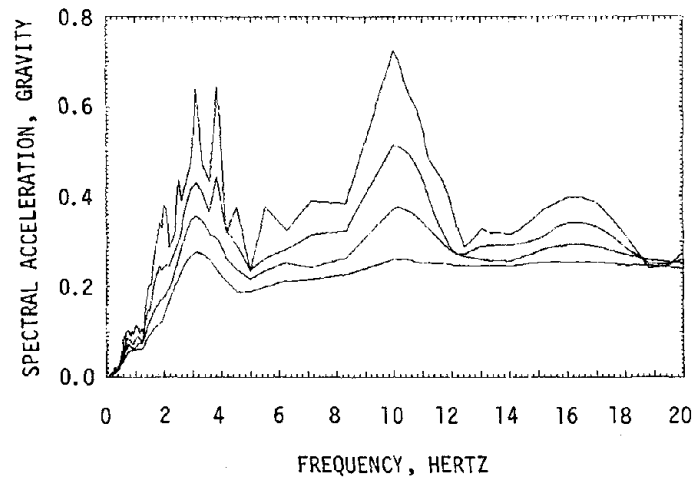


Fig. 4.19 Linear Elastic Response Spectra for Horizontal Base Motions of Test EQ 7

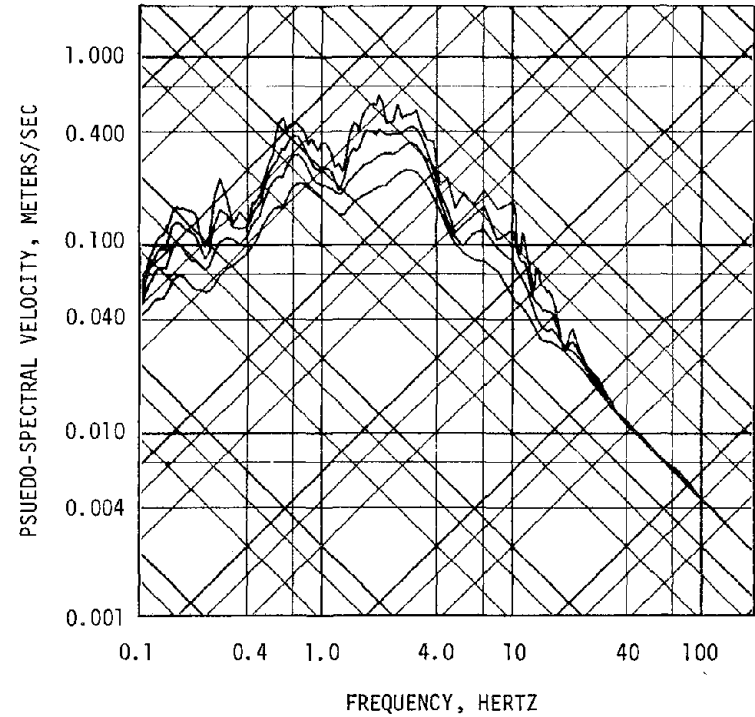
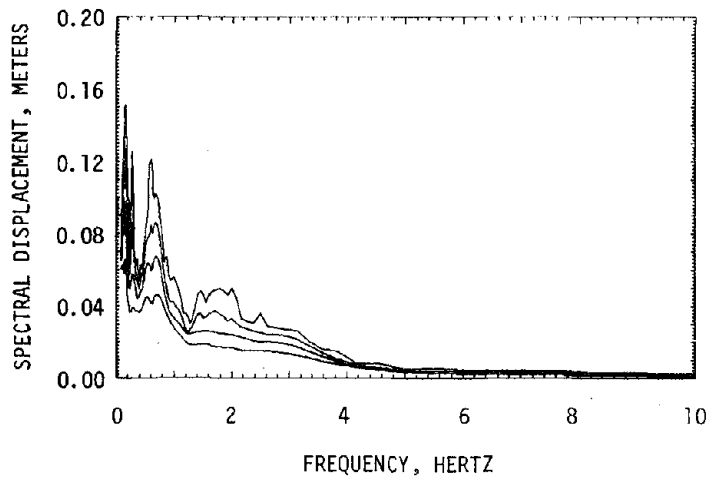
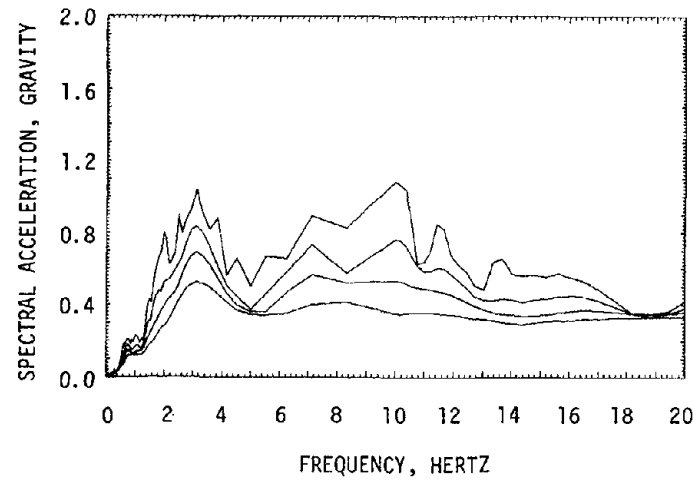


Fig. 4.20 Linear Elastic Response Spectra for Horizontal Base Motions of Test EQ 8

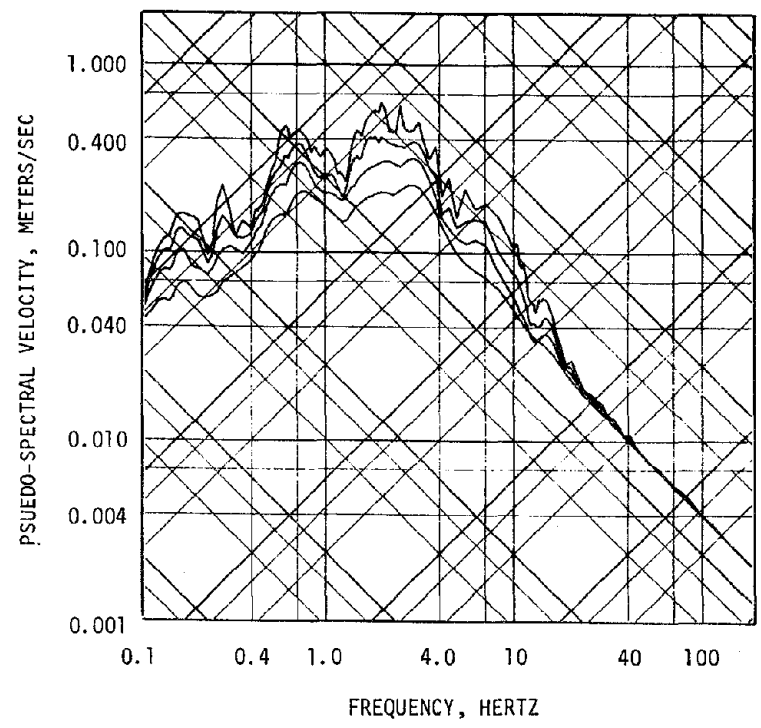
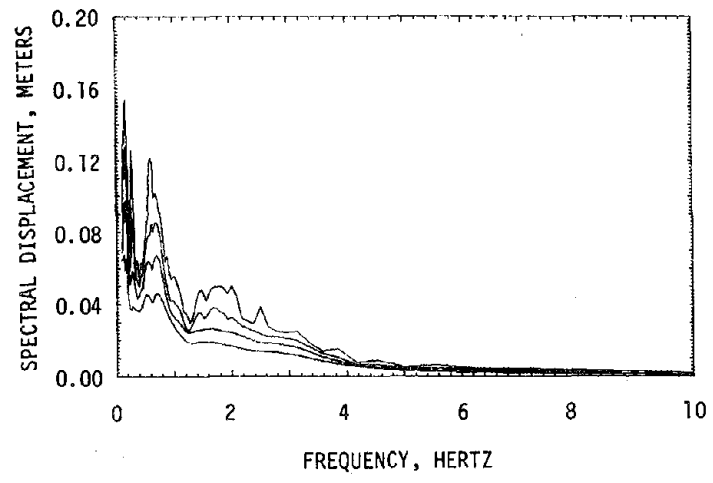
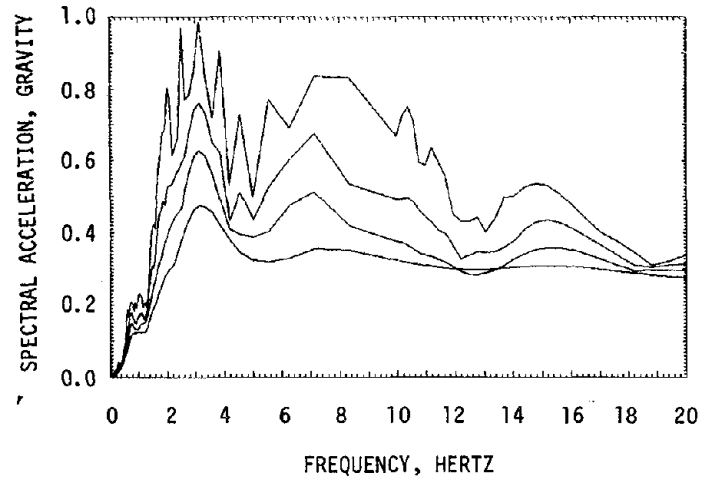


Fig. 4.21 Linear Elastic Response Spectra for Horizontal Base Motions of Test EQ 9

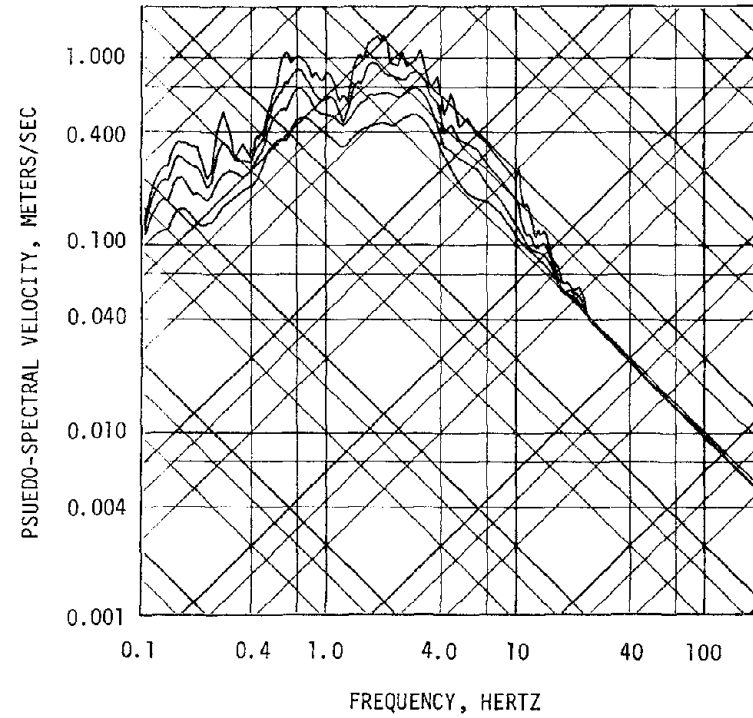
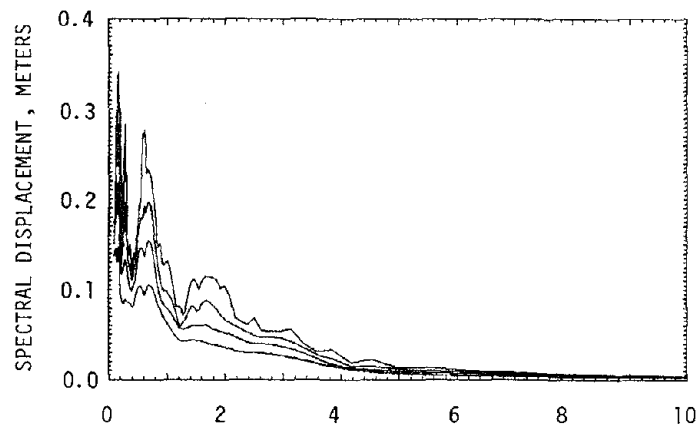
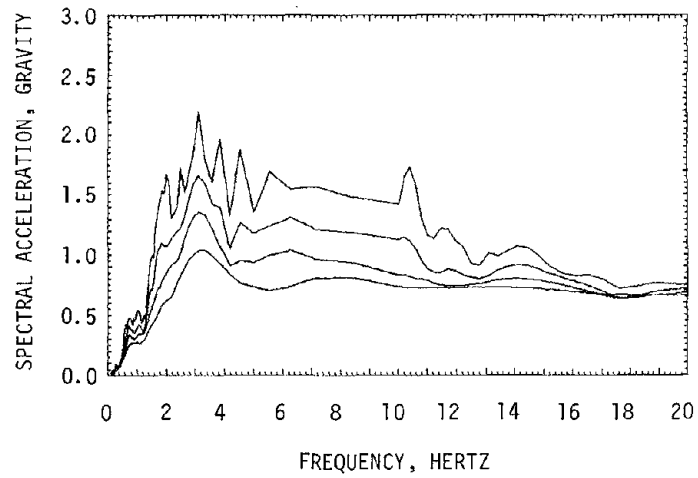


Fig. 4.22 Linear Elastic Response Spectra for Horizontal Base Motions of Test EQ 10

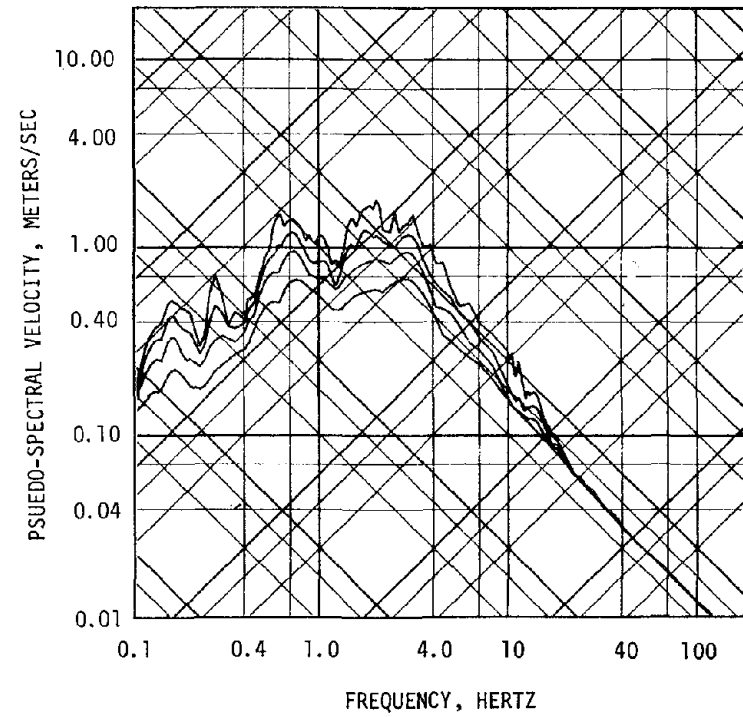
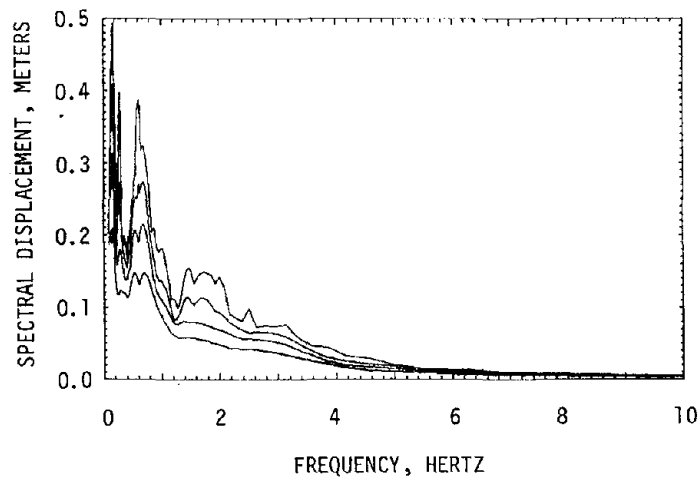
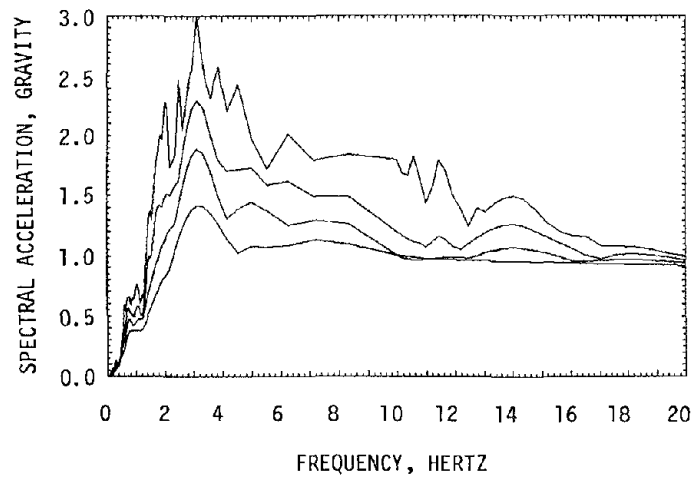


Fig. 4.23 Linear Elastic Response Spectra for Horizontal Base Motions of Test EQ 11

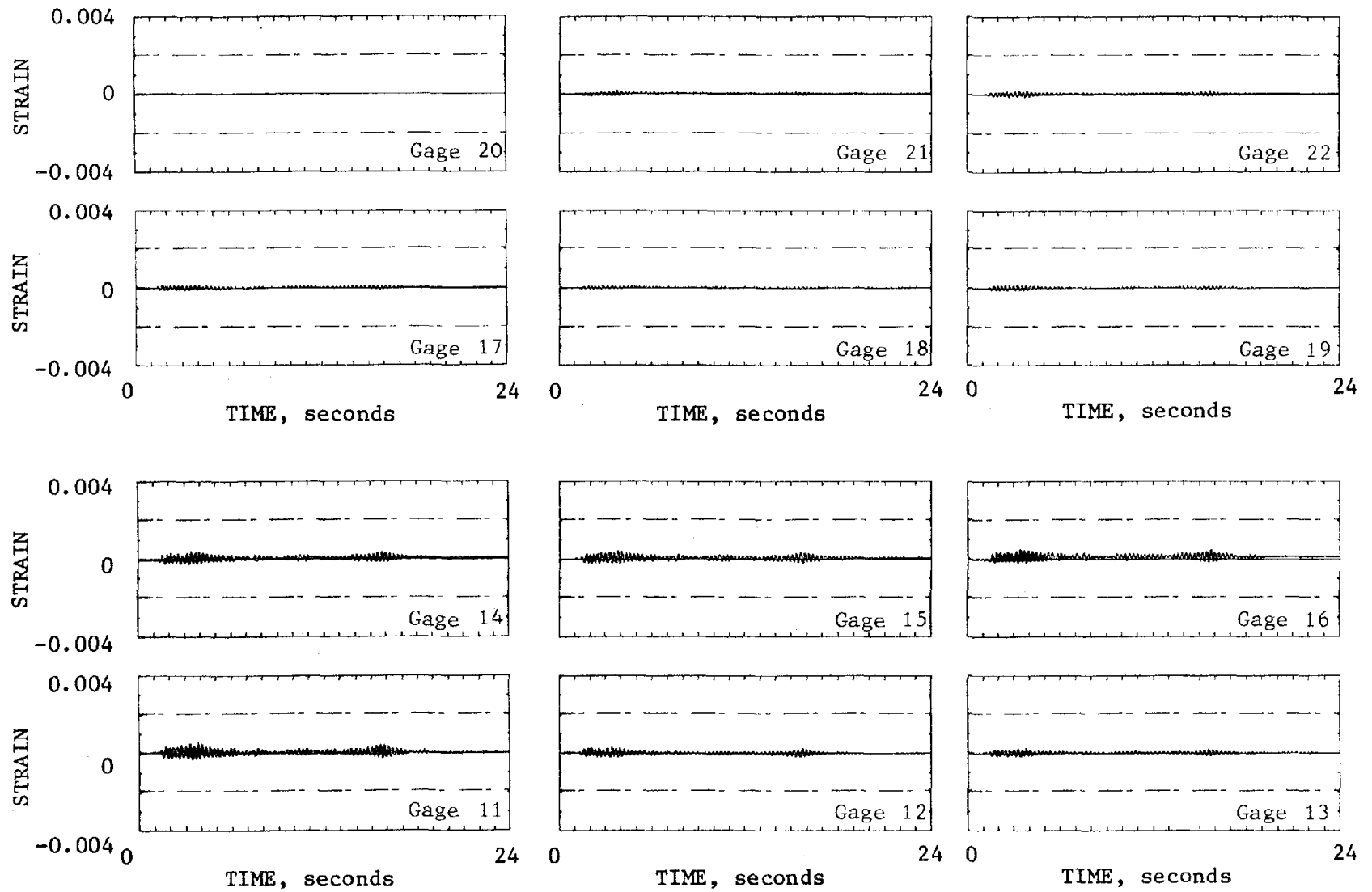


Fig. 4.24 Slab Reinforcement Strains During Test EQ 6

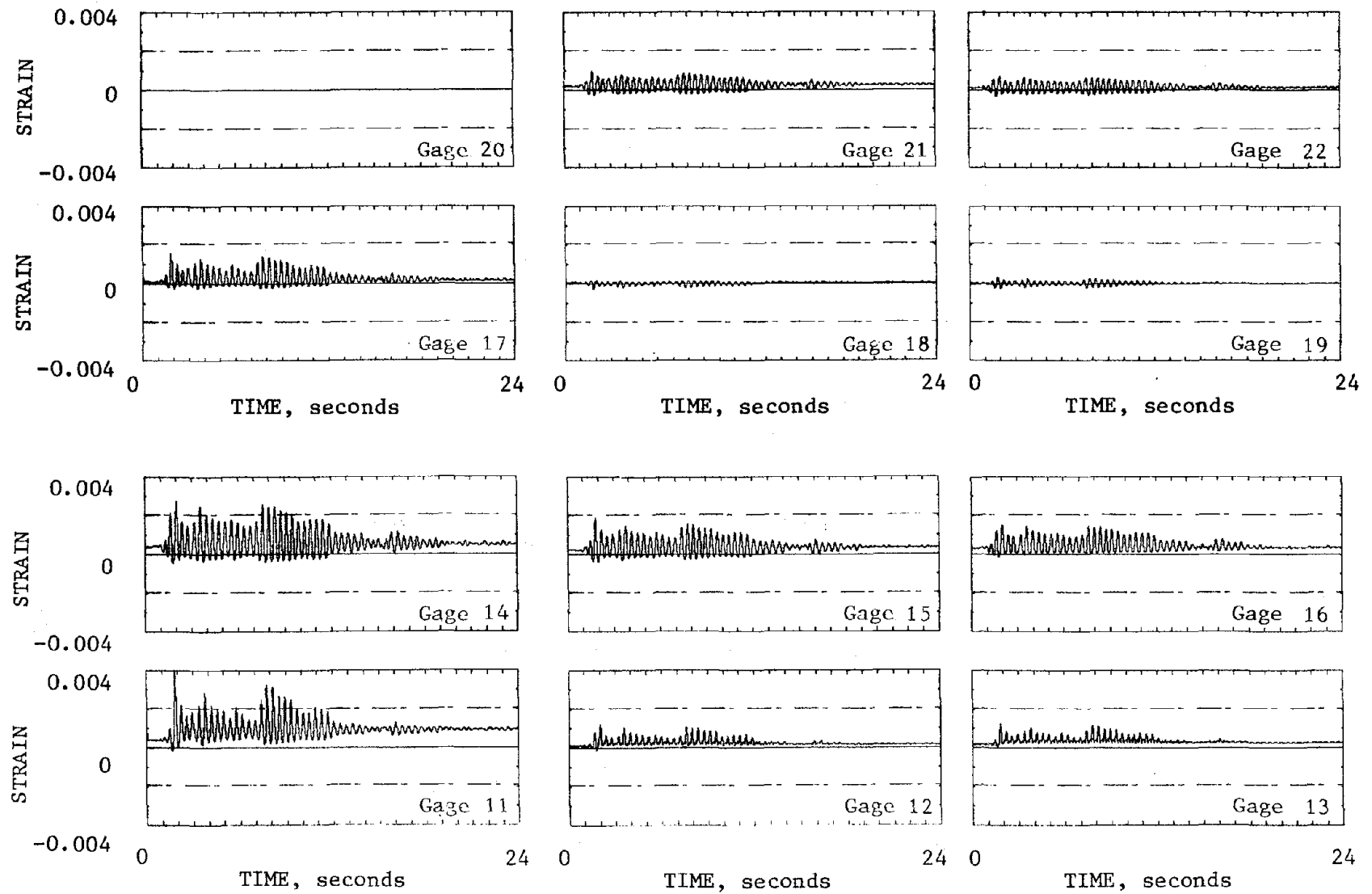


Fig. 4.25 Slab Reinforcement Strains During Test EQ 9

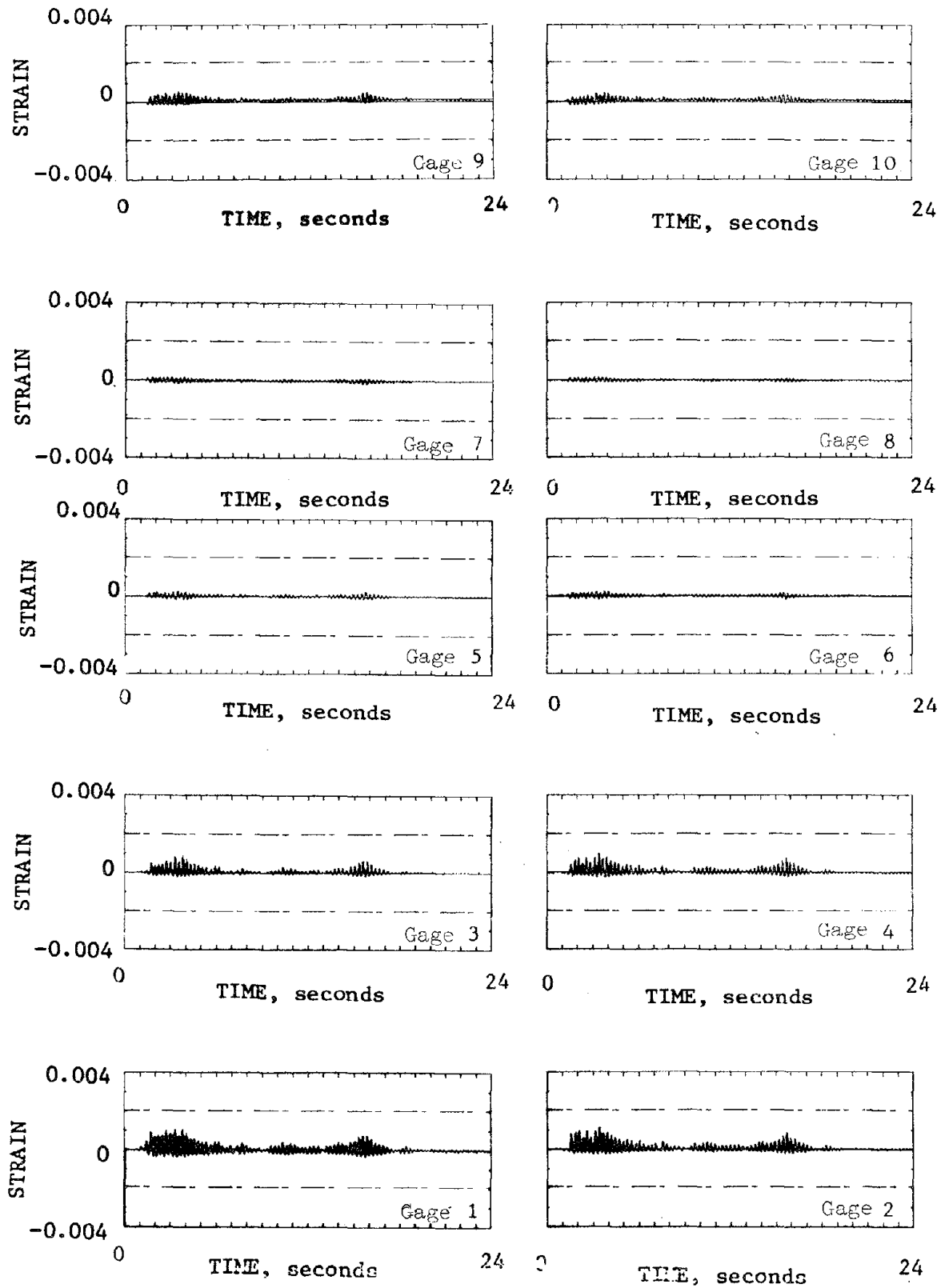


Fig. 4.26 Column Longitudinal Reinforcement Strains During Test EQ 6

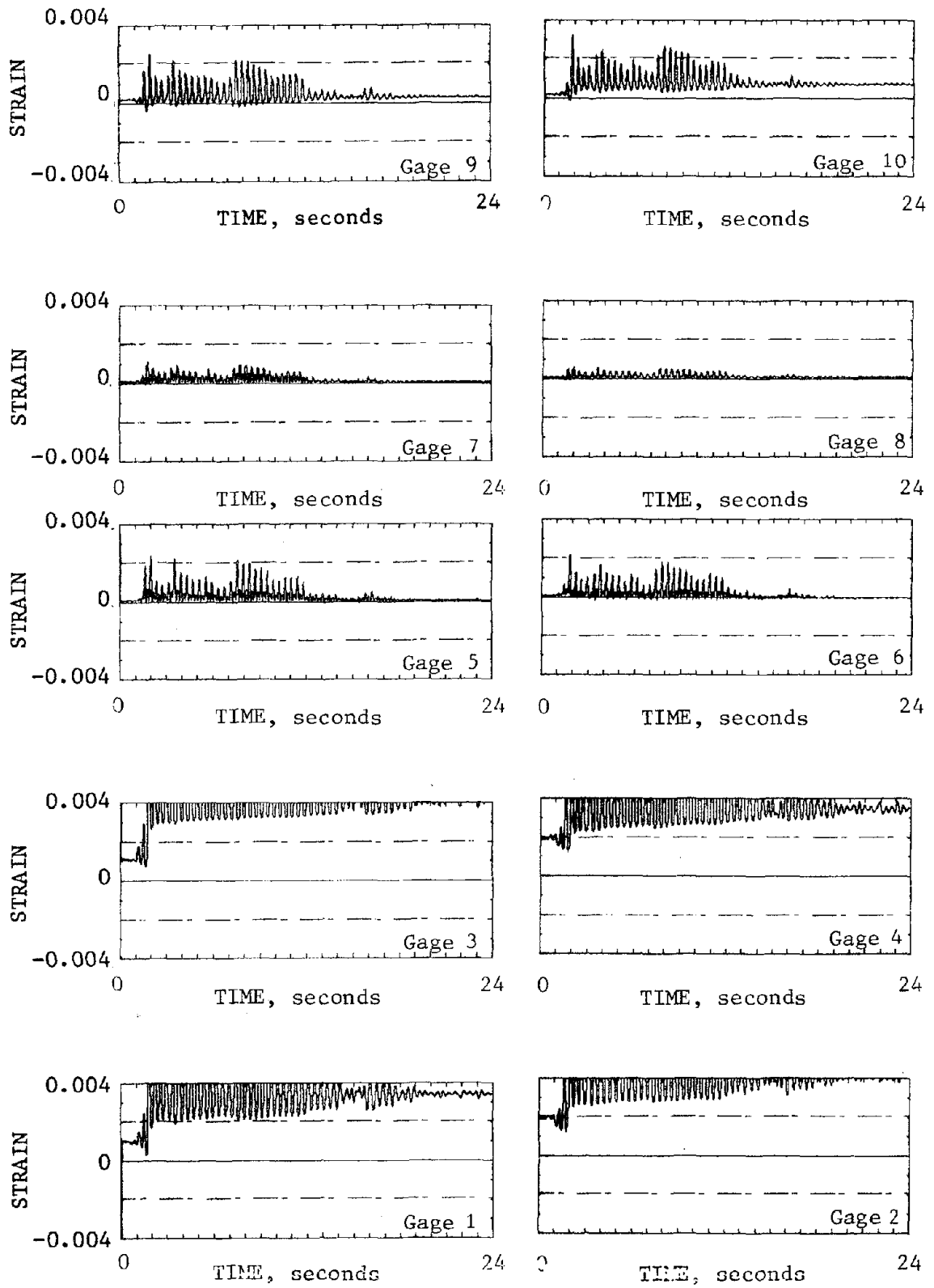


Fig. 4.27 Column Longitudinal Reinforcement Strains During Test EQ 9

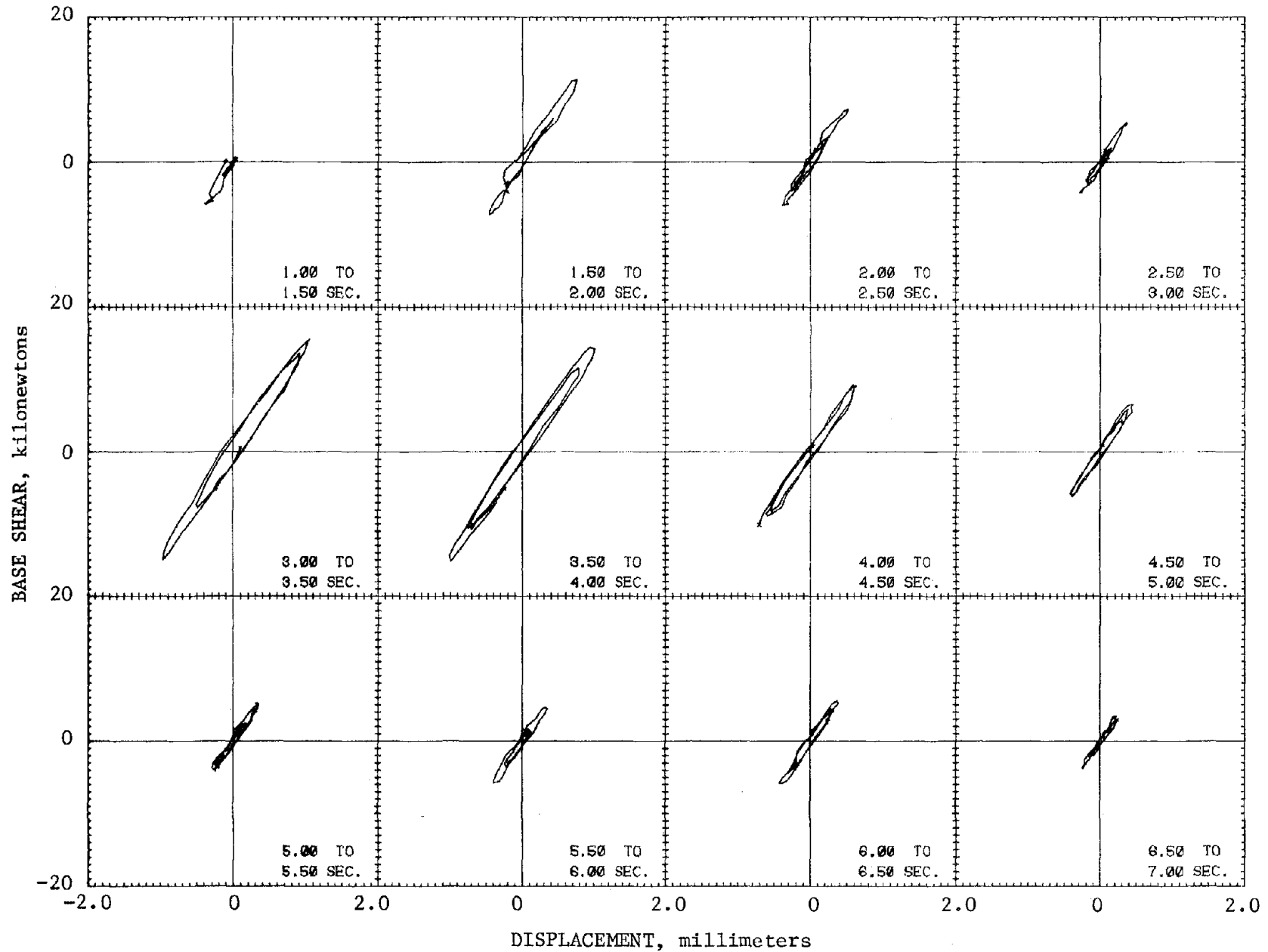


Fig. 4.28 Relation Between Base Shear and Top Floor Displacement During Test EQ 4

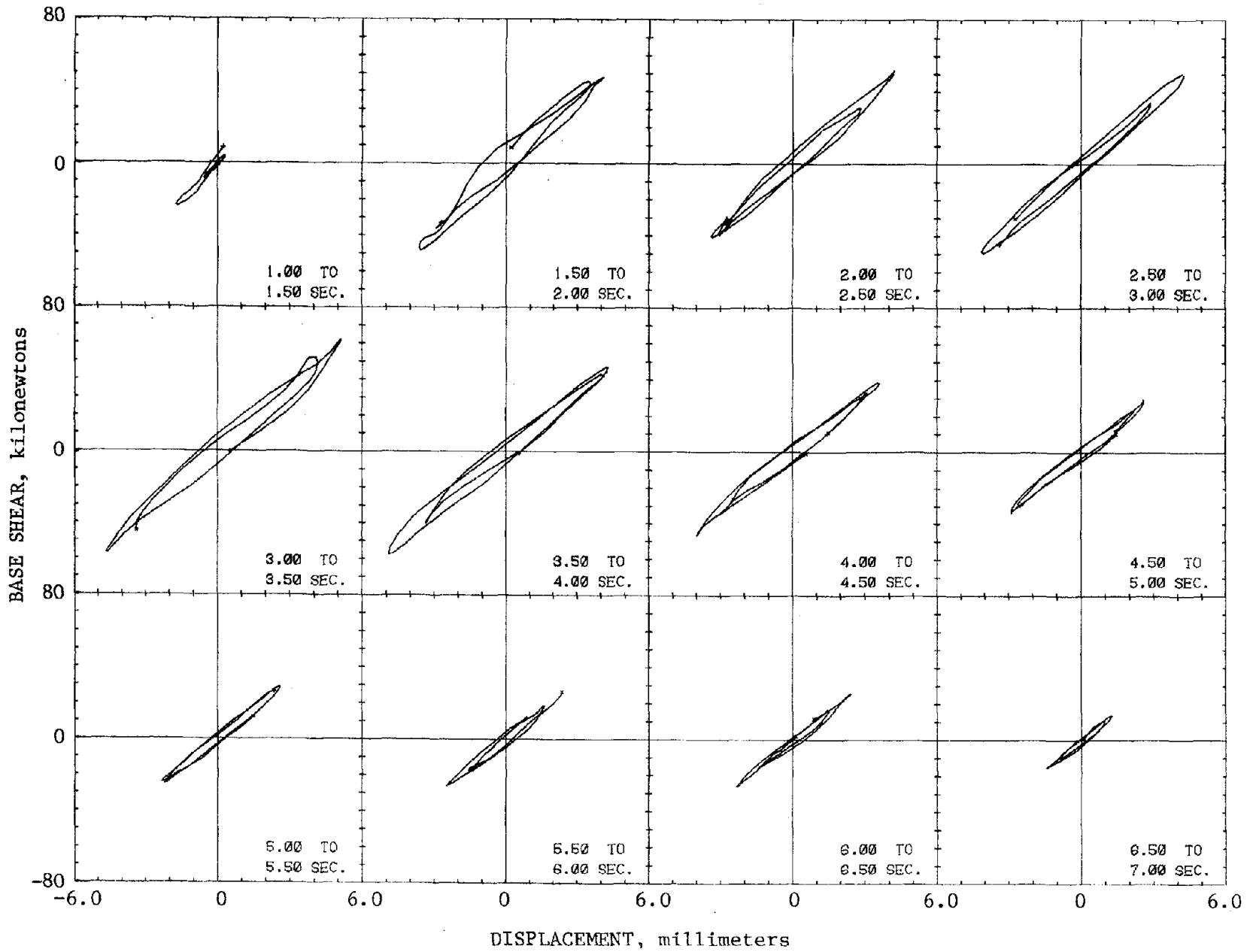


Fig. 4.29 Relation Between Base Shear and Top Floor Displacement During Test EQ 6

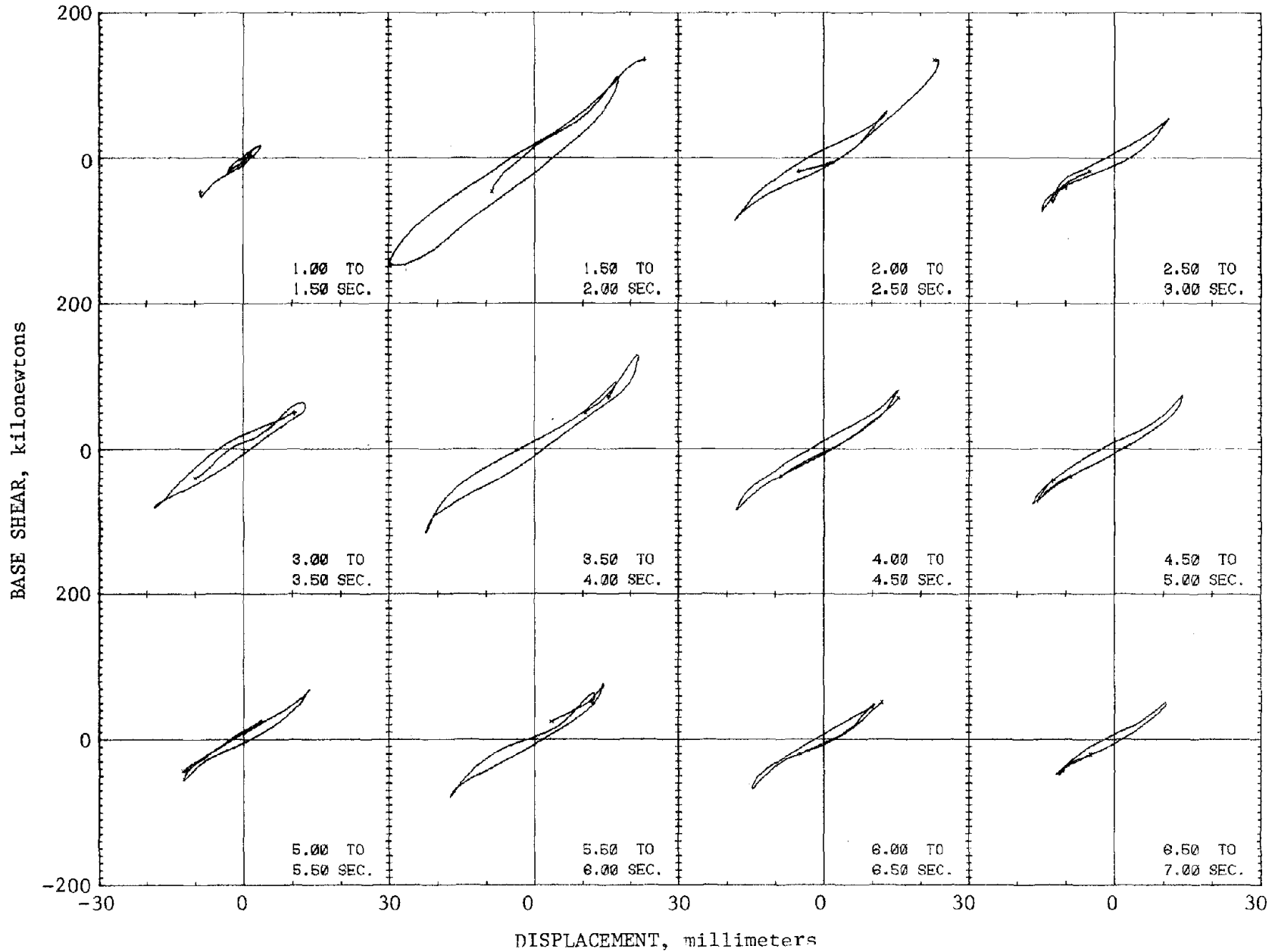


Fig. 4.30 Relation Between Base Shear and Top Floor Displacement During Test EQ 9

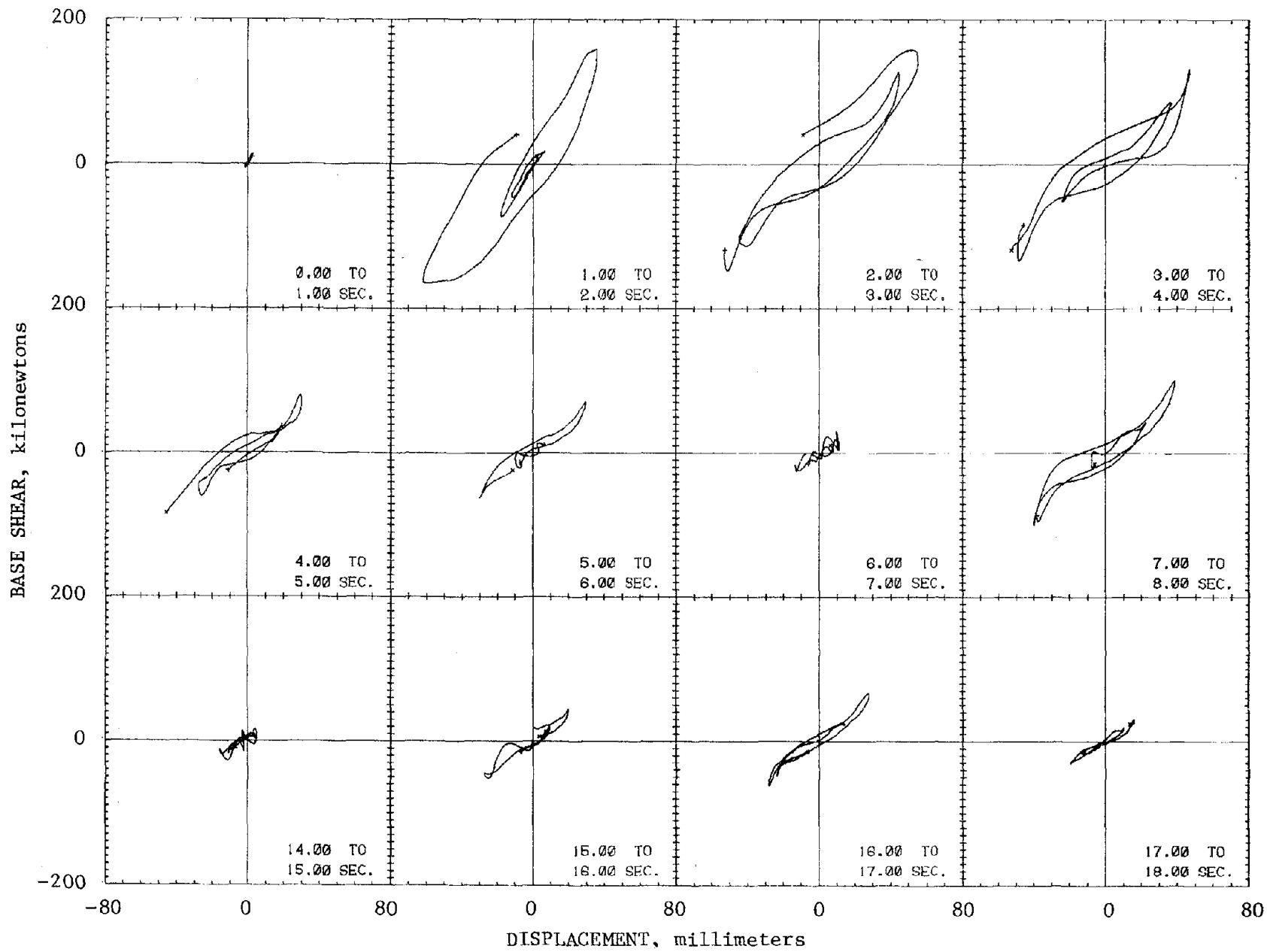


Fig. 4.31 Relation Between Base Shear and Top Floor Displacement During Test EQ 10

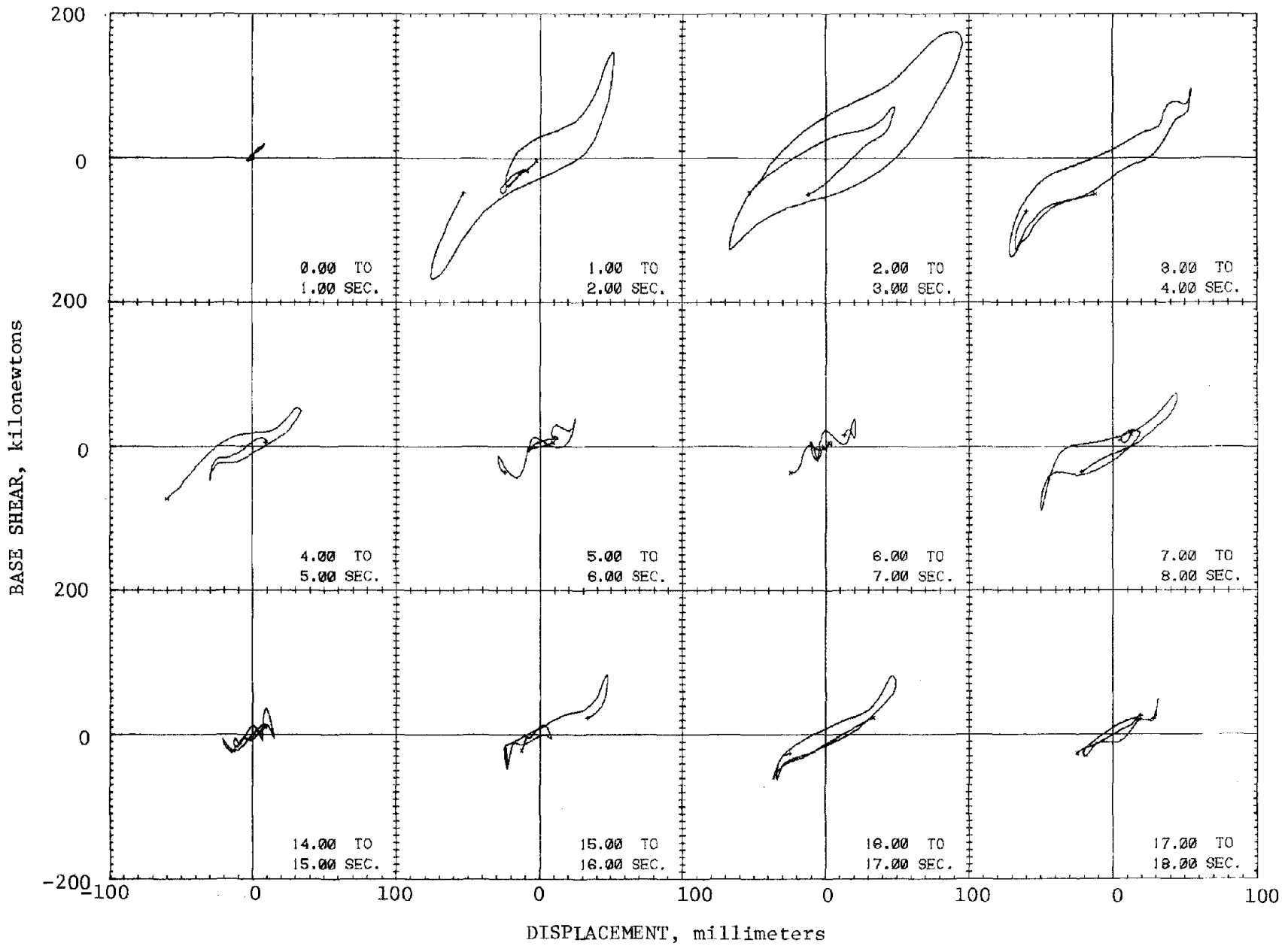


Fig. 4.32 Relation Between Base Shear and Top Floor Displacement During Test EQ 11

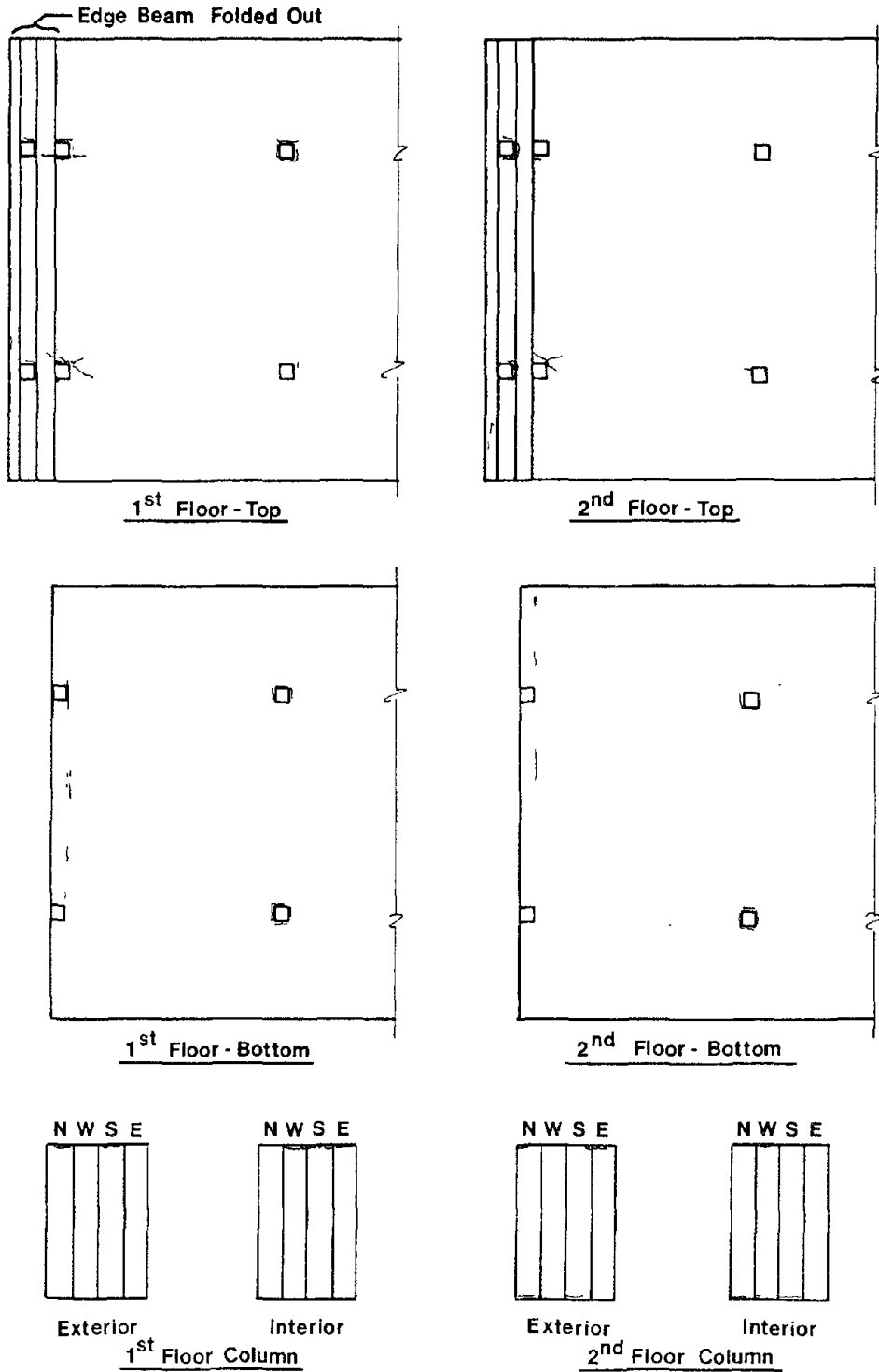


Fig. 4.33 Crack Patterns Observed Before Testing

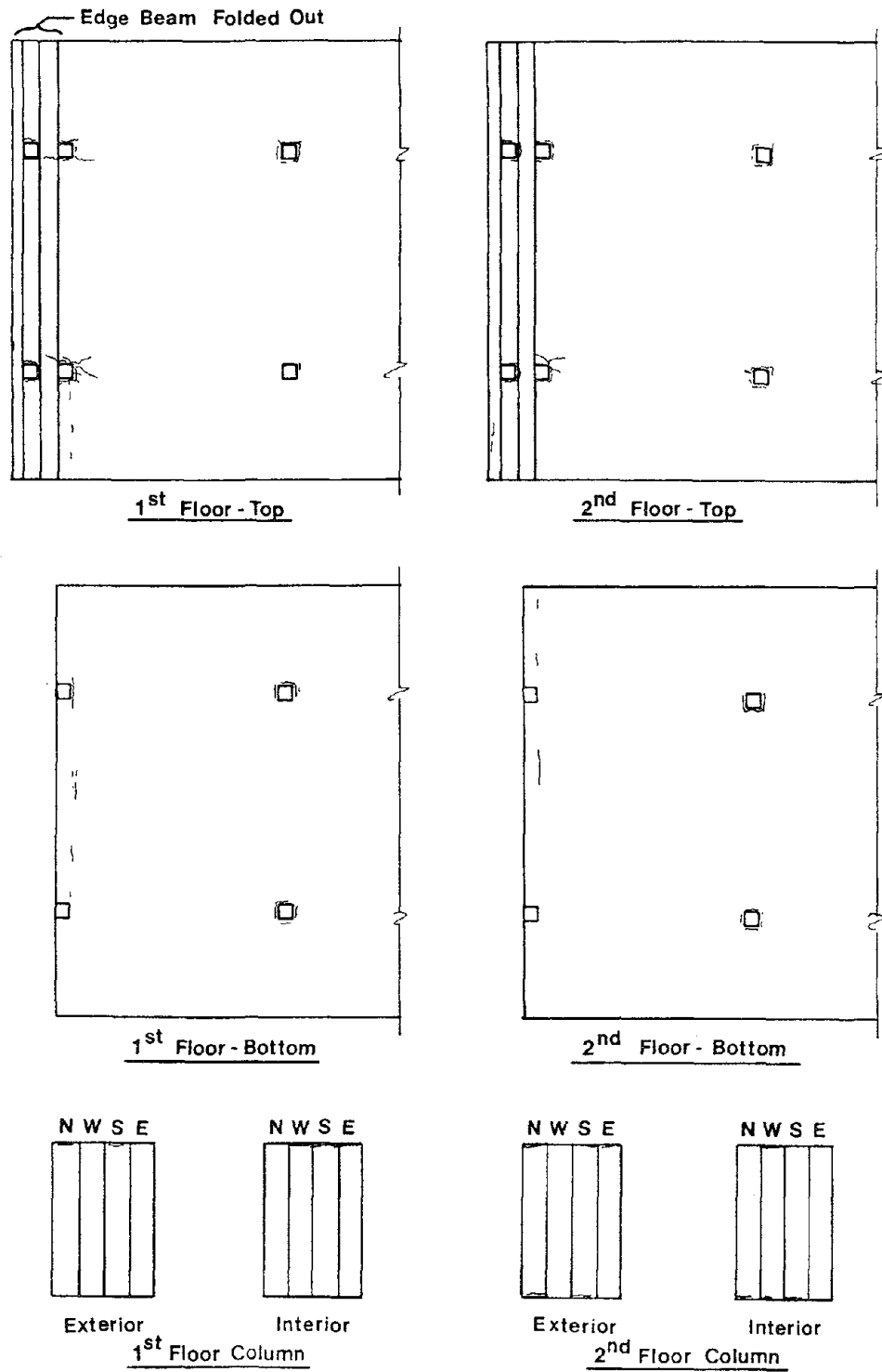


Fig. 4.34 Crack Patterns Observed Following Test EQ 4

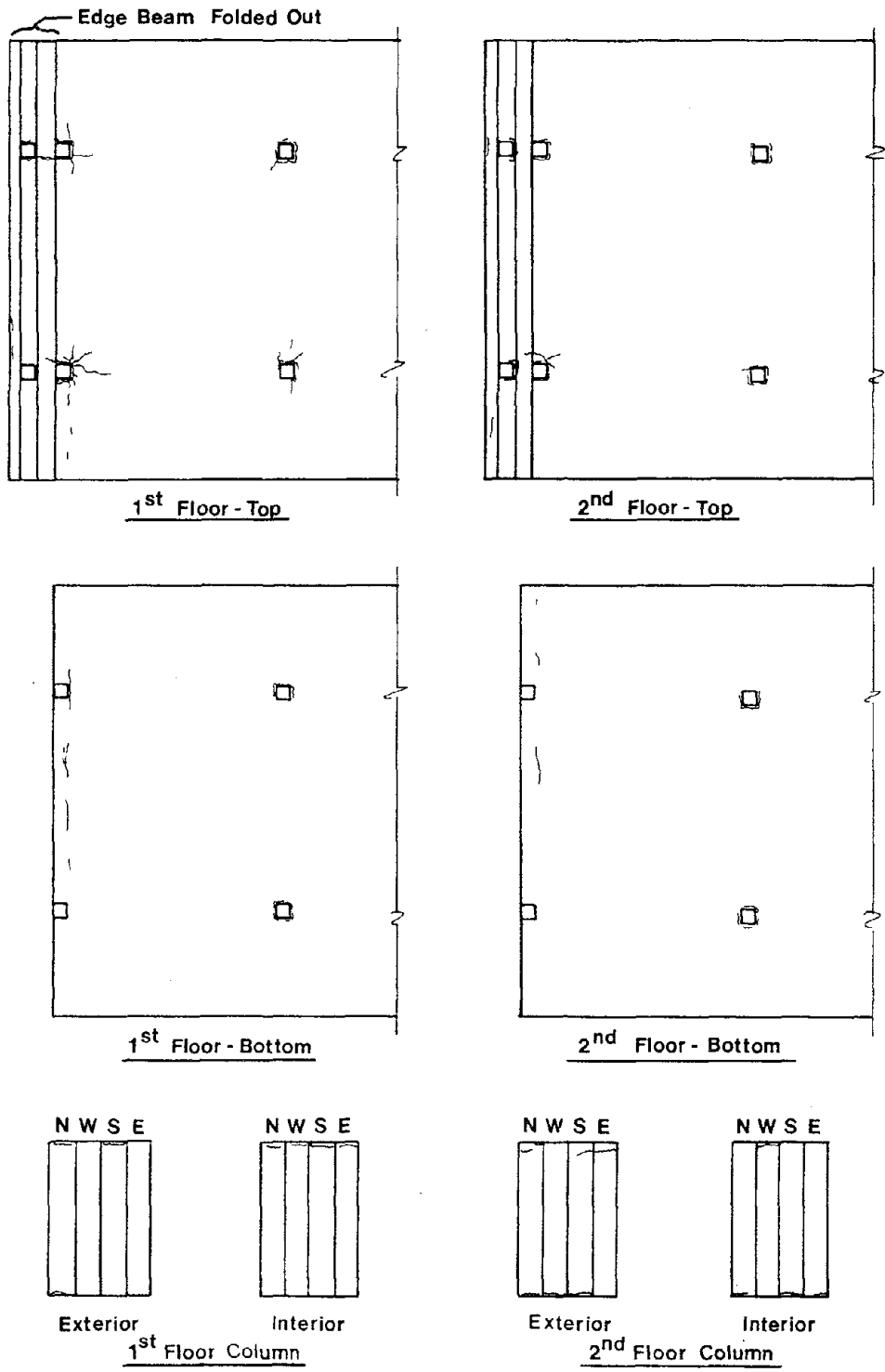


Fig. 4.35 Crack Patterns Observed Following Test EQ 6

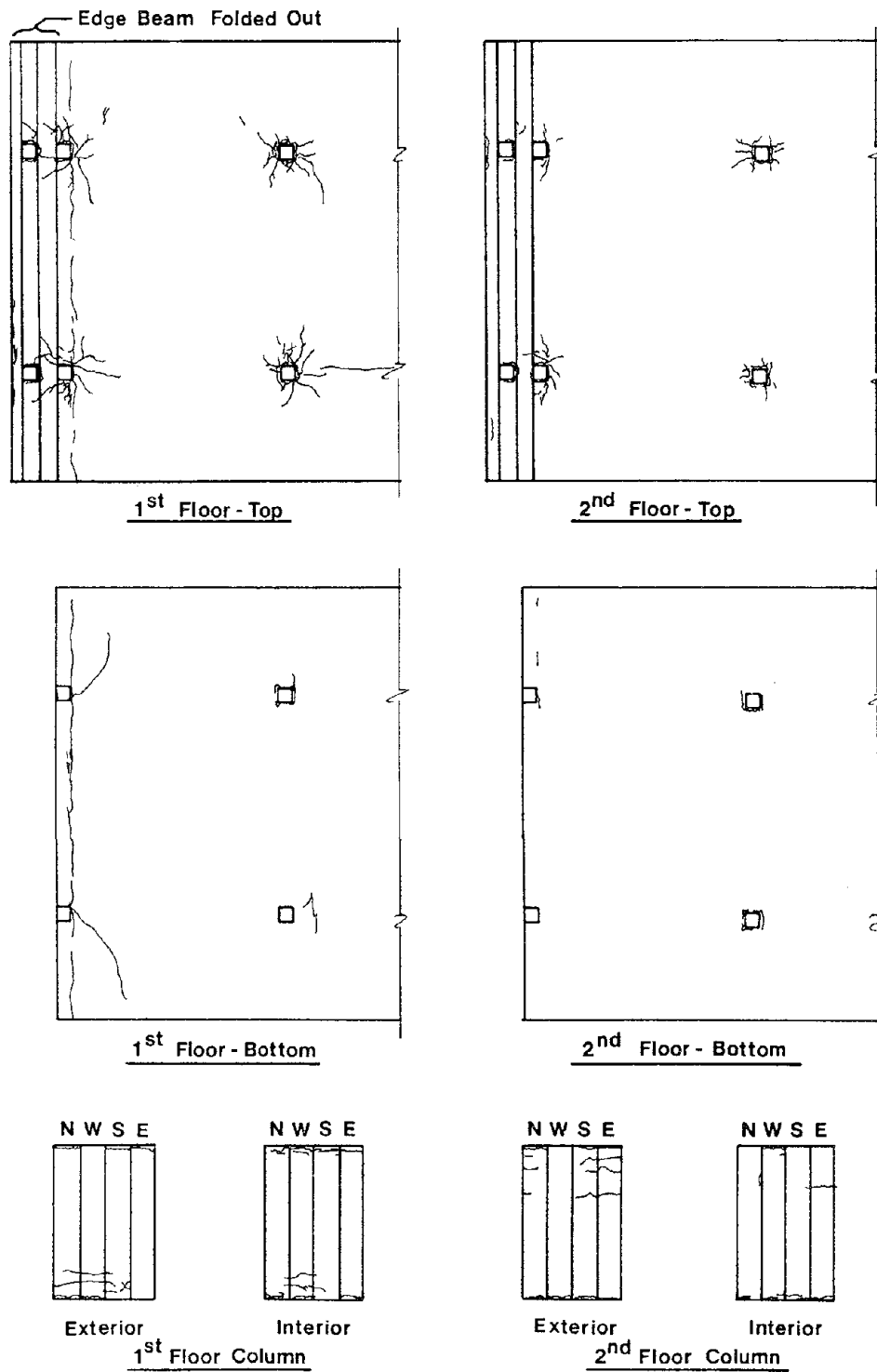


Fig. 4.36 Crack Patterns Observed Following Test EQ 9

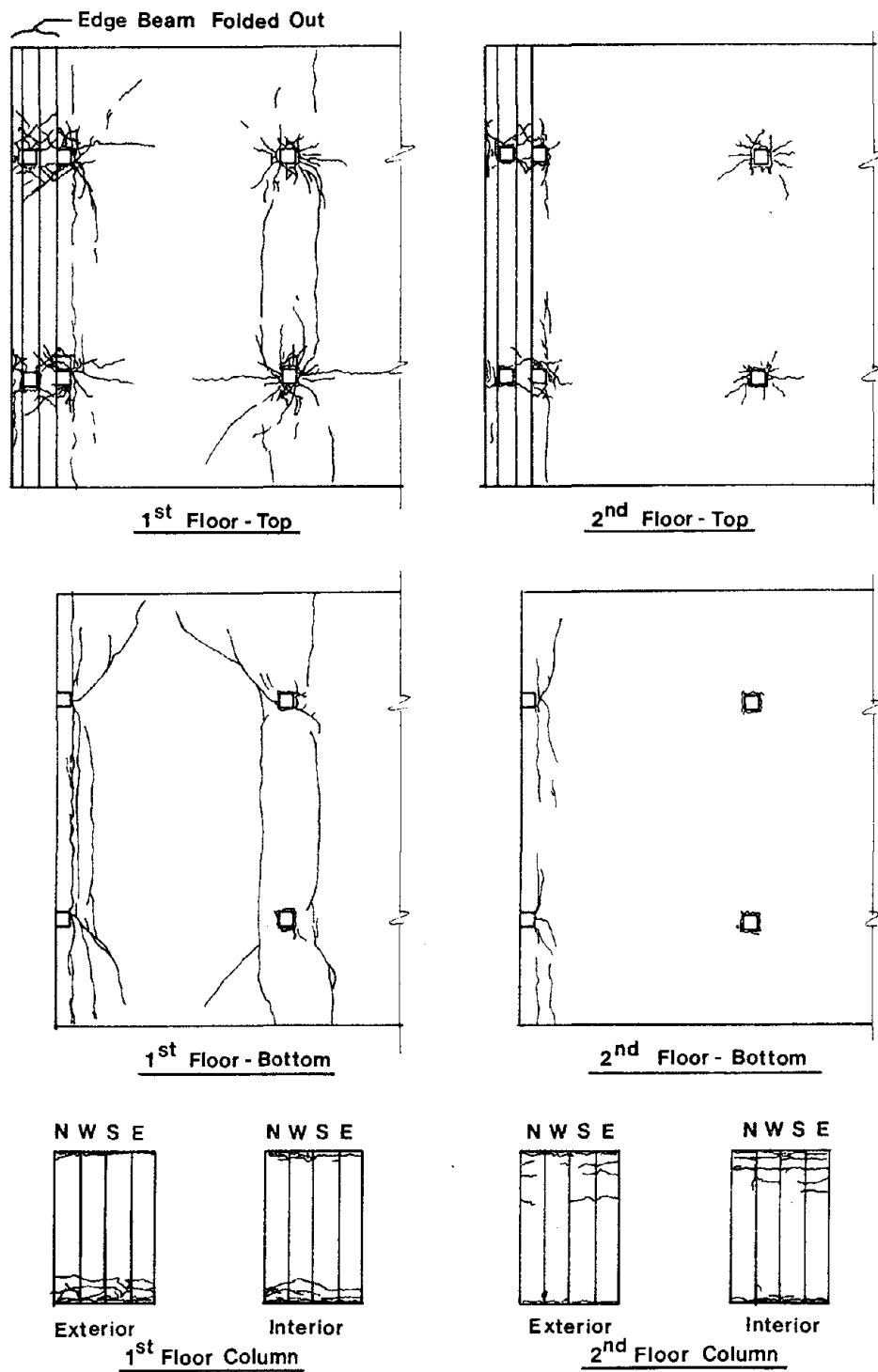


Fig. 4.37 Crack Patterns Observed Following Test EQ 10

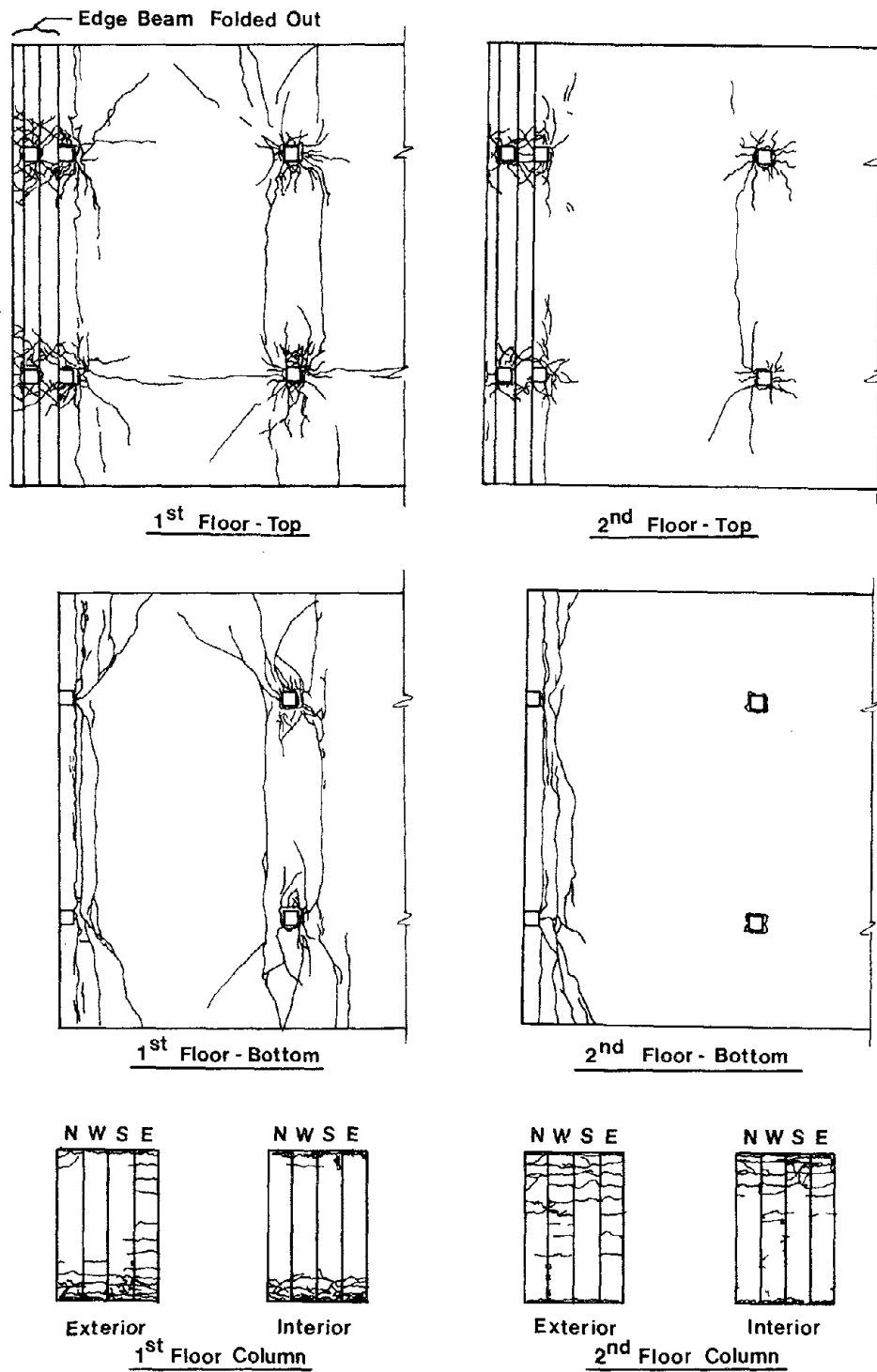
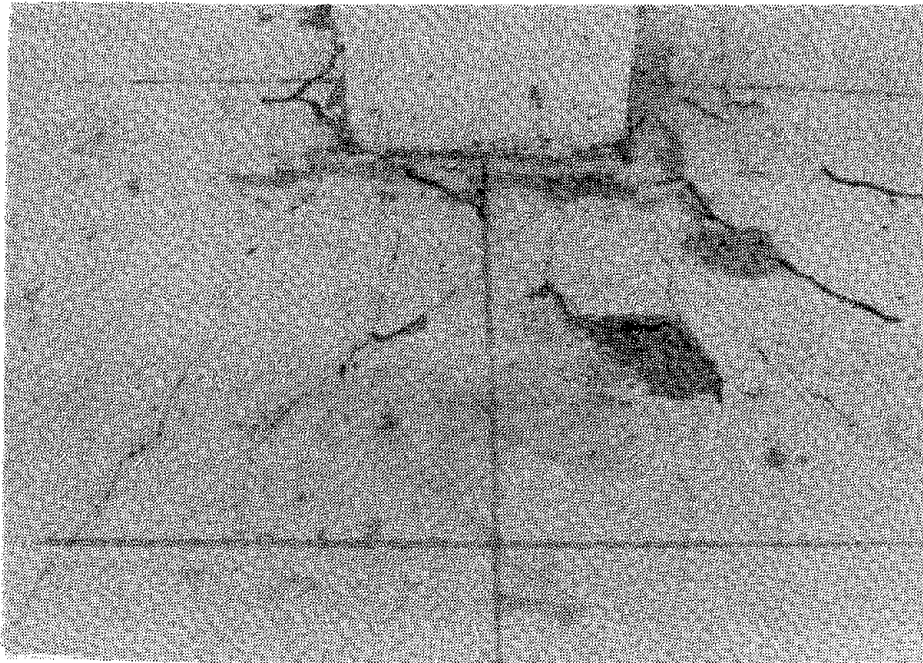
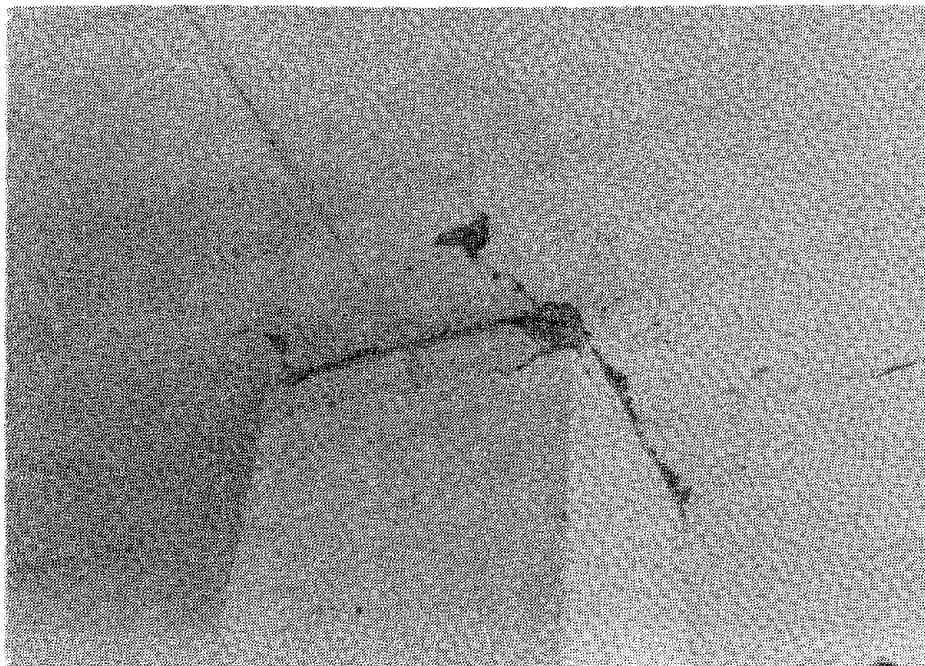


Fig. 4.38 Crack Patterns Observed Following Test EQ 11

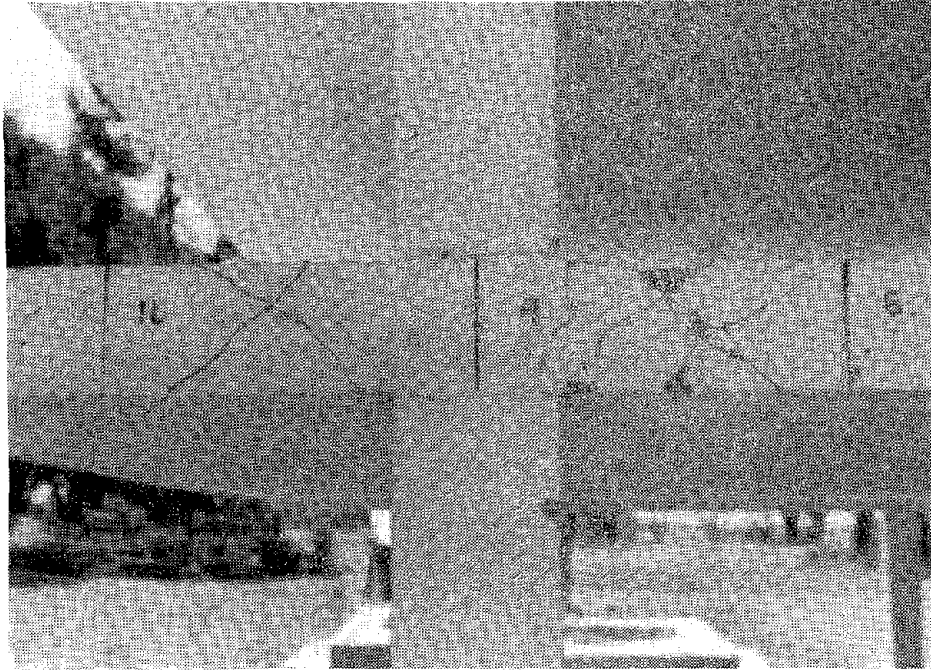


(a) First-Floor Interior Slab-Column Connection Viewed From Top



(b) First-Floor Interior Slab-Column Connection Viewed From Bottom

Fig. 4.39 Photographs of Typical Damage Following Test EQ 11



(c) First-Floor Edge Beam



(d) Exterior Column at Footing

Fig. 4.39 (cont'd.) Photographs of Typical Damage Following Test EQ 11

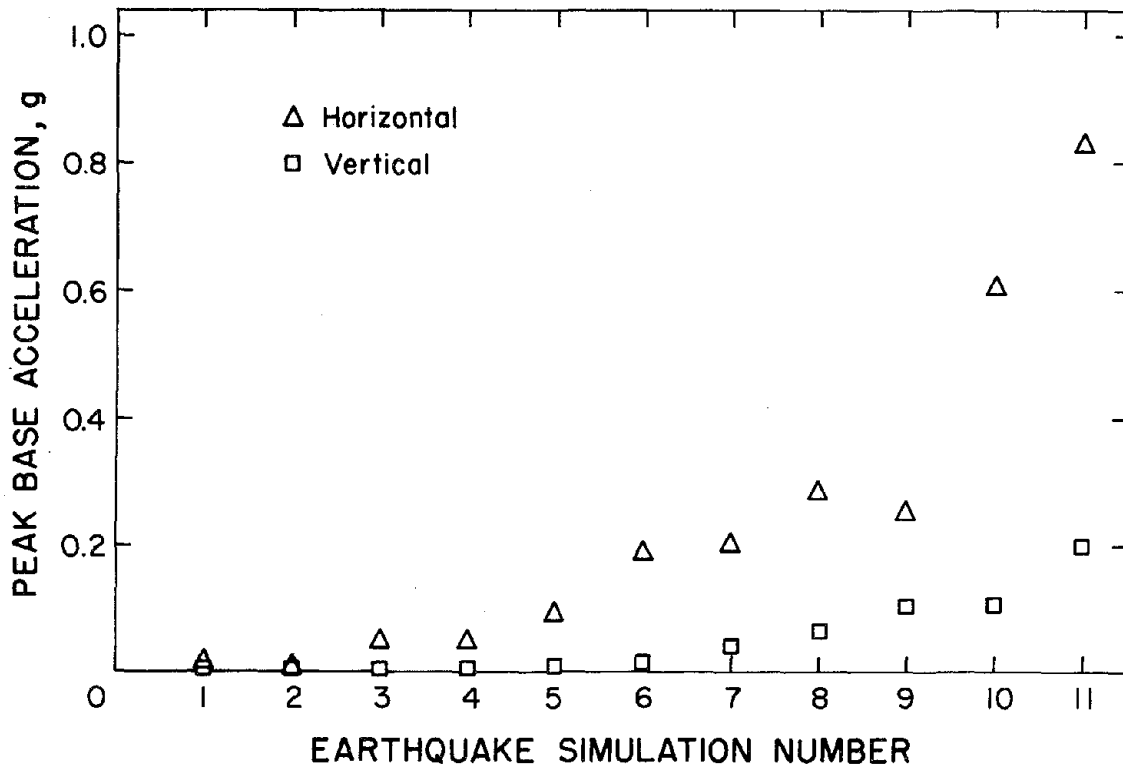


Fig. 5.1 Variation of Peak Horizontal and Vertical Base Accelerations with Test Number

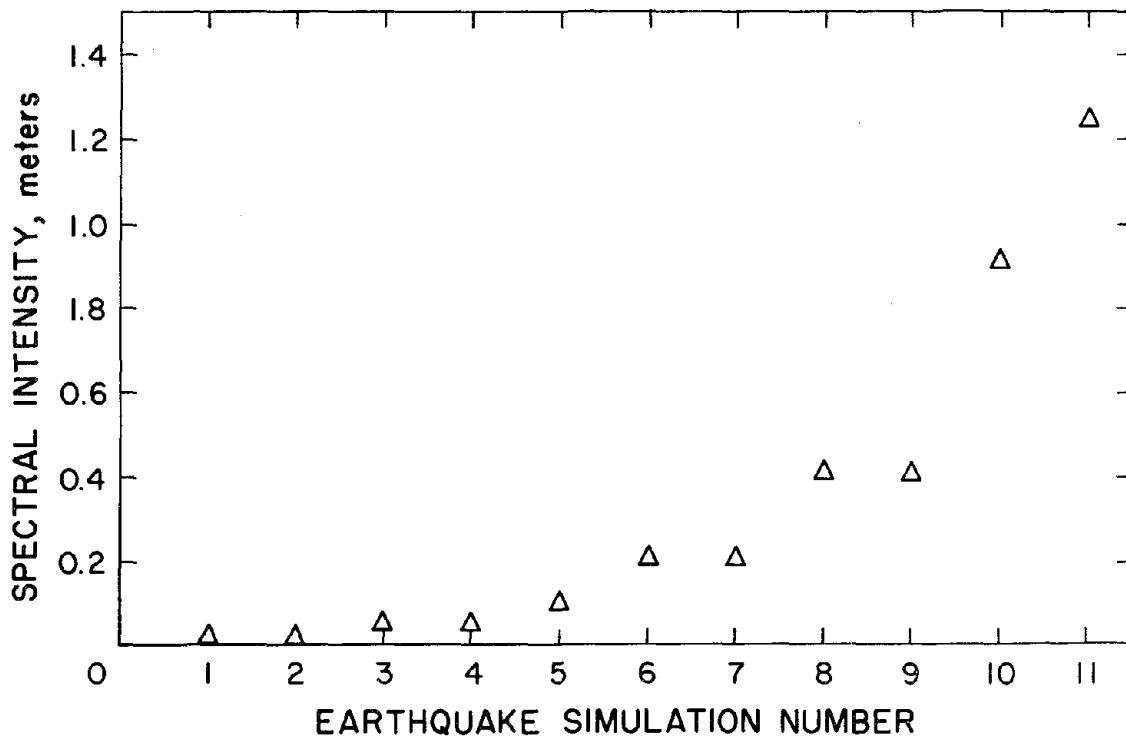


Fig. 5.2 Variation of Five-Percent Damped Spectrum Intensities with Test Number

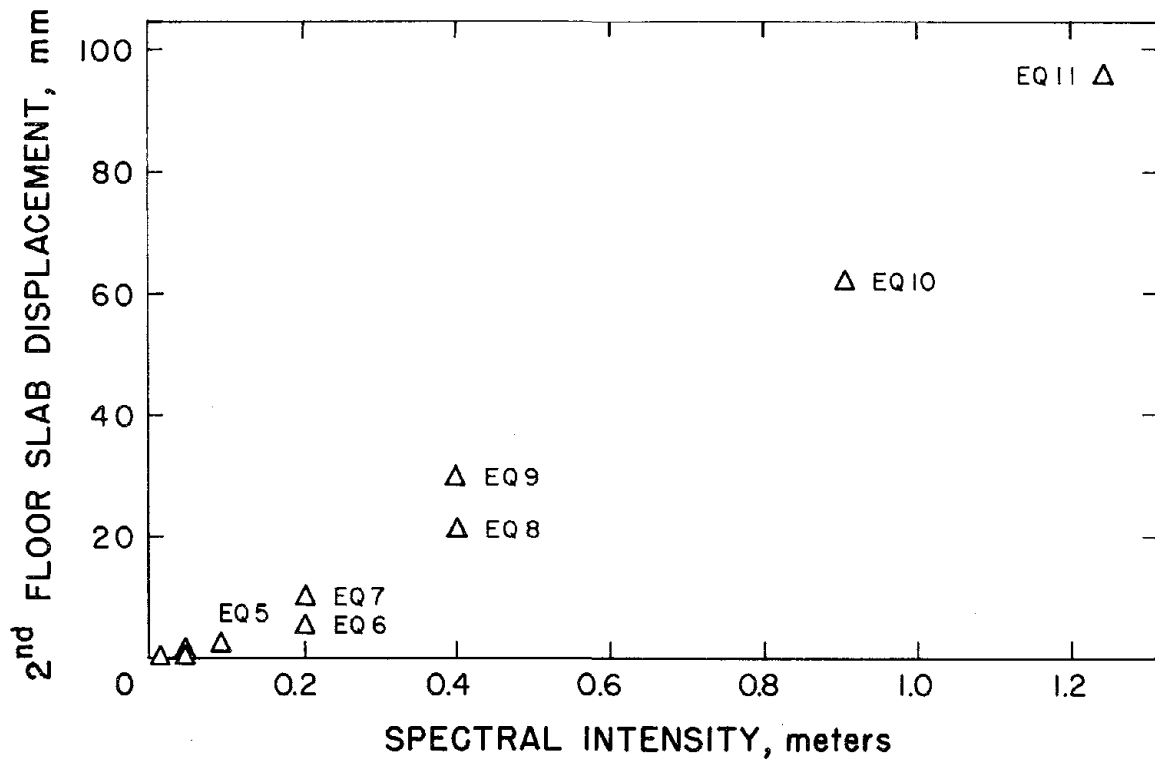


Fig. 5.3 Variation of Peak Second-Floor Relative Displacement with Five-Percent Damped Spectrum Intensity

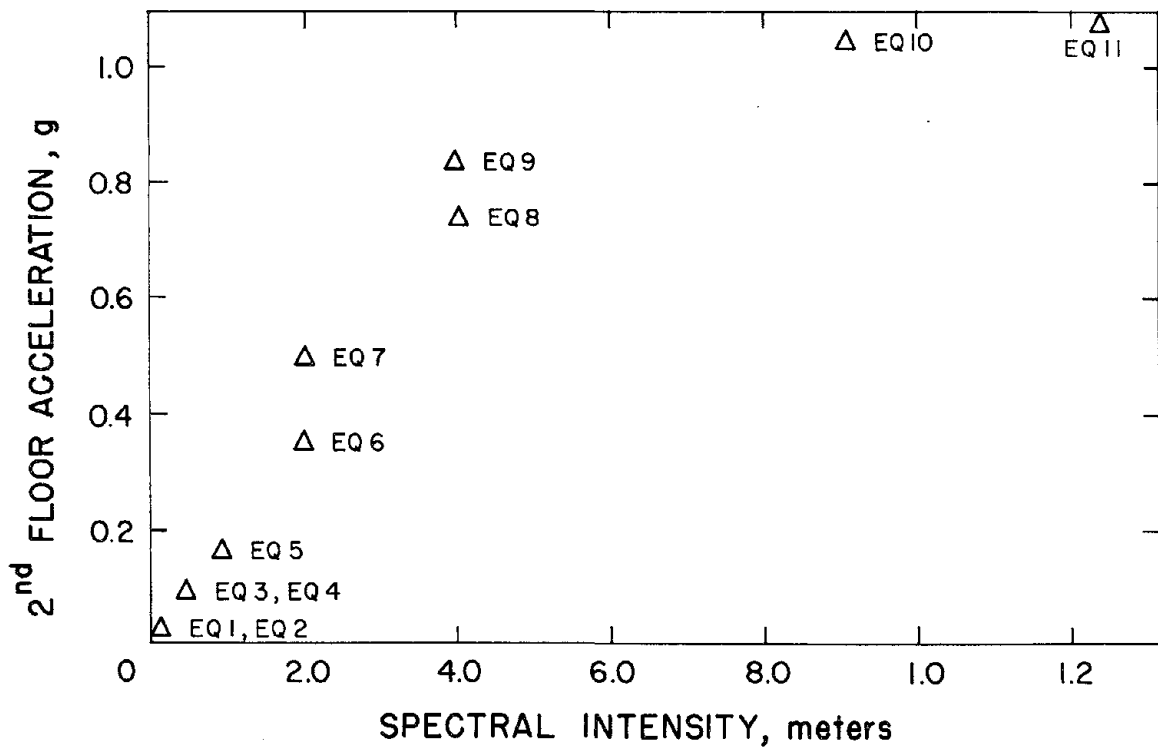


Fig. 5.4 Variation of Peak Second Floor Acceleration with Five-Percent Damped Spectrum Intensity

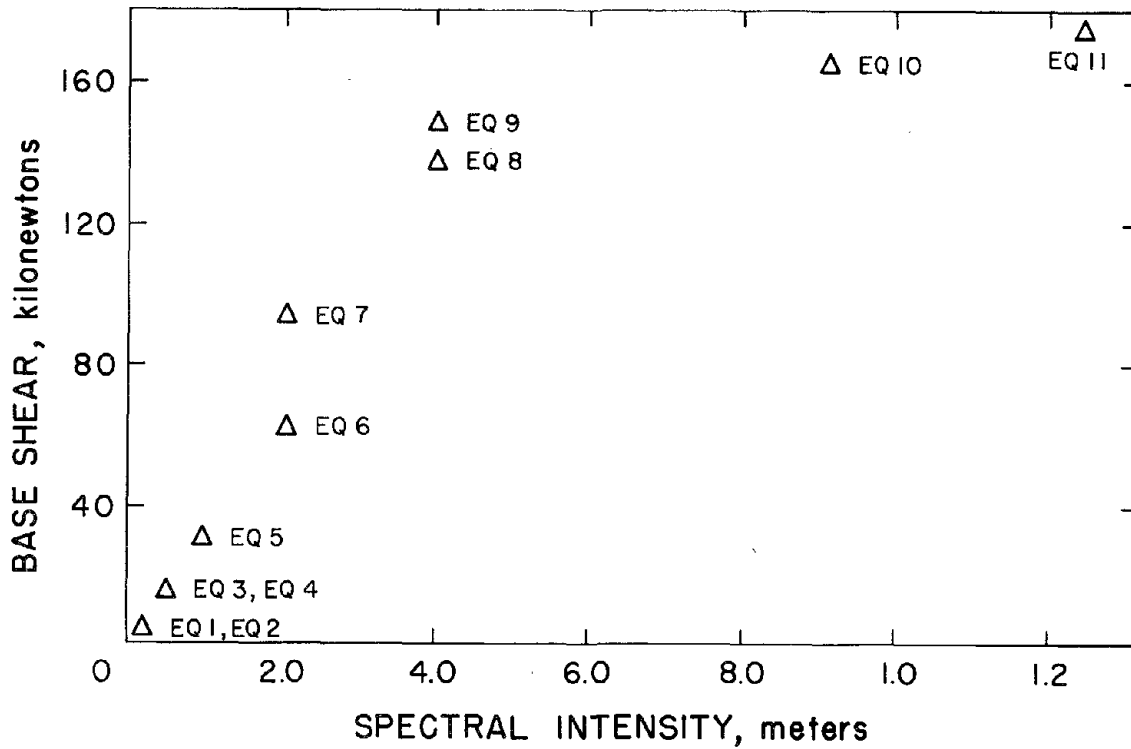


Fig. 5.5 Variation of Peak Base Shear with Five-Percent Damped Spectrum Intensity

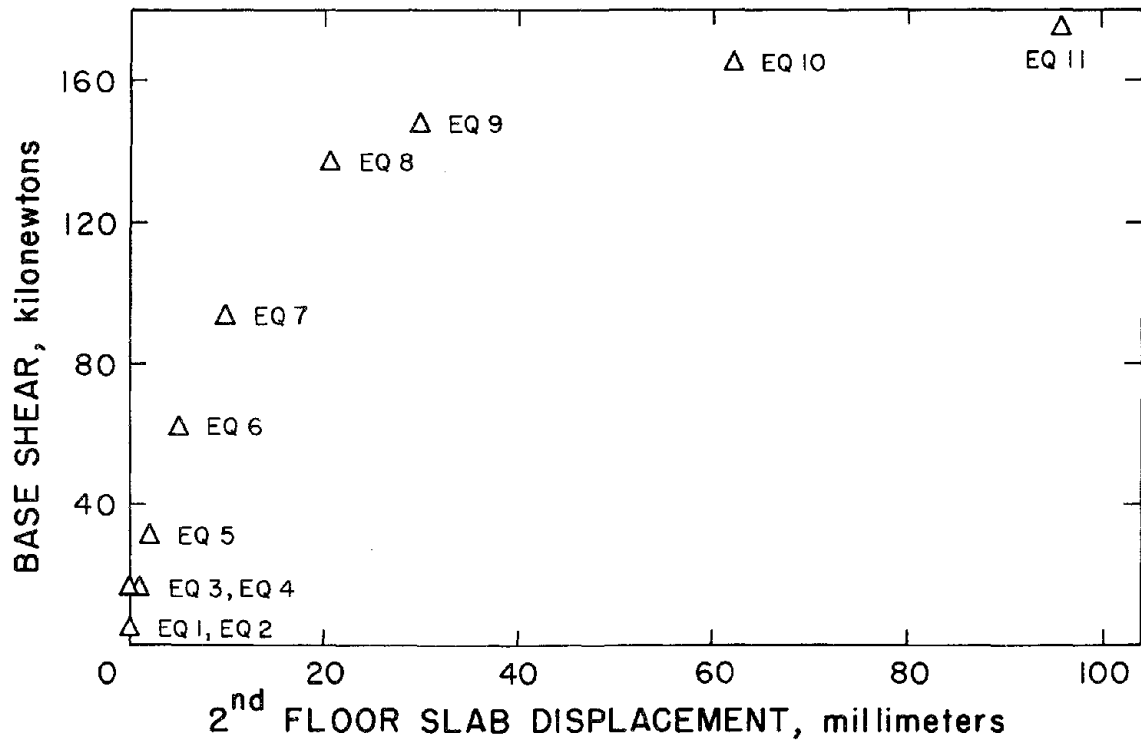


Fig. 5.6 Variation of Peak Base Shear with Peak Second-Floor Relative Displacement

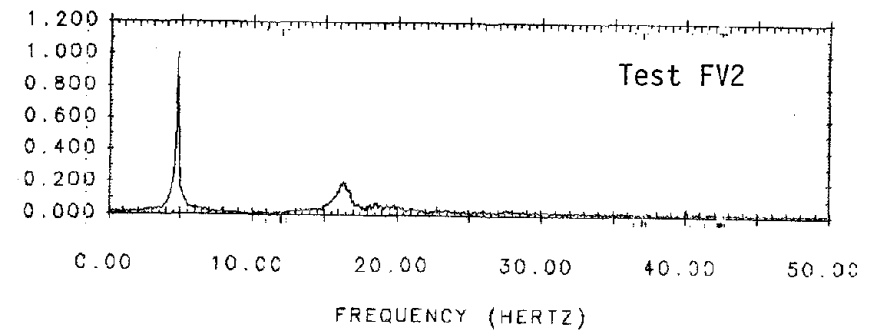
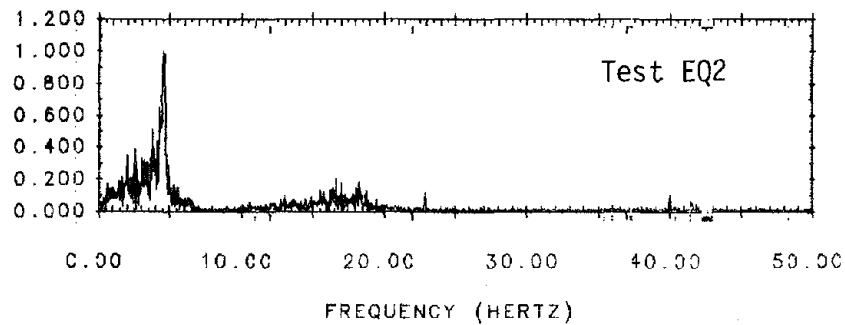
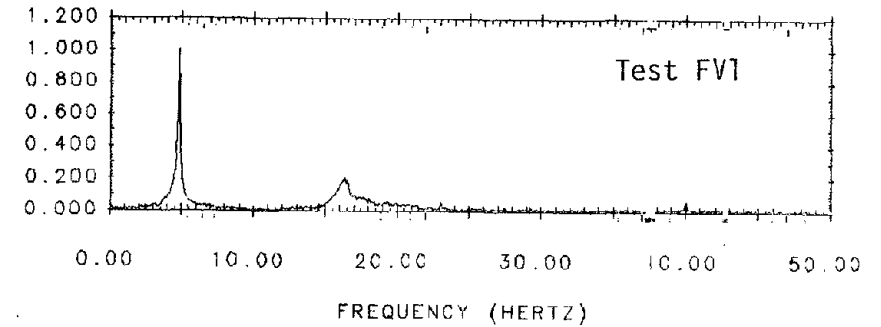
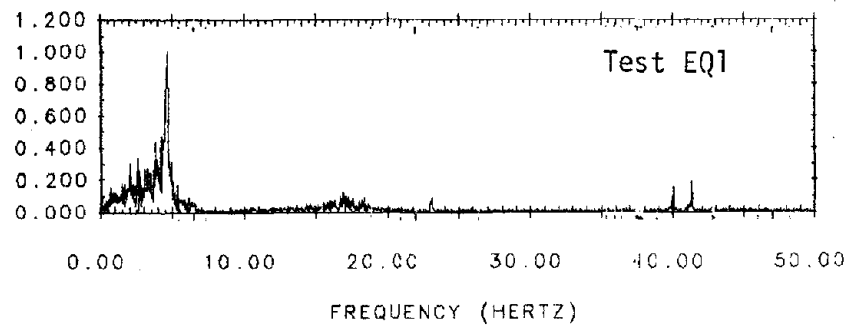
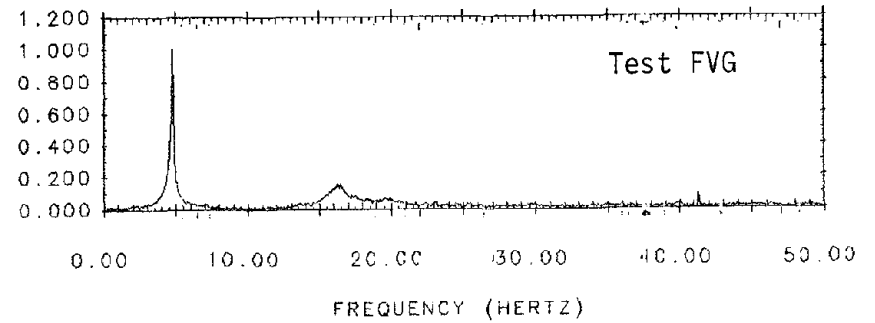
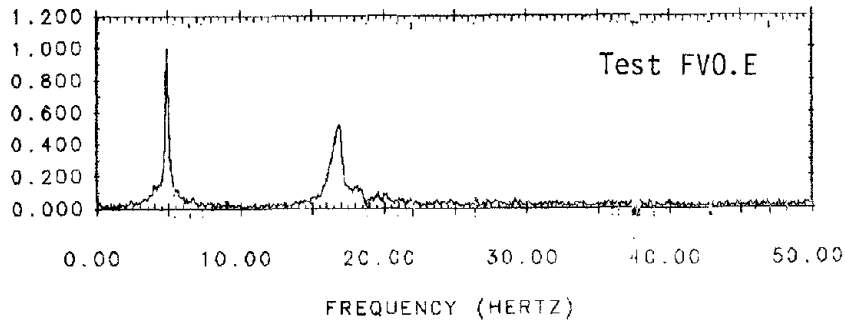


Fig. 5.7 Fourier Amplitude Spectra of First-Floor Free-Vibration and Earthquake Simulation Acceleration Responses

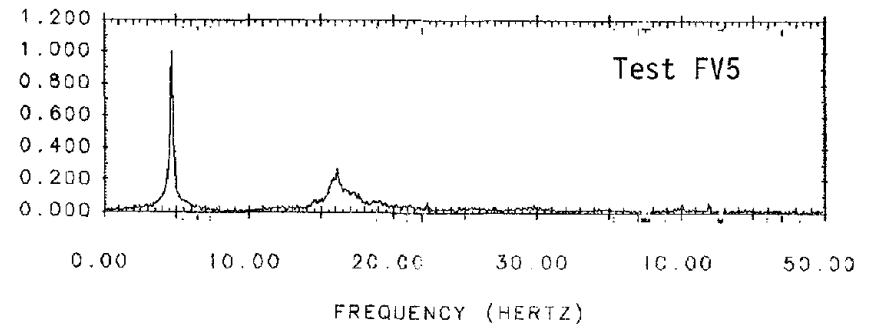
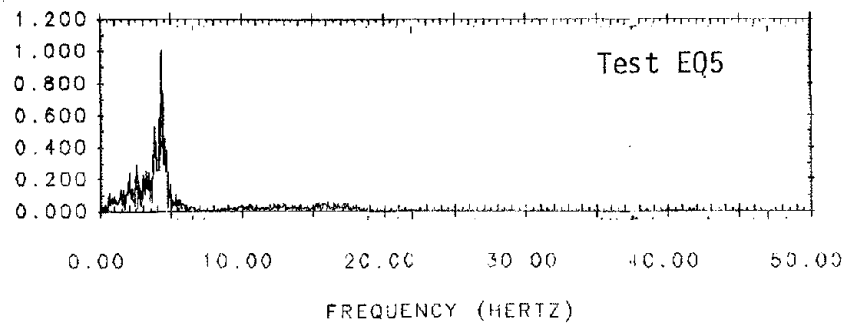
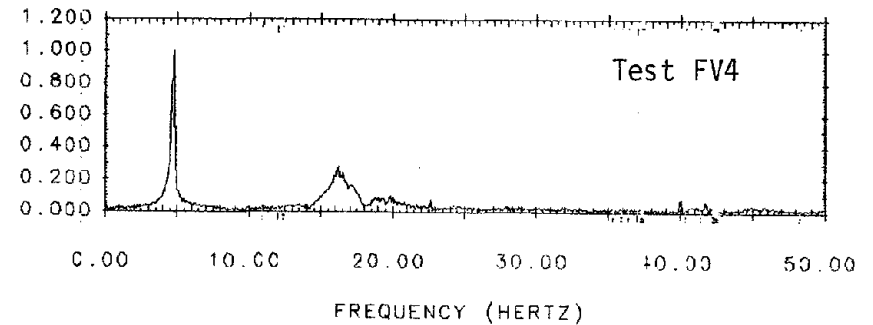
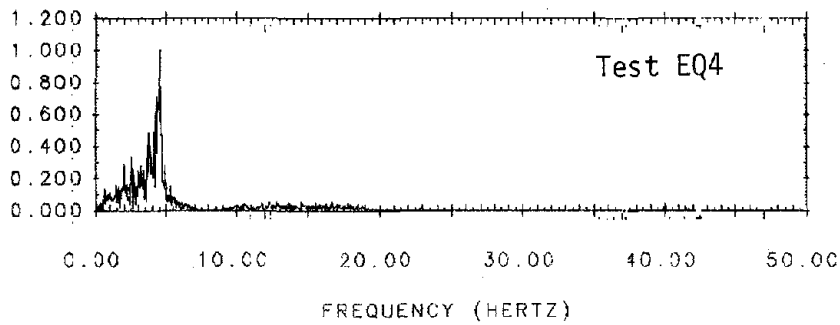
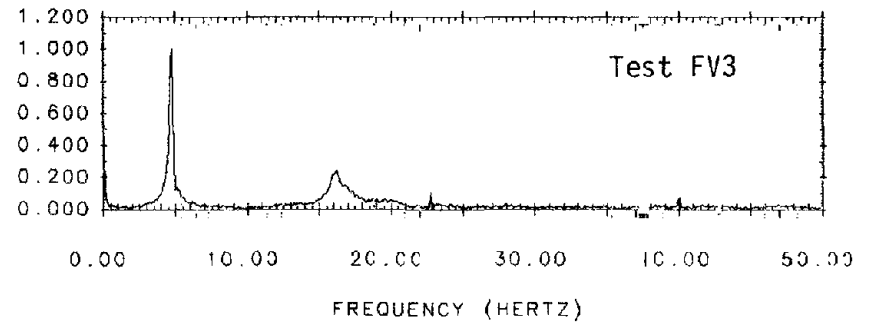
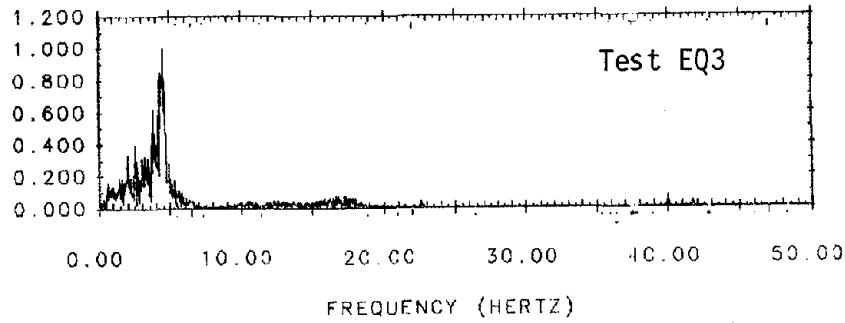


Fig. 5.7 (cont'd.) Fourier Amplitude Spectra of First-Floor Free-Vibration and Earthquake Simulation Acceleration Responses

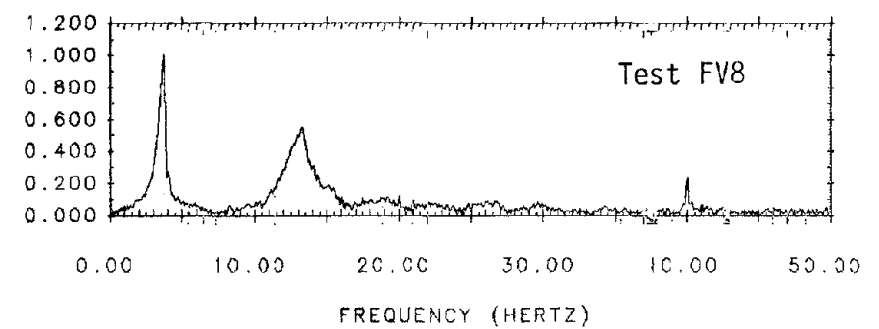
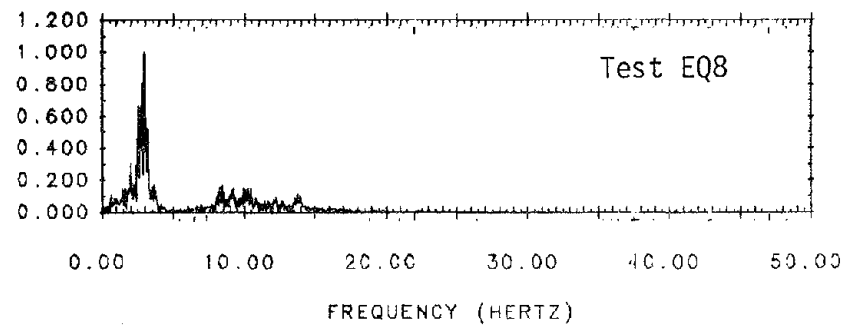
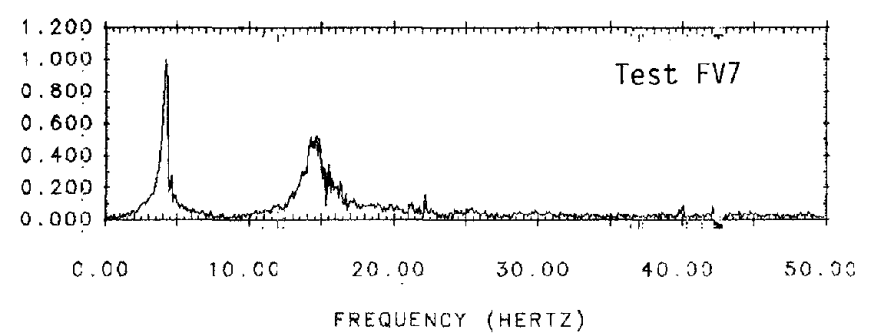
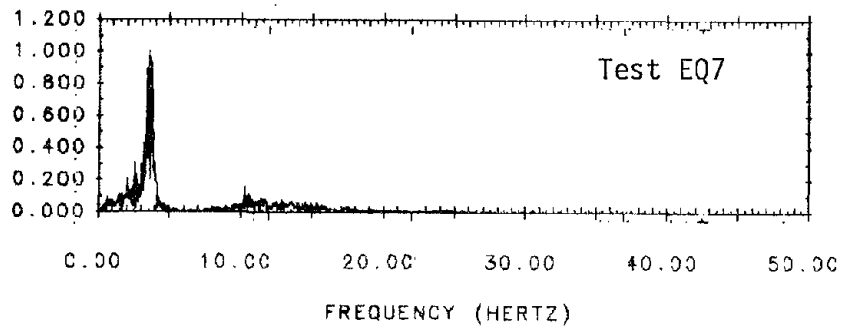
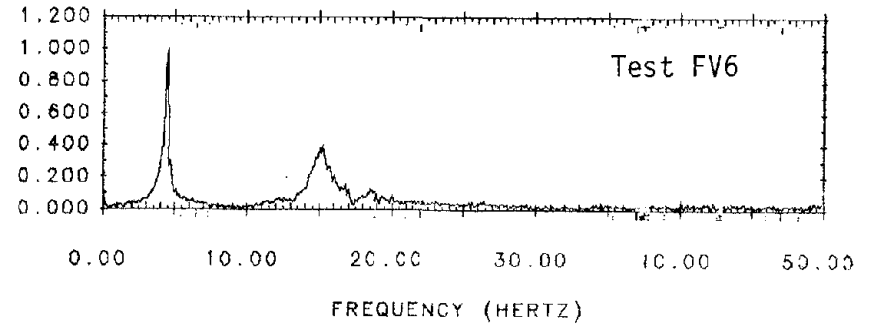
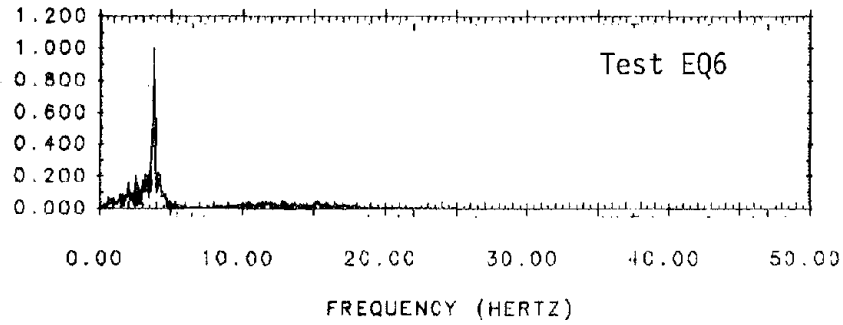


Fig. 5.7 (cont'd.) Fourier Amplitude Spectra of First-Floor Free-Vibration and Earthquake Simulation Acceleration Responses

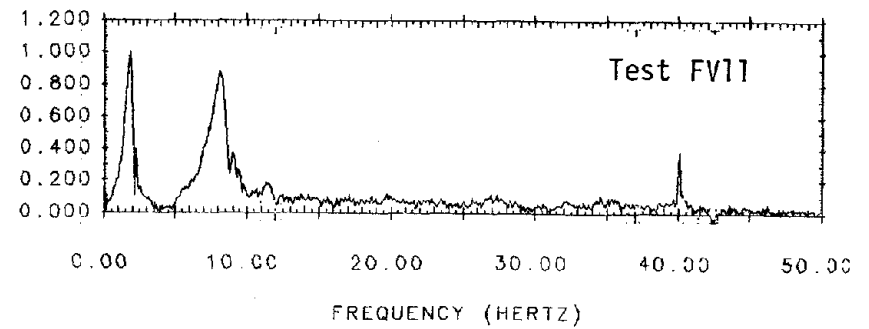
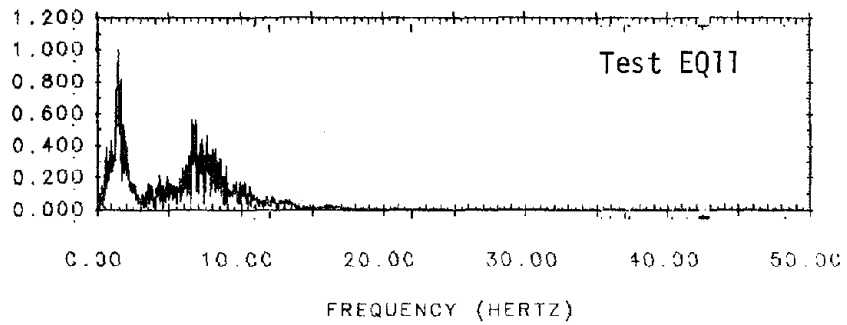
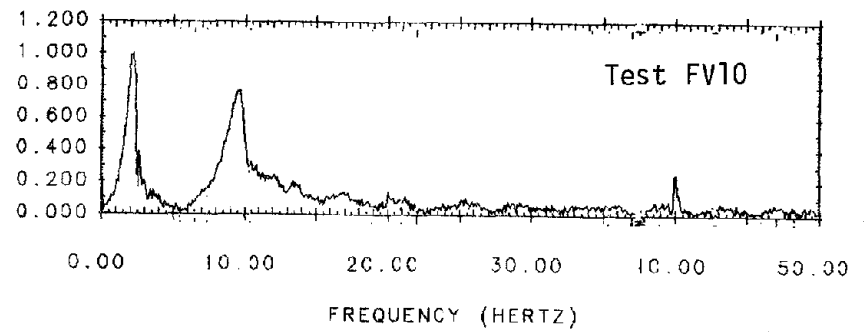
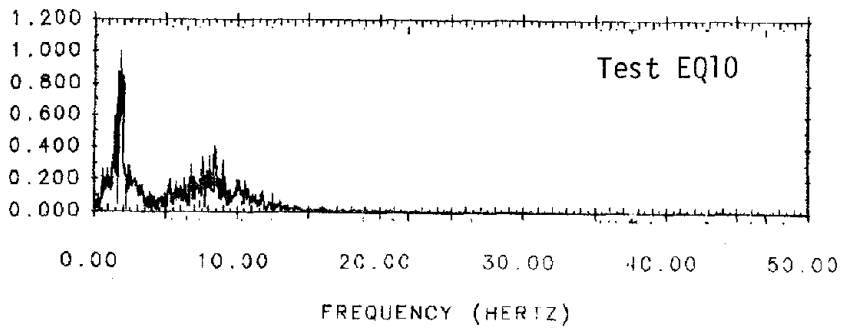
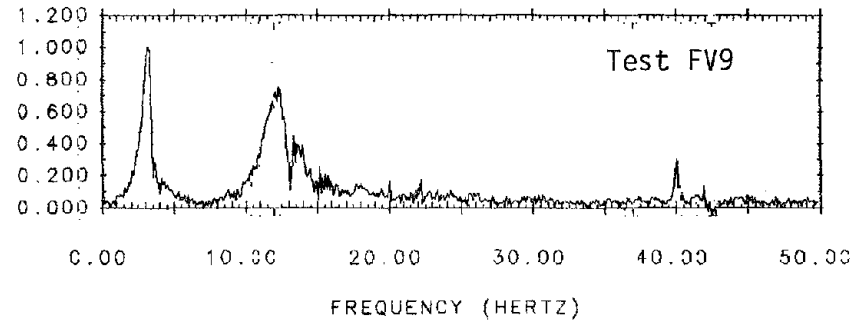
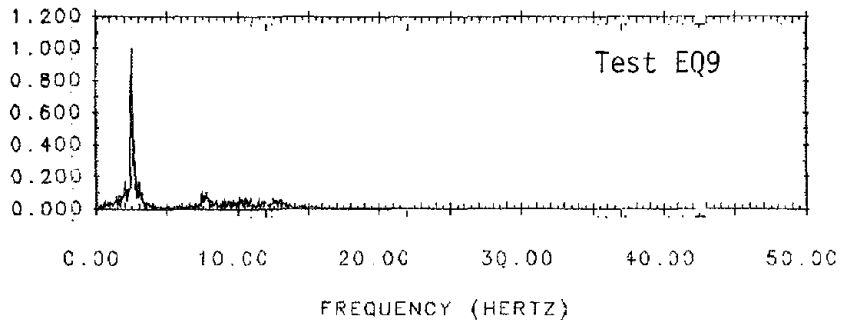


Fig. 5.7 (cont'd.) Fourier Amplitude Spectra of First-Floor Free-Vibration and Earthquake Simulation Acceleration Responses

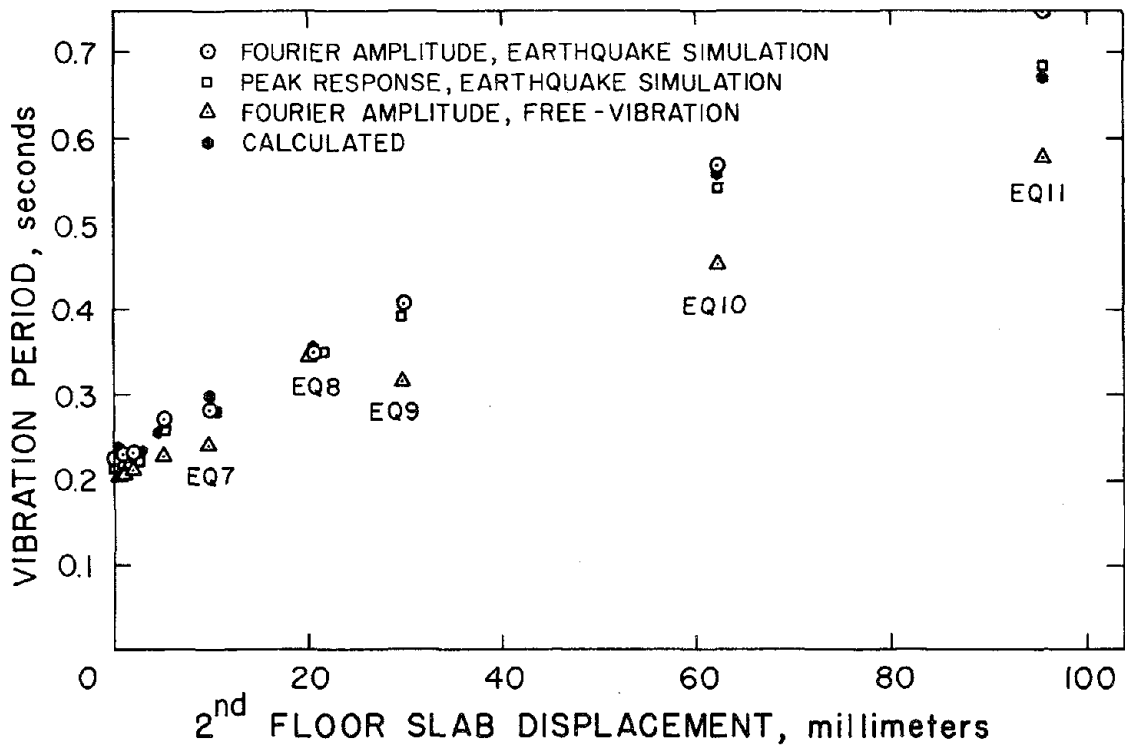


Fig. 5.8 Variation of Apparent First-Mode Vibration Periods with Maximum Second-Floor Relative Displacement

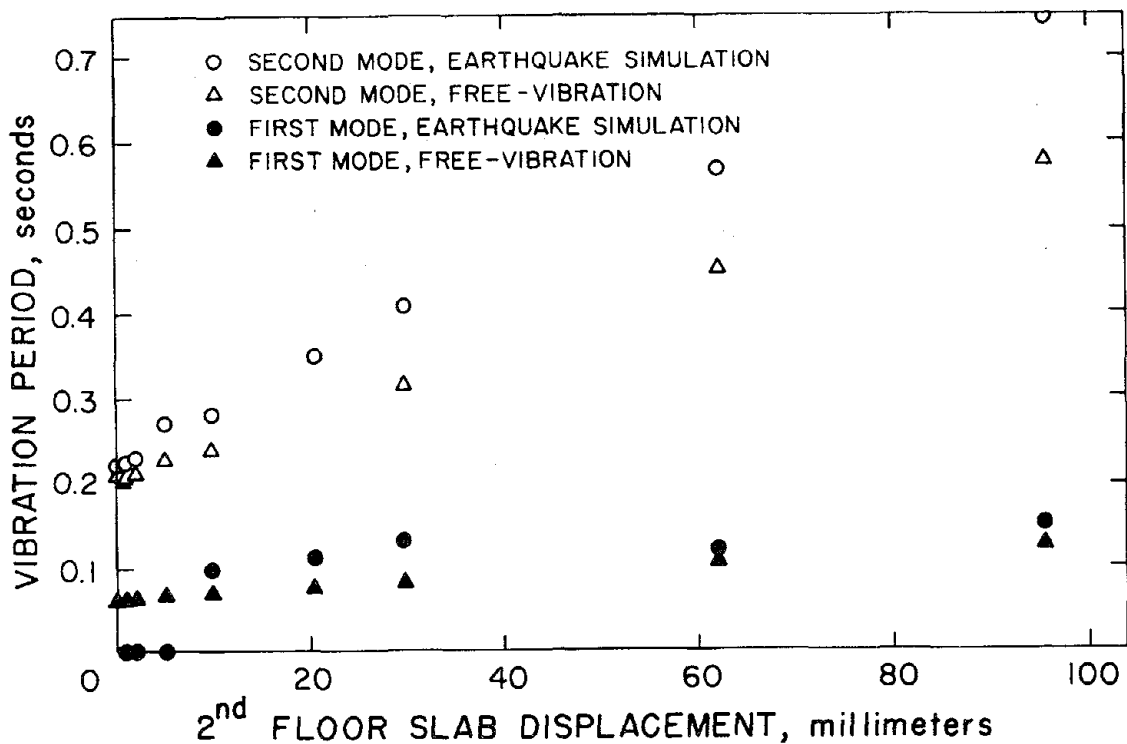


Fig. 5.9 Variation of Apparent First and Second Mode Vibration Periods with Maximum Second-Floor Relative Displacement

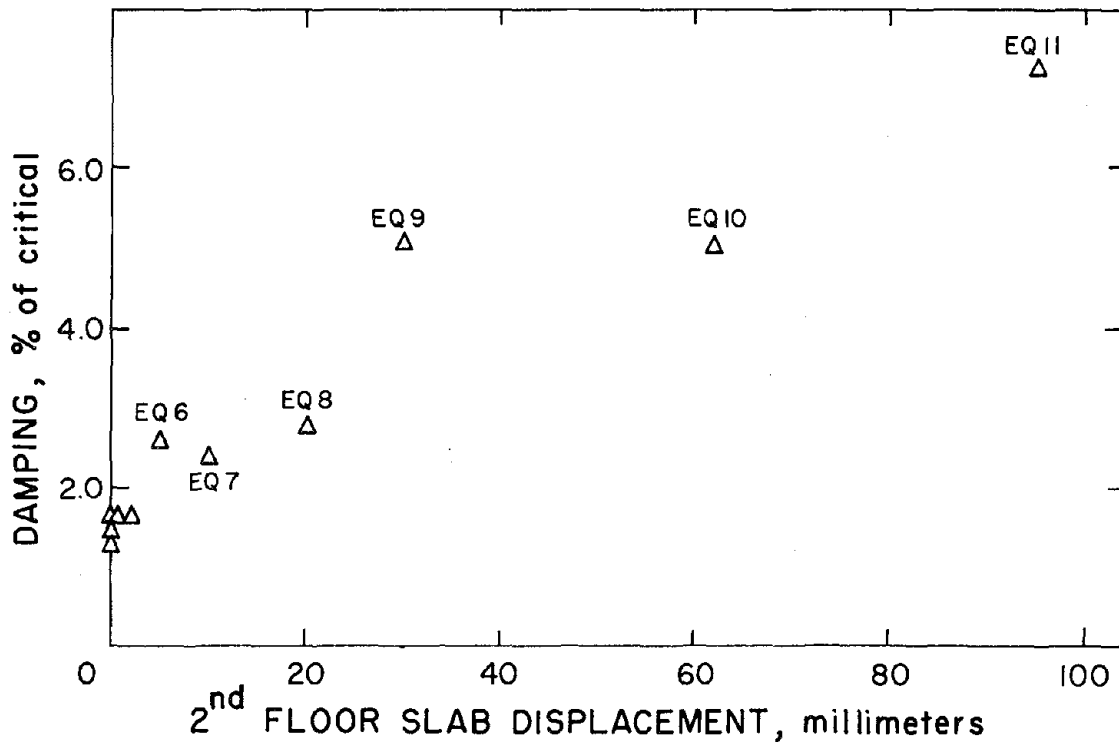


Fig. 5.10 Variation of First-Mode Equivalent Viscous Damping with Maximum Previous Second-Floor Relative Displacement

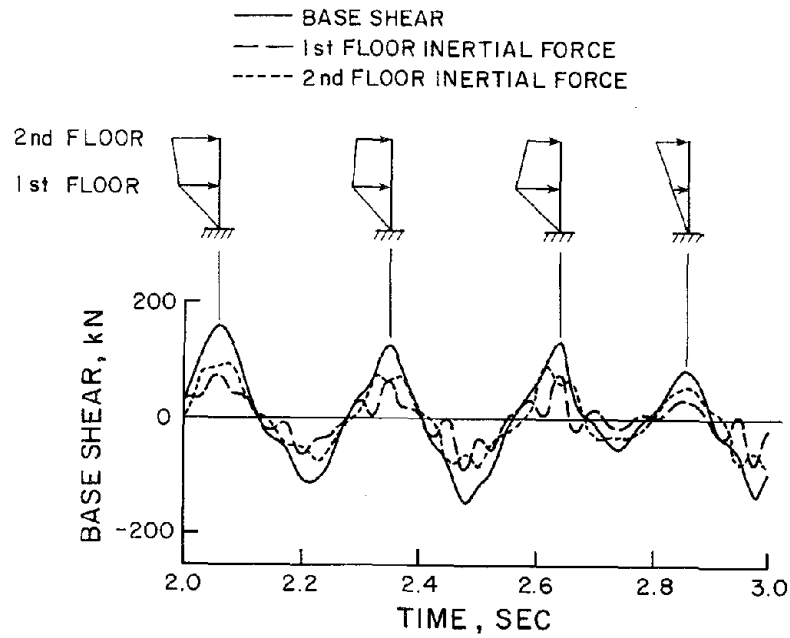


Fig. 5.11 Variation of Inertial Forces During Test EQ10

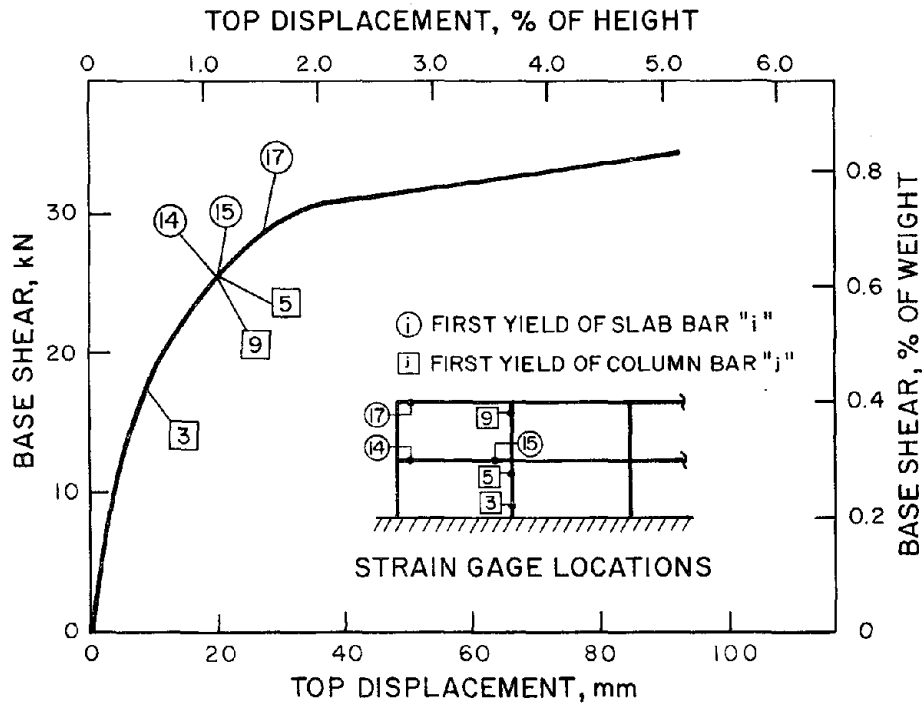


Fig. 5.12 Envelope Relation Between Base Shear and Second-Floor Relative Displacement

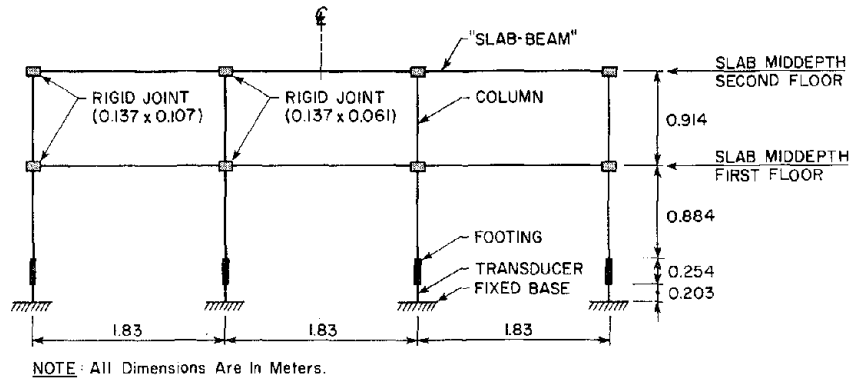


Fig. 6.1 Effective Beam Width Model

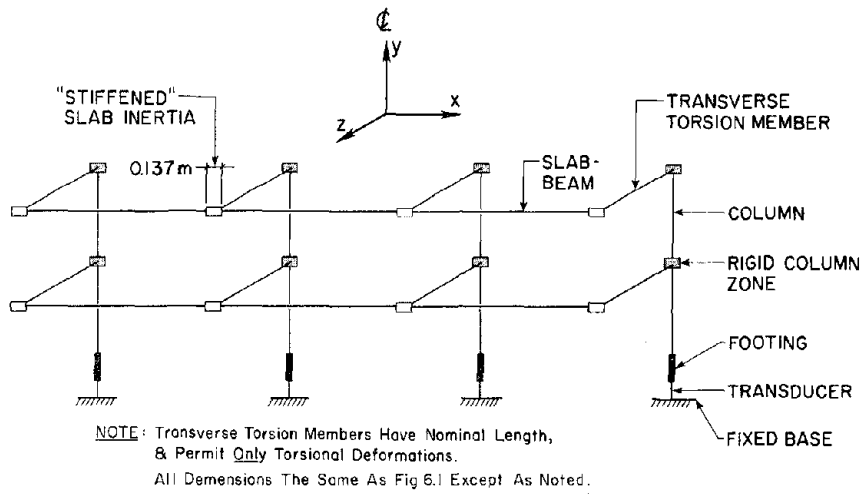


Fig. 6.2 Equivalent Frame Model

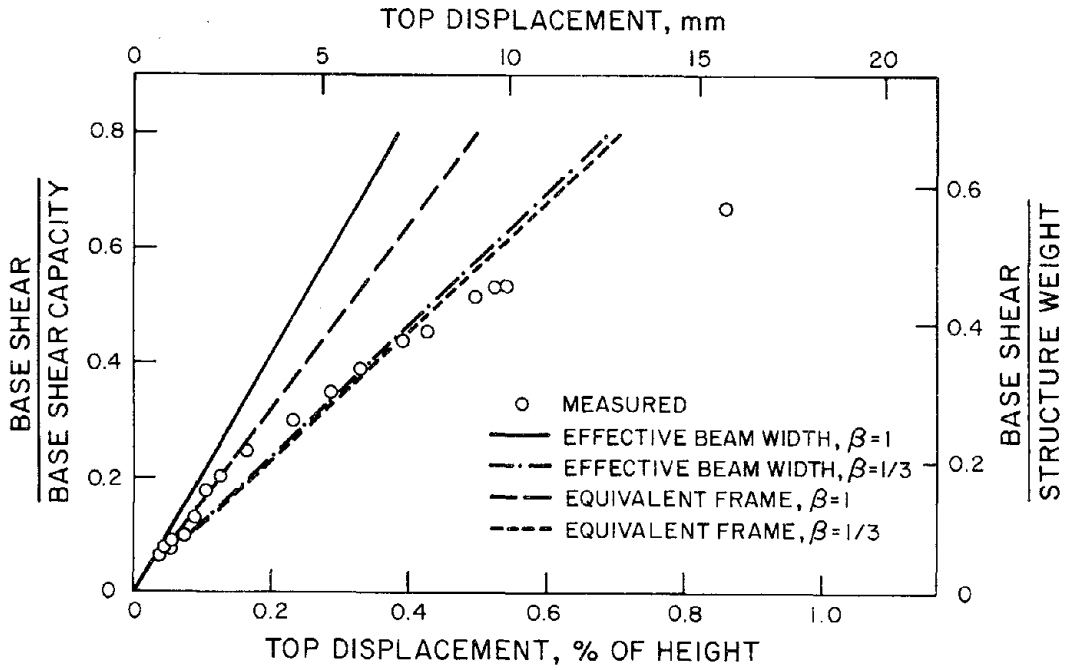


Fig. 6.3 Comparison Between Computed and Measured Lateral-Load Stiffnesses

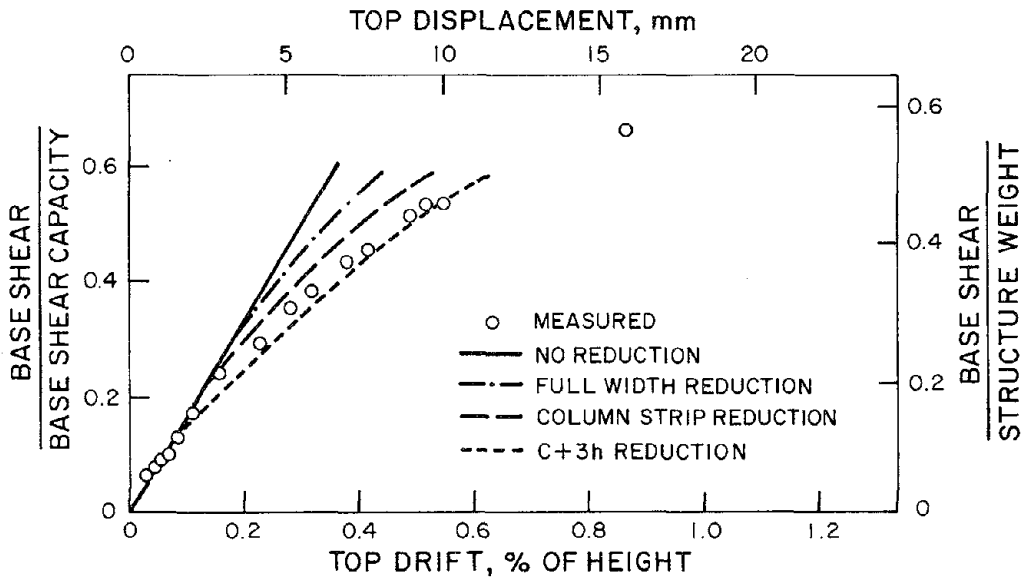


Fig. 6.4 Stiffness Variation of Equivalent Frame Models Modified to Account for Effects of Cracking Due to Applied Loads

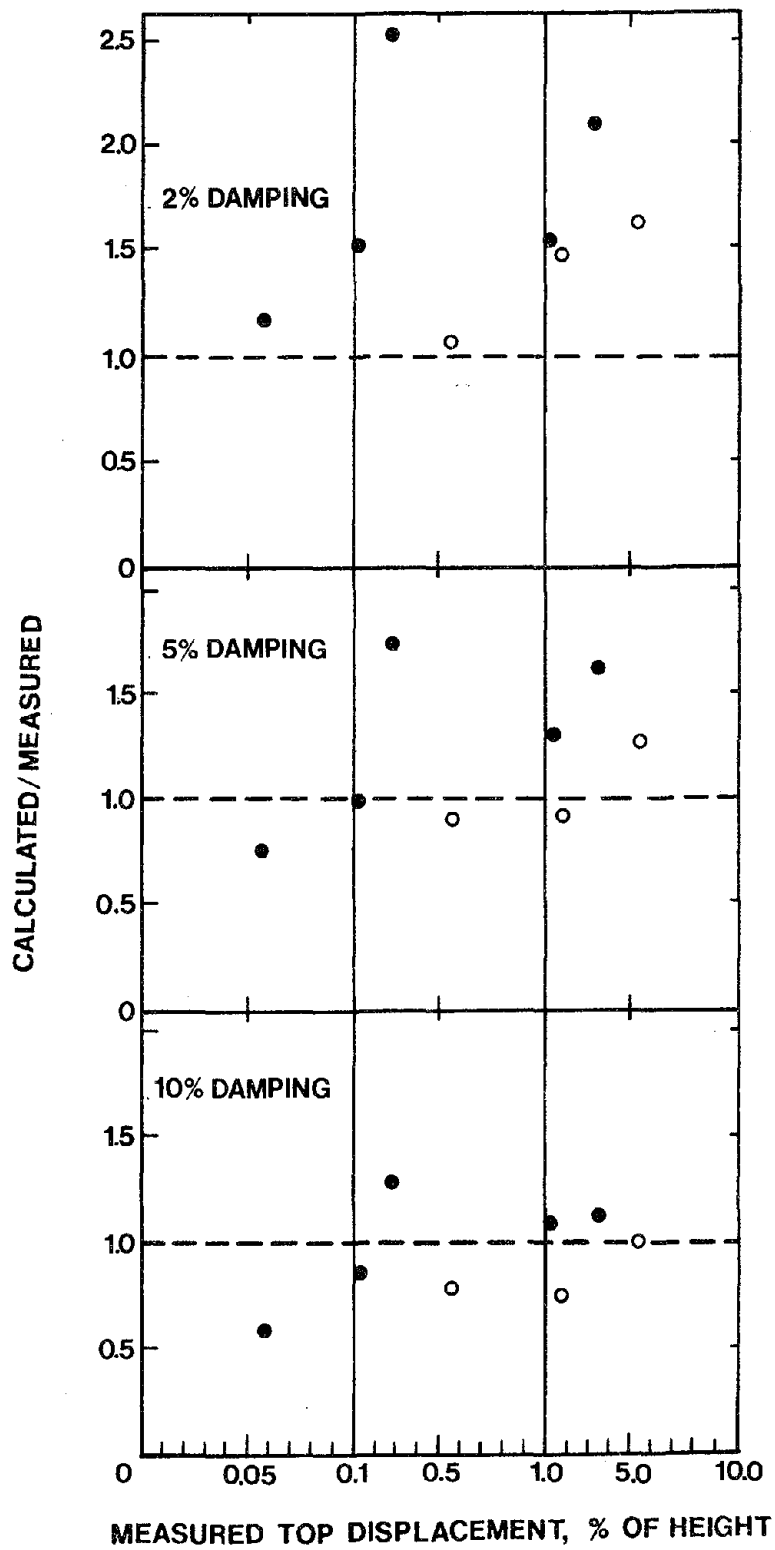


Fig. 6.5 Ratios Between Calculated and Measured Second Floor Displacement Maxima for the "Experimental Model"

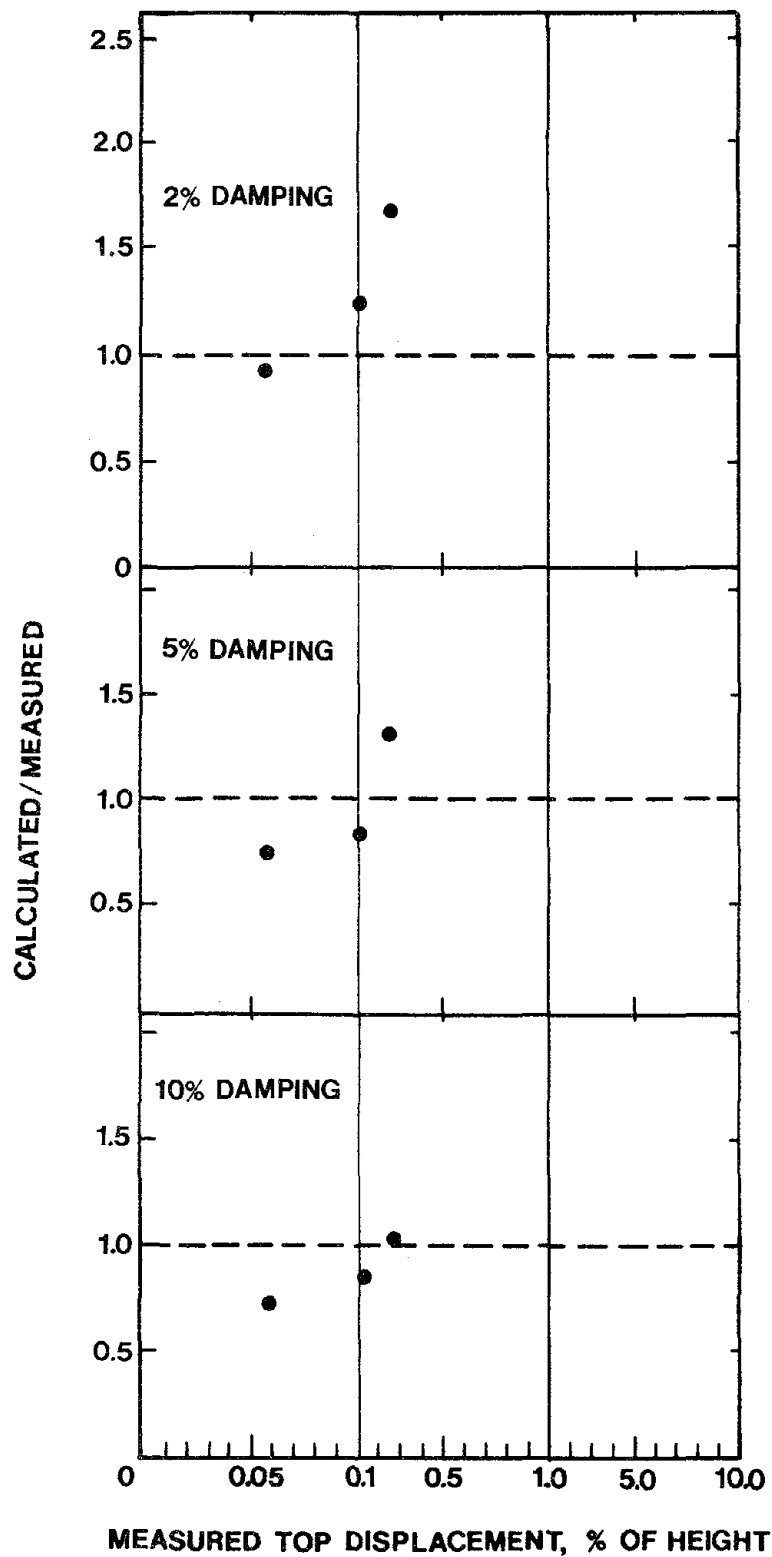
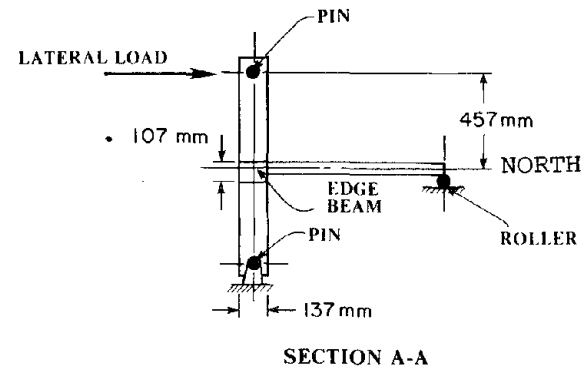
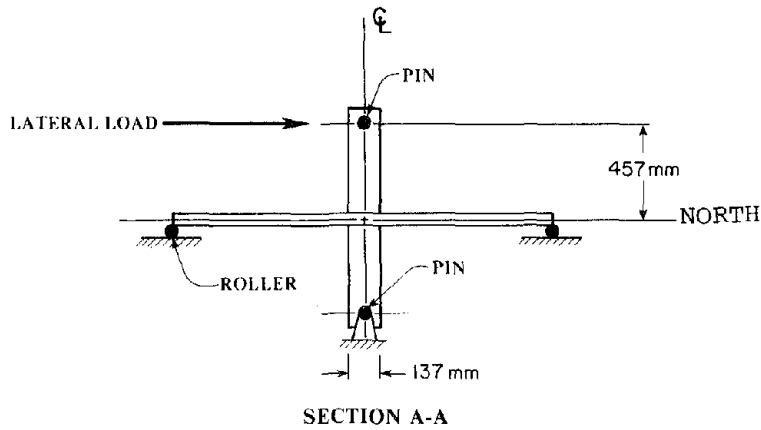
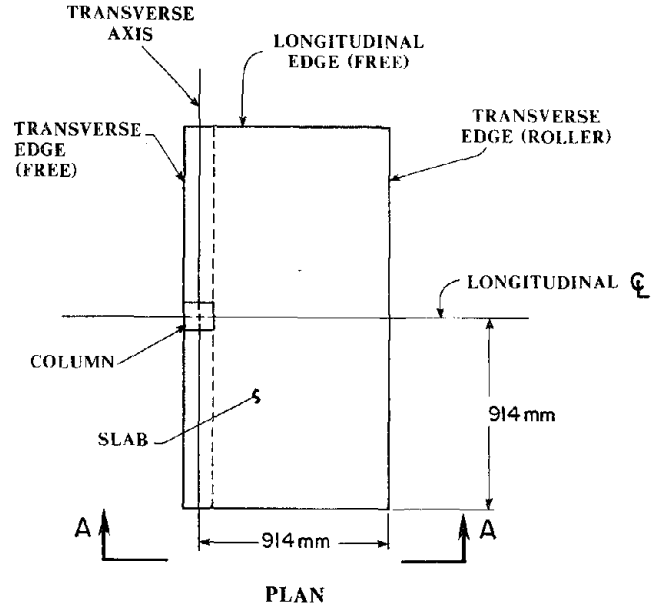
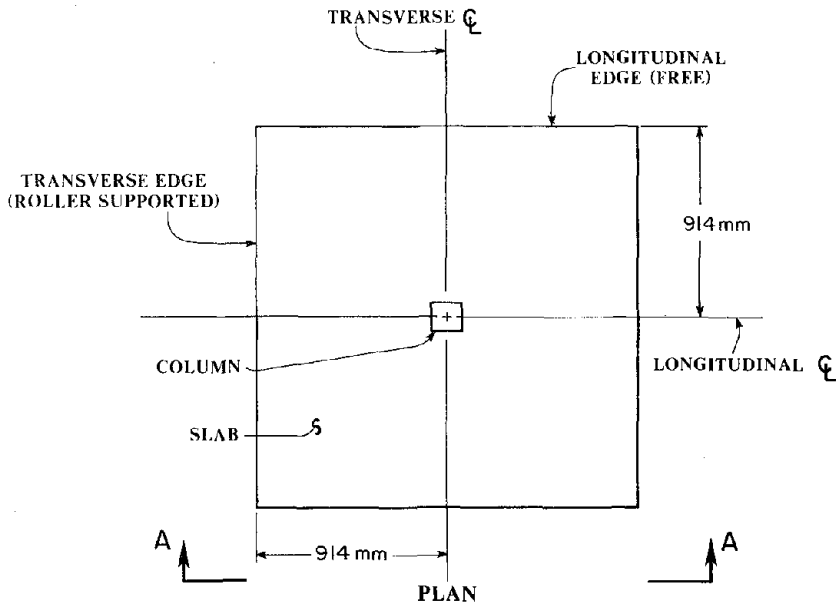


Fig. 6.6 Ratios Between Calculated and Measured Second Floor Displacement Maxima for the "Equivalent Frame Model"



(a) INTERIOR CONNECTION

(b) EXTERIOR CONNECTION

Fig. 7.1 Idealizations of Slab-Column Connection Experiments

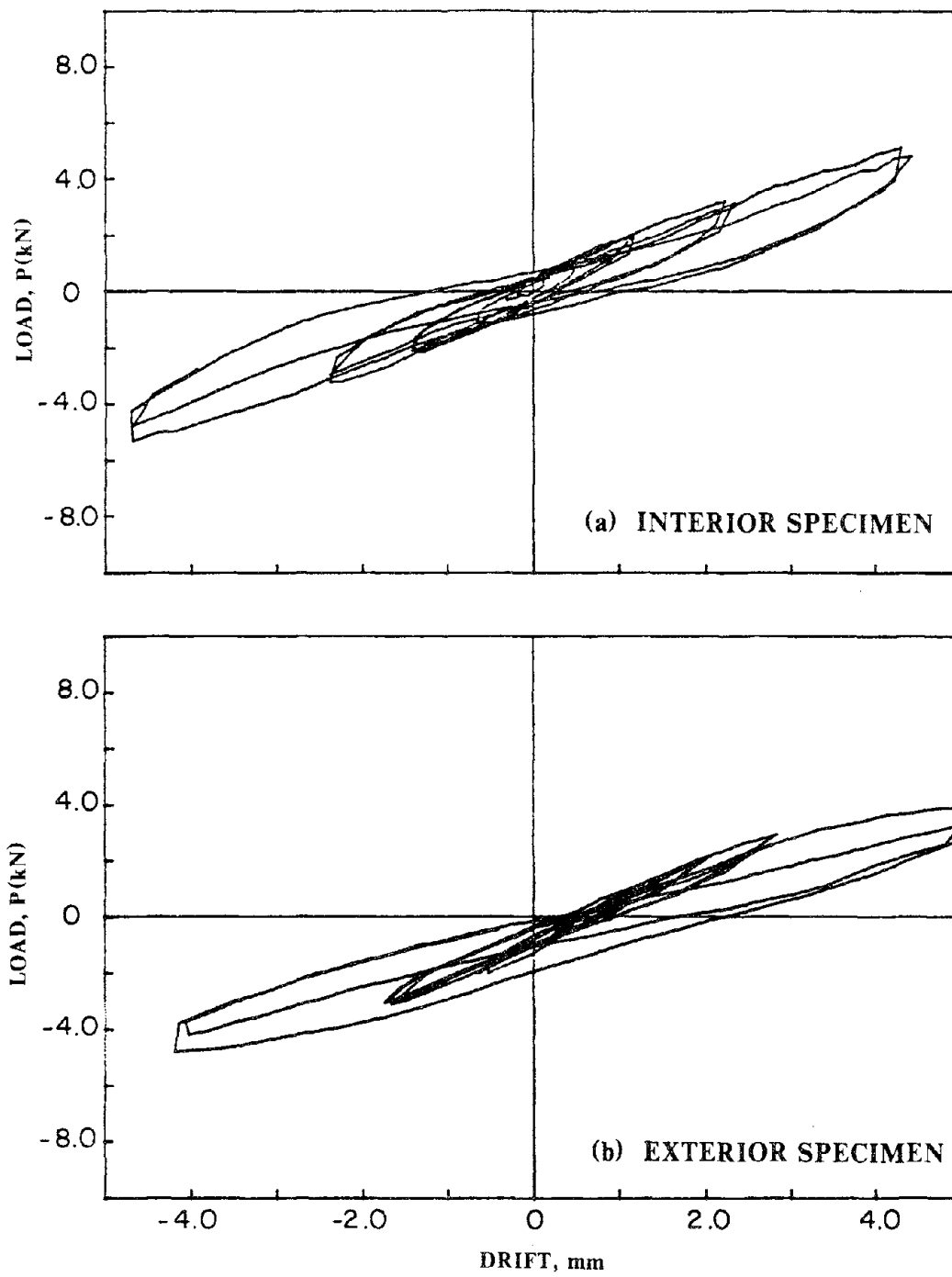


Fig. 7.2 Load-Displacement Relations of Slab-Column Connections

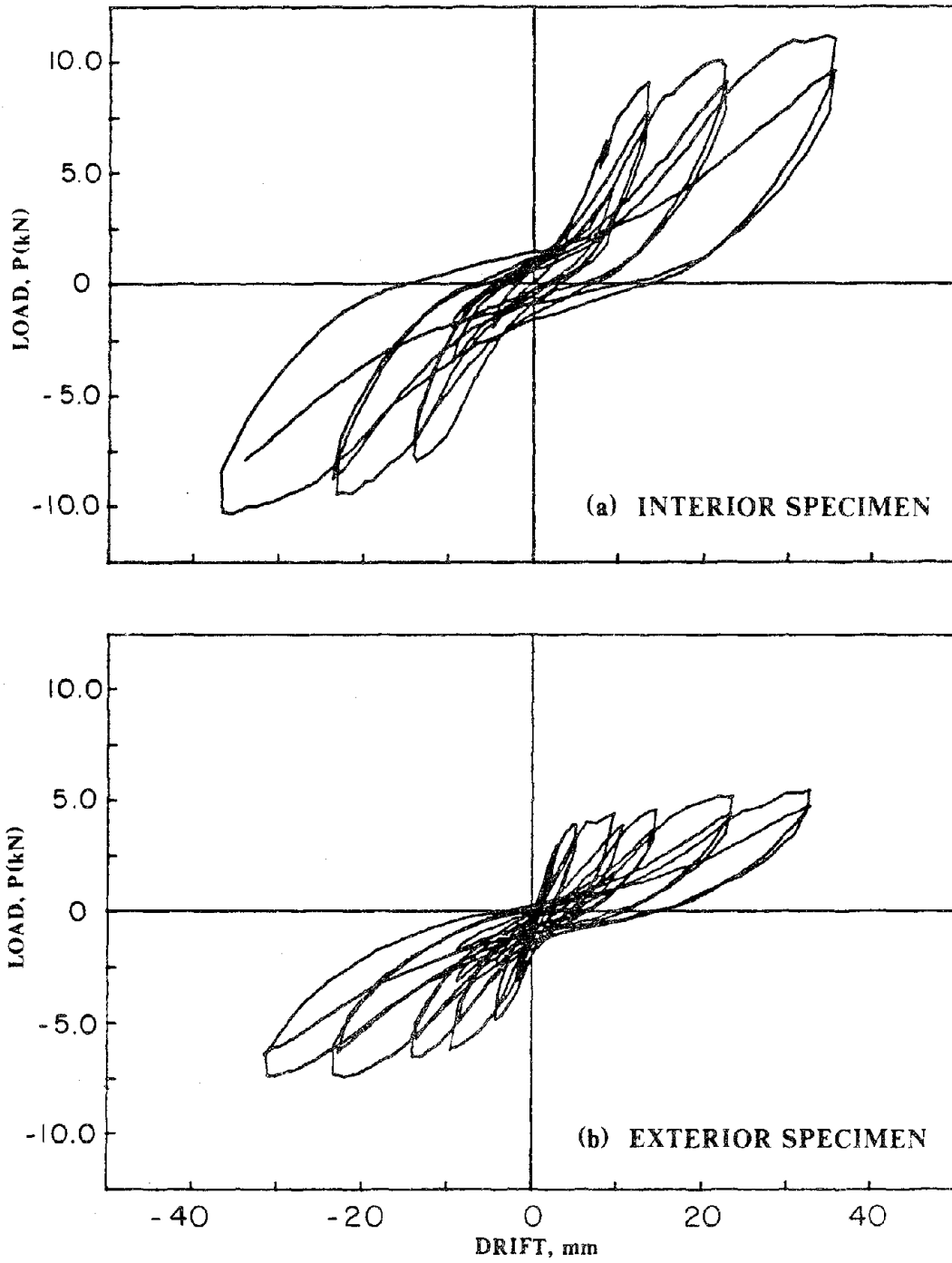
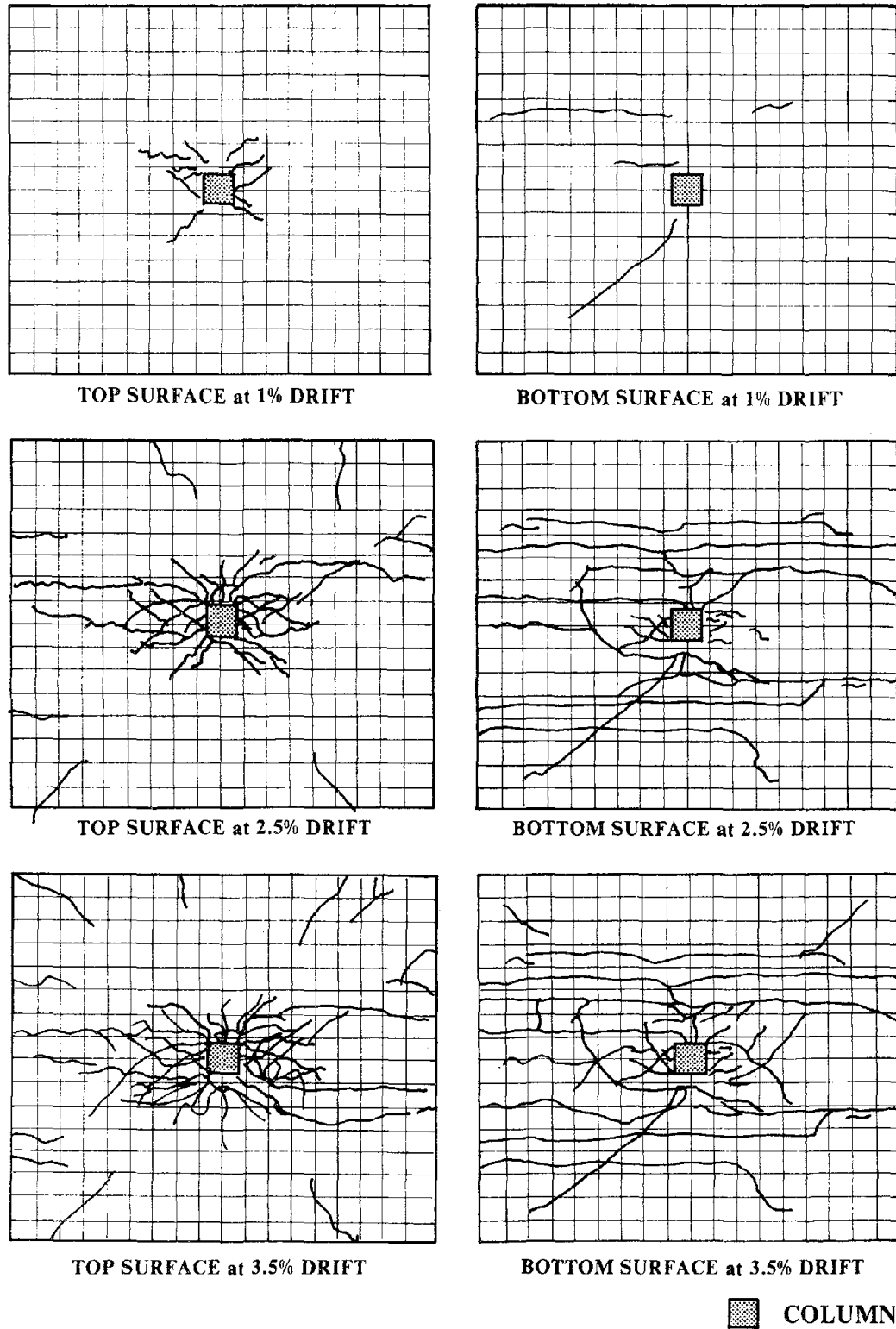
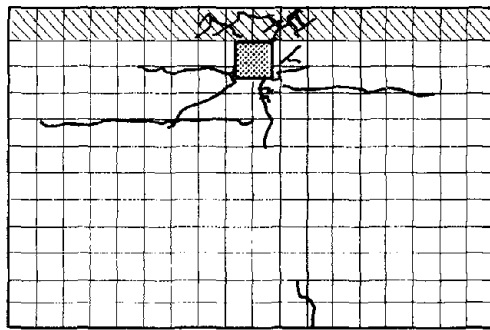


Fig. 7.2 (cont'd.) Load-Displacement Relations of Slab-Column Connections

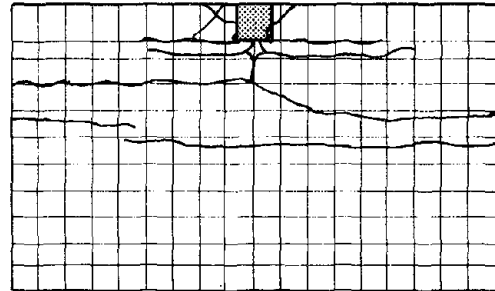


**(a) INTERIOR SPECIMEN**

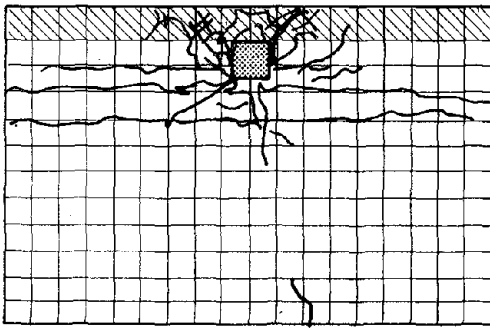
**Fig. 7.3 Progression of Visible Damage in Slab-Column Connections**



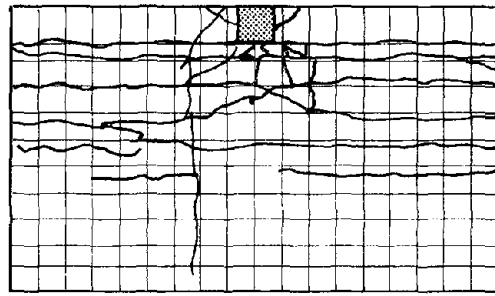
TOP SURFACE at 1% DRIFT



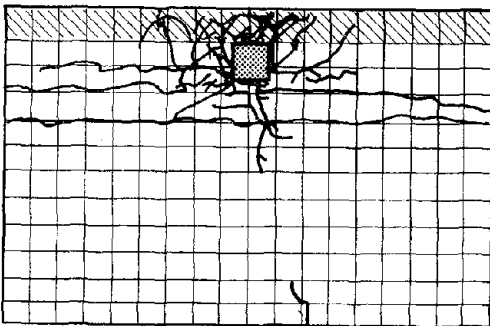
BOTTOM SURFACE at 1% DRIFT



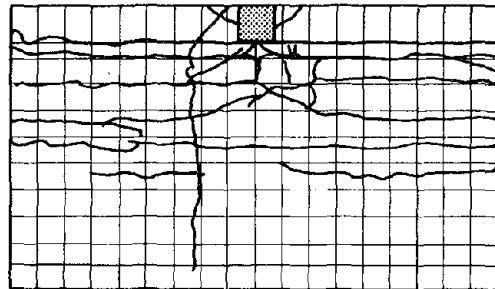
TOP SURFACE at 2.5% DRIFT



BOTTOM SURFACE at 2.5% DRIFT



TOP SURFACE at 3.5% DRIFT



BOTTOM SURFACE at 3.5% DRIFT

 COLUMN

 VERTICAL SIDE OF EDGE BEAM

**(b) EXTERIOR SPECIMEN**

Fig. 7.3 (cont'd.) Progression of Visible Damage in Slab-Column Connections

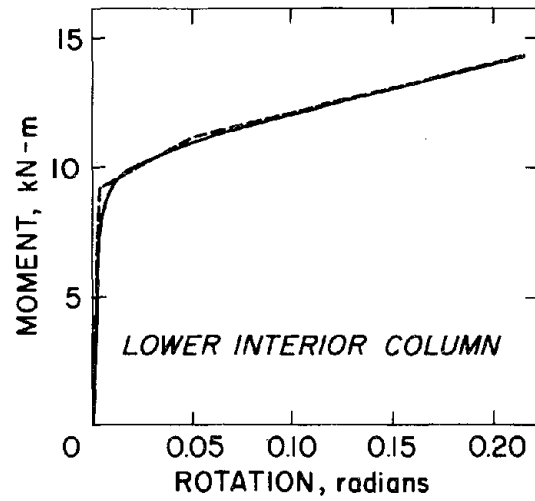
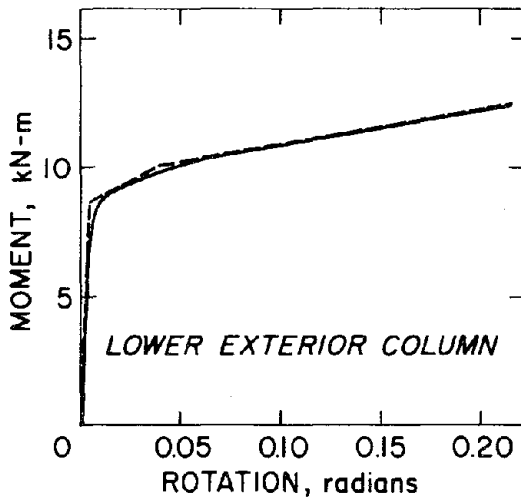
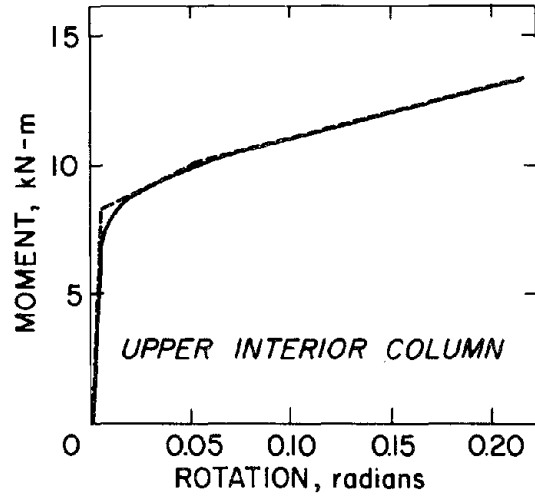
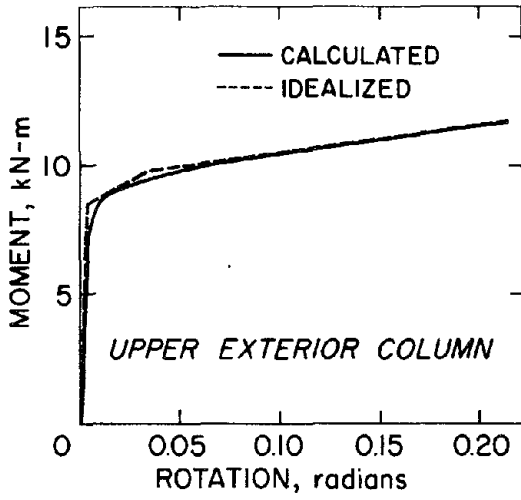


Fig. 7.4 Computed Moment-Rotation Behavior of Columns

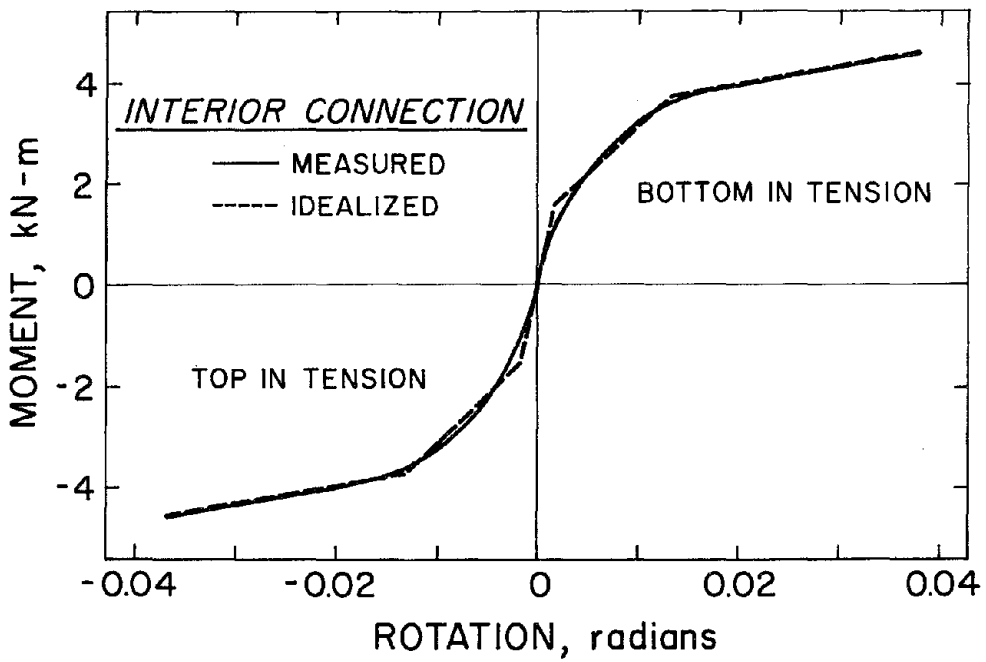
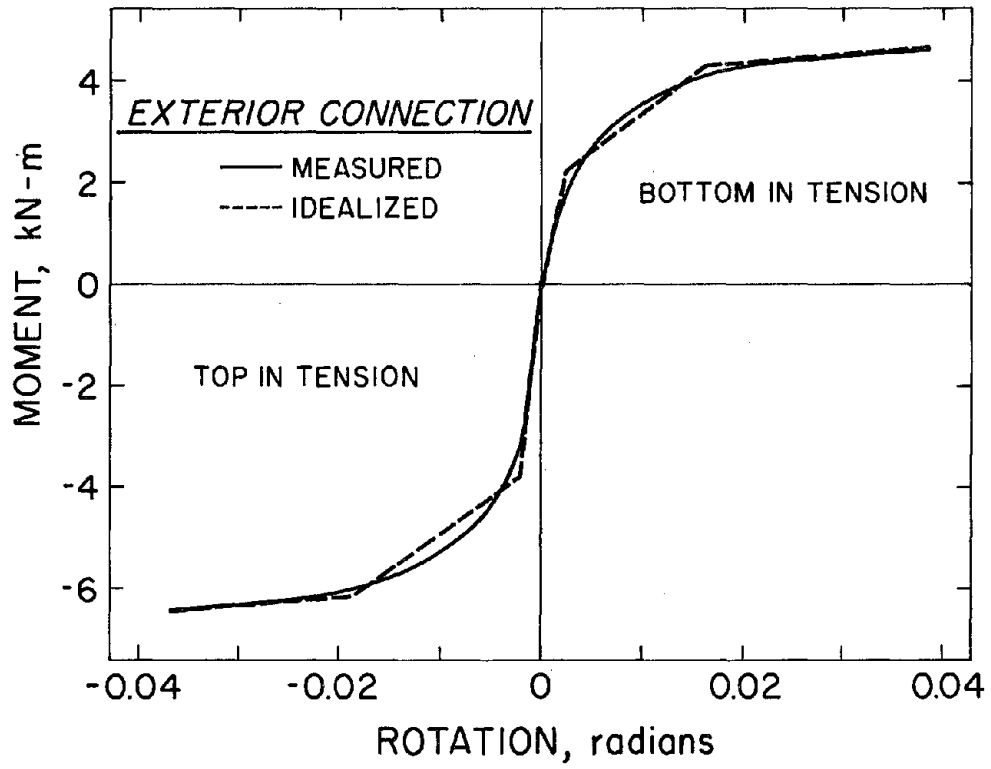


Fig. 7.5 Derived Moment-Rotation Behavior of Slabs

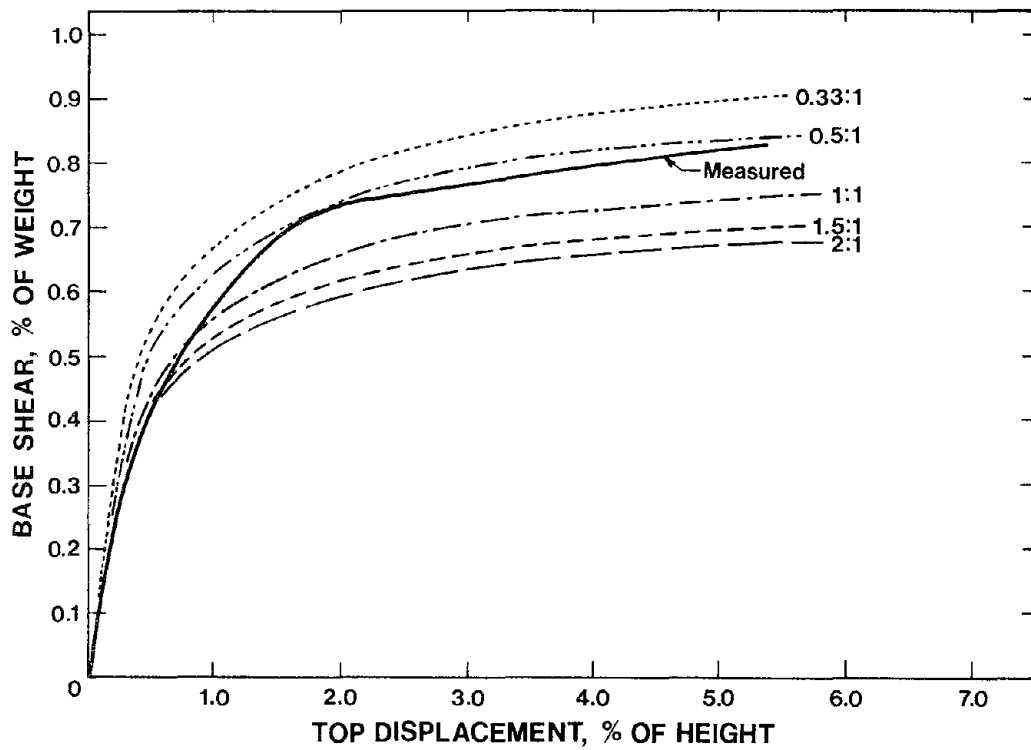


Fig. 7.6 Computed and Measured Relations Between Structure Base Shear and Top Displacement

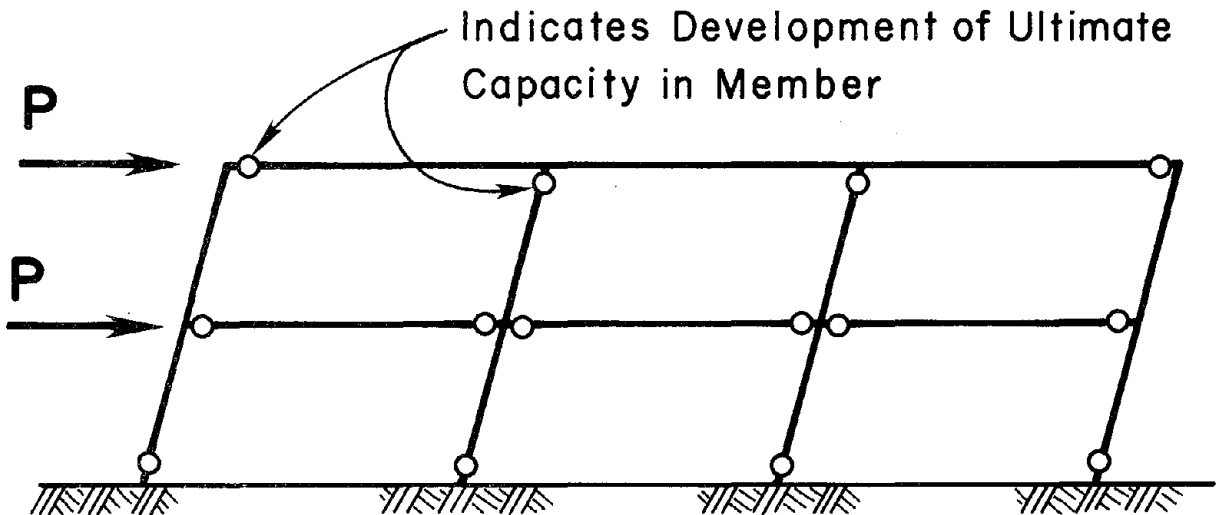


Fig. 7.7 Computed Collapse Mechanism

## APPENDIX A

### DESCRIPTION OF EXPERIMENTAL WORK

This appendix presents experimental details that are not presented in the main body of the report.

#### A.1 Chronology of the Experiments

A chronology of major aspects of the experiments is presented in Table

A.1. The chronology will be referred to in later sections of this appendix.

#### A.2 Test Structure

##### (a) Dimensions

The configuration of the test structure is described in Section 2.1(b) of this report. Nominal dimensions are shown in Fig. 1.2. Gross cross-sectional dimensions were measured at numerous locations before testing to check construction tolerances. Slab thickness was measured along the edge and at 152 of the tie-down locations for the subsidiary lead weights (Fig. A.4 and A.5). Variations of measured dimensions (Table A.2) indicate that actual dimensions were nearly the same as nominal dimensions with small variations.

##### (b) Fabrication

Fabrication was begun by preparing a steel foundation frame for the test structure. The frame had been used as a foundation for previous shaking table experiments. Some modifications were made to accommodate its use for the test structure. Details of the frame are depicted in Fig. A.1.

Reinforced concrete footings were then cast separately from the foundation frame. Footing details are indicated in Fig. A.2. Steel plates

were cast at the bottom of each footing. Column longitudinal reinforcement passed through holes in these plates and was welded on the bottom side. Steel conduits (for bolting the structure to its foundation) and footing reinforcement were tied securely in place for casting of the footings. The top surface of concrete was left rough to ensure a good joint with column concrete that would be cast later.

Following a curing period, the footings were blocked into position above the steel foundation frame (Fig. A.1). Wooden blocks acted as a substitute at this time for the shear and moment transducers that would later be placed between the footings and the foundation frame.

With the footings in place, wooden forms were constructed for the first story columns, slab, and edge beams. All forms were oiled. Following oiling, a plastic sheet was placed over the slab forms to ensure that slab reinforcement did not contact oil. Slab reinforcement was then tied in place, after which time the plastic sheets were removed (Fig. A.3). Short pieces of small diameter plain wire were placed beneath bottom slab bars to ensure proper cover. Specially fabricated steel chairs held the top slab bars at the proper depth. Walking on the slab reinforcement was not permitted (special steps were fabricated to walk on). The first floor columns, edge beams, and slab were cast from a single batch of ready mixed concrete. All concrete was in place within two hours. Slab concrete was trowelled smooth after the initial set.

Forms and shoring were kept in place following casting of the first floor, and were not removed until well after the second floor was cast (Table A.1). Wet burlap and plastic sheets were in place during this period.

The second floor was cast and cured using the procedure described for the

first floor. Relevant dates of casting and time of curing are indicated in Table A.1.

Column stubs above the second floor were cast one week after casting the second floor. Concrete for these stubs was mixed at the casting site.

Forms were stripped at the time indicated in Table A.1. Stripping began at the second floor and proceeded downward. After stripping forms, the shear and moment transducers were hydrostoned one at a time in place beneath the footings. After the hydrostone set, the transducers were bolted to the footings above and the foundation frame below. No movement was detected in the test structure during this operation.

The test structure was painted (Table A.1) with thinned latex paint to facilitate observation of concrete cracks. (Compression experiments on plain and painted concrete cylinders indicated that the paint cracked with the concrete, and greatly facilitated crack detection.)

Following painting, each floor of the test structure was diagonally braced with nominal 2 by 4 lumber. The structure was then rolled carefully to the test platform of the earthquake simulator. The structure was plumbed and centered using a transit. The steel foundation frame was subsequently hydrostoned in place on the test platform and subsequently prestressed to the platform (Fig. A.1).

(c) Subsidiary Weights

Subsidiary lead weights were added to the floor slabs at each floor level to increase the gravity and inertial load effects. Ideally, the objective of placing the weights was to simulate effects of structure dead loads. Given the limitations of the experimental environment, this can be achieved only

approximately. As described below, the subsidiary lead weights were selected and placed only to simulate approximately the effects of prototype slab self weight. Slab live load, and edge beam and column self weights, were not simulated.

To properly simulate effects of prototype slab self weight, the dead load per square meter (or square foot) of the test structure slab plus subsidiary weight should be equal to self weight of the prototype slab. Given that the prototype slab thickness is 203 mm (8 in.), and assuming concrete unit weight of 23.6 kN/m<sup>3</sup> (150 pcf), self weight of prototype slab is 4.79 kN/m<sup>2</sup> (100 psf). Self weight of the model slab is 1.44 kN/m<sup>2</sup> (30 psf). Thus, 3.35 kN/m<sup>2</sup> (70 psf) should be added to the model. This corresponds to a total of 67.3 kN (15.1 kips) of subsidiary weight per floor in the model.

Subsidiary weight in the form of individual lead pigs was selected. Each pig had average weight of 0.435 kN (97.8 lb) and dimensions shown in Fig. A.4. A total of 160 of the pigs were placed on each floor slab, resulting in total subsidiary weight of 69.6 kN (15.6 kips), or three percent in excess of the required subsidiary weight. The weights were positioned as indicated in Fig. A.5. Each weight rested on two pads (Fig. A.4). One of the pads was steel, to minimize movement of the weights during dynamic testing, and the other was rubber, to permit the slab to deform beneath the weight. All interior weights were clamped to the floor slab by steel bolts which passed through oversized conduits in the floor slab (Fig. A.4). Weights over the edge beams were clamped using steel C-clamps in place of the bolts.

The distribution of lead pigs (Fig. A.5) was selected to simulate approximately the prototype slab shear and moment "stresses." To simulate effects in the direction parallel to the three-bay direction, the weights were

positioned approximately uniformly in that direction. Slight deviations from the uniform distribution were required to avoid interference between slab bars and the tie-down bolts. In the transverse direction, the weights were positioned so as to approximate the total connection shears and moments. Because the boundary conditions of the test structure were different from those in the prototype, and because the tie-down system for the weights results in concentrated reactions rather than uniform loads, the required load distribution (Fig. A.5) was distorted from that occurring in the prototype slab.

The equivalent frame method of ACI 318-77 was used to determine approximately the distribution of slab gravity moments in the test structure as compared with those occurring in the uniformly loaded prototype structure. The equivalent frame was defined according to ACI 318-77, with the exception that prismatic columns and slab-beams were assumed. Using the equivalent frame, ideal moments in the prototype were calculated, and then scaled by the factor 0.027 to arrive at corresponding ideal test structure moments. In the transverse direction, multiple bays were assumed for the prototype. Moments in the test structure were calculated similarly for the distribution of loads shown in Fig. A.5. Calculated slab moments in the longitudinal direction compare closely for the scaled prototype and the test structure (Fig. A.6a). Transverse moments for an interior panel (Fig. A.6b) compare well near the columns, but deviate somewhat in the positive moment regions. The deviation in the positive moment regions is probably not of significance, as lateral-load resistance is not likely to be strongly dependent on slab stresses in those locations.

Although no special calculations were made, placement of an equal number of lead weights on either side of a column line (Fig. A.5) is likely to have

resulted in approximately correct slab shear distributions at each connection.

By placing the slab weights above the slab, the vertical distribution of weight is different from that occurring in the prototype. The vertical distribution of weight is summarized in Table A.3. The centroid of the combined slab, subsidiary weights, and tributary columns and edge beams is used in this report to define centroids of lateral floor inertia forces. These centroids are required for determination of overturning moments.

(d) Materials

Concrete

Concrete was designed to be similar to conventional concretes used in full-scale construction. Dry-weight mix proportions were 2.45:2.75:1.00 (course aggregate:fine aggregate:cement) with a water-cement ratio of 0.6. Cement was Type I-II Portland cement. Course aggregate was Radum pea gravel with maximum aggregate size of 10 mm (3/8 in.). Fine aggregate was a mixture of one part Tidewater blend sand and 4.4 parts Radum top sand.

Concrete for footings was batched in the laboratory at Davis Hall of the University of California. Concrete for each of two stories of the test model were ready-mixed and delivered to the casting site at the Earthquake Simulator Laboratory of the Earthquake Engineering Research Center.

Several cylinders and prisms were cast with the footings and with each floor. These were stored with the test structure and received nominally the same treatment as the structure. Compression tests, indirect tension (split cylinder) tests, and modulus of rupture tests were conducted according to ASTM specifications. The tests were conducted following conclusion of shaking table tests on the test structure (Table A.1). The tests and resulting

properties are summarized in Table A.4.

It is noted that mean concrete compression strengths obtained on 75 by 150 mm (3 by 6 in.) cylinders were 37.2 MPa (5390 psi) and 35.9 MPa (5200 psi) for the first and second floors. These values exceed the design compressive strength of 27.6 MPa (4000 psi) by approximately thirty percent. Compressive strengths obtained on 150 by 300 mm (6 by 12 in.) cylinders were approximately 95 percent of the strengths for the smaller cylinders. Splitting tension and modulus of rupture strengths both were approximately thirteen percent of the compressive strengths obtained on the smaller cylinders. This value is considered representative of values obtained for typical large scale concretes.

Mean, upper bound, and lower bound concrete stress-strain relations are plotted in Fig. A.7. The relations were obtained from three tests per floor on 150 by 300 mm (6 by 12 in.) cylinders. The mean secant modulus of elasticity (to 45 percent of compressive strength) was 26000 MPa (3760 ksi) and 25000 MPa (3630 ksi) for first and second floor concretes, respectively.

### Steel

Slab reinforcement comprised 4.5-mm (0.178-in.) diameter deformed wires. The reinforcement was manufactured in the Davis Hall at the University of California. Originally, the reinforcement was plain AISC C-1064 hard drawn steel wire having nominal diameter of 4.76 mm (3/8-in.), initial yield of approximately 1320 MPa (192 ksi) at 0.2 percent offset strain, ultimate stress of 1440 MPa (209 ksi) and ultimate elongation of approximately 3.5 percent. The manufacturing process included two heat treatment cycles in a large commercial oven and cold rolling to obtain desired surface deformations and mechanical properties, as described below.

For the first heat treatment, the virgin wires were packed in 50-mm (2 in.) diameter steel tubes capped with asbestos filler. The tubes facilitated handling and maintenance of uniform temperatures. The wires in the tubes were initially austenized at 816 degrees C for 25 minutes, followed by a slow cool to 650 degrees C, at which temperature the wires were maintained for two hours. This procedure homogenized the microstructure and softened the wire for cold rolling. A tolerance of 15 degrees C was maintained, as verified using thermocouples to measure oven and pipe temperatures at several locations.

Following the first heat treatment, hardened steel rollers deformed the softened wire by "squeezing" the wire at selected locations. The locations which were not squeezed formed the deformations. Nominally, the center to center spacing between circumferential deformations was 0.91 mm (0.036 in.), which corresponds to 0.2 times the nominal diameter. Nominal width of a circumferential deformation was 0.25 mm (0.01 in.). Figure A.8 presents a general view of a deformed bar and mean dimensions from several measurements. The average height of deformations is greater than four percent of the wire diameter which is according to ASTM specifications for deformed rebars. The number of deformations per inch is in excess of the ASTM requirement for deformed wire, but somewhat less than the required deformations for a scaled reinforcing bar.

Cold rolling strained the wires into the strain hardening region, so that a second heat treatment was required. The objective of the second treatment was to obtain properties typical of Grade 60 deformed rebars, and required spheroidizing the carbides and reducing the dislocation density created by rolling. This was achieved by repacking the deformed wires in the tubes and reheating to 650 degrees C, at which temperature they were maintained for two

hours. Again, thermocouples verified uniform and constant treatment.

Stress-strain properties were determined along a 50.8 mm (2.0 in.) gage length on nonmachined bars. Nominal diameter of 4.5 mm (0.178 in.) was used to convert load to stress. Mean stress-strain relations, and 95 percent confidence intervals, are summarized in Fig. A.9. The properties and scatter are not atypical of those obtained for Grade 60 rebar.

Bond stress-slip relations for 4.5-mm bars under monotonic loading are reported elsewhere [56].

Column and edge beam longitudinal reinforcement was deformed 6.4-mm (0.25-in.) rebar. The bars were purchased from the Portland Cement Association, Skokie, Illinois. Stress-strain relations (determined over a 203 mm [8 in.] gage length for nonmachined bars and based on nominal dimensions) are plotted in Fig. A.10.

Column and edge beam transverse reinforcement comprised No. 11 gage bright basic smooth wire (nominal diameter of 3.0 mm [0.12 in.]). The wire was not treated in any manner before using. Mean yield stress and ultimate stress capacities were 622 MPa (90.2 ksi) and 710 MPa (103 ksi), respectively, with mean ultimate elongations of 5.9 percent.

### A.3 Instrumentation and Data Descriptions

Instrumentation was organized so that displacements, accelerations, reinforcement strains, column base forces, and deformations near slab-column and column-footing connections were measured. General descriptions of instrumentation are in Section 3.4. More detailed information is presented in this section. Photographs of instrumentation are in Fig. A.11.

A total of 112 channels of data were recorded digitally for every test using a Neff System 620 analog system processor. Important characteristics of this system have been reported elsewhere [41]. The 112 channels were organized as indicated in Table A.5. Details of the data channels are given in the following paragraphs.

Motion of the test platform of the shaking table was recorded on channels 0-6 and 8-19. Included are average horizontal and vertical displacements and accelerations, pitch, roll, and twist accelerations, and displacements, accelerations, and forces in individual actuators that control movement of the table.

Channels 21-51 recorded data from DCDTs 1 through 32. The DCDTs were used to measure local deformations of interior and exterior connections and footings on the southwest side of the test structure. Locations of the DCDTs on the test structure are indicated in Fig. A.12. Details of the connection system with mean measured dimensions are indicated in Fig. A.13. As shown in that figure, pairs of aluminum collars were fixed (with bolts that had been sharpened to a "point" bearing against concrete) to columns above and below the slab. The collars supported DCDTs that targeted from one collar to another. DCDTs were also fixed to the slab (by aluminum blocks epoxied to slab concrete). These DCDTs were targeted to the column collar of each pair of collars that was nearest to the slab surface. In addition, DCDTs were fixed to a stiff reference frame and targeted to one interior and one exterior footing to measure lateral translation and rotation of the footings relative to the steel foundation frame on which the test structure was supported. DCDTs 30 and 32 (Fig. A.12) were used to measure footing movements only during tests EQ1 through EQ3. After that time, these instruments were relocated to record relative displacements as indicated in Fig. A.14 (Instruments D30 and

D32). They were removed for test EQ11 because lateral drift exceeded the range of the instruments. For test EQ11, relative displacements are calculated as the difference between average slab total displacement and base displacement.

Channels 52-59 recorded data from linear potentiometers that measured absolute displacements of the test structure floor slabs. Locations of the potentiometers is indicated in Fig. A.14. Potentiometers 1 through 4 were fixed to a reference frame that was braced against the exterior walls of the laboratory building. Potentiometers 7 and 8 were fixed to an interior balcony in the laboratory building that was located approximately 4 meters from the North edge of the test structure. All potentiometers were targeted to concrete at slab middepths of the test structure in the locations indicated (Fig. A.14). DCDTs D30 and D32 (Fig. A.14) were placed after test EQ3 to record relative floor displacements.

Channels 60-73 recorded data from accelerometers attached to the test structure. Accelerometers were mounted to aluminum blocks that had been epoxied to concrete. Locations of the accelerometers are in Fig. A.15. Orientations for positive acceleration are indicated by the direction of arrows in that figure.

Transducers to measure shear and moment beneath the footings of the test structure (Fig. A.16) were designed and fabricated for the experiments reported herein. Each transducer was an assemblage of a rectangular steel tube and several steel plates welded together as shown in Fig. A.16. The configuration effectively separated resistance to shear and moment, the shear being carried predominantly by the tube and moment being carried predominantly by the steel plates. This enabled independent selection of shear and moment

resisting elements, resulting in the desirable sensitivities. The configuration also ensures a relatively stiff transducer (desirable from the viewpoint that the transducer should not significantly alter test-structure response), with relatively slender elements (desirable because the strain field is not affected significantly by boundary conditions if slender elements are used).

The side faces of the steel tubes in the transducers were machined to a reduced thickness along the middle third of the tube as shown in Fig. A.16. A foil shear strain gage was attached to the machined faces as shown. The gages were wired into a four arm Wheatstone bridge. In addition, two foil gages, one orientated vertically and the other horizontally, were attached to the outside face of each flexural plate in a transducer (Fig. A.16). These were wired into a four arm Wheatstone bridge to read moment on the transducer. Each transducer was mechanically calibrated prior to installation beneath the test structure. Through experimentation, it was determined that the transducer measurements were insensitive to boundary conditions and independent of the applied shear-to-moment ratio.

Transducer stiffness was computed assuming the plates and tube within each transducer deformed according to the rules of conventional beam theory. Accordingly, a flexural inertia,  $I$ , was computed as

$$\begin{aligned}
 I &= I_{\text{plates}} + I_{\text{tube}} \\
 &= 2 \times (100 \times 6.4)(101^2) + 4.79 \times 10^5 = 1.38 \times 10^7 \text{ mm}^4
 \end{aligned}$$

The effective shear area was computed taking into account the stiffness of the tube. Accordingly, the shear stiffness,  $K$ , is computed as

$$K = \left( \frac{1_{\text{tube}}^3}{12EI_{\text{tube}}} + \frac{1_{\text{tube}}}{GA_{\text{web}}} \right)^{-1} = 0.00555E \text{ kN/mm} \text{ (0.0317E kip/in.)}$$

The transducers were modeled in all analyses using a beam element, as shown in Fig. 6.1. The element had flexural inertia of  $1.38 \times 10^7 \text{ mm}^4$  ( $33.15 \text{ in.}^4$ ) and shear area of  $325 \text{ mm}^2$  ( $0.503 \text{ in.}^2$ ).

Weldable strain gages were attached to longitudinal reinforcement of slabs and columns at one exterior and one interior slab-column connection on the Southwest side of the test structure (Fig. A.17). Gage length was 25.4 mm (1.0 in.). Maximum strain capacity was 0.02. Slab bar gages (located just outside the column face) were attached to top and bottom bars passing through the center of the columns at both floor levels (Fig. 3.7). Column gages were attached to intermediate longitudinal bars just above the footing level at the base, and just below and above the slab level at each floor. Column gages were omitted in the exterior column at the upper level because of limitations on the number of instruments that could be accommodated by the data acquisition system. The strain gage attached to the top slab bar at the exterior connection of the upper floor was damaged during construction. All other gages functioned until they were fractured at large strains during the experiments.

Floor inertial force at any instant in time was obtained from the product between the average floor acceleration and the floor mass. Average floor accelerations were obtained by averaging readings from accelerometers located along each column line. Floor masses include slab self weight, tributary column and edge-beam weights, and lead pigs added to the slab (Table A.3).

Structure base shears were obtained by one of two procedures. The first was by addition of the floor inertial forces. The second was by addition of the shears indicated by shear and moment transducers located below the footings of each column (Fig. A.1). The second measurement includes the

inertial force developed by the footings, whereas the first does not. However, this additional inertial force was negligible relative to the total, and the two methods of obtaining the base shear produced nearly identical results. In this report, only the base shear obtained by adding readings from the shear and moment transducers is presented.

Base moment is defined as the moment at the top of the footings (bottom of the first-story columns). The moment was obtained from the sum of products of floor level inertial forces and the distance from the inertial force to the top of the footings, plus the P-delta moment. Inertial forces are assumed to be centered at the centroid of inertial mass of each floor, considering mass of the slab, edge beams, tributary columns, and subsidiary weights (Table A.3). P-delta moments were calculated as the sum of products between floor gravity loads and lateral displacements relative to the top of the footings. P-delta moments were typically a small fraction of the total. They are included in all reported base moments.

The test structure was oriented on the shaking table with the three-bay direction parallel to a single horizontal direction of base motion (Fig. 3.3). That direction is defined as the East-West direction in this report. Lateral displacements and accelerations of the test platform and of the test structure are considered positive in the West direction. Positive moments and shears are produced at the base of the columns by displacing the structure in the positive direction. Transverse displacements and accelerations are positive in the South direction. Vertical accelerations are positive up. Strain gages indicate positive strain when strained in tension. DCDTs attached to measure relative deformations between slabs and columns at connections, and between the footings and the foundation, measure positive relative displacements when the distance between the instrument and target increases.

Table A.1 Chronology of Experiments

| Event             | Date                |
|-------------------|---------------------|
| Cast Footings     | January 21, 1983    |
| Cast First Floor  | March 28, 1983      |
| Cast First Floor  | May 10, 1983        |
| Cast Column Stubs | May 17, 1983        |
| Strip Forms       | May 24-25, 1983     |
| Paint Structure   | May 31-June 1, 1983 |
| Test Structure    | June 27-29, 1983    |
| Test Concrete     | June 30-31, 1983    |

Table A.2 Comparison Between Nominal and Measured Dimensions, meter

| Dimension                   | Nominal | Mean Measured | Standard Deviation | Maximum Deviation from Nominal |
|-----------------------------|---------|---------------|--------------------|--------------------------------|
| Thickness, Slab 1           | 0.061   | 0.063         | 0.0018             | 0.007                          |
| Thickness, Slab 2           | 0.061   | 0.063         | 0.0014             | 0.006                          |
| Width, Slab 1               | 3.658   | 3.658         | 0.0027             | 0.003                          |
| Width, Slab 2               | 3.658   | 3.658         | 0.0000             | 0.000                          |
| Length, Slab 1              | 5.624   | 5.624         | 0.0033             | 0.004                          |
| Length, Slab 2              | 5.624   | 5.627         | 0.0018             | 0.004                          |
| Height, first-story column  | 0.914   | 0.916         | 0.0019             | 0.003                          |
| Height, second-story column | 0.914   | 0.917         | 0.0022             | 0.005                          |
| Bay Widths                  | 1.829   | 1.830         | 0.0041             | 0.007                          |
| Width, Columns              | 0.137   | 0.136         | 0.0012             | 0.003                          |
| Depth, Edge Beam            | 0.107   | 0.109         | 0.0008             | 0.003                          |
| Width, Edge Beam            | 0.137   | 0.136         | 0.0010             | 0.002                          |
| Length, Edge Beam           | 3.658   | 3.658         | 0.0013             | 0.001                          |

Table A.3 Vertical Weight Distribution

| Floor | Item             | Volume<br>(m <sup>3</sup> ) | Weight, W<br>(kN) <sup>a</sup> | Centroid, Y<br>(m) <sup>b</sup> | W x Y<br>(kN-m) |
|-------|------------------|-----------------------------|--------------------------------|---------------------------------|-----------------|
| 2     | Column Stubs     | 0.023                       | 0.54                           | 1.91                            | 1.0             |
|       | Slab             | 1.297                       | 30.55                          | 1.80                            | 55.0            |
|       | Interior Columns | 0.032                       | 0.75                           | 1.56                            | 1.2             |
|       | Exterior Columns | 0.028                       | 0.66                           | 1.54                            | 1.0             |
|       | Edge Beams       | 0.046                       | 1.08                           | 1.75                            | 1.9             |
|       | Lead Weights     | ---                         | <u>69.60</u>                   | 1.88                            | <u>130.8</u>    |
|       |                  |                             | Sum = 103.18                   |                                 | Sum = 190.9     |
| 1     | Upper Column     | 0.063                       | 1.48                           | 1.13                            | 1.7             |
|       | Slab             | 1.296                       | 30.53                          | 0.88                            | 26.9            |
|       | Interior Columns | 0.032                       | 0.75                           | 0.64                            | 0.5             |
|       | Exterior Columns | 0.028                       | 0.66                           | 0.62                            | 0.4             |
|       | Edge Beams       | 0.046                       | 1.08                           | 0.83                            | 0.9             |
|       | Lead Weights     | ---                         | <u>69.60</u>                   | 0.96                            | <u>66.8</u>     |
|       |                  |                             | Sum = 104.1                    |                                 | Sum = 97.2      |

Weight of Second Floor = 103.2 kN.

Centroid of Second Floor at  $190.9/103.21 = 1.850$  m above top of footing.

Weight of First Floor = 104.1 kN.

Centroid of First Floor at  $97.2/104.1 = 0.934$  m above top of footing.

Note: Total footing weight including tributary columns is 5.77 kN, with centroid at 0.035 m below top of footing.

<sup>a</sup> Reinforced concrete unit weight assumed at 23.6 kN/m<sup>3</sup>.

<sup>b</sup> All centroids are measured relative to top of footings.

Table A.4 Summary of Concrete Properties

| Location     | Compressive Strength <sup>a</sup> |            |                 | Indirect Tension Strength |            |                 | Modulus of Rupture |            |                 | Secant Modulus |            |
|--------------|-----------------------------------|------------|-----------------|---------------------------|------------|-----------------|--------------------|------------|-----------------|----------------|------------|
|              | No. of Tests                      | Mean (MPa) | Std. Dev. (MPa) | No. of Tests              | Mean (MPa) | Std. Dev. (MPa) | No. of Tests       | Mean (MPa) | Std. Dev. (MPa) | No. of Tests   | Mean (MPa) |
| First Story  | 5                                 | 37.2       | 0.76            | 5                         | 4.79       | 0.14            | 5                  | 4.85       | 0.09            | 3              | 25900      |
| Second Story | 10                                | 35.9       | 1.38            | 5                         | 5.03       | 0.21            | 5                  | 4.65       | 0.25            | 3              | 25000      |
| Footings     | 3                                 | 33.0       | 1.52            | 3                         | 4.59       | 0.23            | 0                  | -          | -               | 0              | -          |
| Column Stubs | 3                                 | 33.0       | 0.04            | 2                         | 4.50       | 0.06            | 0                  | -          | -               | 0              | -          |

<sup>a</sup> Compressive strengths are for 75 by 150 mm cylinders. Size factors are presented in Appendix B.

Table A.5 Description of Recorded Data

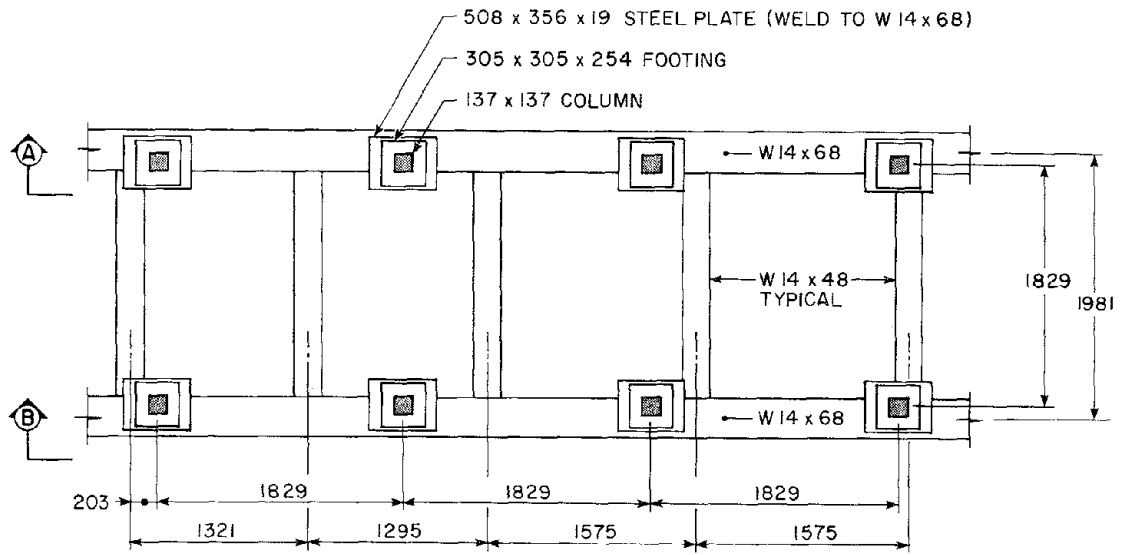
| Channel Number | Name        | Description                           | Units   |
|----------------|-------------|---------------------------------------|---------|
| 0              | AV H T Disp | Average horizontal table displacement | in.     |
| 1              | AV V T Disp | Average vertical table displacement   | in.     |
| 2              | AV H T ACC  | Average horizontal table acceleration | g       |
| 3              | AV V T ACC  | Average vertical table acceleration   | g       |
| 4              | PITCH ACC   | Table pitch acceleration              | rad/s/s |
| 6              | ROLL ACC    | Table roll acceleration               | rad/s/s |
| 7              | BLANK       | Unused channel                        |         |
| 8              | DISP H1     | Displacement of table actuator        | in.     |
| 9              | DISP H2     | Displacement of table actuator        | in.     |
| 10             | DISP H3     | Displacement of table actuator        | in.     |
| 11             | FORCE H1    | Force in table actuator               | kip     |
| 12             | FORCE H2    | Force in table actuator               | kip     |
| 13             | FORCE H3    | Force in table actuator               | kip     |
| 14             | ACC H1      | Horizontal table accelerometer 1      | g       |
| 15             | ACC H2      | Horizontal table accelerometer 2      | g       |
| 16             | DISP V1     | Vertical table displacement           | in.     |
| 17             | DISP V2     | Vertical table displacement           | in.     |
| 18             | DISP V3     | Vertical table displacement           | in.     |
| 19             | DISP V4     | Vertical table displacement           | in.     |
| 20             | DCDT 1      | DCDT D1, Fig. A.12                    | in.     |
| 21             | DCDT 2      | DCDT D2, Fig. A.12                    | in.     |
| 22             | DCDT 3      | DCDT D3, Fig. A.12                    | in.     |
| 23             | DCDT 4      | DCDT D4, Fig. A.12                    | in.     |
| 24             | DCDT 5      | DCDT D5, Fig. A.12                    | in.     |
| 25             | DCDT 6      | DCDT D6, Fig. A.12                    | in.     |
| 26             | DCDT 7      | DCDT D7, Fig. A.12                    | in.     |
| 27             | DCDT 8      | DCDT D8, Fig. A.12                    | in.     |
| 28             | DCDT 9      | DCDT D9, Fig. A.12                    | in.     |
| 29             | DCDT 10     | DCDT D10, Fig. A.12                   | in.     |
| 30             | DCDT 11     | DCDT D11, Fig. A.12                   | in.     |
| 31             | DCDT 12     | DCDT D12, Fig. A.12                   | in.     |
| 32             | DCDT 13     | DCDT D13, Fig. A.12                   | in.     |
| 33             | DCDT 14     | DCDT D14, Fig. A.12                   | in.     |
| 34             | DCDT 15     | DCDT D15, Fig. A.12                   | in.     |
| 35             | DCDT 16     | DCDT D16, Fig. A.12                   | in.     |
| 36             | DCDT 17     | DCDT D17, Fig. A.12                   | in.     |
| 37             | DCDT 18     | DCDT D18, Fig. A.12                   | in.     |
| 38             | DCDT 19     | DCDT D19, Fig. A.12                   | in.     |
| 39             | DCDT 20     | DCDT D20, Fig. A.12                   | in.     |
| 40             | DCDT 21     | DCDT D21, Fig. A.12                   | in.     |
| 41             | DCDT 22     | DCDT D22, Fig. A.12                   | in.     |
| 42             | DCDT 23     | DCDT D23, Fig. A.12                   | in.     |
| 43             | DCDT 24     | DCDT D24, Fig. A.12                   | in.     |
| 44             | DCDT 25     | DCDT D25, Fig. A.12                   | in.     |
| 45             | DCDT 26     | DCDT D26, Fig. A.12                   | in.     |
| 46             | DCDT 27     | DCDT D27, Fig. A.12                   | in.     |
| 47             | DCDT 28     | DCDT D28, Fig. A.12                   | in.     |
| 48             | DCDT 29     | DCDT D29, Fig. A.12                   | in.     |

Table A.5 (cont'd.) Description of Recorded Data

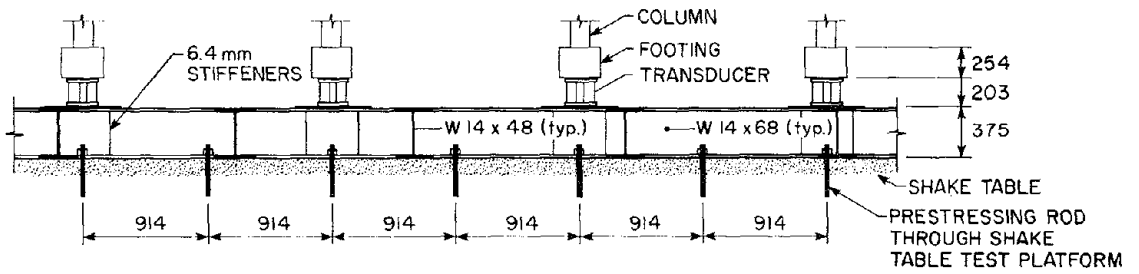
| Channel Name<br>Number | Description | Units  |         |
|------------------------|-------------|--|---------|
| 49                     | DCDT 30     | DCDT D30, Fig. A.12 and A.14   | in.     |
| 50                     | DCDT 31     | DCDT D31, Fig. A.12  | in.     |
| 51                     | DCDT 32     | DCDT D31, Fig. A.12 and A.14   | in.     |
| 52                     | POT 1       | Absolute displacement, slab 1, Fig. A.14                                 | in.     |
| 53                     | POT 2       | Absolute displacement, slab 1, Fig. A.14                                 | in.     |
| 54                     | POT 3       | Absolute displacement, slab 2, Fig. A.14                                 | in.     |
| 55                     | POT 4       | Absolute displacement, slab 2, Fig. A.14                                 | in.     |
| 56                     | POT 5       | Duplicate channel  | in.     |
| 57                     | POT 6       | Duplicate channel  | in.     |
| 58                     | POT 7       | Trans. displacement, slab 2, Fig. A.14                                   | in.     |
| 59                     | POT 8       | Trans. displacement, slab 2, Fig. A.14                                   | in.     |
| 60                     | ACC 1       | Trans. accel., east slab 1, Fig. A.15                                    | g       |
| 61                     | ACC 2       | Vert. accel., slab 1, Fig. A.15  | g       |
| 62                     | ACC 3       | Trans. accel., west slab 1, Fig. A.15                                    | g       |
| 63                     | ACC 4       | Horiz. accel., north slab 1, Fig. A.15                                   | g       |
| 64                     | ACC 5       | Horiz. accel., south slab 1, Fig. A.15                                   | g       |
| 65                     | ACC 6       | Trans. accel., east slab 2, Fig. A.15                                    | g       |
| 66                     | ACC 7       | Trans. accel., west slab 2, Fig. A.15                                    | g       |
| 67                     | ACC 8       | Horiz. accel., north slab 2, Fig. A.15                                   | g       |
| 68                     | ACC 9       | Horiz. accel., south slab 2, Fig. A.15                                   | g       |
| 69                     | ACC 10      | Vert. accel., slab 1, Fig. A.15  | g       |
| 70                     | ACC 11      | Vert. accel., slab 1, Fig. A.15  | g       |
| 71                     | ACC 12      | Vert. accel., slab 1, Fig. A.15  | g       |
| 72                     | ACC 13      | Vert. accel., slab 1, Fig. A.15  | g       |
| 73                     | ACC 14      | Vert. accel., int. footing, Fig. A.15                                    | g       |
| 74                     | SHEAR 1     | Shear, SE exterior footing, Fig. A.14                                    | kip     |
| 75                     | SHEAR 2     | Shear, NE exterior footing, Fig. A.14                                    | kip     |
| 76                     | SHEAR 3     | Shear, SE interior footing, Fig. A.14                                    | kip     |
| 77                     | SHEAR 4     | Shear, NE interior footing, Fig. A.14                                    | kip     |
| 78                     | SHEAR 5     | Shear, SW interior footing, Fig. A.14                                    | kip     |
| 79                     | SHEAR 6     | Shear, NW interior footing, Fig. A.14                                    | kip     |
| 80                     | SHEAR 7     | Shear, SW exterior footing, Fig. A.14                                    | kip     |
| 81                     | SHEAR 8     | Shear, NW exterior footing, Fig. A.14                                    | kip     |
| 82                     | MOMENT 1    | Moment, SE exterior footing, Fig. A.14                                   | kip-in. |
| 83                     | MOMENT 2    | Moment, NE exterior footing, Fig. A.14                                   | kip-in. |
| 84                     | MOMENT 3    | Moment, SE interior footing, Fig. A.14                                   | kip-in. |
| 85                     | MOMENT 4    | Moment, NE interior footing, Fig. A.14                                   | kip-in. |
| 86                     | MOMENT 5    | Moment, SW interior footing, Fig. A.14                                   | kip-in. |
| 87                     | MOMENT 6    | Moment, NW interior footing, Fig. A.14                                   | kip-in. |
| 88                     | MOMENT 7    | Moment, SW exterior footing, Fig. A.14                                   | kip-in. |
| 89                     | MOMENT 8    | Moment, NW exterior footing, Fig. A.14                                   | kip-in. |
| 90                     | STRAIN 1    | Strain, base of SW ext. column, long.<br>bar on W column face, Fig. A.17 | mil/in. |
| 91                     | STRAIN 2    | Strain, base of SW ext. column, long.<br>bar on E column face, Fig. A.17 | mil/in. |
| 92                     | STRAIN 3    | Strain, base of SW int. column, long.<br>bar on W column face, Fig. A.17 | mil/in. |

Table A.5 (cont'd.) Description of Recorded Data

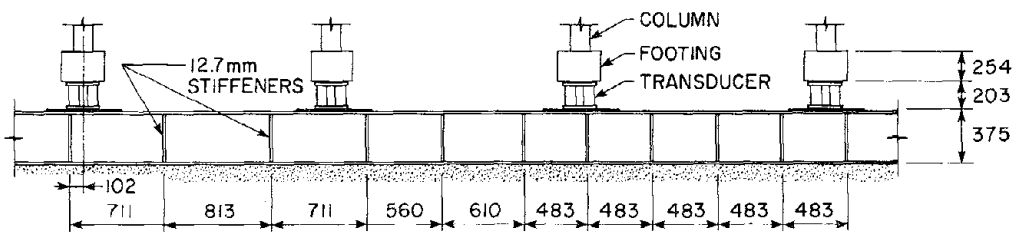
| Channel Name Number | Description  | Units   |
|---------------------|--|---------|
| 93                  | STRAIN 4<br>Strain, base of SW int. column, long. bar on E column face, Fig. A.17          | mil/in. |
| 94                  | STRAIN 5<br>Strain, top 1st floor, SW int. column, long. bar on W face, Fig. A.17          | mil/in. |
| 95                  | STRAIN 6<br>Strain, top 1st floor, SW int. column, long. bar on E face, Fig. A.17          | mil/in. |
| 96                  | STRAIN 7<br>Strain, bottom 2nd floor, SW int. column, long. bar on W face, Fig. A.17       | mil/in. |
| 97                  | STRAIN 8<br>Strain, bottom 2nd floor, SW int. column, long. bar on E face, Fig. A.17       | mil/in. |
| 98                  | STRAIN 9<br>Strain, top 2nd floor, SW int. column, long. bar on W face, Fig. A.17          | mil/in. |
| 99                  | STRAIN 10<br>Strain, top 2nd floor, SW int. column, long. bar on E face, Fig. A.17         | mil/in. |
| 100                 | STRAIN 11<br>Strain, 1st floor, bot. slab long. bar at E face of SW ext. column, Fig. A.17 | mil/in. |
| 101                 | STRAIN 12<br>Strain, 1st floor, bot. slab long. bar at W face of SW int. column, Fig. A.17 | mil/in. |
| 102                 | STRAIN 13<br>Strain, 1st floor, bot. slab long. bar at E face of SW int. column, Fig. A.17 | mil/in. |
| 103                 | STRAIN 14<br>Strain, 1st floor, top slab long. bar at E face of SW ext. column, Fig. A.17  | mil/in. |
| 104                 | STRAIN 15<br>Strain, 1st floor, top slab long. bar at W face of SW int. column, Fig. A.17  | mil/in. |
| 105                 | STRAIN 16<br>Strain, 1st floor, top slab long. bar at E face of SW int. column, Fig. A.17  | mil/in. |
| 106                 | STRAIN 17<br>Strain, 2nd floor, bot. slab long. bar at E face of SW ext. column, Fig. A.17 | mil/in. |
| 107                 | STRAIN 18<br>Strain, 2nd floor, bot. slab long. bar at W face of SW int. column, Fig. A.17 | mil/in. |
| 108                 | STRAIN 19<br>Strain, 2nd floor, bot. slab long. bar at E face of SW int. column, Fig. A.17 | mil/in. |
| 109                 | STRAIN 20<br>Strain, 2nd floor, top slab long. bar at E face of SW ext. column, Fig. A.17  | mil/in. |
| 110                 | STRAIN 21<br>Strain, 2nd floor, top slab long. bar at W face of SW int. column, Fig. A.17  | mil/in. |
| 111                 | STRAIN 22<br>Strain, 2nd floor, top slab long. bar at E face of SW int. column, Fig. A.17  | mil/in. |



NOTE: All Dimensions Are In Millimeters.



SECTION A-A



SECTION B-B

Fig. A.1 Foundation Details

(ALL DIMENSIONS HAVE UNITS OF MILLIMETERS)

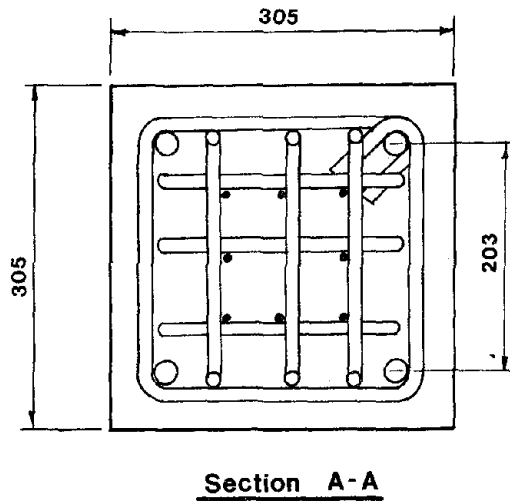
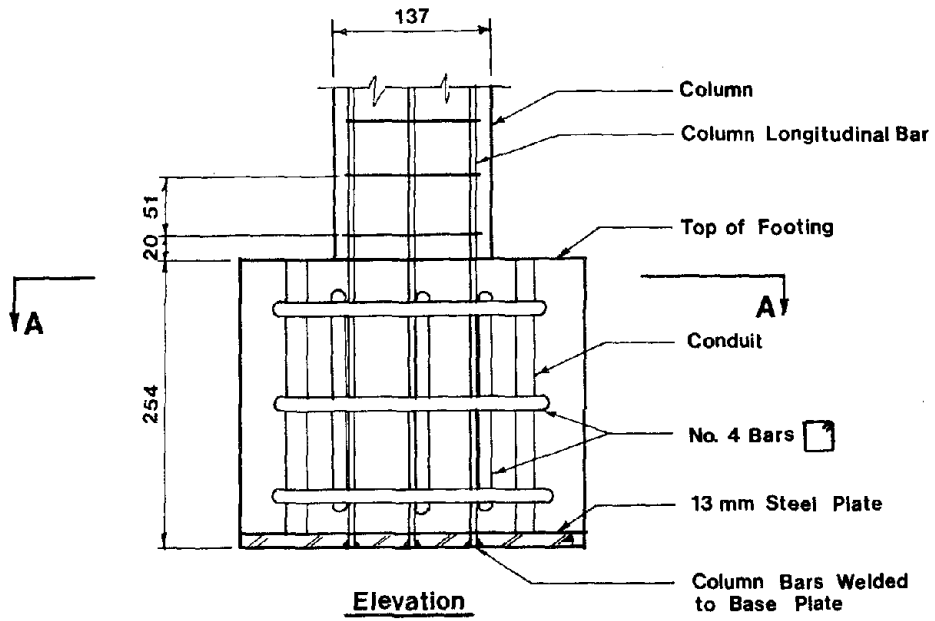
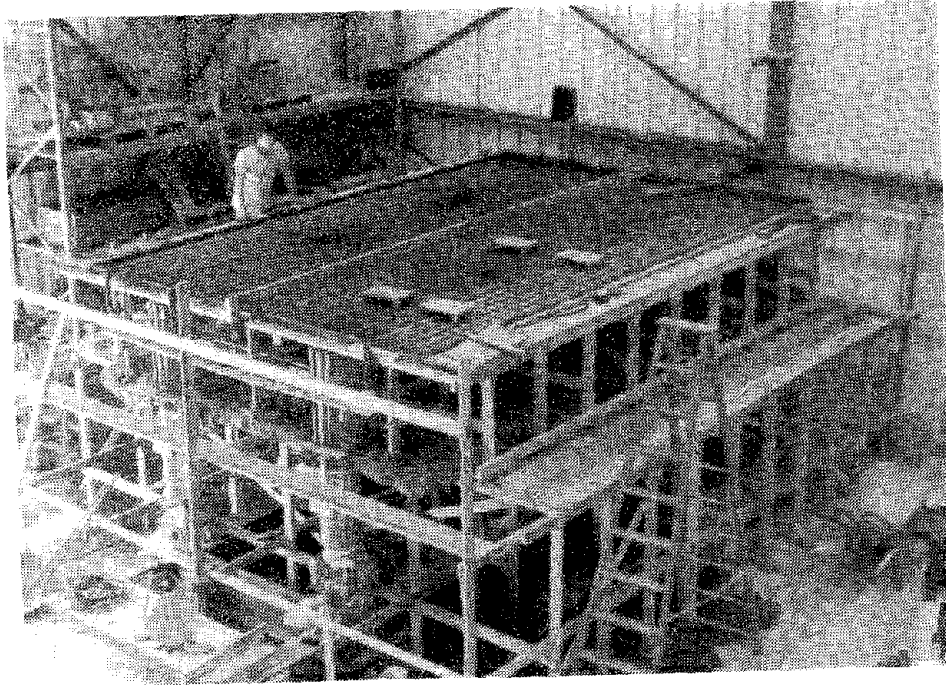
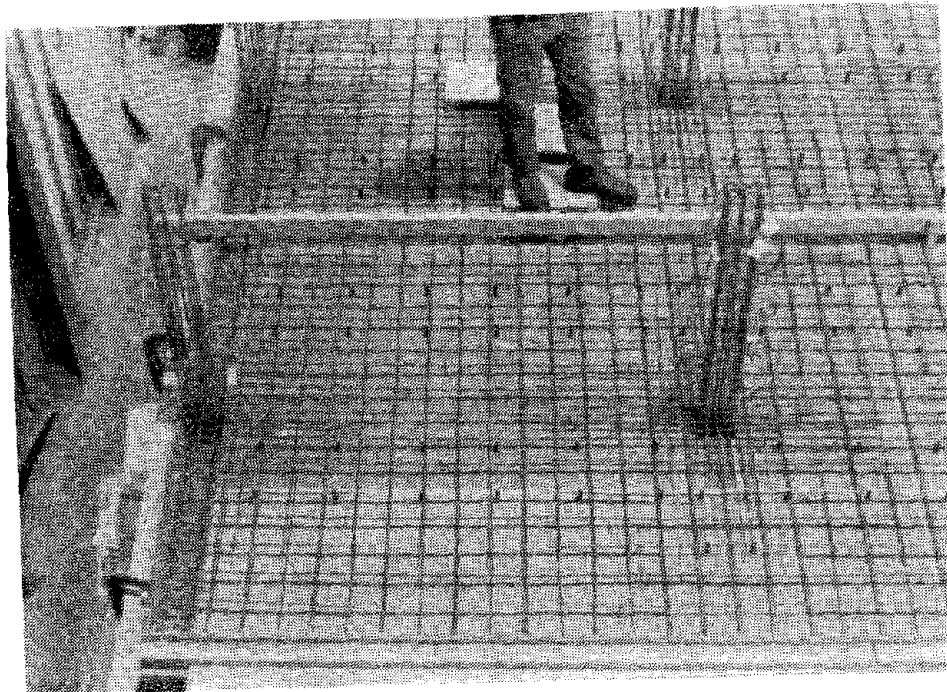


Fig. A.2 Footing Details

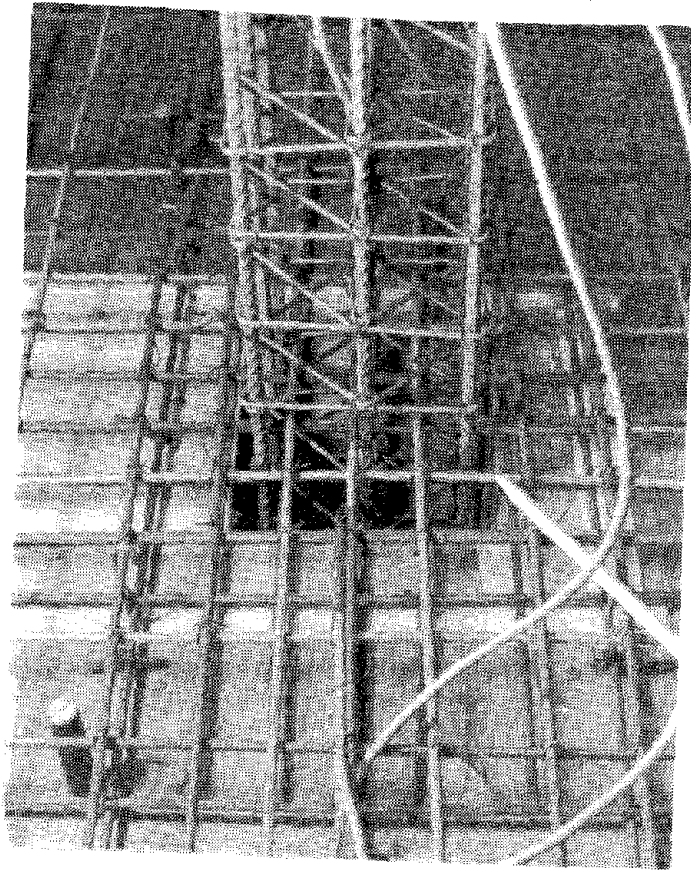


(a) Formwork for Second Floor

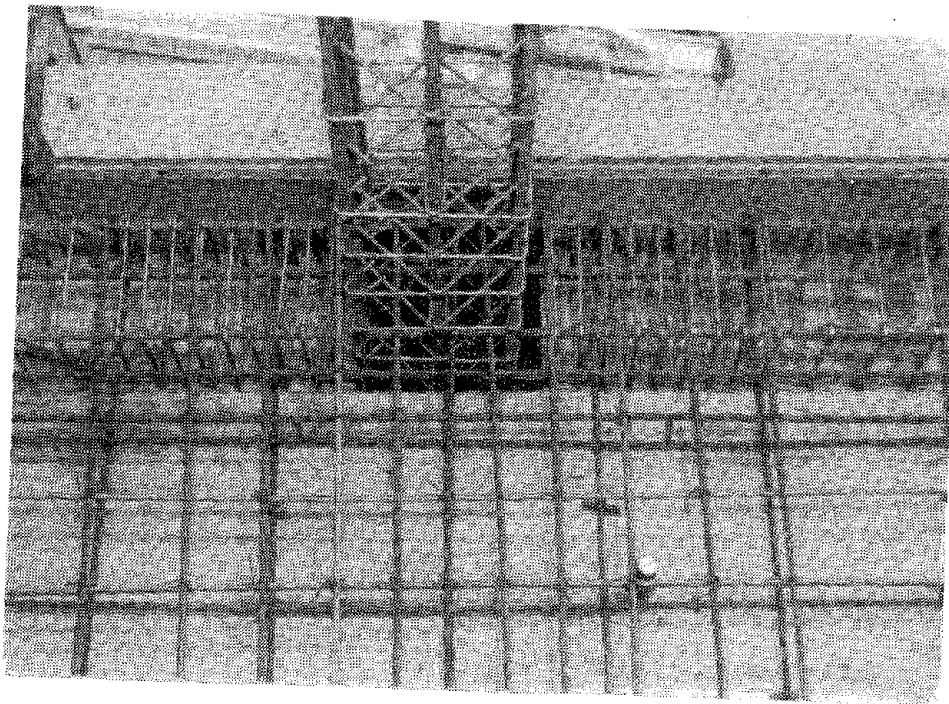


(b) View of Exterior Slab Panel

Fig. A.3 Photographs of Reinforcement Cages Before Casting



(c) Interior Slab-Column Connection



(d) Exterior Slab-Column-Beam Connection

Fig. A.3 (cont'd.) Photographs of Reinforcement Cages Before Casting

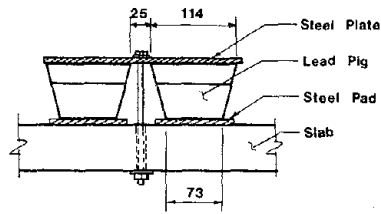
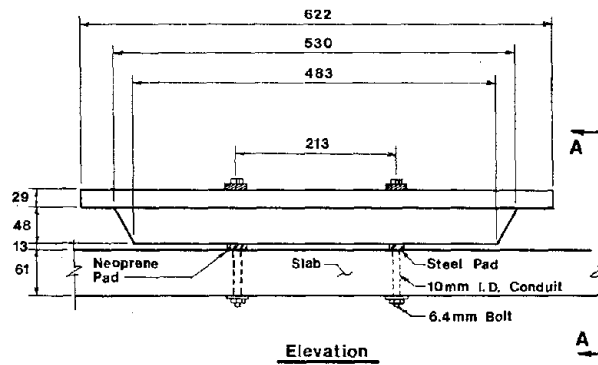


Fig. A.4 Dimensions of Lead Pig

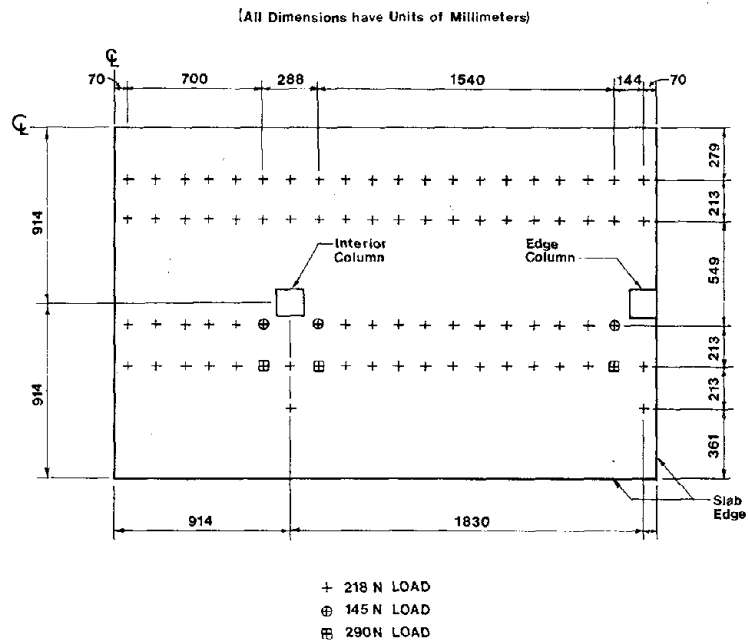
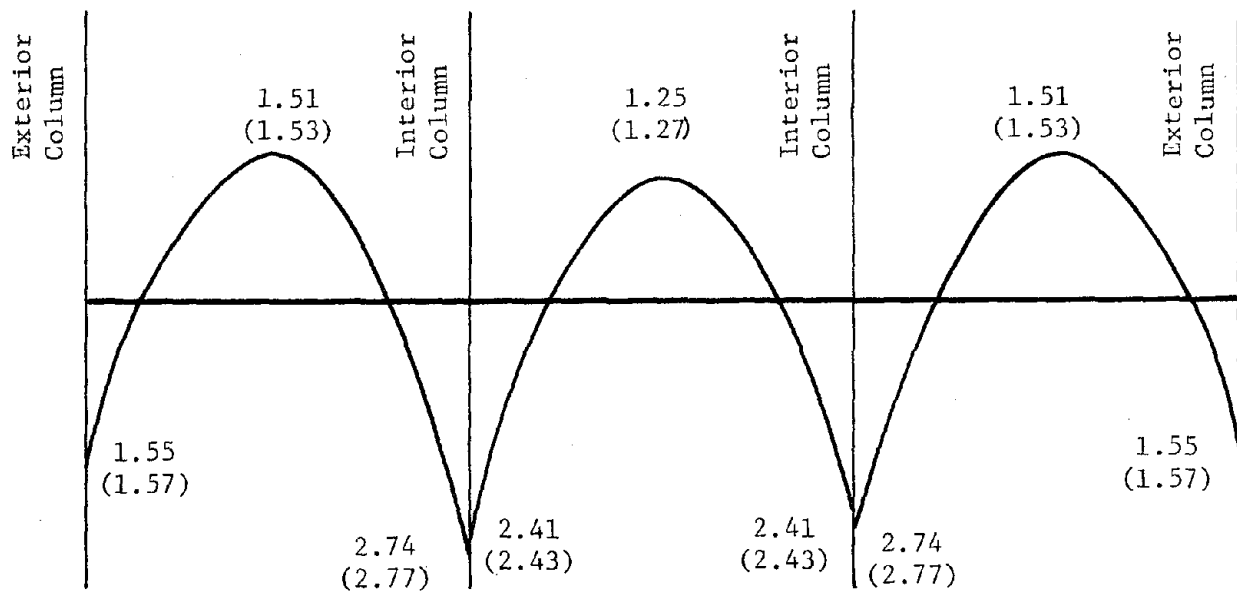
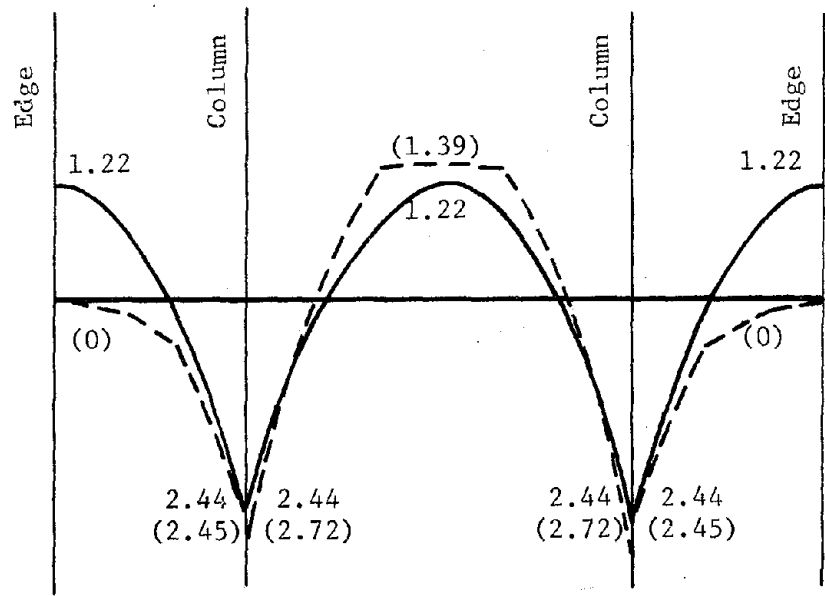


Fig. A.5 Locations and Magnitudes of Lead-Pig Reactions



(a) Longitudinal Moments



(b) Transverse Moments

Fig. A.6 Calculated Ideal and Actual Slab Gravity-Load Moments

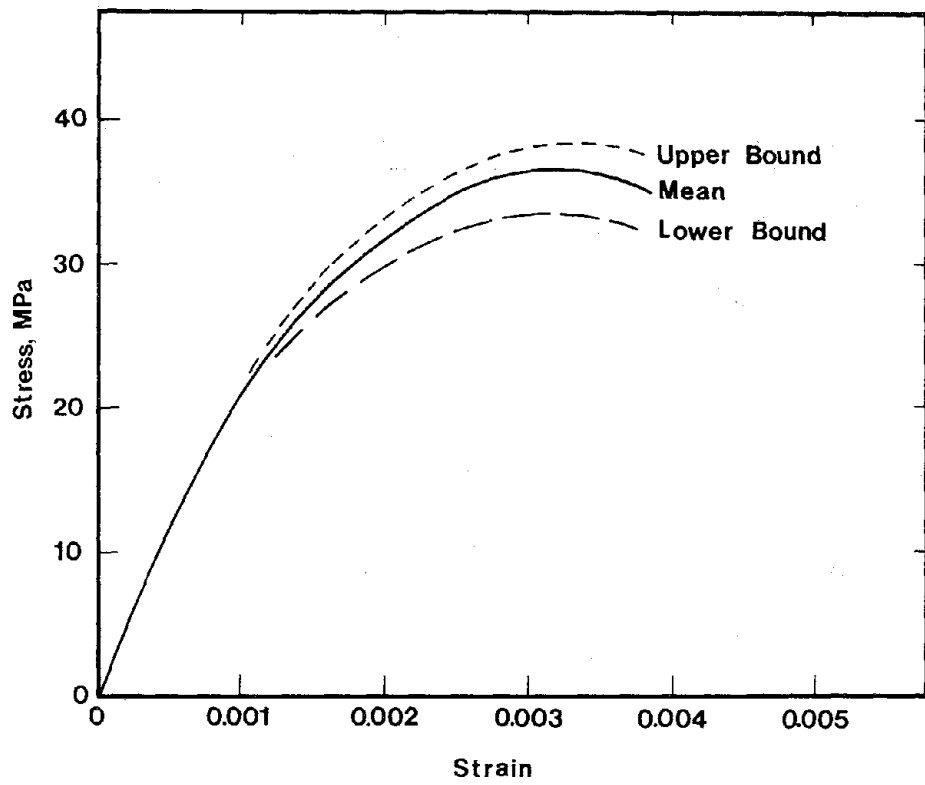
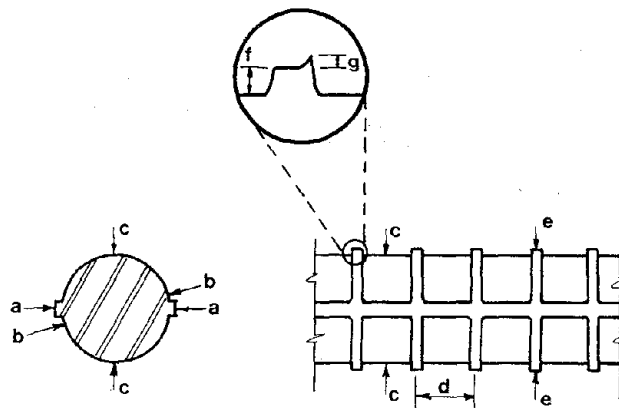


Fig. A.7 Concrete Stress-Strain Relations



| Dimension | a    | b    | c    | d    | e    | f    | g    |
|-----------|------|------|------|------|------|------|------|
| mm        | 5.01 | 4.45 | 4.22 | 2.42 | 4.57 | 0.17 | 0.11 |

Fig. A.8 Slab Reinforcing Bar Dimensions

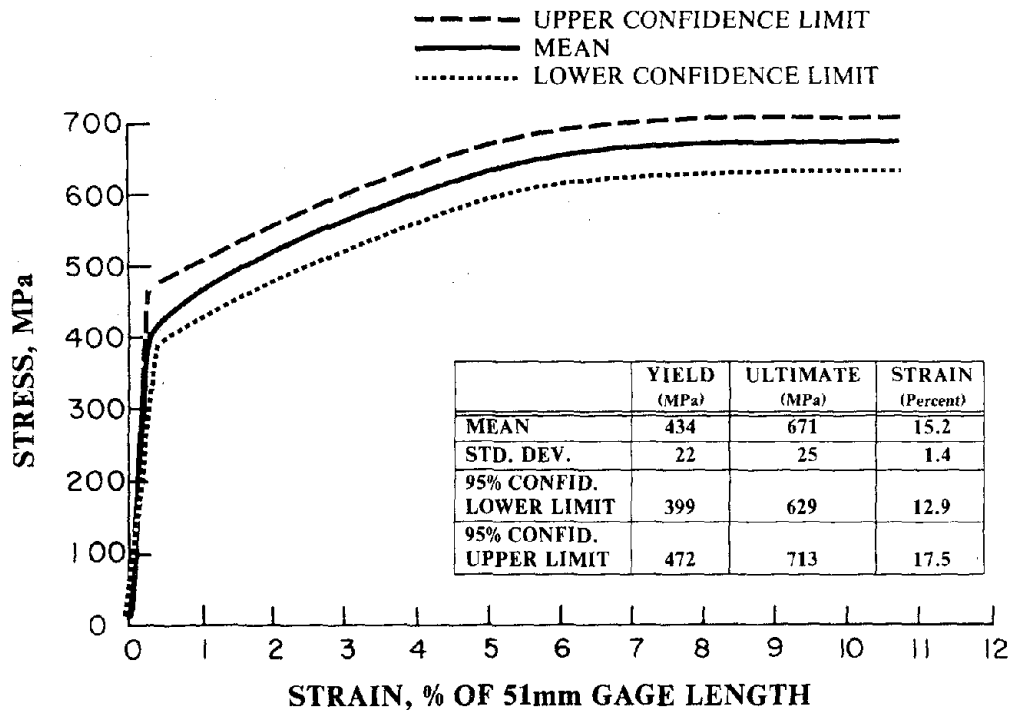


Fig. A.9 Stress-Strain Relation of 4.5-mm Slab Bar

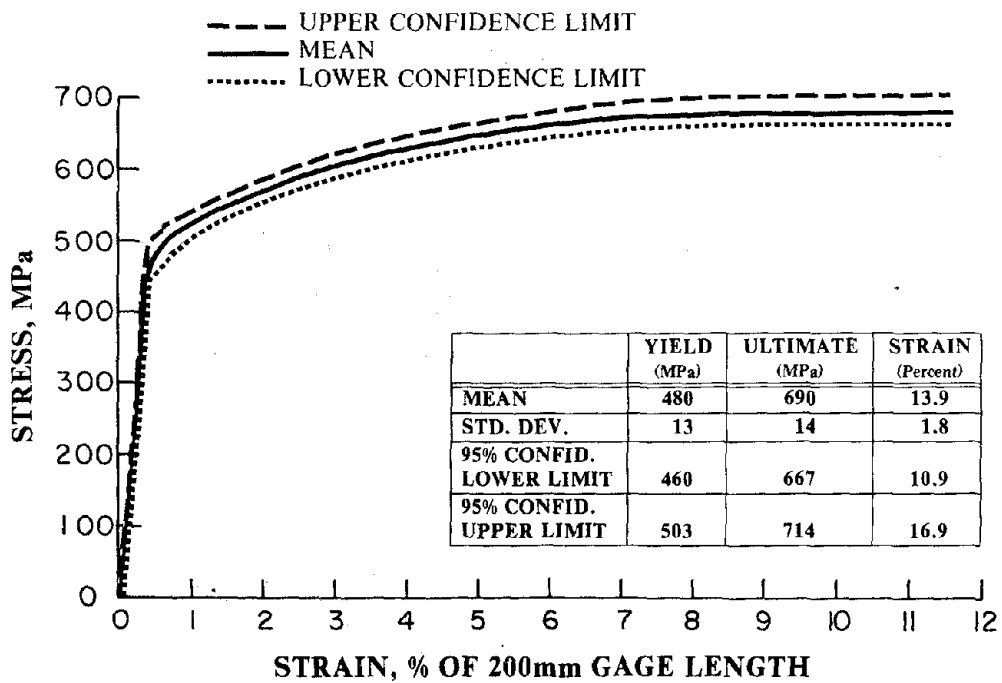
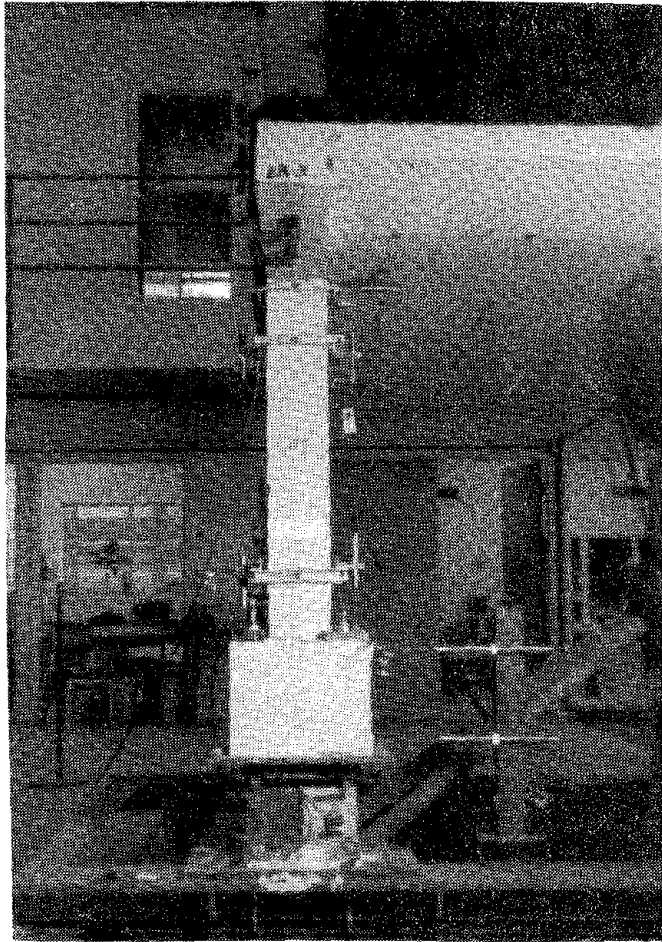
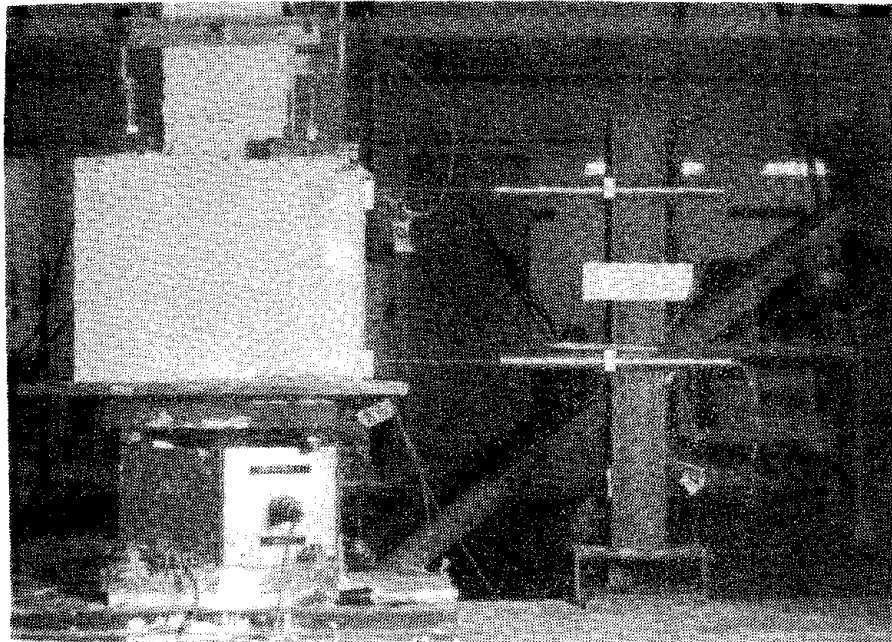


Fig. A.10 Stress-Strain Relation of 6.4-mm Bar

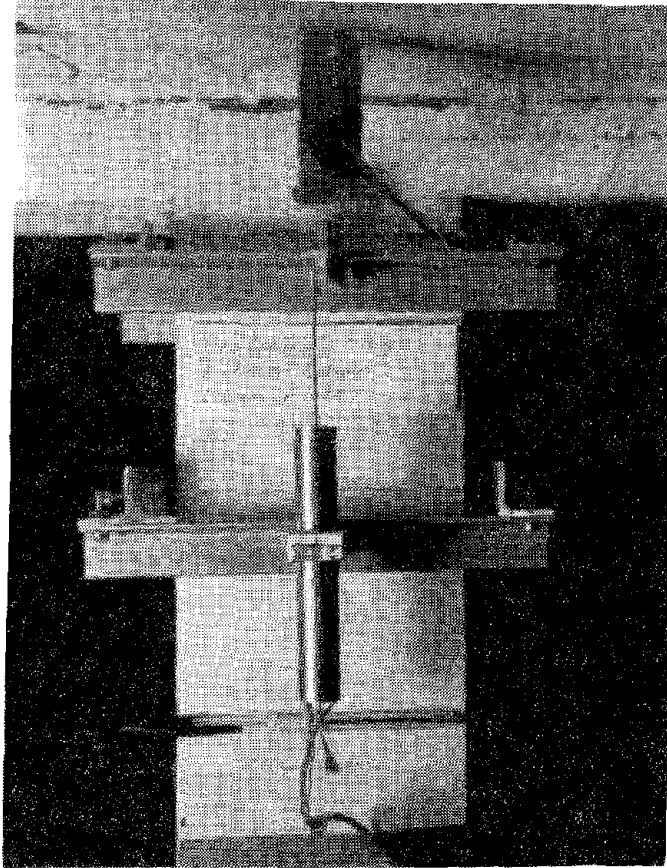


(a) First-Floor Exterior Column, Viewed Transverse to Base Motion

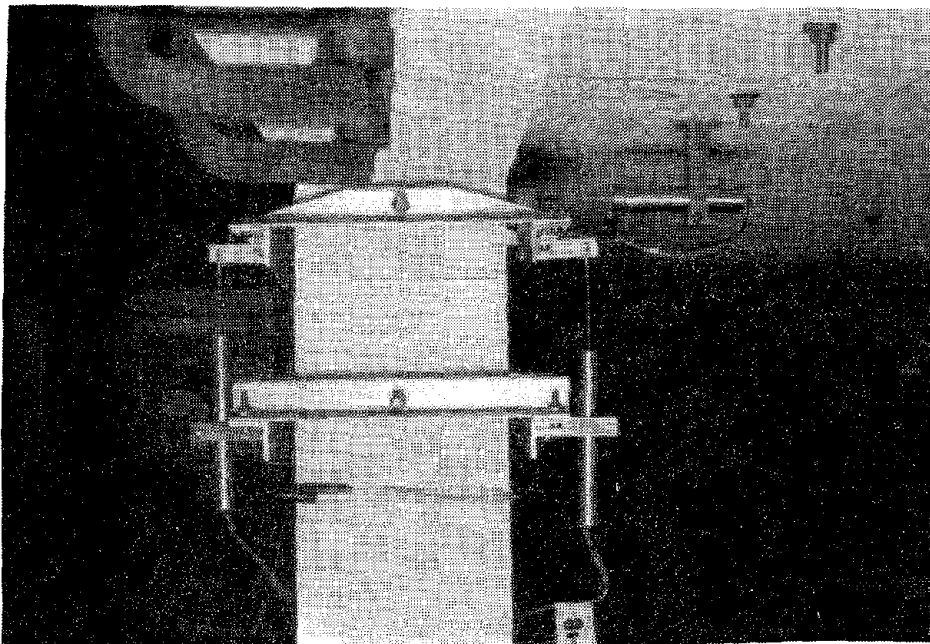


(b) Transducer and Footing Instrumentation

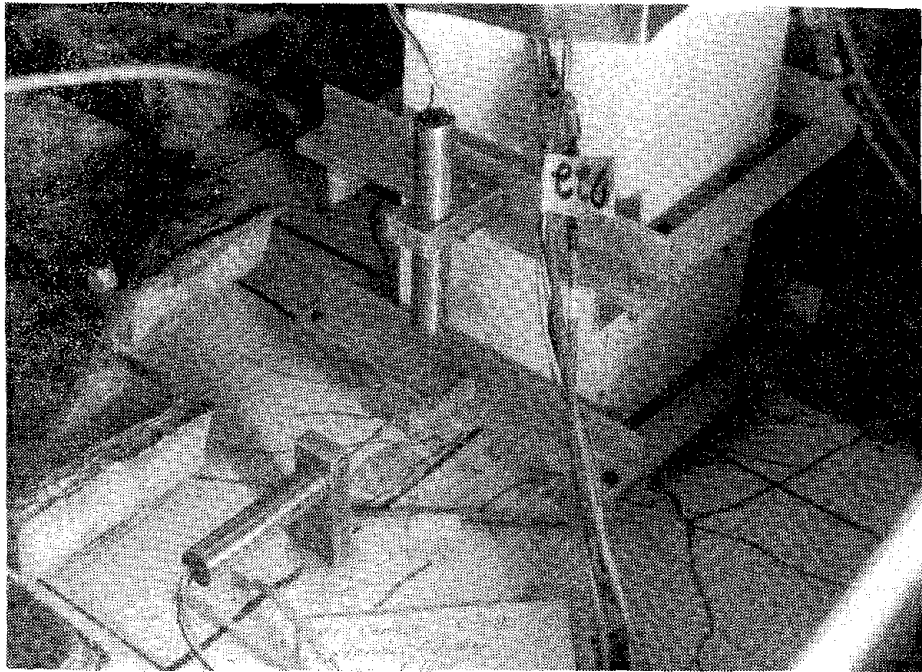
Fig. A.11 Photographs of Instrumentation



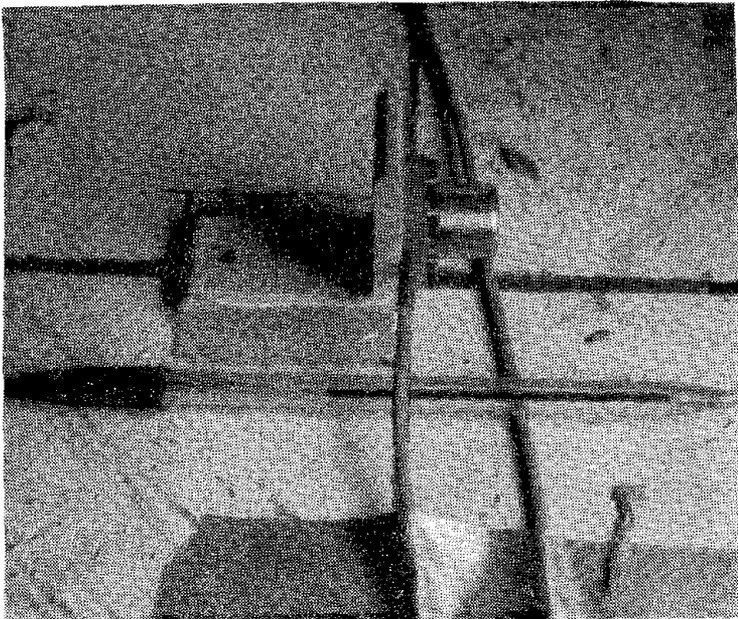
(c) DCDTs at Slab-Column Connection, Viewed Parallel to Base Motion



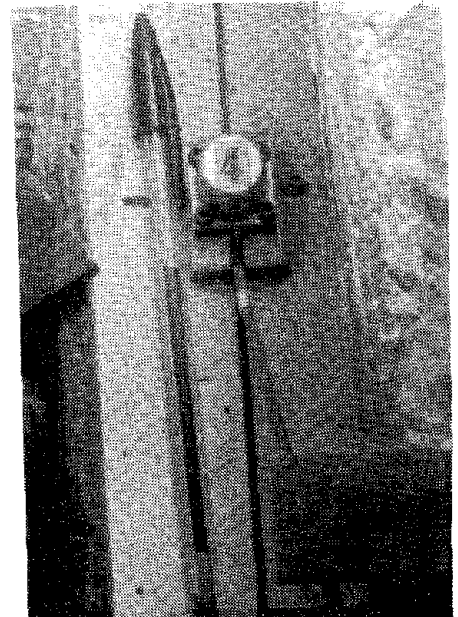
(d) DCDTs at Slab-Column Connection, Viewed Transverse to Base Motion



(e) DCDTs at Slab-Column Connection



(f) Horizontal Floor Slab Accelerometer



(g) Vertical Floor Slab Accelerometer

Fig.A.11 (cont'd.) Photographs of Instrumentation

← WEST —

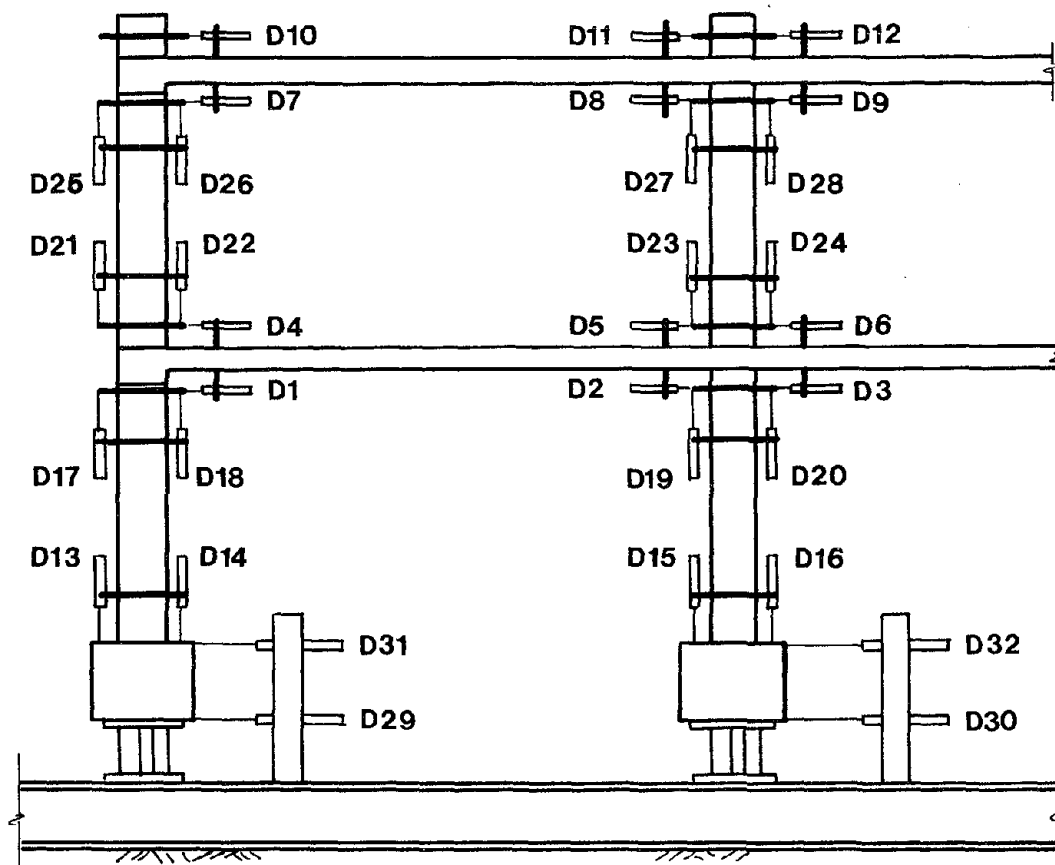


Fig. A.12 DCDT Locations

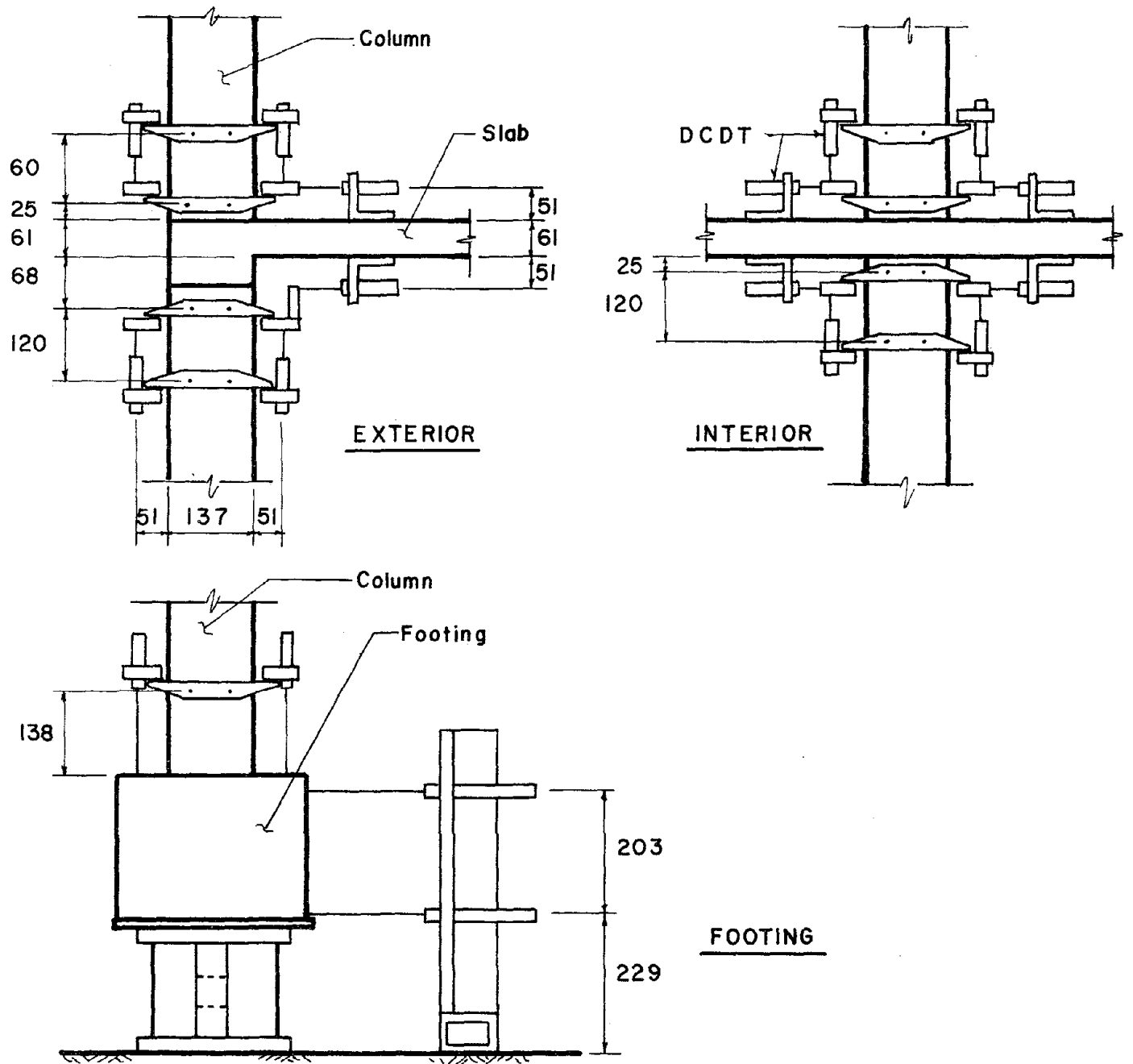
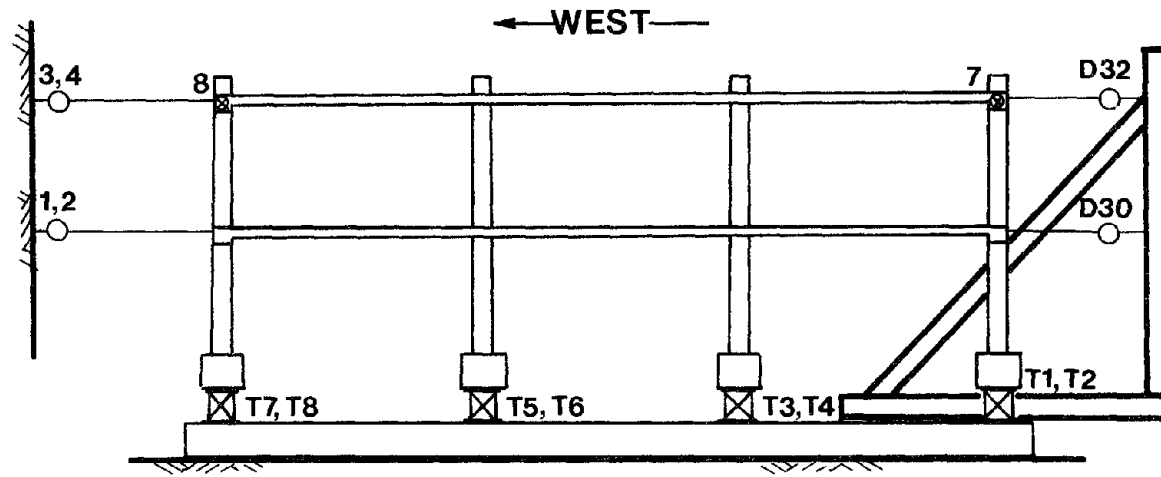
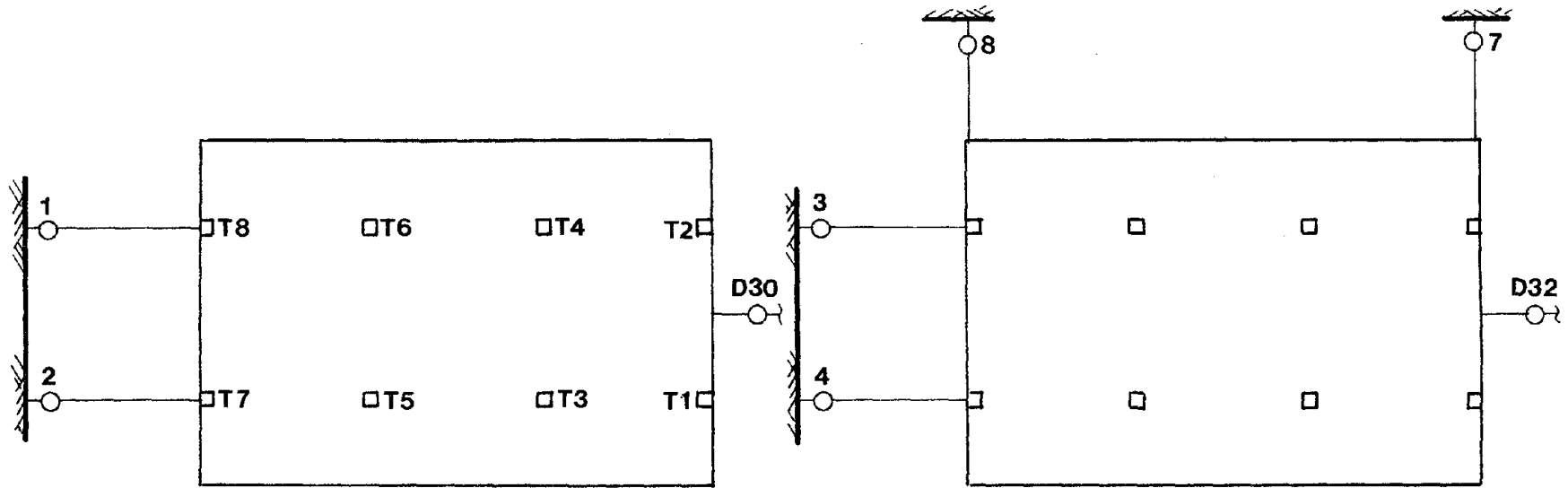


Fig. A.13 Details of DCDT Connections



ELEVATION

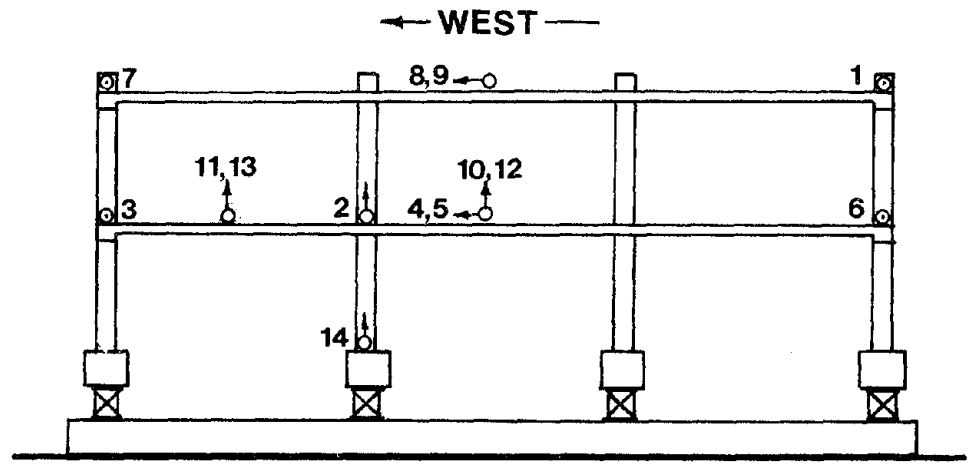
234



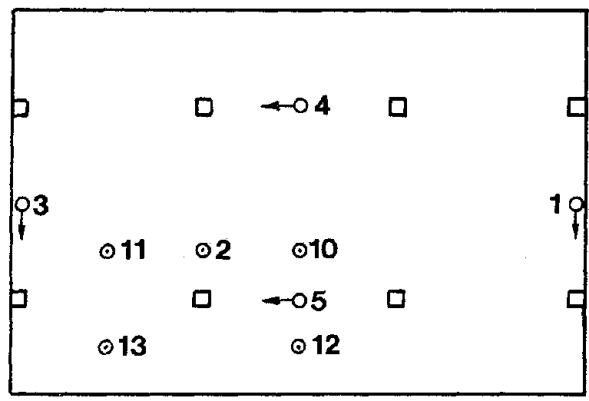
FIRST FLOOR

SECOND FLOOR

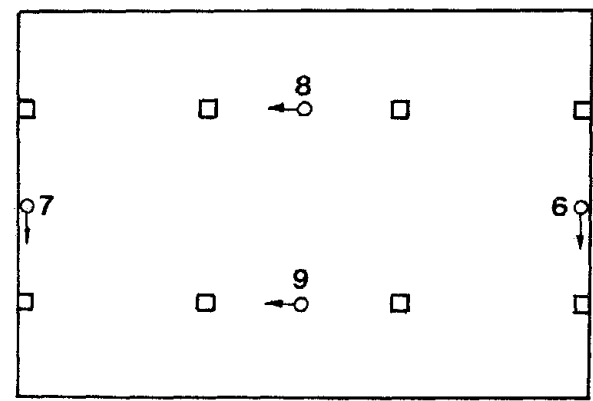
Fig. A.14 Locations of Linear Potentiometers (1-8), DCDTs for Measurement of Relative Displacements (D30, D32), and Transducers (T1-T8)



ELEVATION



FIRST FLOOR



SECOND FLOOR

Fig. A.15 Locations and Orientations of Accelerometers

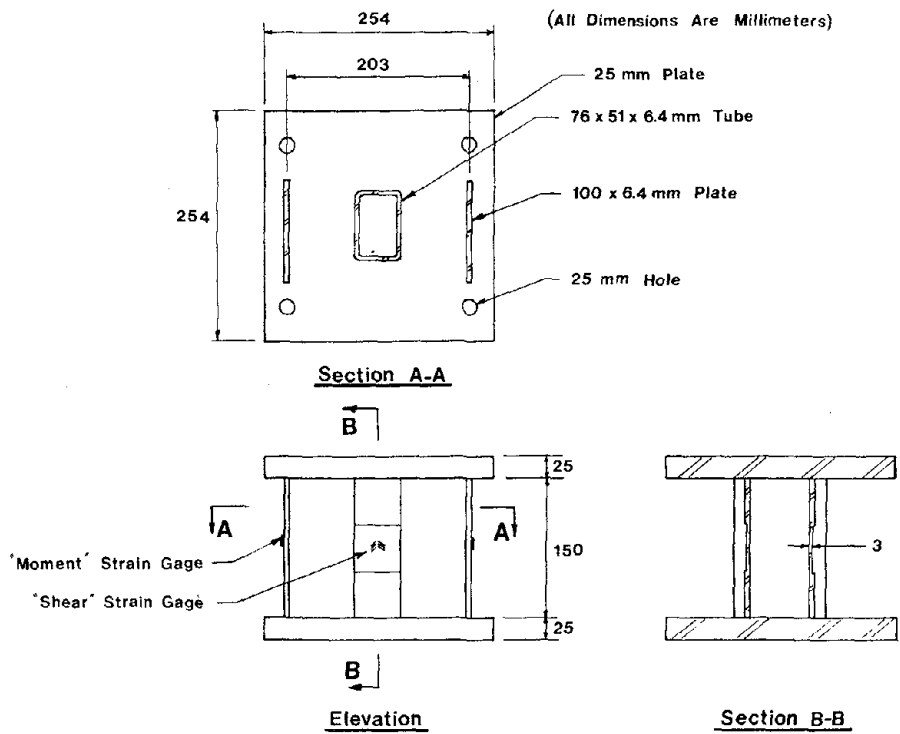


Fig. A.16 Configuration of Shear and Moment Transducer

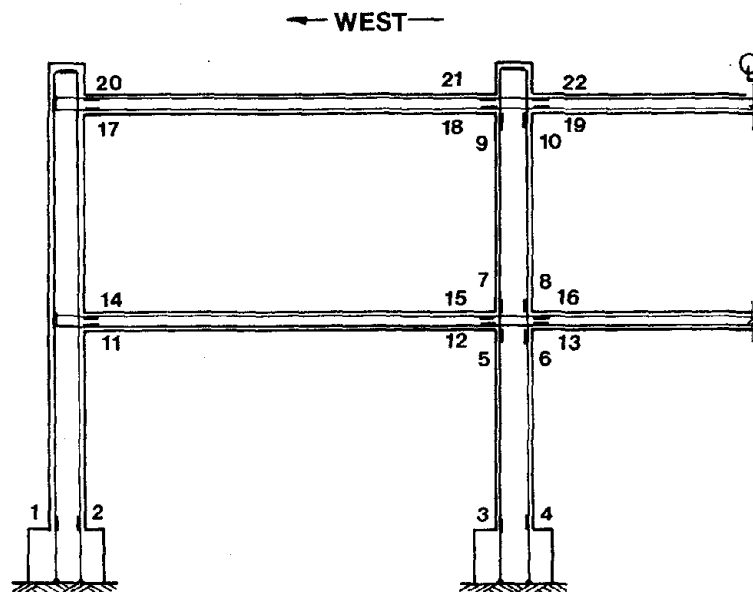


Fig. A.17 Locations of Reinforcement Strain Gages

## APPENDIX B

### NOTATION

The following notation is used in this report:

$A_t$  = cross-sectional area of stirrup leg;

$A_{web}$  = cross-section area of web;

$c$  = column cross-sectional dimension;

$C$  = numerical response coefficient;

$d$  = beam or slab effective depth, taken as mean value for slab shear strength computations;

$D$  = service dead load effect;

$d_b$  = reinforcing bar diameter;

$E$  = service earthquake load effect;

or Young's modulus;

$f$  = subscript indicating quantity measured after placement of subsidiary weights;

$f'_c$  = concrete compression strength;

$f_y$  = steel yield stress;

$G$  = shear modulus;

$h$  = slab thickness;

$H$  = height of structure, measured from top of footing to middepth of second floor slab;

$I$  = occupancy importance factor;

or flexural moment of inertia;

$I_{cr}$  = cracked transformed section flexural moment of inertia;

$I_e$  = effective flexural moment of inertia;

$I_g$  = gross-section flexural moment of inertia;

$K$  = numerical coefficient dependent on type of lateral load resisting system;

or structure stiffness;

$L$  = service live load effect;  
 $l_o$  = column length from face of joint requiring closely-spaced hoops;  
 $M_a$  = maximum applied moment;  
 $M_{cr}$  = cracking moment;  
 $M_s$  = unbalanced moment at slab-column connection;  
 $o$  = subscript indicating quantity measured before placement of subsidiary weights;  
 $R$  = ratio between  $I_e$  and  $I_g$ ;  
 $s$  = stirrup or hoop spacing;  
 $S$  = numerical coefficient for site-structure resonance;  
 $T$  = vibration period, in sec;  
 $U_g$  = factored design gravity load effect;  
 $V$  = service level design base shear;  
 $W$  = structure weight, not including footings and foundation;  
 $x_f$  = ordinate of mode shape at top of footing;  
 $x_t$  = ordinate of mode shape at top of transducer;  
 $x_1$  = ordinate of mode shape at middepth of first-level slab;  
 $x_2$  = ordinate of mode shape at middepth of second-level slab;  
 $Z$  = numerical coefficient dependent on seismic zone;  
 $\beta$  = factor by which slab flexural inertia is reduced;  
 $\epsilon_{cmax}$  = maximum concrete compression strain assumed at ultimate.

## EARTHQUAKE ENGINEERING RESEARCH CENTER REPORTS

NOTE: Numbers in parentheses are Accession Numbers assigned by the National Technical Information Service; these are followed by a price code. Copies of the reports may be ordered from the National Technical Information Service, 5285 Port Royal Road, Springfield, Virginia, 22161. Accession Numbers should be quoted on orders for reports (PB --- ---) and remittance must accompany each order. Reports without this information were not available at time of printing. The complete list of EERC reports (from EERC 67-1) is available upon request from the Earthquake Engineering Research Center, University of California, Berkeley, 47th Street and Hoffman Boulevard, Richmond, California 94804.

- UCB/EERC-79/01 "Hysteretic Behavior of Lightweight Reinforced Concrete Beam-Column Subassemblages," by B. Forzani, E.P. Popov and V.V. Bertero - April 1979(PB 298 267)A06
- UCB/EERC-79/02 "The Development of a Mathematical Model to Predict the Flexural Response of Reinforced Concrete Beams to Cyclic Loads, Using System Identification," by J. Stanton & H. McNiven - Jan. 1979(PB 295 875)A10
- UCB/EERC-79/03 "Linear and Nonlinear Earthquake Response of Simple Torsionally Coupled Systems," by C.L. Kan and A.K. Chopra - Feb. 1979(PB 298 262)A06
- UCB/EERC-79/04 "A Mathematical Model of Masonry for Predicting its Linear Seismic Response Characteristics," by Y. Mengi and H.D. McNiven - Feb. 1979(PB 298 266)A06
- UCB/EERC-79/05 "Mechanical Behavior of Lightweight Concrete Confined by Different Types of Lateral Reinforcement," by M.A. Manrique, V.V. Bertero and E.P. Popov - May 1979(PB 301 114)A06
- UCB/EERC-79/06 "Static Tilt Tests of a Tall Cylindrical Liquid Storage Tank," by R.W. Clough and A. Niwa - Feb. 1979 (PB 301 167)A06
- UCB/EERC-79/07 "The Design of Steel Energy Absorbing Restrainers and Their Incorporation into Nuclear Power Plants for Enhanced Safety: Volume 1 - Summary Report," by P.N. Spencer, V.F. Zackay, and E.R. Parker - Feb. 1979(UCB/EERC-79/07)A09
- UCB/EERC-79/08 "The Design of Steel Energy Absorbing Restrainers and Their Incorporation into Nuclear Power Plants for Enhanced Safety: Volume 2 - The Development of Analyses for Reactor System Piping," "Simple Systems" by M.C. Lee, J. Penzien, A.K. Chopra and K. Suzuki "Complex Systems" by G.H. Powell, E.L. Wilson, R.W. Clough and D.G. Row - Feb. 1979(UCB/EERC-79/08)A10
- UCB/EERC-79/09 "The Design of Steel Energy Absorbing Restrainers and Their Incorporation into Nuclear Power Plants for Enhanced Safety: Volume 3 - Evaluation of Commercial Steels," by W.S. Owen, R.M.N. Pelloux, R.O. Ritchie, M. Faral, T. Ohhashi, J. Toplosky, S.J. Hartman, V.F. Zackay and E.R. Parker - Feb. 1979(UCB/EERC-79/09)A04
- UCB/EERC-79/10 "The Design of Steel Energy Absorbing Restrainers and Their Incorporation into Nuclear Power Plants for Enhanced Safety: Volume 4 - A Review of Energy-Absorbing Devices," by J.M. Kelly and M.S. Skinner - Feb. 1979(UCB/EERC-79/10)A04
- UCB/EERC-79/11 "Conservatism In Summation Rules for Closely Spaced Modes," by J.M. Kelly and J.L. Sackman - May 1979(PB 301 328)A03
- UCB/EERC-79/12 "Cyclic Loading Tests of Masonry Single Piers; Volume 3 - Height to Width Ratio of 0.5," by P.A. Hidalgo, R.L. Mayes, H.D. McNiven and R.W. Clough - May 1979(PB 301 321)A08
- UCB/EERC-79/13 "Cyclic Behavior of Dense Course-Grained Materials in Relation to the Seismic Stability of Dams," by N.G. Banerjee, H.B. Seed and C.K. Chan - June 1979(PB 301 373)A13
- UCB/EERC-79/14 "Seismic Behavior of Reinforced Concrete Interior Beam-Column Subassemblages," by S. Viathanatepa, E.P. Popov and V.V. Bertero - June 1979(PB 301 326)A10
- UCB/EERC-79/15 "Optimal Design of Localized Nonlinear Systems with Dual Performance Criteria Under Earthquake Excitations," by M.A. Bhatti - July 1979(PB 80 167 109)A06
- UCB/EERC-79/16 "OPTDYN - A General Purpose Optimization Program for Problems with or without Dynamic Constraints," by M.A. Bhatti, E. Polak and K.S. Pister - July 1979(PB 80 167 091)A05
- UCB/EERC-79/17 "ANSR-II, Analysis of Nonlinear Structural Response, Users Manual," by D.P. Mondkar and G.H. Powell July 1979(PB 80 113 301)A05
- UCB/EERC-79/18 "Soil Structure Interaction in Different Seismic Environments," A. Gomez-Masso, J. Lysmer, J.-C. Chen and H.B. Seed - August 1979(PB 80 101 520)A04
- UCB/EERC-79/19 "ARMA Models for Earthquake Ground Motions," by M.K. Chang, J.W. Kwiatkowski, R.F. Nau, R.M. Oliver and K.S. Pister - July 1979(PB 301 166)A05
- UCB/EERC-79/20 "Hysteretic Behavior of Reinforced Concrete Structural Walls," by J.M. Vallenias, V.V. Bertero and E.P. Popov - August 1979(PB 80 165 905)A12
- UCB/EERC-79/21 "Studies on High-Frequency Vibrations of Buildings - 1: The Column Effect," by J. Lubliner - August 1979 (PB 80 158 553)A03
- UCB/EERC-79/22 "Effects of Generalized Loadings on Bond Reinforcing Bars Embedded in Confined Concrete Blocks," by S. Viathanatepa, E.P. Popov and V.V. Bertero - August 1979(PB 81 124 018)A14
- UCB/EERC-79/23 "Shaking Table Study of Single-Story Masonry Houses, Volume 1: Test Structures 1 and 2," by P. Gülkan, R.L. Mayes and R.W. Clough - Sept. 1979 (HUD-000 1763)A12
- UCB/EERC-79/24 "Shaking Table Study of Single-Story Masonry Houses, Volume 2: Test Structures 3 and 4," by P. Gülkan, R.L. Mayes and R.W. Clough - Sept. 1979 (HUD-000 1836)A12
- UCB/EERC-79/25 "Shaking Table Study of Single-Story Masonry Houses, Volume 3: Summary, Conclusions and Recommendations," by R.W. Clough, R.L. Mayes and P. Gülkan - Sept. 1979 (HUD-000 1837)A06

- UCB/EERC-79/26 "Recommendations for a U.S.-Japan Cooperative Research Program Utilizing Large-Scale Testing Facilities," by U.S.-Japan Planning Group - Sept. 1979(PB 301 407)A06
- UCB/EERC-79/27 "Earthquake-Induced Liquefaction Near Lake Amatitlan, Guatemala," by H.B. Seed, I. Arango, C.K. Chan, A. Gomez-Masso and R. Grant de Ascoli - Sept. 1979(NUREG-CR1341)A03
- UCB/EERC-79/28 "Infill Panels: Their Influence on Seismic Response of Buildings," by J.W. Axley and V.V. Bertero Sept. 1979(PB 80 163 371)A10
- UCB/EERC-79/29 "3D Truss Bar Element (Type 1) for the ANSR-II Program," by D.P. Mondkar and G.H. Powell - Nov. 1979 (PB 80 169 709)A02
- UCB/EERC-79/30 "2D Beam-Column Element (Type 5 - Parallel Element Theory) for the ANSR-II Program," by D.G. Row, G.H. Powell and D.P. Mondkar - Dec. 1979(PB 80 167 224)A03
- UCB/EERC-79/31 "3D Beam-Column Element (Type 2 - Parallel Element Theory) for the ANSR-II Program," by A. Riahi, G.H. Powell and D.P. Mondkar - Dec. 1979(PB 80 167 216)A03
- UCB/EERC-79/32 "On Response of Structures to Stationary Excitation," by A. Der Kiureghian - Dec. 1979(PB 80166 929)A03
- UCB/EERC-79/33 "Undisturbed Sampling and Cyclic Load Testing of Sands," by S. Singh, H.B. Seed and C.K. Chan Dec. 1979(ADA 087 298)A07
- UCB/EERC-79/34 "Interaction Effects of Simultaneous Torsional and Compressional Cyclic Loading of Sand," by P.M. Griffin and W.N. Houston - Dec. 1979(ADA 092 352)A15
- UCB/EERC-80/01 "Earthquake Response of Concrete Gravity Dams Including Hydrodynamic and Foundation Interaction Effects," by A.K. Chopra, P. Chakrabarti and S. Gupta - Jan. 1980(AD-A087297)A10
- UCB/EERC-80/02 "Rocking Response of Rigid Blocks to Earthquakes," by C.S. Yim, A.K. Chopra and J. Penzien - Jan. 1980 (PB80 166 002)A04
- UCB/EERC-80/03 "Optimum Inelastic Design of Seismic-Resistant Reinforced Concrete Frame Structures," by S.W. Zagajeski and V.V. Bertero - Jan. 1980(PB80 164 635)A06
- UCB/EERC-80/04 "Effects of Amount and Arrangement of Wall-Panel Reinforcement on Hysteretic Behavior of Reinforced Concrete Walls," by R. Iliya and V.V. Bertero - Feb. 1980(PB81 122 525)A09
- UCB/EERC-80/05 "Shaking Table Research on Concrete Dam Models," by A. Niwa and R.W. Clough - Sept. 1980(PB81 122 368)A06
- UCB/EERC-80/06 "The Design of Steel Energy-Absorbing Restrainers and their Incorporation into Nuclear Power Plants for Enhanced Safety (Vol 1A): Piping with Energy Absorbing Restrainers: Parameter Study on Small Systems," by G.H. Powell, C. Oughourlian and J. Simons - June 1980
- UCB/EERC-80/07 "Inelastic Torsional Response of Structures Subjected to Earthquake Ground Motions," by Y. Yamazaki April 1980(PB81 122 327)A08
- UCB/EERC-80/08 "Study of X-Braced Steel Frame Structures Under Earthquake Simulation," by Y. Ghanaat - April 1980 (PB81 122 335)A11
- UCB/EERC-80/09 "Hybrid Modelling of Soil-Structure Interaction," by S. Gupta, T.W. Lin, J. Penzien and C.S. Yeh May 1980(PB81 122 319)A07
- UCB/EERC-80/10 "General Applicability of a Nonlinear Model of a One Story Steel Frame," by B.I. Sveinsson and H.D. McNiven - May 1980(PB81 124 877)A06
- UCB/EERC-80/11 "A Green-Function Method for Wave Interaction with a Submerged Body," by W. Kioka - April 1980 (PB81 122 269)A07
- UCB/EERC-80/12 "Hydrodynamic Pressure and Added Mass for Axisymmetric Bodies," by F. Nilrat - May 1980(PB81 122 343)A08
- UCB/EERC-80/13 "Treatment of Non-Linear Drag Forces Acting on Offshore Platforms," by B.V. Dao and J. Penzien May 1980(PB81 153 413)A07
- UCB/EERC-80/14 "2D Plane/Axisymmetric Solid Element (Type 3 - Elastic or Elastic-Perfectly Plastic) for the ANSR-II Program," by D.P. Mondkar and G.H. Powell - July 1980(PB81 122 350)A03
- UCB/EERC-80/15 "A Response Spectrum Method for Random Vibrations," by A. Der Kiureghian - June 1980(PB81 122 301)A03
- UCB/EERC-80/16 "Cyclic Inelastic Buckling of Tubular Steel Braces," by V.A. Zayas, E.P. Popov and S.A. Mahin June 1980(PB81 124 885)A10
- UCB/EERC-80/17 "Dynamic Response of Simple Arch Dams Including Hydrodynamic Interaction," by C.S. Porter and A.K. Chopra - July 1980(PB81 124 000)A13
- UCB/EERC-80/18 "Experimental Testing of a Friction Damped Aseismic Base Isolation System with Fail-Safe Characteristics," by J.M. Kelly, K.E. Beucke and M.S. Skinner - July 1980(PB81 148 595)A04
- UCB/EERC-80/19 "The Design of Steel Energy-Absorbing Restrainers and their Incorporation into Nuclear Power Plants for Enhanced Safety (Vol 1B): Stochastic Seismic Analyses of Nuclear Power Plant Structures and Piping Systems Subjected to Multiple Support Excitations," by M.C. Lee and J. Penzien - June 1980
- UCB/EERC-80/20 "The Design of Steel Energy-Absorbing Restrainers and their Incorporation into Nuclear Power Plants for Enhanced Safety (Vol 1C): Numerical Method for Dynamic Substructure Analysis," by J.M. Dickens and E.L. Wilson - June 1980
- UCB/EERC-80/21 "The Design of Steel Energy-Absorbing Restrainers and their Incorporation into Nuclear Power Plants for Enhanced Safety (Vol 2): Development and Testing of Restraints for Nuclear Piping Systems," by J.M. Kelly and M.S. Skinner - June 1980
- UCB/EERC-80/22 "3D Solid Element (Type 4-Elastic or Elastic-Perfectly-Plastic) for the ANSR-II Program," by D.P. Mondkar and G.H. Powell - July 1980(PB81 123 242)A03
- UCB/EERC-80/23 "Gap-Friction Element (Type 5) for the ANSR-II Program," by D.P. Mondkar and G.H. Powell - July 1980 (PB81 122 285)A03

- UCB/EERC-80/24 "U-Bar Restraint Element (Type 11) for the ANSR-II Program," by C. Oughourlian and G.H. Powell July 1980(PB81 122 293)A03
- UCB/EERC-80/25 "Testing of a Natural Rubber Base Isolation System by an Explosively Simulated Earthquake," by J.M. Kelly - August 1980(PB81 201 360)A04
- UCB/EERC-80/26 "Input Identification from Structural Vibrational Response," by Y. Hu - August 1980(PB81 152 308)A05
- UCB/EERC-80/27 "Cyclic Inelastic Behavior of Steel Offshore Structures," by V.A. Zayas, S.A. Mahin and E.P. Popov August 1980(PB81 196 180)A15
- UCB/EERC-80/28 "Shaking Table Testing of a Reinforced Concrete Frame with Biaxial Response," by M.G. Oliva October 1980(PB81 154 304)A10
- UCB/EERC-80/29 "Dynamic Properties of a Twelve-Story Prefabricated Panel Building," by J.G. Bouwkamp, J.P. Kollegger and R.M. Stephen - October 1980(PB82 117 128)A06
- UCB/EERC-80/30 "Dynamic Properties of an Eight-Story Prefabricated Panel Building," by J.G. Bouwkamp, J.P. Kollegger and R.M. Stephen - October 1980(PB81 200 313)A05
- UCB/EERC-80/31 "Predictive Dynamic Response of Panel Type Structures Under Earthquakes," by J.P. Kollegger and J.G. Bouwkamp - October 1980(PB81 152 316)A04
- UCB/EERC-80/32 "The Design of Steel Energy-Absorbing Restrainers and their Incorporation into Nuclear Power Plants for Enhanced Safety (Vol 3): Testing of Commercial Steels in Low-Cycle Torsional Fatigue," by P. Spencer, E.R. Parker, E. Jongewaard and M. Drory
- UCB/EERC-80/33 "The Design of Steel Energy-Absorbing Restrainers and their Incorporation into Nuclear Power Plants for Enhanced Safety (Vol 4): Shaking Table Tests of Piping Systems with Energy-Absorbing Restrainers," by S.F. Stiemer and W.G. Godden - Sept. 1980
- UCB/EERC-80/34 "The Design of Steel Energy-Absorbing Restrainers and their Incorporation into Nuclear Power Plants for Enhanced Safety (Vol 5): Summary Report," by P. Spencer
- UCB/EERC-80/35 "Experimental Testing of an Energy-Absorbing Base Isolation System," by J.M. Kelly, M.S. Skinner and K.E. Beucke - October 1980(PB81 154 072)A04
- UCB/EERC-80/36 "Simulating and Analyzing Artificial Non-Stationary Earthquake Ground Motions," by R.F. Nau, R.M. Oliver and K.S. Pister - October 1980(PB81 153 397)A04
- UCB/EERC-80/37 "Earthquake Engineering at Berkeley - 1980," - Sept. 1980(PB81 205 874)A09
- UCB/EERC-80/38 "Inelastic Seismic Analysis of Large Panel Buildings," by V. Schriker and G.H. Powell - Sept. 1980 (PB81 154 338)A13
- UCB/EERC-80/39 "Dynamic Response of Embankment, Concrete-Gravity and Arch Dams Including Hydrodynamic Interaction," by J.F. Hall and A.K. Chopra - October 1980(PB81 152 324)A11
- UCB/EERC-80/40 "Inelastic Buckling of Steel Struts Under Cyclic Load Reversal," by R.G. Black, W.A. Wenger and E.P. Popov - October 1980(PB81 154 312)A08
- UCB/EERC-80/41 "Influence of Site Characteristics on Building Damage During the October 3, 1974 Lima Earthquake," by P. Repetto, I. Arango and H.B. Seed - Sept. 1980(PB81 161 739)A05
- UCB/EERC-80/42 "Evaluation of a Shaking Table Test Program on Response Behavior of a Two Story Reinforced Concrete Frame," by J.M. Blondet, R.W. Clough and S.A. Mahin
- UCB/EERC-80/43 "Modelling of Soil-Structure Interaction by Finite and Infinite Elements," by F. Medina - December 1980(PB81 229 270)A04
- UCB/EERC-81/01 "Control of Seismic Response of Piping Systems and Other Structures by Base Isolation," edited by J.M. Kelly - January 1981 (PB81 200 735)A05
- UCB/EERC-81/02 "OPTNSR - An Interactive Software System for Optimal Design of Statically and Dynamically Loaded Structures with Nonlinear Response," by M.A. Bhatti, V. Ciampi and K.S. Pister - January 1981 (PB81 218 851)A09
- UCB/EERC-81/03 "Analysis of Local Variations in Free Field Seismic Ground Motions," by J.-C. Chen, J. Lysmer and H.B. Seed - January 1981 (AD-A099508)A13
- UCB/EERC-81/04 "Inelastic Structural Modeling of Braced Offshore Platforms for Seismic Loading," by V.A. Zayas, P.-S.B. Shing, S.A. Mahin and E.P. Popov - January 1981(PB82 138 777)A07
- UCB/EERC-81/05 "Dynamic Response of Light Equipment in Structures," by A. Der Kiureghian, J.L. Sackman and B. Nour-Omid - April 1981 (PB81 218 497)A04
- UCB/EERC-81/06 "Preliminary Experimental Investigation of a Broad Base Liquid Storage Tank," by J.G. Bouwkamp, J.P. Kollegger and R.M. Stephen - May 1981(PB82 140 385)A03
- UCB/EERC-81/07 "The Seismic Resistant Design of Reinforced Concrete Coupled Structural Walls," by A.E. Aktan and V.V. Bertero - June 1981(PB82 113 358)A11
- UCB/EERC-81/08 "The Undrained Shearing Resistance of Cohesive Soils at Large Deformations," by M.R. Pyles and H.B. Seed - August 1981
- UCB/EERC-81/09 "Experimental Behavior of a Spatial Piping System with Steel Energy Absorbers Subjected to a Simulated Differential Seismic Input," by S.F. Stiemer, W.G. Godden and J.M. Kelly - July 1981

- UCB/EERC-81/10 "Evaluation of Seismic Design Provisions for Masonry in the United States," by B.I. Sveinsson, R.L. Mayes and H.D. McNiven - August 1981 (PB82 166 075)A08
- UCB/EERC-81/11 "Two-Dimensional Hybrid Modelling of Soil-Structure Interaction," by T.-J. Tzong, S. Gupta and J. Penzien - August 1981(PB82 142 118)A04
- UCB/EERC-81/12 "Studies on Effects of Infills in Seismic Resistant R/C Construction," by S. Brokken and V.V. Bertero - September 1981 (PB82 166 190)A09
- UCB/EERC-81/13 "Linear Models to Predict the Nonlinear Seismic Behavior of a One-Story Steel Frame," by H. Valdimarsson, A.H. Shah and H.D. McNiven - September 1981(PB82 138 793)A07
- UCB/EERC-81/14 "TLUSH: A Computer Program for the Three-Dimensional Dynamic Analysis of Earth Dams," by T. Kagawa, L.H. Mejia, H.B. Seed and J. Lysmer - September 1981(PB82 139 940)A06
- UCB/EERC-81/15 "Three Dimensional Dynamic Response Analysis of Earth Dams," by L.H. Mejia and H.B. Seed - September 1981 (PB82 137 274)A12
- UCB/EERC-81/16 "Experimental Study of Lead and Elastomeric Dampers for Base Isolation Systems," by J.M. Kelly and S.B. Hodder - October 1981 (PB82 166 182)A05
- UCB/EERC-81/17 "The Influence of Base Isolation on the Seismic Response of Light Secondary Equipment," by J.M. Kelly - April 1981 (PB82 255 266)A04
- UCB/EERC-81/18 "Studies on Evaluation of Shaking Table Response Analysis Procedures," by J. Marcial Blondet - November 1981 (PB82 197 278)A10
- UCB/EERC-81/19 "DELIGHT.STRUCT: A Computer-Aided Design Environment for Structural Engineering," by R.J. Balling, K.S. Pister and E. Polak - December 1981 (PB82 218 496)A07
- UCB/EERC-81/20 "Optimal Design of Seismic-Resistant Planar Steel Frames," by R.J. Balling, V. Ciampi, K.S. Pister and E. Polak - December 1981 (PB82 220 179)A07
- UCB/EERC-82/01 "Dynamic Behavior of Ground for Seismic Analysis of Lifeline Systems," by T. Sato and A. Der Kiureghian - January 1982 (PB82 218 926)A05
- UCB/EERC-82/02 "Shaking Table Tests of a Tubular Steel Frame Model," by Y. Ghanaat and R. W. Clough - January 1982 (PB82 220 161)A07
- UCB/EERC-82/03 "Behavior of a Piping System under Seismic Excitation: Experimental Investigations of a Spatial Piping System supported by Mechanical Shock Arrestors and Steel Energy Absorbing Devices under Seismic Excitation," by S. Schneider, H.-M. Lee and W. G. Godden - May 1982 (PB83 172 544)A09
- UCB/EERC-82/04 "New Approaches for the Dynamic Analysis of Large Structural Systems," by E. L. Wilson - June 1982 (PB83 148 080)A05
- UCB/EERC-82/05 "Model Study of Effects of Damage on the Vibration Properties of Steel Offshore Platforms," by F. Shahrivar and J. G. Bouwkamp - June 1982 (PB83 148 742)A10
- UCB/EERC-82/06 "States of the Art and Practice in the Optimum Seismic Design and Analytical Response Prediction of R/C Frame-Wall Structures," by A. E. Aktan and V. V. Bertero - July 1982 (PB83 147 736)A05
- UCB/EERC-82/07 "Further Study of the Earthquake Response of a Broad Cylindrical Liquid-Storage Tank Model," by G. C. Manos and R. W. Clough - July 1982 (PB83 147 744)A11
- UCB/EERC-82/08 "An Evaluation of the Design and Analytical Seismic Response of a Seven Story Reinforced Concrete Frame - Wall Structure," by F. A. Charney and V. V. Bertero - July 1982(PB83 157 628)A09
- UCB/EERC-82/09 "Fluid-Structure Interactions: Added Mass Computations for Incompressible Fluid," by J. S.-H. Kuo - August 1982 (PB83 156 281)A07
- UCB/EERC-82/10 "Joint-Opening Nonlinear Mechanism: Interface Smeared Crack Model," by J. S.-H. Kuo - August 1982 (PB83 149 195)A05
- UCB/EERC-82/11 "Dynamic Response Analysis of Tachi Dam," by R. W. Clough, R. M. Stephen and J. S.-H. Kuo - August 1982 (PB83 147 496)A06
- UCB/EERC-82/12 "Prediction of the Seismic Responses of R/C Frame-Coupled Wall Structures," by A. E. Aktan, V. V. Bertero and M. Piazza - August 1982 (PB83 149 203)A09
- UCB/EERC-82/13 "Preliminary Report on the SMART 1 Strong Motion Array in Taiwan," by B. A. Bolt, C. H. Loh, J. Penzien, Y. B. Tsai and Y. T. Yeh - August 1982 (PB83 159 400)A10
- UCB/EERC-82/14 "Shaking-Table Studies of an Eccentrically X-Braced Steel Structure," by M. S. Yang - September 1982 (PB83 260 778)A12
- UCB/EERC-82/15 "The Performance of Stairways in Earthquakes," by C. Roha, J. W. Axley and V. V. Bertero - September 1982 (PB83 157 693)A07
- UCB/EERC-82/16 "The Behavior of Submerged Multiple Bodies in Earthquakes," by W.-G. Liao - Sept. 1982 (PB83 158 709)A07
- UCB/EERC-82/17 "Effects of Concrete Types and Loading Conditions on Local Bond-Slip Relationships," by A. D. Cowell, E. P. Popov and V. V. Bertero - September 1982 (PB83 153 577)A04

- UCB/EERC-82/18 "Mechanical Behavior of Shear Wall Vertical Boundary Members: An Experimental Investigation," by M. T. Wagner and V. V. Bertero - October 1982 (PB83 159 764)A05
- UCB/EERC-82/19 "Experimental Studies of Multi-support Seismic Loading on Piping Systems," by J. M. Kelly and A. D. Cowell - November 1982
- UCB/EERC-82/20 "Generalized Plastic Hinge Concepts for 3D Beam-Column Elements," by P. F.-S. Chen and G. H. Powell - November 1982 (PB83 247 981)A13
- UCB/EERC-82/21 "ANSR-III: General Purpose Computer Program for Nonlinear Structural Analysis," by C. V. Oughourlian and G. H. Powell - November 1982 (PB83 251 330)A12
- UCB/EERC-82/22 "Solution Strategies for Statically Loaded Nonlinear Structures," by J. W. Simons and G. H. Powell - November 1982 (PB83 197 970)A06
- UCB/EERC-82/23 "Analytical Model of Deformed Bar Anchorages under Generalized Excitations," by V. Ciampi, R. Elieghausen, V. V. Bertero and E. P. Popov - November 1982 (PB83 169 532)A06
- UCB/EERC-82/24 "A Mathematical Model for the Response of Masonry Walls to Dynamic Excitations," by H. Sucuoğlu, Y. Mengi and H. D. McNiven - November 1982 (PB83 169 011)A07
- UCB/EERC-82/25 "Earthquake Response Considerations of Broad Liquid Storage Tanks," by F. J. Cambra - November 1982 (PB83 251 215)A09
- UCB/EERC-82/26 "Computational Models for Cyclic Plasticity, Rate Dependence and Creep," by B. Mosaddad and G. H. Powell - November 1982 (PB83 245 829)A08
- UCB/EERC-82/27 "Inelastic Analysis of Piping and Tubular Structures," by M. Mahasverachai and G. H. Powell - November 1982 (PB83 249 987)A07
- UCB/EERC-83/01 "The Economic Feasibility of Seismic Rehabilitation of Buildings by Base Isolation," by J. M. Kelly - January 1983 (PB83 197 988)A05
- UCB/EERC-83/02 "Seismic Moment Connections for Moment-Resisting Steel Frames," by E. P. Popov - January 1983 (PB83 195 412)A04
- UCB/EERC-83/03 "Design of Links and Beam-to-Column Connections for Eccentrically Braced Steel Frames," by E. P. Popov and J. O. Malley - January 1983 (PB83 194 811)A04
- UCB/EERC-83/04 "Numerical Techniques for the Evaluation of Soil-Structure Interaction Effects in the Time Domain," by E. Bayo and E. L. Wilson - February 1983 (PB83 245 605)A09
- UCB/EERC-83/05 "A Transducer for Measuring the Internal Forces in the Columns of a Frame-Wall Reinforced Concrete Structure," by R. Sause and V. V. Bertero - May 1983 (PB84 119 494)A06
- UCB/EERC-83/06 "Dynamic Interactions between Floating Ice and Offshore Structures," by P. Croteau - May 1983 (PB84 119 486)A16
- UCB/EERC-83/07 "Dynamic Analysis of Multiply Tuned and Arbitrarily Supported Secondary Systems," by T. Igusa and A. Der Kiureghian - June 1983 (PB84 118 272)A11
- UCB/EERC-83/08 "A Laboratory Study of Submerged Multi-body Systems in Earthquakes," by G. R. Ansari - June 1983 (PB83 261 842)A17
- UCB/EERC-83/09 "Effects of Transient Foundation Uplift on Earthquake Response of Structures," by C.-S. Yim and A. K. Chopra - June 1983 (PB83 261 396)A07
- UCB/EERC-83/10 "Optimal Design of Friction-Braced Frames under Seismic Loading," by M. A. Austin and K. S. Pister - June 1983 (PB84 119 288)A06
- UCB/EERC-83/11 "Shaking Table Study of Single-Story Masonry Houses: Dynamic Performance under Three Component Seismic Input and Recommendations," by G. C. Manos, R. W. Clough and R. L. Mayes - June 1983
- UCB/EERC-83/12 "Experimental Error Propagation in Pseudodynamic Testing," by P. B. Shing and S. A. Mahin - June 1983 (PB84 119 270)A09
- UCB/EERC-83/13 "Experimental and Analytical Predictions of the Mechanical Characteristics of a 1/5-scale Model of a 7-story R/C Frame-Wall Building Structure," by A. E. Aktan, V. V. Bertero, A. A. Chowdhury and T. Nagashima - August 1983 (PB84 119 213)A07
- UCB/EERC-83/14 "Shaking Table Tests of Large-Panel Precast Concrete Building System Assemblages," by M. G. Oliva and R. W. Clough - August 1983
- UCB/EERC-83/15 "Seismic Behavior of Active Beam Links in Eccentrically Braced Frames," by K. D. Hjelmstad and E. P. Popov - July 1983 (PB84 119 676)A09
- UCB/EERC-83/16 "System Identification of Structures with Joint Rotation," by J. S. Dimsdale and H. D. McNiven - July 1983
- UCB/EERC-83/17 "Construction of Inelastic Response Spectra for Single-Degree-of-Freedom Systems," by S. Mahin and J. Lin - July 1983

- UCB/EERC-83/18 "Interactive Computer Analysis Methods for Predicting the Inelastic Cyclic Behaviour of Structural Sections," by S. Kaba and S. Mahin - July 1983 (PB84 192 012) A06
- UCB/EERC-83/19 "Effects of Bond Deterioration on Hysteretic Behavior of Reinforced Concrete Joints," by F.C. Filippou, E.P. Popov and V.V. Bertero - August 1983 (PB84 192 020) A10
- UCB/EERC-83/20 "Analytical and Experimental Correlation of Large-Panel Precast Building System Performance," by M.G. Oliva, R.W. Clough, M. Velkov, P. Gavrilovic and J. Petrovski - November 1983
- UCB/EERC-83/21 "Mechanical Characteristics of Materials Used in a 1/5 Scale Model of a 7-Story Reinforced Concrete Test Structure," by V.V. Bertero, A.E. Aktan, H.G. Harris and A.A. Chowdhury - September 1983 (PB84 193 697) A05
- UCB/EERC-83/22 "Hybrid Modelling of Soil-Structure Interaction in Layered Media," by T.-J. Tzong and J. Penzien - October 1983 (PB84 192 178) A08
- UCB/EERC-83/23 "Local Bond Stress-Slip Relationships of Deformed Bars under Generalized Excitations," by R. Eligehausen, E.P. Popov and V.V. Bertero - October 1983 (PB84 192 848) A09
- UCB/EERC-83/24 "Design Considerations for Shear Links in Eccentrically Braced Frames," by J.O. Malley and E.P. Popov - November 1983 (PB84 192 186) A07
- UCB/EERC-84/01 "Pseudodynamic Test Method for Seismic Performance Evaluation: Theory and Implementation," by P.-S. B. Shing and S. A. Mahin - January 1984 (PB84 190 644) A08
- UCB/EERC-84/02 "Dynamic Response Behavior of Xiang Hong Dian Dam," by R.W. Clough, K.-T. Chang, H.-Q. Chen, R.M. Stephen, G.-L. Wang, and Y. Ghanaat - April 1984
- UCB/EERC-84/03 "Refined Modelling of Reinforced Concrete Columns for Seismic Analysis," by S.A. Kaba and S.A. Mahin - April, 1984
- UCB/EERC-84/04 "A New Floor Response Spectrum Method for Seismic Analysis of Multiply Supported Secondary Systems," by A. Asfura and A. Der Kiureghian - June 1984
- UCB/EERC-84/05 "Earthquake Simulation Tests and Associated Studies of a 1/5th-scale Model of a 7-Story R/C Frame-Wall Test Structure," by V.V. Bertero, A.E. Aktan, F.A. Charney and R. Sause - June 1984
- UCB/EERC-84/06 "R/C Structural Walls: Seismic Design for Shear," by A.E. Aktan and V.V. Bertero
- UCB/EERC-84/07 "Behavior of Interior and Exterior Flat-Plate Connections subjected to Inelastic Load Reversals," by H.L. Zee and J.P. Moehle
- UCB/EERC-84/08 "Experimental Study of the Seismic Behavior of a two-story Flat-Plate Structure," by J.W. Diebold and J.P. Moehle